Development of silicon-based microsensor for the detection of some volatile organic compounds

Ibrahim Musa

N°d'ordre : NNT : 2022LYSE1034

THESE de DOCTORAT DE L'UNIVERSITE DE LYON

Opérée au sein de

L'Université Claude Bernard Lyon 1

Ecole Doctorale N° 206

Chimie, Procédés, Environnement

Spécialité de doctorat : Chimie

Discipline : Chimie Physique

Soutenue publiquement le 18 mars 2022, par :

Ibrahim MUSA

Development of silicon-based micro-sensor for the detection of some volatile organic compounds

Devant le jury composé de :

LEONARD, Didier	Professeur des universités (UCBL, ISA)	Président
KORRI-YOUSSOUFI, Hafsa	Directrice de recherche CNRS	Rapporteure
KANOUN, Olfa	Professeure des universités (Allemagne)	Rapporteure
BAUSELLS ROIGE, Joan	Directeur de recherche (Espagne)	Examinateur
ERRACHID El-SALHI, Abdelhamid	Professeur des universités (UCBL, ISA)	Directeur de thèse
RAFFIN, Guy	Ingénieur de recherche CNRS (ISA)	Co-directeur de thèse
JAFFREZIC, Nicole	Directeur de recherche émérite CNRS (ISA)	Invitée

UNIVERSITE CLAUDE BERNARD – LYON 1

Président de l'Université	M. Frédéric FLEURY
Président du Conseil Académique	M. Hamda BEN HADID
Vice-Président du Conseil d'Administration	M. Didier REVEL
Vice-Président du Conseil des Etudes et de la Vie Universitaire	Mme Céline BROCHIER
Vice-Président de la Commission de Recherche	M. Petru MIRONESCU
Directeur Général des Services	M. Pierre ROLLAND

COMPOSANTES SANTE

Département de Formation et Centre de Recherche en Biologie Humaine	Directrice : Mme Anne-Marie SCHOTT
Faculté d'Odontologie	Doyenne : Mme Dominique SEUX
Faculté de Médecine et Maïeutique Lyon Sud - Charles Mérieux	Doyenne : Mme Carole BURILLON
Faculté de Médecine Lyon-Est	Doyen : M. Gilles RODE
Institut des Sciences et Techniques de la Réadaptation (ISTR)	Directeur : M. Xavier PERROT
Institut des Sciences Pharmaceutiques et Biologiques (ISBP)	Directeur : M. Claude DUSSART

COMPOSANTES & DEPARTEMENTS DE SCIENCES & TECHNOLOGIE

Département Génie Electrique et des Procédés (GEP)	Directrice : Mme Rosaria FERRIGNO
Département Informatique	Directeur : M. Behzad SHARIAT
Département Mécanique	Directeur M. Marc BUFFAT
Ecole Supérieure de Chimie, Physique, Electronique (CPE Lyon)	Directeur : Gérard PIGNAULT
Institut de Science Financière et d'Assurances (ISFA)	Directeur : M. Nicolas LEBOISNE
Institut National du Professorat et de l'Education	Directeur : M. Pierre CHAREYRON
Institut Universitaire de Technologie de Lyon 1	Directeur : M. Christophe VITON
Observatoire de Lyon	Directrice : Mme Isabelle DANIEL
Polytechnique Lyon	Directeur : Emmanuel PERRIN
UFR Biosciences	Admin provisoire : Mme Kathrin GIESELER
UFR des Sciences et Techniques des Activités Physiques et Sportives (STAPS)	Directeur : M. Yannick VANPOULLE
UFR Faculté des Sciences	Directeur : M. Bruno ANDRIOLETTI

To my Family and Friends

Acknowledgments

It gives me great pleasure and honor to thank Prof. Abdelhamid ERRACHID El-SALHI, Head of the Micro and Nano Biotechnology Group, MNBT, ISA, Lyon, for guiding me over the hilly terrain of research during the previous three years. I want to take this occasion to convey my heartfelt gratitude for allowing me to research under his supervision and for maintaining his faith in my capacities. He has been a great help throughout my thesis with his tolerance and knowledge, allowing me to work in my way. I appreciate his support and excitement, which helped me stay motivated even when things were difficult. Emeritus Prof. Nicole JAFFREZIC deserves my gratitude for providing me with a research-oriented environment, as well as her unwavering encouragement and support. I would like to express my gratitude to my co-supervisor, Mr. Guy RAFFIN, a specialist in thermal analysis, gas, and VOCs at ISA Lyon, for his support and guidance throughout my Ph.D. work. I have expanded my understanding in many areas of gas detection, from employing the theory of gas chromatography-mass spectroscopy to how to treat data, thanks to his abundance of information, direction, and leadership. To me, he has always been the epitome of a passionate and motivating mentor. His scientific judgment is perfect, and his patience and motivation helped me adopt a scientific approach. He inspired me to think for myself and develop new ideas for my research. I would like to express my gratitude to jury members Prof. KANOUN Olfa and Dr. KORRI-YOUSSOUFI Hafsa for giving their time to review my thesis. I would also want to express my gratitude to Prof. BAUSSELS ROIGE Joan and LEONARD Didier for agreeing to serve on this committee.

Prof. Abdelhamid ELAISSARI, Dr. Nadia ZINE, Dr. Francesca BELLAGAMBI, and Marie HANGOUET deserve my heartfelt gratitude for their guidance, cooperation, and technical advice during the process of completing this thesis. Their assistance in revising this thesis is gratefully appreciated. Nothing is possible without the help of one's family. I want to express my heartfelt gratitude to my late Parent, whose memory has always served as a source of inspiration, even in the darkest of circumstances. I would want to convey my heartfelt gratitude to my wife for her unwavering support, encouragement, eternal love, and sacrifices I would have never been able to fulfill my objectives. Her unfailing love and patience will serve as an inspiration and source of strength for the rest of my life. My beautiful girls, MUSA Haleemah and MUSA Yousrah deserve my eternal thanks for their unwavering support and understanding of my ambitions and desires, as well as the patience to suffer my absence. I would like to

express my gratitude to Christophe Pages, Catherine Jose, and Marie Martin for their technical assistance. I also appreciate the contributions of Prof. Peter Goekjian, Anis Madaci, Mathieu Verpillat, Pouyan Razmshoar, Muhammad Sani Ismail, Imen Boubezari, Farez Zouaoui, Hamdi Ben Halima, Nazha Hilali, and Musbahu Aminu Abdullahi for their scientific bits of advice. My thanks also go to my colleagues and friends Dr. Idris, Dr. Isah, Dr. Joseph, Dr. Taoheed, Christopher, Dr. Sumera, Michel, Eslam, Dr. Muhammad, Yahaya, Aliyu, Garba, Umar, Garkuwa, Abdullahi, Isaac, Dr. Muna, and all other lab mates for their timely help, and contribution to creating a friendly and cooperative atmosphere in the laboratory. I would want to convey my heartfelt gratitude to everyone who has lent a helping hand in the successful completion of this thesis work, as well as my regret for not being able to name everyone individually.

Finally, I want to express my gratitude to the Almighty for giving me the fortitude to face life's challenges and accomplish this endeavor.

Table of Contents

Résumé

L'analyse de l'air expiré des COV fournit des informations très vitales, du point de vue médical, sur l'état métabolique immédiat, démontrant l'état de santé actuel du patient et la possibilité de prévoir toute maladie maintenant ou à venir. La plupart des maladies, comme le cancer, sont dans la plupart des cas détectées à un stade avancé de la maladie, probablement après la production de l'ensemble de la tumeur, puisqu'elle est difficile à diagnostiquer et elle doit alors être traitée de manière invasive. Ce manuscrit a examiné les inconvénients des technologies traditionnelles dans l'analyse des COV respiratoires et s'est concentré sur le développement de micro-capteurs pour l'amélioration des technologies de nez électroniques dans le diagnostic des maladies. Les polymères conducteurs et le biopolymère de chitosane déposés électrochimiquement sur une électrode en or, ont été considérés par divers chercheurs comme un aspirant potentiel en tant qu'outils de détection de gaz, du fait qu'ils possèdent les propriétés requises ; combinaisons chimiques intéressantes et ajustables, caractéristiques électriques et structurelles. Les polymères conducteurs utilisés pour les capteurs de gaz, jusqu'à présent, pour n'en citer que quelques-uns, comprennent le polypyrrole, le polythiophène, la polyaniline et le polyéther et d'une certaine manière un biopolymère, le chitosane, leurs dérivés sont utilisés comme membrane sensible déposée sur des électrodes d'or interdigitées pour les capteurs de gaz conductométriques en raison de leur capacité à acquérir des propriétés conductrices. Le principal avantage du capteur à base de polymère est de fonctionner à température ambiante par rapport aux autres types de capteurs, principalement à base d'oxydes métalliques présentant une efficacité de fonctionnement à très haute température (300-700°C). Par la suite, les scientifiques ont tenté d'obtenir un capteur de gaz avec des propriétés 3S (sensibilité, sélectivité et stabilité) pour répondre au besoin essentiel des capteurs de gaz en santé publique pour le diagnostic des maladies et le contrôle de l'environnement. Les microcapteurs de gaz sont préférés aux techniques de détection de gaz conventionnelles en raison de leur nature non invasive, de leur taille portable, de leur détection rapide et de leur capacité à fonctionner dans des conditions atmosphériques. Cette étude se concentre principalement sur les avancées précédentes dans les capteurs de gaz à base de polymères conducteurs électrodéposés établis sur des transducteurs. Des études approfondies ont révélé que la capacité de détection du polymère électrodéposé pourrait être plus efficace par dopage ou fonctionnalisation chimique : nanostructuration et mélange d'autres matériaux fonctionnels pour produire un nanocomposite ou des matériaux hybrides, comme cela a été rapporté lorsque des polymères avec phtalocyanines incorporées

sont utilisés comme matériau sensible pour l'application à la détection de gaz. Les microcapteurs de gaz fabriqués à partir de l'électropolymérisation de chitosane dopé avec les phthalocyanines de nickel (NiPc) et de nanofibres de PVC électrofilées incorporant des phthalocyanines de nickel comme matériau de détection de base, présentent plusieurs avantages, notamment des propriétés réglables, la détection à la température ambiante et le potentiel de se prêter aux processus d'impression. Des composites en couche mince de chitosane/NiPc ont été déposés par voie électrochimique sur les électrodes en or interdigitées. Alors que les nanofibres de PVC ont été électrofilées sur une surface d'électrode en or interdigitée. La membrane polymère seule et le polymère dopé NiPc sont caractérisés par la microscopie électronique à balayage (MEB), par des spectres de dispersion d'énergie (EDS), par la spectrométrie infrarouge à transformée de Fourier (FTIR) et par une analyse thermogravimétrique (TGA).

Les propriétés de détection de vapeurs d'acétone, d'éthanol et de méthanol des films préparés dans des conditions optimales ont été étudiées à température ambiante en utilisant des mesures différentielles à une fréquence optimale de 10 kHz. La fibre PVC dopée NiPc pour la détection du méthanol a la sensibilité, la limite de détection (LOD), le temps de réponse et le temps de récupération suivants : 505 µS/cm $(v/v)^{-1}$, 500 ppm, 13 secondes et 25 secondes respectivement. Par rapport au film de chitosane dopé avec NiPc, le capteur de méthanol obtenu présente les caractéristiques suivantes : sensibilité : 60,21µS/cm $(v/v)^{-1}$, limite de détection : 700 ppm, temps de réponse : 31 secondes et temps de récupération : 38 secondes. L'étude a également montré une meilleure sélectivité et répétabilité pour cette configuration vis-à-vis du méthanol par rapport à l'éthanol et à l'acétone. L'appareil est insensible à l'interférence de la vapeur d'eau, ce qui le rend bien adapté à la détection des COV en présence d'humidité.

Abstract

Exhaled breath analysis of Volatile Organic Compounds (VOCs) from the medical point of view provides very vital information on the immediate metabolic state demonstrating the patient's current health status and the possibility of forecasting any disease now or soon. Most diseases as if cancer, are in most cases detected at the late stage of the disease, probably after the tumor most have been produced which makes it difficult to diagnose and must be treated in an invasive way. This manuscript looked at the drawbacks of the traditional technologies in breath VOCs analysis and focused on micro sensors developments for improved e-nose technologies in disease diagnosing. Conducting polymers and chitosan biopolymer electrochemically deposited on a gold electrode, has been considered by various researchers to be a potential aspirant for gas sensing tools. They present required properties, interesting and tunable chemical combinations, electrical and structural characteristics. The conducting polymers used for gas sensors, so far, to mention but few, comprises polypyrrole, polythiophene, polyaniline, and polyether and in some way chitosan biopolymer. Their derivatives are utilized as sensitive membrane deposited on interdigitated gold electrodes for conductometric gas sensors because of the ability to acquire conducting properties. The polymer-based sensor's main advantage is operating at room temperature over the other types of sensors, primarily based on metal oxides with operation efficiency at a very high temperature (300-700^{o}C). Subsequently, scientists attempted to attain a gas sensor with 3S properties (sensitivity, selectivity, and stability) due to gas sensors' critical role in public health for disease diagnoses and environmental control. Gas micro sensors are chosen over conventional gas detection techniques due to their non-invasive nature, portable size, rapid detection, and ability to work in atmospheric conditions. This study focuses more on the previous advances in electrodeposited conducting polymer-based gas sensors established on different transducers application. Improved in-depth studies revealed that the electrodeposited polymer's sensing ability could be more efficient through incorporation or chemical functionalization: nanostructuration and mixing other functional materials to yield a nanocomposite or hybrid materials, as was reported where polymer/phthalocyanines are employed as sensitive material for gas sensing application. Gas micro sensors made from electropolymerization of chitosan doped nickel phthalocyanines and electrospun PVC nanofibers incorporated with nickel phthalocyanines film as the base sensing material have several advantages including tunable properties, room temperature sensing, and the potential of being amenable to the printing processes. Thin-film composite of chitosan/NiPc were electrochemically deposited across the

fingers of interdigitated gold electrodes. Whereas PVC nanofibers were electrospun on interdigitated gold electrode surface. The sole polymer membrane and the polymer doped with NiPc undergo chemical characterization by scanning electron microscopy (SEM) images, energy dispersive spectra (EDS), Fourier transform infrared spectrometry (FTIR), and thermal gravimetric analysis (TGA).

Acetone, ethanol, and methanol head space gas-sensing properties of the films prepared at optimum conditions were studied at ambient temperature using differential measurements at an optimized frequency of 10 kHz. The methanol sensor based on PVC fiber doped with NiPc presents the sensitivity, the LOD, the response time, and the recovery time with the following values: 505 $\mu S/cm(v/v)^{-1}$, 500 ppm, 13 seconds, and 25 seconds respectively. Compared to the methanol sensor based on chitosan film doped with NiPc, its characteristics are the following ones: sensitivity: 60.21 $\mu S/cm(v/v)^{-1}$, LOD: 700 ppm, response time: 31 seconds, and recovery time: 38 seconds. The study also showed better selectivity and repeatability for this configuration towards methanol in comparison to ethanol and acetone. The device is unaffected by the interfering water vapor, which makes it well suitable for VOC sensing in presence of humidity.

List of Abbreviations

APCI-MS …… Atmospheric Pressure Chemical Ionization-Mass Spectroscopy

AuNP ……... Gold Nanoparticles

CA …… Chronoamperometry

CE ……..……Counter Electrode

CNT …….. Carbon Nano Tubes

CV …… Cyclic Voltammetry

CVD …… Chemical Vapor Deposition

FET …….. Field Effect Transistor

GC-MS …… Gas Chromatography-Mass Spectroscopy

IDEs …… Interdigitated Electrodes

ITO …….. Indium Tin Oxide

LCU …… Liquid Calibration Unit

Mos …….. Metal Oxides Semiconductor

MWCNT …… Multi-Wall Carbon Nano Tube

NiPc …… Nickel Phthalocyanines

PANI …… Polyaniline

PPy …….. Polypyrrole

PTh …….. Polythiophenes

PTR-MS …….. Proton Transfer Reactions-Mass Spectroscopy

PVA …… Polyvinyl Alcohol

PVC …… Polyvinyl Chloride

QCM …… Quartz Microbalance

RE …… Reference Electrode

SAW …… Surface Acoustic Wave

VOCs ……Volatile Organic Compounds

WE ……... Working Electrode

List of Figures

List of Tables

Chapter I

Basic Overview and Design of the Thesis

I.1. Summary:

The first section of this dissertation covers a basic overview of the subject and explains the problem and the thesis' background. This opening chapter also highlights the thesis' structure and contents. The manuscript's outline is portrayed briefly, with the focus of each chapter highlighted.

I.2. General Introduction & context of the thesis

For people with headaches, tiredness, nausea, impaired vision, convulsion, and even blindness, tumors, and cancer, survival is dependent especially on early diagnosis for patients and researchers are working round the clock to create technologies that can identify biomarkers related to the diseases quickly.

Breath analysis has emerged as a non-invasive method for predicting lung cancer diagnosis, as lung cancer patients' breath extracts have been discovered to contain increased quantities of various volatile organic compounds (VOCs). Until breath testing becomes a clinical reality, a rapid, reliable, cost-effective, and portable technique developed before early diagnosis will be achieved.

These conditions can be possible with polymer-based gas sensor arrays, providing a solid platform for identifying disease-related VOC fingerprints in exhaled breath. In terms of sensitivity and selectivity, sensor researchers, including our team, have already demonstrated that conductive polymer nanocomposites outperform virgin nanomaterials such as polypyrrole (PPy) polythiophene (PTh), polyaniline (PANI), polyether, and biopolymer chitosan. The main objective of this thesis is to speed up the development of chitosan biopolymer nanocomposite, as well as PVC electrospun nanofibers, for the development of vapor sensors with h igh sensitivity and tunable selectivity towards specifically targeted VOC biomarkers. Finally, to construct a system that will integrate and validate the obtained data by coupling our micro sensor with GC-MS, LCU and, Lock-in amplifier to measure VOC at low concentrations.

I.3. The manuscript's design

The dissertation's content can be summarized in a few words. The next chapter focuses on synthesizing bibliographic data after a broad introduction to provide the content of the thesis in this current **chapter I**. The background of various types of malignancy is presented in **Chapter II**. An overview of cancer-related deaths worldwide is offered to demonstrate how carcinoma has become a significant health issue for humanity. Following that, the inadequacies of present cancer diagnostic procedures are discussed, and the necessity of breath analysis is acknowledged as a noninvasive tool for cancer prediction. The potential of biomarker analysis using an electronic nose with conductometric VOC sensors over other traditional exhaled breath analysis methods is also discussed. Finally, different polymer materials employed as the base of VOC sensors have received much attention. A comprehensive review of the literature on the various methodologies for structuring conductive networks and functionalizing polymer and metallo-phthalocyanines is also discussed.

The following three chapters provide the results and discussion of all the experiments for this dissertation. Practical approaches were devised to fabricate sensors that are selective for different types of VOC targets. In these chapters, each of the methodologies employed to generate other deposition techniques of chitosan biopolymer and their vapor sensing capability was discussed independently. The creation of a chitosan-based conductometric sensor for gas sensing applications is discussed in **Chapter III**. This chapter covers the synthesis, construction, and VOC sensing performance of a collection of functionalized chitosan sensors using interdigitated electrodes as the transducer. This technique aims to tune the selectivity of these sensors by varying the organic functionality on the sensitive membrane. The development of conductive nanohybrids, which are multicomponent systems in which two or more nanomaterials are integrated for the objective of synthesizing a novel nanomaterial with desirable multifunctionality, is discussed in **Chapter IV**. The development and vapor sensing applications of electropolymerization chitosan and nickel phthalocyanines-based hybrid sensors are shown in the totality of this chapter. The effect of humidity on the selectivity of the sensors was investigated in depth. The synthesis and vapor sensing characterization of electrospun polyvinyl chloride (PVC) nanofibers are the emphases of **Chapter V**. Our group's researchers have already employed this method in the past few years, which is made up of traditional electrospinning and has been proven to respond selectively to target VOCs when the suitable polymer matrix is used. However, this section incorporates the polymer matrix of electrospun PVC nanofiber, with Nickel phthalocyanines as a controlling parameter of the VOC

sensors' stability selectivity and sensitivity. Finally, the concluding aspect of the manuscript presents observations and future perspectives on developing conductive nanocomposite capable of detecting lower concentrations of VOCs for illness prediction.

After this manuscript, a complete explanation of all the used materials, methodologies, tools, and synthesis operations is gathered in an appendix to make it easier to understand.

This appendix also includes a list of the fundamental ELECTRODEPOSITION AND ELECTROSPINNING employed in this study and a systematic procedure for fabricating them. Morphological, thermal, and structural characterization approaches were all taken into consideration.

Chapter II

Bibliographic Chapter

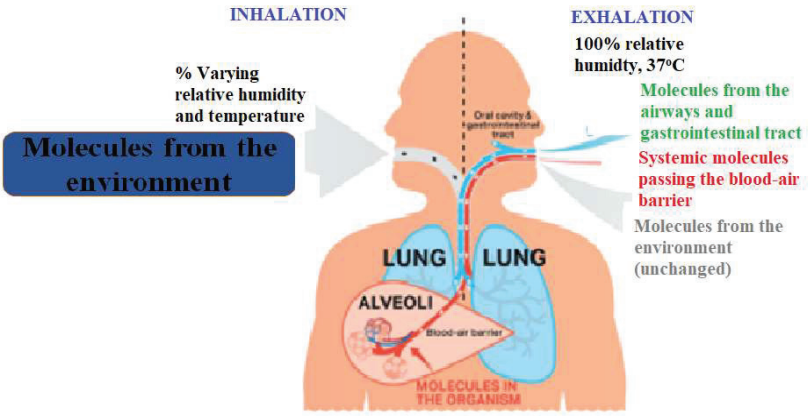

II.1. Introduction

Medical check-up techniques and diagnostics procedures are the essential tools that help physicians differentiate a healthy individual from a sick person and can predict incoming health consequences [1]. The idea of disease detection at the earliest stage creates the possibility for a victorious diagnosis and provides a suitable treatment protocol. It requires the involvement of a cheap, non-invasive, and proactive way of diagnosing diseases [2]. However, it is conceivable that blood and urine are the widely used biological fluids in laboratory testing, but in recent decades, alternative biological specimens such as exhaled breath have gained importance as sources of clinical information [3], both for diagnosis and therapy monitoring, since this breath can reflect biological activities as well as health status, and it can also be collected easily and painlessly [4]. For these reasons, exhaled breath testing has become an increasingly essential non-invasive diagnostic tool for assessing health status and disease types [5]. Furthermore, breath tests have been used to successfully diagnose symptoms such as lung disease, oxidative stress, gastrointestinal disease, metabolic abnormalities, and Helicobacter pylori infection in clinical trials [6]. Breath analysis is a growing field of research with implications for both fundamental and clinical applications, and early diagnostics is a dynamic and expanding subject that uses nanotechnology and molecular diagnostics to aid in the identification of some VOCs and systemic disorders [7]. As a result, VOCs present in exhaled breath has become a valuable tool for assessing physiological and pathological states in humans [8]. Similarly, an examination of the breath may reveal more health information's. Exhaled air can thus identify a variety of clinically relevant substances (e.g., disease biomarkers, drug metabolites) as well as indicators of pollution exposure. Because these compounds were created from both endogenous and exogenous sources, monitoring them might provide information on physiological processes that happened in the body and along the channels of ingestion or absorption.

However, advanced analytical technologies for detecting and measuring volatile organic compounds in clinical matrices raised significant concern for their application in evaluating VOCs' diagnostic potential for different types of diseases [9]. VOCs were initially analyzed by analytical techniques such as gas chromatography-mass spectroscopy (GC-MS), proton transfer reaction mass spectroscopy (PTR-MS), or chemiluminescence [10]. Indeed, the GC-MS operates for the first time to separate the VOCs in a chromatography column, then their identification by mass spectroscopy [11]. This technique has a low detection limit of about one hundred ppb and good selectivity. However, it involves complex measurement procedures and

imposes expensive laboratory measurements. (PTR-MS), is an analytical chemistry technique that uses gas phase hydronium reagent ions which are produced in an ion source. It is a technique for monitoring volatile organic compounds in ambient air. With detection limits in the single digit pptv or even ppqv range, real-time. Complex measurement techniques are often imposed. It involves employing an expert and costly laboratory measurements. As for chemiluminescence, it consists of studying the light produced by returning to the ground state of a molecule previously excited by a chemical reaction [12]. It has the advantage of being a portable technique; however, it causes analytical difficulties for multiple detections of distinct species [13]. As such, these traditional approaches of analyzing VOCs become time-consuming, convoluted, very expensive, and unsuitable for widespread screening.

In this respect, discovering a rapid, reliable, economical, and portable method is of uttermost need before breath analysis attains a clinical reality [14].

While, trying to make some progress, a new trend of analysis has emerged in the last three decades, based on developing gas micro-sensors capable of selectively detecting and quantifying VOCs characteristic of different diseases syndrome [15]. Portability, real-time acquisition, efficiency, non-invasive, and low cost are the keys to manufacturing these innovative micro-sensors [16]. Researchers paid much attention worldwide to numerous gas species detection; quite many transduction principles focused with a high percentage pointed at the miniaturized ones. The main form of operation studied in sensing approaches and promoting sensing results is outlined here: sensing transducers based on metal oxides [17], acoustic waves [18], cantilever resonance [19], resonance [20], resistance, or capacitive changes [21]. The last among the sensor, as mentioned earlier, is capacitively described by the possession of a) devices where the variations in device capacitance formed from the change in the dielectric permittivity of chemically sensitive materials and (b) silicon/polymer biomorphs working in the form of resonance or static bonding [22]. These devices listed above are formed from a flexible or rigid electrode, whereas covered utilizing sensitive materials (predominantly a polymer) through a chemical reaction carried out on the surface, which can expand the volume in the presence of the detecting molecule. This review will implement distinct conducting polymeric and derivatives sensitive membranes developed based on the previous research to detect gaseous compounds.

For these recent developments, electrodeposited conducting polymers on given transducers for gas sensing ability has received much attention due to their promising sensing characteristics, including sensitivity, selectivity, stability, and short response time. These features are operated at room temperature. The development is an additional advantage since most commercially

available microsensors, generally based on metal oxides, operate at very high temperatures (300-700°C). Among the conducting polymers reported to have been used as sensitive membranes since the early 1980s are polypyrrole (PPy) [23], polythiophene (PTh) [24], polyaniline (PANI) [25], polyether [26], chitosan bio polymer [27], and their derivatives. These polymers above were synthesized via chemical or electrochemical procedures. Chemical oxidation is considered the most suitable and straightforward synthesis technique because it involves blending a monomer with an oxidant in each solution.

Nevertheless, electrochemical synthesis proved more efficient than chemical synthesis because it controls the polymerization and doping level [28]. It could also be made over several substrates for the sole purpose of device fabrication directly. The working electrode, mostly interdigitated gold microelectrode, counter (Pt-Electrode), and a reference electrode (Ag/AgCl /3M KCl) are the three-electrode system usually used for electrochemical polymerization of the sensitive materials. Cyclic voltammetry (CV) and chronoamperometry (CA) are the two most known electrochemical deposition techniques for depositing polymeric materials on a given transducer. Surface morphology, porosity, mechanical properties, and thermal stability significantly impact the polymer film coating's physical characteristics [29]. Further research on polymeric sensor fabrication highlights that, to broaden and upgrade the sensor performance, electrodeposited polymers are consistently incorporated with some sensitive materials like coordination compounds (Metallo-phthalocyanines) [30] and metal nanoparticles (Zeolites) [31], metal oxide nanoparticles, and carbon nanotubes to develop composites of higher sensitivity toward gas detection. The analytes detection process proceeds via converting chemical information to an electrical signal [32].

II.2. Brief perception of cancer

Cancer is caused by the rapid development and expansion of aberrant cells. Cell division happens in a normal human being to replace or rather damage a cell and heal injuries. Cancer takes numerous forms, but the causal agent is the out-of-control development of aberrant cells along with the invasion of other organs. Injured DNA in a normal cell neither heals nor dies; instead, the cell continues to make new cells with the same damaged DNA. Consequently, the tumor is produced in most cases. This cancer cell spreads to other parts of the body, where it grows and creates new tumors, which eventually replace normal tissues. Metastasis is the word for this process. Metastasis is the final stage of a tumor's progression. External causes (tobacco, pathogenic organisms, radiation, and chemicals) and internal factors cause cancer (inherited

mutations, hormones, immune condition, and the mutation from the metabolism). Finding a way to initiate or trigger cancer development, the causal cause may occur all at once or in series. The time between exposure to an external factor and cancer detection is frequently more than ten years [33].The International Agency for Research on Cancer's GLOBOCAN 2020 estimates of cancer incidence and mortality update the worldwide cancer burden. In 2020, an estimated 19.3 million new cancer cases (18.1 million excluding nonmelanoma skin cancer) will be diagnosed worldwide, with around 10.0 million cancer deaths (9.9 million excluding nonmelanoma skin cancer). With a projected 1.8 million fatalities (18%), lung cancer remained the top cause of cancer death, followed by colorectal (9.4%), liver (8.3%), stomach (7.7%), and female breast (6.9%) cancers demonstrated in Figure 1. Tumor rates are typically highest in countries with the most considerable life expectancy, educational attainment, and style of living. However, the opposite is true for some cancers, such as cervical cancer, and the incidence rate is more remarkable in countries with low population density [34].

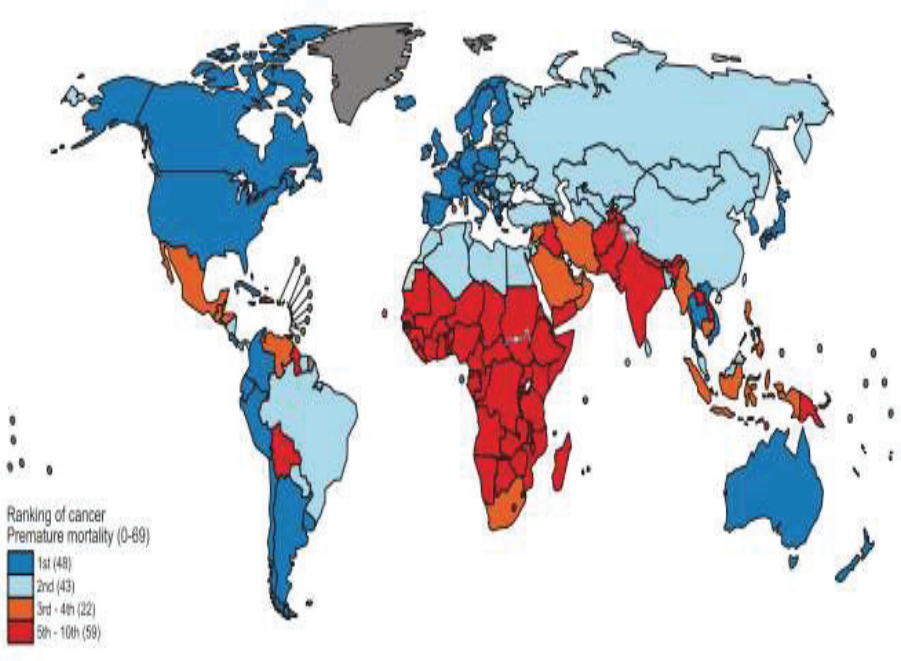

Figure 1. Global Map Showing Cancer's National Ranking as a Cause of Death in People under 70 Years in 2015

The legend of Fig. 1 includes the number of countries represented in each ranking category. (From World Health Organization (WHO)).

The World Health Assembly passed a resolution on cancer prevention and control through an integrated approach (WHA 70.12) in 2017, urging governments and the WHO to take

immediate action to meet the targets set out in the Global Action Plan and the 2030 UN Agenda for Sustainable Development to reduce cancer-related premature mortality.

II.3. Tools for Conventional diagnosis of cancer

Lung cancer is a severe threat to human survival on our planet. The difficulty in detecting lung cancer is the inability to recognize signs in the early stages of the disease. Unfortunately for us, the most common procedures for diagnosing lung cancer nowadays can indeed miss gradual development of the tumors because the diagnosis is focused on determining the size of the tumor [35]. This method is likewise considered prohibitively expensive and unsuitable for extensive screening.

PAPANICOLAU test to detect cervical cancer in women, mammography (an X-ray image used to examine breast tumors), and endoscopic examinations (usually for inspecting the gastrointestinal tract, bronchial tubes, cervix, prostate, bladder, or head, and neck region) are the traditional ways of diagnosing cancer [35]. Ultrasound tests, magnetic resonance imaging, computed tomography, and other methods of cancer screening are among the others [37]. As indicated in (Table 1), each of these approaches has certain flaws in one way or another because the efficiency of detection is dependent on the size of the tumor. As a result, none of the procedures can detect cancer in its early stages. Some of them are costly, while others are invasive and painful to use. As a result, considerable study into the development of cancer biomarker sensors that could aid in the early detection of cancer is critical [36].

Table 1. Cancer Screening

Cancer	Screening	Screening	Frequency
Breast	Breast self-exam chemical test exam mammogram ultrasonography resonance imaging	40-50 years	Every 12 years
Skin/Mucosa	Pap test Human pappillomavirus (HPV)	21 years	21-29 years
Prostate	Prostate specific antigen (PSA) Digital rectal exam	50 years	14 years
Lung	Baseline low dose computed tomography (CT) scan	55 years withs risk factors (smoking history)	Yearly
Colorectal	Guaiac-based fecal occult blood test (gFOBT) fecal immunochemical test stool DNA test CT colonography Double-contrast barium enema sigmoidaoscopy colonoscopy	50 years	Depending on the test 10 years and yearly respectively

II.4. Clinical manifestation of lung cancer

Lung cancer symptoms are divided into two groups: those induced by the tumor's direct mass effect or invasion and those caused by paraneoplastic symptoms, which are systemic symptoms caused by compounds secreted by the tumor (Table 2). Cough, hemoptysis, wheezing, shortness of breath, obstructive pneumonia due to endobronchial tumor development, chest wall pain, and shortness of breath due to restrictive functionality due to peripheral tumor growth are all symptoms of direct tumor invasion. Regional tumor migration into the thorax might induce symptoms depending on the organs involved. The tumor's invasion of the trachea can induce dyspnea, the esophagus can produce dysphagia, the recurrent laryngeal nerve can create hoarseness, and the diaphragmatic nerve can cause respiratory distress due to diaphragm paralysis. Horner's syndrome, marked by enophthalmos, ptosis, miosis, and anhydrosis, is also caused by the invasion of the sympathetic nerves of the cervical spinal cord. Pancoast syndrome, produced by an attack of the 8th cervical and 1st or 2nd thoracic nerves, manifests

as shoulder discomfort radiating along with the ulnar nerve distribution. In contrast, superior vena cava syndrome is caused by an invasion of the superior vena cava [38]. Lung cancer can spread to any organ in the body, causing symptoms specific to the metastatic lesion [39].

Table 2. Lung cancer signs and symptoms

	Comments
Symptoms from direct tumor invasion	
Symptoms associated with central or endobronchial growth of tumor	Cough, hemoptysis, wheezing, shortness of breath, obstructive pneumonia
Symptoms associated with peripheral growth of tumor	Pleural and chest wall pain, pneumonia
Horners syndrome	Sympathetic nerve paralysis, enophthalmos; ptosis, miosis, and a hydrolysis
Pan coast syndrome	Involvement of the 8th cervical and 1-2 thoracic nerve, shoulder pain, radiating ulnar destruction of the arm
Superior vena cava syndrome	Facial edema, right arm edema
Symptoms associated with extra-thoracic metastatic disease	
Paraneoplastic syndrome	
Humoral hypercalcemia of malignancy	Ectopic secretion of PTHrP Squamous cell lung cancer
Syndrome of inappropriate antidiuretic hormone secretion	Ectopic secretion of vasopressin, common in the tumor with neuroendocrine features, such as small cell lung cancer
Ectopic syndrome	Ectopic ACTH production, common in the neuroendocrine tumor, such as small lung cancer
Skeletal-connective tissue syndrome	Clubbing hypertrophic primary osteoarthropathy
Neurologic-myopathic syndrome	Ecto-lambert syndrome retinal blindness with SCLC, peripheral neuropathies, subacute cerebellar degeneration, cortical degeneration polymyositis

The biopsy is now required to diagnose lung cancer, which involves confirming the existence of cancer cells and selecting appropriate treatment, which involves molecular genetic testing. Several tools for lung tissue biopsy are currently in use for lung cancer diagnosis and staging. The location and features of the lesion, the general state of the patient, and the level of

experience of the technician performing the examination should all be considered when choosing diagnostic equipment (Table 3).

Table 3. Advantages and disadvantages of commonly used biopsy procedures for lung cancer

	Advantages	Disadvantages
FSB	High diagnostic yield for central and endobronchial lesion	Low diagnostic yield for non-endobronchial lesion and peripheral lesion
EBUS-TBNA	Acquisition of real time ultrasound images. Accessibility to central lung lesion and some L/N (located in mediastinal, paratracheal, subcarinal, hilar, and interlobar area)	Limitation in evaluation peripheral lung lesion and other L/N
EBUS-GS	Acquisition of real time ultrasound images. Improved accessibility for more peripheral lesion. Collection of cells and some lung tissue	Requirements of Professional training expensiveness
Navigation bronchoscopy	Acquisition of reconstructed and virtual map to target. Improved accessibility to more peripheral lesion. Collection of cells and some lung tissue	Requirements of navigation programs
CT-NAB	High diagnostic yield for peripheral lung lesion (diameter above 2 cm)	Need patients' cooperation (keep posture and holding breath)
GUN biopsy	High diagnostic yield using core-biopsy needles. Collection of relatively sufficient lung tissue	Need patients' cooperation (keep posture and holding breath). Relatively prevalent complication. Pneumothorax and pulmonary hemorrhage

II.5. Cancer biomarker detection

Lung cancer detection at an initial stage can help to reduce mortality rates and save lives [40]. Biomarkers have shifted attention to a new era of cancer diagnosis at an early stage [41]. Any material or activity that may be objectively identified and assessed as an indicator for a normal

biological process, pathogenic process, or pharmacological responses to therapeutic intervention," according to the definition of a biomarker. DNA, mRNA, enzymes, metabolites, transcription factors, cell surface receptors, and certain VOCs are among the species encountered by cancer biomarkers discovered in tumor tissues or serum given in Figure 2 [42]. Different noninvasive gas sensing systems are discussed in this overview. The main goal of a cancer biomarker study is to develop reliable, cost-effective, sensitive, and monitoring strategies for cancer risk detection, early cancer detection, and tumor classification. Patients can receive appropriate treatment, and experts can track disease progression, relapse, and recurrence [43].

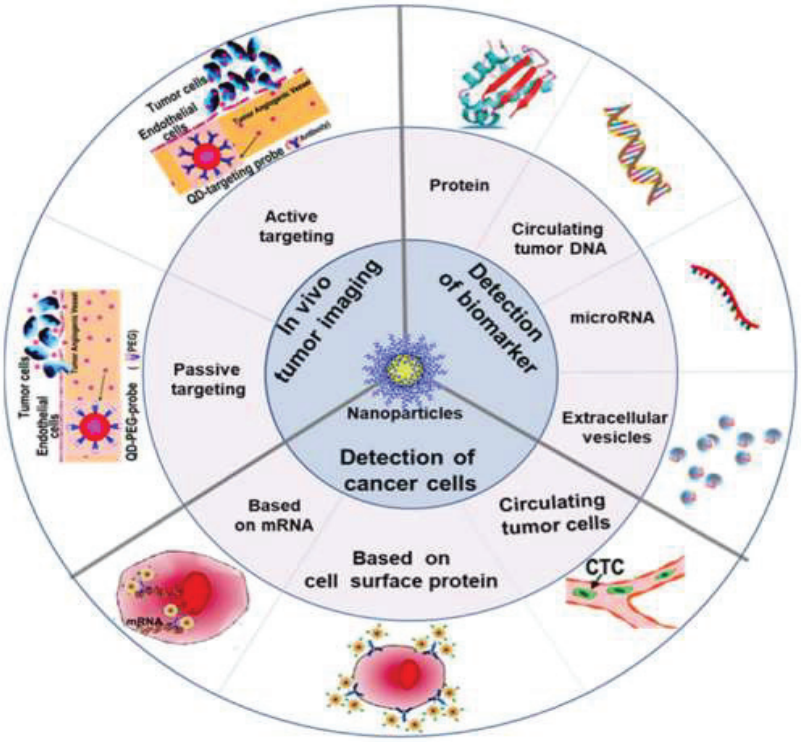

Figure 2. Schematic illustration of various cancer biomarkers

VOC sensors had a lot of promise around cancer detection recently, because the number of VOCs observed in human exhaled breath was the subject of the matter to provide vital information. VOCs' pattern identification distinguished the exhaled breath VOC of cancer patients' exhaled breath and VOC profile of a healthy subject [43]. According to data acquired from a study using a PTR-MS and GC-MS coupled pre-concentrator, chemicals of interest were discovered at concentrations of 1-20 ppb in healthy subjects and 10-100 ppb in cancer patients' exhaled breath. There are two types of VOC biomarkers for cancer patients: polar and non-polar molecules. In exhaled breath, polar VOCs fall into the categories of alcohol, carbonyl

compounds (aldehyde and ketone), and while non-polar VOCs fall into the categories of alkane and aromatic hydrocarbons (Table 4) [44].

Table 4. Breath VOC biomarkers for cancer

Cancer	Detected VOC	VOC biomarkers	Ref
Lung cancer	Alcohols	methanol, ethanol, isopropanol,1-propanol	
	Aliphatic hydrocarbons	heptane, decane, undecane, cyclopentane, 1,3-butadiene, octane, 1-hexene, nonane, methyl heptene, cyclohexane, pentane	
	Aromatic hydrocarbons	isoprene, benzene, toluene, ethyl benzene, xylene, styrene, propyl benzene, trichlorofluoro benzene, 1,2,4-trimethyl benzene, 1,4-dimethyl benzene	
	Carbonyl compounds	formaldehyde, propanal, butanal, pentanal, hexanal, heptanal, octanal, nonanal, acetone, Butanone	[45]
Skin cancer	Alcohols	ethyl hexanol, cyclohexanol	
	Aliphatic hydrocarbons	cyclohexane, nonane, decane, heptadecane	
	Aromatics	benzaldehyde, benzyl alcohol, 1,4-dimethyl benzene, 1,2,4-trimethyl benzene	[46]
Breast cancer	Aliphatic hydrocarbons	nonane, 5-methyl tridecane, 3-methyl undecane, 6-methyl pentadecane, 2-methyl propane, 3-methyl nonadecane, 4-methyl dodecane, 2-methyl octane	
	Carbonyl compounds	heptanal and hexanal	[47]

Because of the low concentration of VOC biomarkers, pre-concentration is required. The human respiratory system produces many volatile organic compounds from many sources (Figure 3).

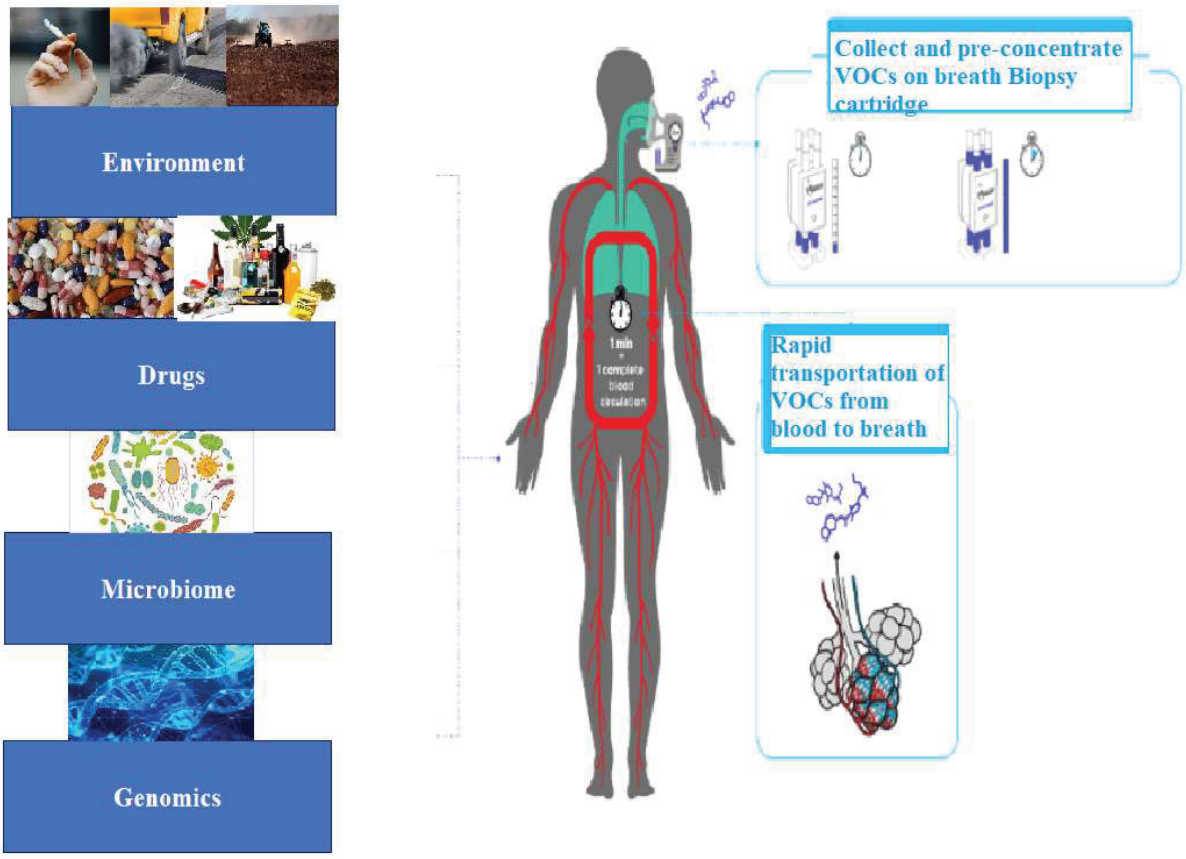

Figure 3. VOCs originating from the entire body and the collection from exhaled breath

VOCs can be endogenous, meaning they come from the body, or exogenous, meaning they come from the environment. After passing via the respiratory tract, they may be of systemic origin.

II.5.1. Alcohol

Alcohols are often derived from foods and alcoholic beverages, and they are absorbed from all regions of the gastrointestinal tract, primarily through simple diffusion into the bloodstream. Alcohols are also produced via the breakdown of hydrocarbons. Alcohol is prevalent in bodily tissues and fluids and is easily absorbed in circulation due to its high affinity for water [48]. 1-propanol was identified in higher concentrations in lung cancer patients than healthy controls [49]. Furthermore, Bajtarevic et al. demonstrated in 2005 that lung cancer patients' breath extract contains methanol, ethanol, and isopropanol [50]. On the other hand, Ethyl hexanol and cyclohexanol are skin cancer indicators [51].

II.5.2. Aromatic hydrocarbons

Philips et al [52]. found a mixture of VOCs styrene, propyl-benzene, trichlorofluorobenzene, 1,2,4-trimethylbenzene, 2-methyl isoprene, 1,4-dimethyl benzene, and 1-methylethenyl benzene to yield a breath print of lung cancer. Poli et al [53]. found a combination of VOCs such as benzene, toluene, ethylbenzene, isoprene, xylene, and styrene to be non-small cell lung cancer biomarkers. In 2005, Machado et al. demonstrated that lung cancer patients' breath extract contained various VOCs such as isoprene, benzene, and toluene [54]. Several aromatic hydrocarbons have been found as skin cancer biomarkers, including benzaldehyde, benzyl alcohol, 1,4-dimethyl benzene, and 1,2,4-trimethyl benzene [55].

II.5.3. Carbonyl compounds

All C_1-C_9 straight-chain aldehydes were discovered in human breath extract. Apart from acetaldehyde, all of them were found in the breath of lung cancer patients. Formaldehyde is also a potential biomarker for bladder and prostate cancer, according to Li et al [56].
Other aldehydes, such as heptanal and hexanal, are also associated with people with breast cancer [57]. Because it is generated under metabolic conditions associated with a high fatty acid oxidation rate in lung cancer, acetone is one of the most common compounds in-breath and a significant lung cancer biomarker [58]. It was discovered that acetone and methyl ethyl ketone are lung cancer indicators as reported in 1985, acetone can also be used to determine the level of glucose in the blood [59]. The level of acetone in a healthy person's breath extract is typically 5 ppm, whereas diabetic patients' breath extract can include up to 300 ppm acetone [60].

II.5.4. Aliphatic hydrocarbons

Gordon et al. identified multiple alkanes and monomethylated alkanes in lung cancer patients' exhaled breath in 1985 [61]. Philips et al [52] observed a combination of VOCs such as 2,2,4,6,6-pentamethyl heptane, 2-methyl heptane, decane, undecane, cyclopentane, methyl-cyclopropane, 1-methyl-2-pentyl-methane, 1,3-butadiene, 3-methyl-octane, 1-hexene, nonane, [53] and also found a combination of VOCs such as pentane, 2-methyl pentane, heptane, octane, decane, and pentamethyl heptanes to be non-small cell lung cancer biomarkers. Belizario et al. studied in 2005 lung cancer patients' breath extract of MPM patients [62], malignant pleural mesothelioma (MPM) being cancer caused mostly by asbestos exposure, It contains many VOCs, including pentane [63] and cyclohexane, being the most specific component in the breath. Breast cancer is related to increased oxidative stress [64], which leads to increased

pentane concentration [63]. Phillips et al. reported nonane, 5-methyl tridecane, 3-methyl undecane, 6-methyl pentadecane, 2-methyl propane, 3-methyl nonadecane, 4-methyl dodecane, and 2-methyl octane as breast cancer biomarkers in 2003 [65]. Melanoma cancer biomarkers have been discovered to include nonane, decane, and heptadecane [66].

II.6. Interest in Exhaled Breath Analysis

Exhaled breath represents one of the most accessible diagnostic samples because large quantities are released spontaneously. At least 10,000 L of air is inhaled and subsequently exhaled by a human being each day [67]. Breath odors were considered for disease recognition in the past before the current development diagnostics: a pleasant smell linked to diabetes mellitus, fish-like odor associated with liver sickness, and urine-like odor with kidney problems [68]. The estimated composition of the exhaled breath of a normal human being is mainly nitrogen, oxygen, carbon dioxide, argon, and water vapors. However, the volatile organic compounds that might diagnostically be vital are present in very trace concentrations [69], as reported in Table 5.

Table 5. Major VOCs and range of concentrations for healthy persons

S/N	VOCs from exhaled breath	Concentrations range
1	Formaldehyde	ppmv-ppbv
2	Acetaldehyde	ppbv
3	Pentanal, Hexanal	ppbv-pptv
4	Acetone	ppmv-ppbv
5	Ethyl Acetate	ppbv
6	Furan, 2,5-Dimethyl	ppbv
7	Furan, -2 Ethyl	ppbv
8	Isoprene	ppbv-pptv
9	Ethane, Pentane	ppbv-pptv
10	Ethanol	ppmv-pptv
11	2- Propanol	ppmv-pptv
12	Benzene, P-Xylene, Toluene	ppbv
13	Nitric Oxide (NOx)	ppbv
14	Carbon disulfide	ppbv
15	Carbonyl sulfide	ppbv

The Identification of VOCs in exhaled breath has reached a level of sustained interest in breath diagnosis because of its non-invasive nature. The concept behind breath metabolomics (mostly known as breathomics) is that VOCs profile in breath will be changed when switch from a normal to a pathological state occurs, which can be detected and partially used for diagnosis and monitoring [70]. VOCs present in exhaled breath are endogenous or exogenous evolved during different biochemical activities in living organisms. Secondly, they are carried out with food, inhaled in the air, or absorbed by the skin [60].

PAULING discovered in 1971 that normal human breath included about 200 VOCs, indicating that it might be a source of information for both systemic and lung physiology [53]. Only 1% of these VOCs can be used as a biomarker for a specific disease; 75% of them are common to all patients and may be used to differentiate between them when concentration levels change, while 25% of this 1% are uncommon volatiles that could be used as biomarkers for specific diseases [72]. Breath VOCs are found at very trace levels, and their reliable sensing poses a great challenge, hence the typical sample pre-concentration approach with a susceptible analytical instrument [71].

II.7. Physiology of human exhaled breath

The exhaled air is like a flow of gas-carrying molecules that reflect the state of the body of a human being. The development of devices for measuring exhaled air has made it possible to

identify many of these substances [74]. The cells produced VOCs during biochemical processes, then transported via the bloodstream to the lungs and exhaled only a few minutes after their creation.

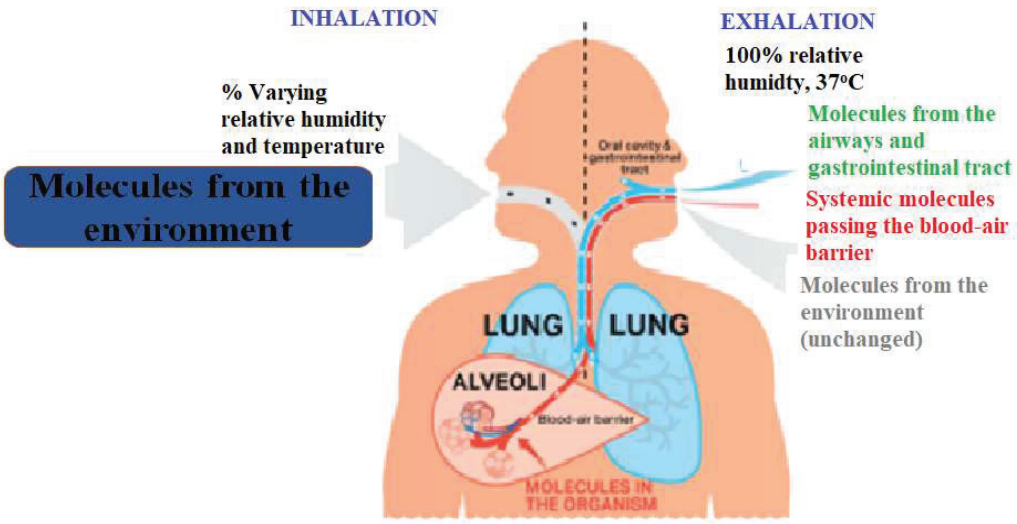

Figure 4. Exhaled molecule pathway in the human body

As illustrated in Figure 4, the passage of air exhaled by humans through the respiratory tract is separated into the dead zone and the alveolar site [77]. The dead zone collects the air that has been trapped in the nasal and oral cavities, as well as the trachea and bronchi, in a volume of around 150 mL. The alveolar zone is made up of the air enclosed in the lungs' alveoli, which has a capacity of about 350 mL. Most exhaled air is broken down into carbon, nitrogen, oxygen, water, and inert gases. More than 1000 distinct molecules make up the remaining fraction, including inorganics like carbon monoxide (CO) and monoxide nitrogen (NO) and organics like acetone and ethanol (VOCs). They are hard to differentiate since they are present in traces of exhaled breath.

II.8. VOC biomarker of diseases

The number of VOCs found has risen exponentially since the start of this study axis in 1971, providing a better knowledge of human metabolism. However, developing a full-fledged diagnostic model remains a challenge. Exhaled air VOC composition changes qualitatively and quantitatively depending on patients, especially concerning numerous criteria such as their sex, physical state, and way of life. GC-MS studied exhaled air in 50 healthy adults in 1999 [72],

which we shall briefly describe this chapter. In specifically, the average occurrence of 204 VOCs per person was discovered. Furthermore, 27 VOCs were discovered to be familiar to all participants out of 3481 VOCs detected in these same patients. Extensive research on breathed air has uncovered a set of biomarkers whose concentration variations are crucial in the case of various disorders. Table 6 lists some of the most common VOCs, as well as their concentrations in healthy people and diseases linked to high amounts [73].

Table 6. Exhaled air biomarkers, related disorders, and measured concentrations

S/N	**Volatile Organic Compounds**	**Related Disease**	**Concentrations**
1	Acetone ($(CH_3)_2CO$)	Diabetes Heart failure Lung cancer	0-1 ppm
2	Acetaldehyde (CH_3CHO)	Lung cancer Alcoholism Liver disease	0-1 ppm
3	Ammonia (NH_3)	Kidney disease	0-1 ppm
4	Benzene (C_6H_6)	Breast cancer Lung cancer	0-10 ppb
5	Hydrogen (H_2)	digestion disorder	-
6	Ethane (C_2H_6)	Breast cancer Oxidative stress Vitamin E deficiency	0-10 ppb
7	Ethanol (C_2H_5OH)	Hepatitis obesity	0-1 ppm
8	Isoprene (C_5H_8)	Hypercholesterolemia	50-200 ppb
9	Methane (CH_4)	Intestinal problems	2-10 ppm
10	Nitrogen Oxide (Nox)	Asthma Pulmonary Disease Lung cancer Rhinitis	10-50 ppb
11	Carbon monoxide (CO)	Cystic fibrosis Oxidative stress Pulmonary inflammation	0-1 ppm
12	Pentane C_5H_{12}	Breast cancer Oxidative stress Lung disease Asthma Schizophrenia Myocardial infarction	0-10 ppb
13	Carbonyl sulfide	Liver disease	0-10 ppb

As a result, nitric oxide has been identified as a target molecule for asthma diagnostics [74]. These biomarkers are found in modest levels in the air exhaled by healthy people, but it rises significantly when the airways are irritated or narrowed [75]. The amounts of exhaled NO molecules measured in patients make it possible to diagnose asthma on the one hand and to validate the efficacy of prescribed anti-inflammatory drugs on the others, corticosteroids, for example. This molecule has also been verified as a biomarker for numerous biomedical uses, particularly lung cancer research [76].

In another development, some disease diagnoses are adressed through exhaled breath analysis. Stress oxidant, a pathogenic mechanism that develops from significant diseases such as cancer, heart failure, or neurological problem [77], has also been connected to fluctuating VOC concentrations. It shows up as abnormalities in physiological species responsible for redox reactions in the human body, resulting in the emergence of chemical processes that cause free radical generation. These radicals continue to destroy saturated and unsaturated lipids in the human body, resulting in severe cellular damage. The concentration of aldehyde, isoprene, ethane, and pentane molecules in exhaled air rises due to this disease [78]. We are interested in detecting the acetone, ethanol, and methanol molecules in expired air as part of this thesis, as it is one of the most prevalent VOCs in people. In recent years, there has been a lot of research on the effects of the VOCs, as mentioned earlier, on human metabolism [79]. Preliminary determination of the metabolic origin of the volatile biomarkers has limited the progress of the scientific and practical applications. To overcome the current limitations, we developed a metabolism tracking approach combining stable isotope labeling and conductometric analysis of volatiles to trace the intracellular metabolism-derived volatiles and to reveal their relation to various types of diseases pathways. This analytical strategy represents a potential cutting-edge tool in elucidating the biochemical authenticity of diseases volatiles and further expanding our understanding of the metabolic network of airborne metabolites. Metabolic problems are usually the result of an endocrine organ, such as the liver, not functioning correctly. The mechanism of molecular acetone synthesis in the liver is depicted in Figure 5. Metabolic events in the human body go wrong when using fat stores for energy instead of glucose. In hepatocytes, oxidation of fatty acids results in the development of excess acetyl-coenzyme, as much as peroxidation of lipids results in excess acetoacetate formation. By decarboxylation of these molecules present in excess, acetone is produced, resulting in an increase in the amount of acetone in the human body. As a result, this molecule has been identified as a diabetes or fat loss biomarker [80]. Healthy people, for example, have acetone concentrations of less than 0.8 ppm, whereas diabetic patients have values of more than 1.8 ppm [81].

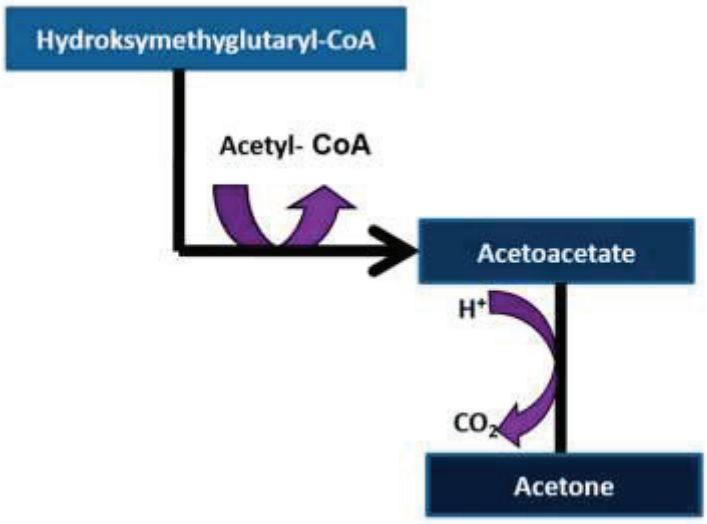

Figure 5. Decarboxylation of ketone bodies

Furthermore, advances in VOC detection and analysis techniques have allowed researchers to dig further into the effects of the VOC molecules on human metabolism [86]. These molecules have recently been identified as an HF syndrome biomarker [82]. These studies clearly show that most volatile organic compounds can diagnose related disease symptoms because they can effectively distinguish between healthy people and patients. Furthermore, the molecular acetone can determine the severity of heart failure. Before moving on to the numerous VOC detection methods in the literature, we'll look at how the exhaled air of patients is collected, conditioned, and analyzed in the next section.

II.9. The versatile use of exhaled VOCs in human health and disease

Gordon et al. were the first to analyze VOCs in exhaled breath from a lung cancer patient in 1985. Their study used gas chromatography-mass spectrometry (GC-MS) [83]. Since then, there has been a surge in interest in the clinical diagnostic potential of exhaled breath studies in early cancer diagnosis, as evidenced by a significant increase in the number of publications during the last three decades. Many of these studies used a control strategy. Lung cancer patients who had not been clinically diagnosed were used as the case group, and cancer subjects were used as the control group, with the VOC profile evaluated and compared between them. VOC biomarkers are a group of organic compounds whose concentrations are statistically different between two groups. Propanol, isoprene, benzene, acetone, pentane, hexanal, toluene, and ethylbenzene are the most discovered VOCs as lung cancer biomarkers employing GC-MS, PTR-MS, and ion mobility mass spectrometry as analytical equipment (Figure 6) [84].

However, these procedures are believed to be either incredibly expensive or non-portable, despite the need for a low-cost, portable, and sensitive exhaled breath analysis apparatus [85].

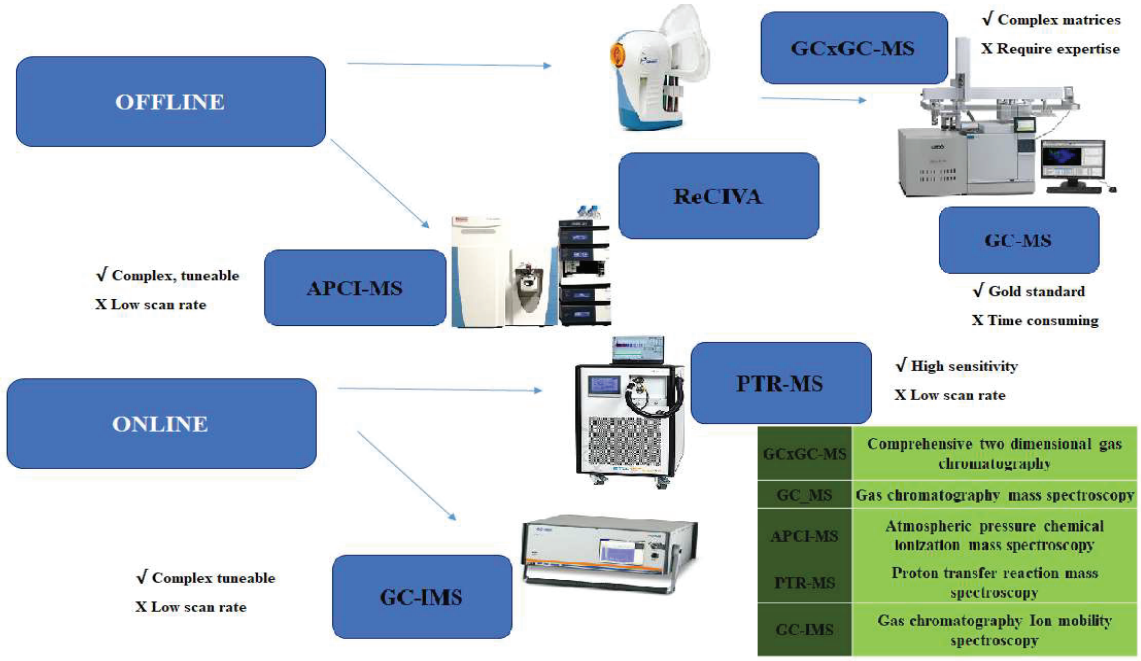

Figure 6. Traditional techniques of analyzing VOCs Offline and Online

Biomarkers have gained prominence because of their rapid release and ability to conduct non-invasive health assessments. Biomarkers are measurable indicators of the condition of a biological process [86]. They are used to screen for diseases, track their progression, and assess therapeutic response [87]. In this regard, researchers are investigating the possibility of developing non-invasive approaches for diagnosing cancer by detecting specific cancer VOCs [88]. It was discovered to be an exceptionally fascinating approach since it allowed for the early detection of tumor cells while they were still localized. One of the most important ways to reduce cancer-related morbidity and mortality is to educate people about the condition [89]. Breath analysis is fascinating, but it suffers from the disadvantages of a large amount of water and a very low concentration of VOC biomarkers (in parts per billion levels) [90].

II.10. Techniques for biomarker analysis

Exhaled breath analysis utilizing gas chromatography-mass spectrometry as the detecting instrument was the subject of many articles at first. Following that, ion flow tube mass spectroscopy, proton transfer reaction-mass spectroscopy, chemo-luminescence sensors, opto-chemical fibers, infrared spectroscopy, and polymer-coated surface acoustic wave sensors were

discussed. To date, the need to continue employing these techniques to detect volatile chemicals has been stifled by factors like cost, the degree of skill required to operate such large instruments, the necessity for pre-concentration, non-portability, and a long response time [91].

II.11. Progressive development in gas analysis

Micro-sensors are already a crucial source of innovation [92]. In recent years, there have been significant improvements in sensor design and fabrication methods and significant advancements in micro-sensor technologies using newly designed materials, resulting in high-sensitivity gas sensors. Gas sensors are particularly effective type of profound sensing device, with a broad array of applications in the health care field attracting huge interest worldwide [93]. Several characteristics, such as device sensitivity, selectivity, precision, limit of detection (LOD), resolution, accuracy, reversibility, recovery time, and response time, are used to evaluate detection capability [94]. Furthermore, device miniaturization and power consumption, costly materials, and extended lifetimes are essential variables in developing sensors in various applications. We highlighted in the following subchapter the contributions of chromatography, electrochemical sensors (metal oxide semiconductor and organic-based chemiresistive gas sensors), carbon nano-tube sensors, acoustic gas sensors (surface acoustic wave, capacitive micro-machine gas sensor), optical sensors, and photonic crystal gas sensors.

II.11.1. Gas chromatography

Chromatography is a long-established method for separating and analyzing a complex mixture of volatile organic and inorganic substances. Chromatography works by splitting a mix through percolation via selectively adsorbing medium and detecting chemicals of interest quickly [95]. It begins with injecting a mixture of chemicals into a chromatograph fitted with a specified column. The sample goes down the column at varying rates, resulting in a different time interval between reaching the column's terminal point. Ion mobility spectrometry and mass spectrometry are two techniques used [96]. The fundamental limitations of these techniques are their non-portability, high cost, and reliance on an expert for handling efficiency. They are currently unsuitable for in-situ applications [97].

II.11.2. Carbon Nano-tube based Sensors

Microfabrication innovation has progressed that carbon nanotubes (CNTs) sensors are now available [98]. CNT as a sensing material with qualities dependent on its shape is a typical feature of these sensors. Single-walled carbon nanotubes (SWCNT) and multi-walled carbon

nanotubes (MWCNT) are two carbon nanotube sensing transducers. The former has only one layer of CNTs, the latter having numerous layers of CNTs within one another. Based on their modes of functioning, they are a significant candidate in gas detecting applications. Gas sorption, ionization, capacitive, and resonant frequency gas sensors are available. CNTs react with the target gas in this scenario, causing a charge transfer between the CNT and the gas. The conductivity of the carbon nanotube sensing material changes due to this process.

II.11.3. Acoustic gas sensors

The acoustic sensor responds to analyte absorption in the detecting film and detects gas species immobilized on the device's surface. The analytes that generate the optimum chemical reactions are generally examined at deficient concentration levels for these sorts of sensors [99]. The fundamental disadvantage of these sensors is their limited selectivity due to the widespread use of sensing materials. Various strategies for enhancing the sensor's selectivity have been published, including using multiple sensors with diverse chemical interfaces and pattern recognition algorithms to measure gaseous analytes. In addition to coupling the sensor to a chromatographic column for separating different types of absorbed analytes, quartz crystal microbalance (QCM), surface acoustic waves (SAW), flexural plate wave (FPW), and thin rod sensors are among the acoustic gas sensors that have been proposed and studied [18].

II.11.4. Optical sensors

In an active site where the detection of photons transforms into electronic signals, the optical sensor conducts based manipulation, control, or sensing of the propagation of visible light or any other type of electromagnetic waves. The sensitivity of these sensors to VOCs can be helpful, but they can also be costly. Fiber-optical gas and photonic crystal gas sensors are the most often tested optical sensors. A fiber-optic sensor is created by attaching an optical fiber to the substrate and depositing sensitive materials. The optical fiber is housed in a V-shaped curve channeled on the quartz substrate with a desired radius of curvature [100]. The sensing film coated on the upper side of the structure using the required procedure based on the chosen sensing material for a specific application.

On the other hand, photonic crystal gas sensors are created utilizing advanced micro patterning and deposition techniques such as e-beam lithography and physical and CVD techniques [101]. The dimensions and shape of the patterns are carefully controlled [102]. However, as compared to other procedures, this technique can be costly. For detecting a gaseous analyte, the detection technique is based on the phenomena of optical absorption.

II.11.5. Electrochemical sensors

There are four main axes in electrochemical sensors:

- Amperometric sensors,
- Potentiometric sensors,
- Field Effect Transistor FETs,
- Conductometric sensors.

However, in the case of gas sensors, the first two types are rarely used. An electrochemical sensor uses an electrical variation to reflect the chemical reaction between the target species and the sensor's sensitive portion. These groups are frequently mentioned in the literature on aqueous media analyses [103]. The current arising from the oxidation or reduction of electro species active in a biological activity on the sensor surface can usually be measured using amperometry [104].

In an electrochemical cell, when no current flows, potentiometric sensors assess the accumulation of a charge potential around the working electrode relative to a reference electrode; they convert ionic activity into an electrochemical reaction [105]. Because the application of these approaches to detecting gaseous analytes is not optimal, we will not go into greater depth about how they work. The other two types of sensors, FET and conductometric sensors, will now be discussed. The FET is a semiconductor system of the transistor family. It uses an electric field to control the shape and conductivity of a channel in a semiconductor material. It consists of three electrodes, the gate, the drain, and the source. As for a bipolar transistor, a distinction is made between channel type N and channel type P FETs.

We are talking about a junction FET transistor (JFET). Establish a bias voltage sufficient at the level of the grid will make it possible to attract or repel the charge carriers in the channel. The charge carrier depletion zone is thus created to form a zone of conduction in the canal. The conductance between the drain and the source of the transistor is thus measured. In linear mode, the transistor acts as a resistor and switch between a non-conduction state or conduction. In saturated mode, the transistor acts as a current source and can be used as a voltage amplifier. FETs are generally used in applications where the signals in play are weak or high impedance. It is therefore relevant that this type of sensor is used for electrochemical analyzes. Although many investigations on these types of transistors for the detection of VOCs have been undertaken, the MOSFET category is widely regarded to be the most successful as a gas sensor. Conductometric sensors being used in this work, are presented in Chapter III.4.

II.12. Gas Sensors Based on Electrodeposited Conducting Polymers

Conducting polymers transformed into a new era of chemically flexible, mechanically versatile, solution-developed electronic materials [106]. Integrating aromatic repeat units to form well-conjugated backbones leads to extensive delocalization of π-electrons and efficient charge transfer. Numerous semiconductor gas/vapor sensors apply conductive polymers as part of the electrode material. Organic polymers are mostly considered electrically non-conductive. However, conductive polymers produce a channel for electrons to move through the polymer chain or jump from one chain to another [107]. Inherently, conducting polymers, polyaniline, polyacetylene, polypyrrole, poly (p-phenylene), polythiophene, poly (p-phenylenevinylene), chitosan-based bio polymer, and their derivatives possess the properties to be active layers of gas/vapor sensors. Polyaniline (PANI) is the most used [108]. Conductive polymer reacts with gaseous/vapor species as an electron acceptor or electron donor. In a situation where p-type conductive polymer donates the electron to the gaseous species, its whole conductivity multiplies reversibly; when the polymers act as an electron acceptor, its conductivity becomes less. Conductive polymer possesses a very high conductance of roughly 10^3 S/cm compared to indium tin oxide (ITO) [109]. They can also enable the development of a film by a spin coating that is much cheaper and convenient. Nevertheless, the side effect of conducting polymer is property change while producing the doped polymer composition. Recently there was shift of interest in using chitosan as a potential novel bio polymer for gas sensing technology [110].

II.13. Polymer functionalized transducers as versatile gas sensing materials

The amalgamation of two functional material components brings about an unintended development of a newly discovered function of different features of the individual starting materials [111]. Most laboratory analyses reported that molecular weight [112], dispersity [113], and end-groups of the synthesized conjugated polymer [114] could have reasonable effects on gas sensing devices. The alternating double bond-single bond chemical structure of conjugated polymers mostly depends on a cross-coupling reaction. As a result, synthesis is more commonly done by polycondensation reactions that proceed via the uncontrolled step-growth mechanism. Notwithstanding, to access the full potential of semiconducting polymers, the formation of synthetic methods that follow a controlled chain-growth mechanism is compulsory. An artificial technique that triggered precise control over molecular weight, dispersity, and end-groups will pave the way to optimize polymer properties for industrial applications in electronic sensing devices.

II.14. Polymer deposited on gold microelectrode

Gold nanoparticles (AuNPs) are applied widely owing to their interesting catalytic properties. The conducting polymers combined with AuNPs as nanostructured products exhibit unique electrical, optical, and catalytic properties. These novel synthesized nanocomposites detect gases like hydrogen, ammonia, nitrate, hydrogen peroxide, hydrogen sulfide, and acetone. Various technologies were employed in the preparation of these nanocomposites, to mention but few are chemical, electrochemical, thermal evaporation, hydrothermal, and spin-coating techniques. Recently, polymer film deposition into metal nanocomposites has been considered the best technique for polymer-nanocomposites synthesis [115]. Metal nanocomposites are produced on the surface or instead in bulk through the process of drop-casting or incorporation of pre-synthesized nanoparticles at the time of electrochemical deposition of conducting polymers. Electrochemical polymerization is interestingly achieved by applying one of the three techniques. These techniques comprise of the use of (a) a constant voltage (potentiostatic), (b) a variable current and voltage (potentiodynamic), and (c) a constant current (galvanostatic) to a solution of the polymer. The three electrode systems are needed to perform electro-polymerization by applying the earlier techniques. The calomel or AgCl (KCl) electrode are the reference electrode, platinum is the counter electrode, and gold is the working electrode. The conducting polymer is deposited onto the working electrode. An anion is also used for charge neutrality, such as an acid (HA) [115].

II.15. Electrochemical Deposition Protocols for Conducting Polymers

Working electrodes are prepared using either of the two techniques: cyclic voltammetry (CV) and chronoamperometry (CA). The characterization of the electrodes was mostly done using cyclic voltammetry, as viewed from different articles. Cyclic voltammetry (CV) is an electrochemical technique that evolves in an electrochemical cell. CV has been done by cycling the potential of a working electrode and analyzing the resulting current. In contrast, Chronoamperometry, an electrochemical method where the working electrode's potential is constant and the resulting current from faradaic processes occurring at the electrode (produced by the applied potential), is observed as a function of time. The functional exchange between current response and time is measured after applying a constant potential to the electrochemical system's working electrode. As discussed later, these techniques are repeatedly used in gas sensors preparation and characterization. From literature, a group of researchers used composites films based on poly (3, 4-ethylene dioxythiophene) in the presence of palladium

nanoparticles for the sensitive detection of hydrogen peroxide by employing the chronoamperometry technique as a mode of electrodeposition, the polymer deposition was done at a constant potential of 1 V. The deposition time was 60 -120 seconds [115]. In another development, a gas sensor based on polyaniline doped with [3, 3'-Co(1,2-C2B9H11)2]$^{-1}$ anion (PANI/COSANE) for the detection and quantification of acetone in human breath was prepared. Cyclic voltammetry technique was used under the following conditions: electrochemical polymerization was performed to prepare a sensitive layer of PANI/COSANE. Ten potential sweep cycles between 0.5 V and 2.0 V at a scan rate of 80 mV/s were applied. Electrochemical polymerization to prepare a sensitive layer of PANI/NITRATE onto the gold microelectrode was done by applying a potential sweep of 0 V and 0.95 V at a scan rate of 100m V/s [116].

Different techniques for depositing sensitive materials on the transducers are implemented (Table 7)

Table 7. Different deposition techniques of sensitive materials on transducers

Transducer	Sensitive membrane	Deposition Technique	VOC	LOD	Ref
IDEs	Ppy/silver nanocomposites	Nano pipette/spincoated	NH_3	0.25 ppm	[117]
IDEs	CuO/polyether	Solvated thermal	Ethanol, Methanol, Humidity	380 ppm	[118]
IDEs	PEDOT: PSS	Drop casting	Ethanol, Methanol, Acetone, Pentanol, THF	300 ppm	[119]
IDEs	PANI/CNT	Drop casting	NH_3, Ethanol,	250 ppm	[120]
IDEs	Poly(3-hexyl thiophene P3HT	Spin coating	NH_3	100 ppm	[121]
IDEs	P3HT:Au:ZnO NPs	Drop casting	NO_2	500 ppm	[122]
IDEs	PPy	Drop casting	NH_3	100 ppb	[123]
IDEs	PANI/COSANE	Electrochemical deposition	Acetone	8 ppm	[116]
IDEs	Poly(3,4-etylenedioxythophene	Electrochemical deposition	Hydrogen Peroxide	50 ppm	[124]
IDEs	PANI/CuBr nanocomposites	Electrochemical deposition	Hydrogen Disulphide	100 ppm	[125]
IDEs	PANI/Cu, PANI/Pd, PANI/TiO_2	Electrochemical deposition	VOCs	×	[126]

II.16. Chitosan-based sensitive layer

Due to its capacity to form films, chitosan is a biocompatible polymer commonly employed in creating gas sensors. This polymer has mostly been used in the literature as a biomolecule immobilization matrix [127]. It appears to be a viable material for developing room-temperature

gas sensors that respond to gas vapors [128]. The acid-base properties of the polymer allow it to be electrodeposited on the surface of a conducting electrode. Ammonia [129], alcohol vapors [130], and gaseous acetone [131] have all been described as examples of its usage in sensor design.

It's relevant to our research. The project aims to create a gas sensor capable of measuring VOC concentrations range in the hundreds of parts per billion for medical purposes

II.17. Chitosan as a sensitive membrane for gas sensing ability

When the chitosan film is exposed to ambient air, the oxygen atoms present in the medium are chemi-absorbed on its surface [132]. Once the film is subjected to a potential, the quantity of free electrons circulating randomly in the conduction band decreases. The absorbed oxygen species trap electrons and transfers from one chitosan particle to another [133]. The resistance of the sensor then increases and a decrease in the response of the sensor is generally observed [134]. This depends on the saturation of the oxygen species according to a certain equilibrium. This phenomenon depends on the saturation of the oxygen species according to a certain equilibrium.

Moreover, when the sensor is subjected to a specific flow of carrier gas enriched in VOC, this gas flow has a certain number of water molecules reflecting the gas' relative humidity. These water molecules will affect the film and change the chemical balance achieved. The molecules bonded to the chitosan particles' surface will react with the O- species, resulting in the degassing of O_2 and release of the trapped electrons.

Moreover, the presence of the water molecules also creates surface tension on the chitosan film. This tension promotes the movement of electrons by allowing them to escape oxygen species. These are again free in the conduction band, which increases the electrical conduction of the membrane. However, free electrons may not move quickly between available particles due to gaps between adjacent particles. The structure of the carbonic chain of chitosan improves the circulation of electrons [135]. The hydrogen of the amine groups binds to the oxygen of water molecules to form hydrogen bonds, as shown in the Figure 7.

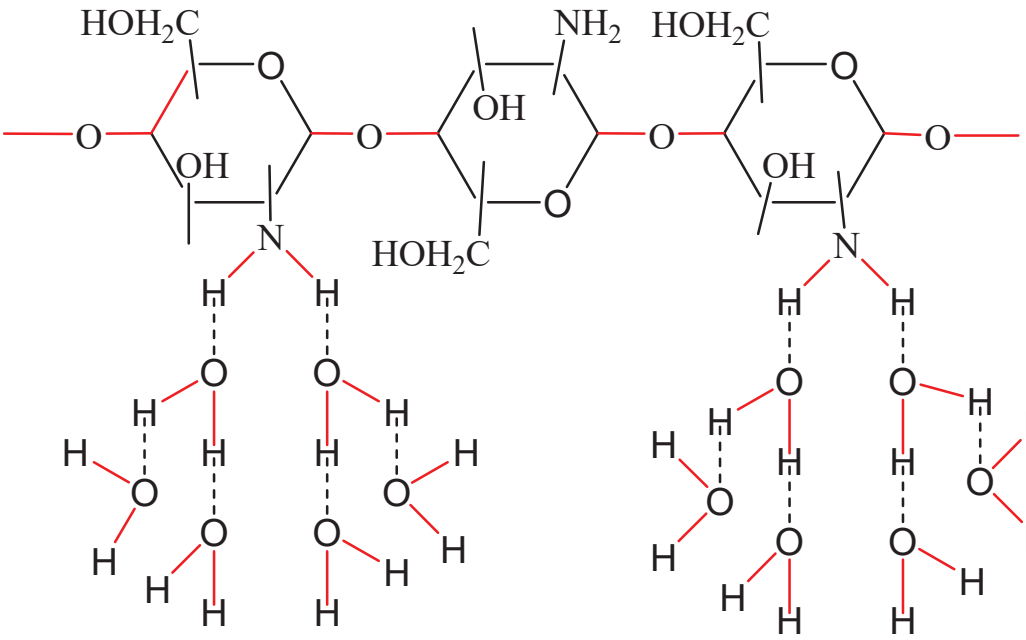

Figure 7. Chitosan reaction with water vapor

These hydrogen bridges act as electrical bridges to transfer electrons between particles. This theory, therefore, reveals that the conductivity of the sensitive layer is highly dependent on the water molecules present in the gas. In this sense, we can consider that its response will depend on the relative humidity of the gas. The sensors' response will be more significant with high relative humidity because of the many water molecules.

VOCs, however, do not have a factor in what we have presented so far. Chitosan is mainly sensitive to water molecules and not to VOCs. The presence of VOC in the carrier gas changes the membrane's conductivity by affecting the flow of electrons in the conduction band. Indeed, the acetone molecules have an inherent molecular vibration and affect the water molecules on the film's surface. The previously established surface tension is then broken, which causes the vaporization of the water molecules. The interaction between water molecules and oxygen species is thus reduced, which directly affects the increase in the film's conductivity caused by water molecules [127].

II.18. Membrane design

If it is in solution, chitosan goes from a soluble state in acid solution to a precipitated hydrogel state when the pH increases. Different groups conducted many studies based on this principle to deposit a sensitive layer of chitosan on the electrode's surface [134]. According to the same

direction, our membrane's production is mainly based on an electro-polymerization deposition technique presented in Figure 8.

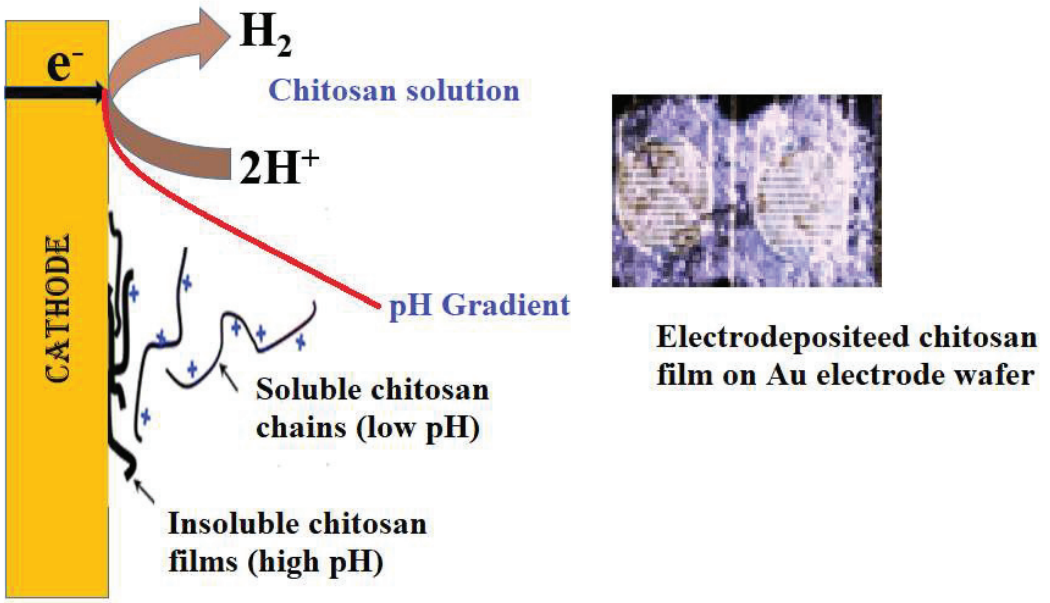

Figure 8. Chitosan deposition mechanism

It allows controlled electro-addressing of the polymer on a conductive electrode such as gold. When the reduction of H^+ ions of an acid solution of chitosan is carried out, a sudden increase of the pH on the electrode's surface is caused. This causes the precipitation of the polymer and the formation of a homogeneous membrane on the conductor's surface. Moreover, this technique makes it possible to incorporate nanoparticles into the polymeric membrane. When nanoparticles are suspended in the solution of chitosan, they are found "sucked" during the precipitation of the polymer and are present in the membrane, thus deposited. We, therefore, can consider enriching our chitosan membrane with some molecules sensitive to certain VOCs to increase the sensitivity of our sensor.

II.19. Metallo-Phthalocyanines-Polymer blend enhances gas-sensing ability

Metallo-phthalocyanines are organometallic compounds, which tend to have the capability to act as a chemically reactive and sensitive film as a factor of enormous physical properties impelled upon them through interaction with many volatile organic compounds (VOCs) [136]. They are primarily used as thin-film semiconducting gas sensors to detect various VOCs. The main properties of phthalocyanines in detection abilities for environmentally relevant volatile organic compounds are particularly their ionization potentials ability, which can as well be

varied by metal-ion insertion and besides by the attachment of other atoms or groups that trigger or diminish the ionization potential in preference of their position in the electronegativity scale [137]. Substituents' variation in the side chain and the ligand or μ-bridge in their polymers [138], which are a fundamental approach to get control of some of the physical limitations of most phthalocyanines, including the lousy processability and higher crystallinity for chemosensing, comprises combining these materials with polymers, such as polyvinyl alcohol (PVA), polystyrene (PS), polymethyl methacrylate (PMMA) [139], etc. Phthalocyanines are incorporated in the polymer by dissolution in a common solvent and deposited by a common solution processing. These techniques are solvent casting, spin coating, electrostatic layer-by-layer process, or in some cases, to see the possibility of electrochemical deposition [140]. Abdulameer and his coworkers, in 2017 in their work [141] reported that polymers-phthalocyanines blend materials demonstrated as less crystalline, higher conductivity, and more efficient gas sensing than the pure phthalocyanines. This ability paves the way for the careful fabrication and design of an optimized thin film having different high degrees of sensitivity, selectivity, and stability (3S). However, these films undergo high chemical and thermal stability concerning many environmental conditions. The membrane is easily made through the following coating techniques, sublimation, spraying, spin, and smearing coating or through electrochemical deposition.

Studies have classified the interactions between the metallo-phthalocyanine and VOCs into the irreversible chemical affinity, reversible (normal charge-transfer) chemical reaction, or in some time, bulk sorption [140]. We will focus more on the different VOC sensors concerning metallo-phthalocyanines blends with co-polymers discussed under the film structures and the electrical properties. The gas sensors in the discussion are primarily based on indium tin oxide electrodes, quartz crystal’s microbalance, and interdigitated electrode transducers. However, these techniques seem to be essential by controlling the deposition conditions in a well-articulated manner, which involves the concentration of the solution, the applied current, number of cycles, possibly scan rate at the successive number of cycles for cyclic voltammetry. Electrochemical deposition can yield a highly reproducible film/membrane in thickness and homogeneity, as seen in the work of Singh et al, where they used CuPc/ Ppy/CTAB as sensitive material on gold electrode transducers [137]. Previous research reveals that phthalocyanines of metals mixed with an insulating polymer, the product of the blend hybrid material, have the potential of being more resistive for conductometric measurements. Even though other transduction means can also be applied. This work will discuss the different copolymers incorporated with Metallo-phthalocyanines, transducers, deposition techniques, and the various volatile organic

compounds detected. Figure 9 below demonstrates how we carried out electrodeposition of chitosan biopolymer incorporated with NiPc on IDEs as the sensitive materials for VOCs conductometric detection, the result is presented in chapter 4.

Figure 9. Chitosan-Nickel-phthalocyanine composites formation for gas sensing ability

II.20 Metallo-Phthalocyanines-Polymer blend material Deposition Techniques

Metallo-phthalocyanines are considered to demonstrate excellent electrocatalytic activities through oxidation and reduction of numerous common chemical substances with sensing of toxic gases. An example of gases that have been detected is ammonia using carbon black-phthalocyanines composites resistors [142]. Nitrogen dioxide was sensed by copper phthalocyanines [143], hydrogen by phthalocyanines with palladium-coated SAW [144]. Additionally, ozone was detected using an immobilized metal complex and conducting polymer in the presence of surfactants for the electrode modification in methanol media. Again, copper phthalocyanines in the presence of surfactants through electrochemical polymerization of pyrrole were conducted, knowing well that CuPc is a molecular semiconducting substance [145], and widely utilized for gas sensing applications due to conjugated π systems present. It triggers the transferring or acceptance of electrons on the electrode surface.

In developing a susceptible and reproducible gas sensor, many techniques were reported for growing a thin film of co-polymer/metal phthalocyanines onto transducers with common identification (gold electrode). This deposition technique involves vacuum deposition, casting

in matrices, spin coating, self-assembling, electro-polymerization, and Langmuir-Blodgett techniques [146]. Although these techniques were mentioned above, it was reported that the electrochemical method has merits over the remaining procedures in terms of deposition simplicity, reproducibility, and the ability for an in-situ production of a thin and stable membrane of homogeneity and controlled thickness [147]. Furthermore, interdigitated electrode transducers are primary capacitive chemical sensors [22]. Studies have recently shown that a polymer incorporated with phthalocyanine materials film was used as the chemical interface for volatile organic vapors in the air. The capacitance differentials (ΔC) as determined using interdigitated capacitors might come up because of the changes from the relative dielectric coefficients ἐi in the gaseous gas phase (I=1), in the sensitive layer (I=2) and from the changes of the adequate thickness (Δd) of the exposed membrane. Changes in the substrate-related dielectric co-efficient ἐi might be neglected. Generally, the dielectric coefficient of the substrate remains constant. Polymers-phthalocyanines blend materials demonstrated low crystallinity, higher conductivity, and more efficient gas sensing. Much attention is focused on incorporating polymer-phthalocyanines in achieving a low-cost, sensitive, selective, and stable micro gas sensor for disease diagnosis through exhaled breath analysis. Zhou and his co-worker in 1993 reported sensitivity properties of coatings with monomeric, polymeric, and polymer-bound phthalocyanines for the development of a micro sensor for the detection of NO_2 as demonstrated elsewhere [148].

In his research, Gaudillat and his team of scientists used S-CoPc, CuTsPc, and PANI for the gaseous detection of ammonia; ITO electrode was employed as the working transducer [152]. The deposition of the PANI-phthalocyanines sensitive membrane was carried out through a layer-by-layer hybrid film casting technique. The investigation reported the limit of detection for ammonia as 0.7 ppm. This article provides previous works to develop a sensitive gas microsensor by incorporating co-polymers-metallo-phthalocyanine as a sensitive layer. The deposition was done on various transducers, and numerous deposition techniques were applied for different gases. The limit of detection of the research was also reported, as seen in Table 8.

Table 8. Various techniques adopted for metallo-phthalocyanines incorporated polymer deposition for VOCs detection on standard transducer IDEs

S/N	Transducers	Sensitive layer	Deposition technic	Target analyte	LOD	Reference
1	ITO Electrode	S-CoPc, CuTsPc and PVP, PEG, PAA-AM, and PANI	Hybrid films solvent casting (layer by layer)	Ammonia	0,7 ppm	[149]
2	QCM Tranducers	Axially substituted TiOPcs from the reaction of 2,2,3,3-tetraflouropropyloxy phthalonitriles with Ti(IV) n-butane	Coating Deposition from solution	VOCs	5 ppm	[150]
3	QCM Tranducers	NiPc based vic-dioximes functionalized with hexafluoroisopropanol	Coating Deposition from solution	VOCs	100 ppm	[151]
4	IDEs	CNTs@PANI/TcPcCo	Coating Deposition from solution	Ammonia	5 ppm	[152]
5	IDEs	Copper t-4-(2,4-di-t-amyl-phenylsulphonyl)phthalocyanines	Coating Deposition from solution	NO_2	1 ppm	[153]
6	QCM Tranducers	R Flouroalkyloxy Substituted NiTsPc and ZnTsPc	Coating Deposition from solution	VOCs	2 ppm	[154]
7	QCM and SAW Transducers	Fluorinated and non-fluorinated alkyl and aryloxy substituents of NiTsPc and ZnTsPc	Spray coating techniques	DMMP	0,6 ppm	[155]
8	ITO Electrode	CuTsPc/Alq_3 thin film with Toluene surface treatment	Spin Coating	NO_2	NO	[141]
9	ID Gold Electrode	PANI/NiTsPc	Electrochemical deposition	Ammonia	5 ppm	[156]
10	Glass substrate fitted with IGE	Triazine of Co(II) and Zn (II) Pc	Spin coating	CO_2	500 ppm	[157]
11	Interdigital tranducer	Polysiloxane/CuPc	Drop coating deposition	Methanol	5 ppm	[158]

II.21. References

[1] V. Dal Bello-Haas, "Core competencies for health care professionals: what medicine, nursing, occupational and physiotherapy share.," *Journal of Physical Therapy Education*, vol. 21, no. 1, p. 76, Spring 2007, Accessed: Apr. 17, 2022. [Online]. Available: https://journals.lww.com/jopte/Citation/2007/01000/Core_competencies_for_health_care_professionals_.12.aspx

[2] J. Fitzgerald and H. Fenniri, "Cutting Edge Methods for Non-Invasive Disease Diagnosis Using E-Tongue and E-Nose Devices," *Biosensors (Basel)*, vol. 7, no. 4, p. E59, Dec. 2017, doi: 10.3390/bios7040059.

[3] W. Miekisch, J. K. Schubert, and G. F. E. Noeldge-Schomburg, "Diagnostic potential of breath analysis—focus on volatile organic compounds," *Clinica Chimica Acta*, vol. 347, no. 1, pp. 25–39, Sep. 2004, doi: 10.1016/j.cccn.2004.04.023.

[4] F. Di Francesco, R. Fuoco, M. G. Trivella, and A. Ceccarini, "Breath analysis: trends in techniques and clinical applications," *Microchemical Journal*, vol. 79, no. 1, pp. 405–410, Jan. 2005, doi: 10.1016/j.microc.2004.10.008.

[5] B. Buszewski, M. Kesy, T. Ligor, and A. Amann, "Human exhaled air analytics: biomarkers of diseases," *Biomed Chromatogr*, vol. 21, no. 6, pp. 553–566, Jun. 2007, doi: 10.1002/bmc.835.

[6] G. D. Miller, R. M. Van Wagoner, B. J. Bruno, J. D. Husk, M. N. Fedoruk, and D. Eichner, "Investigating oral fluid and exhaled breath as alternative matrices for anti-doping testing: Analysis of 521 matched samples," *J Pharm Biomed Anal*, vol. 176, p. 112810, Nov. 2019, doi: 10.1016/j.jpba.2019.112810.

[7] I. Horváth, J. Hunt, and P. J. Barnes, "Exhaled breath condensate: methodological recommendations and unresolved questions," *European Respiratory Journal*, vol. 26, no. 3, pp. 523–548, Sep. 2005, doi: 10.1183/09031936.05.00029705.

[8] P. Sukul, J. K. Schubert, K. Zanaty, P. Tretz, A. Sinha, S. Kamysek, W. Meikisch., "Exhaled breath compositions under varying respiratory rhythms reflects ventilatory variations: translating breathomics towards respiratory medicine," *Sci Rep*, vol. 10, no. 1, Art. no. 1, Aug. 2020, doi: 10.1038/s41598-020-70993-0.

[9] K. Schmidt and I. Podmore, "Current Challenges in Volatile Organic Compounds Analysis as Potential Biomarkers of Cancer," *J Biomark*, vol. 2015, p. 981458, 2015, doi: 10.1155/2015/981458.

[10] O. Lawal, W. M. Ahmed, T. M. E. Nijsen, R. Goodacre, and S. J. Fowler, "Exhaled breath analysis: a review of 'breath-taking' methods for off-line analysis," *Metabolomics*, vol. 13, no. 10, p. 110, 2017, doi: 10.1007/s11306-017-1241-8.

[11] E. A. Reber, "Gas Chromatography-Mass Spectrometry (GC-MS): Applications in Archaeology," in *Encyclopedia of Global Archaeology*, C. Smith, Ed. Cham: Springer International Publishing, 2018, pp. 1–17. doi: 10.1007/978-3-319-51726-1_340-2.

[12] T. L. Mathew, P. Pownraj, S. Abdulla, and B. Pullithadathil, "Technologies for Clinical Diagnosis Using Expired Human Breath Analysis," *Diagnostics (Basel)*, vol. 5, no. 1, pp. 27–60, Feb. 2015, doi: 10.3390/diagnostics5010027.

[13] X. Liu, S. Cheng, H. Liu, S. Hu, D. Zhang, and H. Ning, "A Survey on Gas Sensing Technology," *Sensors*, vol. 12, no. 7, Art. no. 7, Jul. 2012, doi: 10.3390/s120709635.

[14] J. Grlica, T. Martinović, and H. Džapo, "Capacitive sensor for respiration monitoring," in *2015 IEEE Sensors Applications Symposium (SAS)*, Apr. 2015, pp. 1–6. doi: 10.1109/SAS.2015.7133567.

[15] N. Nasiri and C. Clarke, "Nanostructured Gas Sensors for Medical and Health Applications: Low to High Dimensional Materials," *Biosensors (Basel)*, vol. 9, no. 1, p. 43, Mar. 2019, doi: 10.3390/bios9010043.

[16] J. Wang, Q. Zhou, S. Peng, L. Xu, and W. Zeng, "Volatile Organic Compounds Gas Sensors Based on Molybdenum Oxides: A Mini Review," *Frontiers in Chemistry*, vol. 8, 2020, Accessed: Apr. 17, 2022. [Online]. Available: https://www.frontiersin.org/article/10.3389/fchem.2020.00339

[17] W. Guan, N. Tang, K. He, X. Hu, M. Li, and K. Li, "Gas-Sensing Performances of Metal Oxide Nanostructures for Detecting Dissolved Gases: A Mini Review," *Frontiers in Chemistry*, vol. 8, 2020, Accessed: Apr. 17, 2022. [Online]. Available: https://www.frontiersin.org/article/10.3389/fchem.2020.00076

[18] Y. Huang, P. Kr. Das, and V. R. Bhethanabotla, "Surface acoustic waves in biosensing applications," *Sensors and Actuators Reports*, vol. 3, p. 100041, Nov. 2021, doi: 10.1016/j.snr.2021.100041.

[19] R. Blue, J. G. Brown, L. Li, R. Bauer, and D. Uttamchandani, "MEMS Gas Flow Sensor Based on Thermally Induced Cantilever Resonance Frequency Shift," *IEEE Sensors Journal*, vol. 20, no. 8, pp. 4139–4146, Apr. 2020, doi: 10.1109/JSEN.2020.2964323.

[20] Z. Branković and Y. Rostovtsev, "A resonant single frequency molecular detector with high sensitivity and selectivity for gas mixtures," *Sci Rep*, vol. 10, no. 1, Art. no. 1, Jan. 2020, doi: 10.1038/s41598-020-58473-x.

[21] D. Barauskas, D. Pelenis, G. Vanagas, D. Viržonis, and J. Baltrušaitis, "Methylated Poly(ethylene)imine Modified Capacitive Micromachined Ultrasonic Transducer for Measurements of CO2 and SO2 in Their Mixtures," *Sensors*, vol. 19, no. 14, Art. no. 14, Jan. 2019, doi: 10.3390/s19143236.

[22] S. P. Lee, "Electrodes for Semiconductor Gas Sensors," *Sensors (Basel)*, vol. 17, no. 4, Mar. 2017, doi: 10.3390/s17040683.

[23] K. J. Dunst, K. Cysewska, P. Kalinowski, and P. Jasiński, "Polypyrrole based gas sensor for ammonia detection," *IOP Conf. Ser.: Mater. Sci. Eng.*, vol. 104, p. 012028, Jan. 2016, doi: 10.1088/1757-899X/104/1/012028.

[24] A. Ashraf, U. Farooq, B. A. Farooqi, and K. Ayub, "Electronic structure of polythiophene gas sensors for chlorinated analytes," *J Mol Model*, vol. 26, no. 3, p. 44, Feb. 2020, doi: 10.1007/s00894-020-4287-x.

[25] A. Yadav, A. Agarwal, P. B. Agarwal, and P. Saini, "Ammonia Sensing by PANI-DBSA Based Gas Sensor Exploiting Kelvin Probe Technique," *Journal of Nanoparticles*, vol. 2015, p. e842536, Nov. 2015, doi: 10.1155/2015/842536.

[26] R. Rodrigues,S. I. C. S. Palma, G. V. Correia, L. Padrao, J. Pais, E. Ramou, P. C. Silva, A. C. A. Roque., "Sustainable plant polyesters as substrates for optical gas sensors," *Materials Today Bio*, vol. 8, p. 100083, Sep. 2020, doi: 10.1016/j.mtbio.2020.100083.

[27] S. Mallakpour, E. Azadi, and C. M. Hussain, "Chitosan/carbon nanotube hybrids: recent progress and achievements for industrial applications," *New J. Chem.*, vol. 45, no. 8, pp. 3756–3777, Mar. 2021, doi: 10.1039/D0NJ06035F.

[28] M. N. Gueye, A. Carella, J. Faure-Vincent, R. Demadrille, and J.-P. Simonato, "Progress in understanding structure and transport properties of PEDOT-based materials: A critical review," *Progress in Materials Science*, vol. 108, p. 100616, Feb. 2020, doi: 10.1016/j.pmatsci.2019.100616.

[29] M. I. J. Ibrahim, S. M. Sapuan, E. S. Zainudin, and M. Y. M. Zuhri, "Physical, thermal, morphological, and tensile properties of cornstarch-based films as affected by different plasticizers," *International Journal of Food Properties*, vol. 22, no. 1, pp. 925–941, Jan. 2019, doi: 10.1080/10942912.2019.1618324.

[30] S. Radhakrishnan and S. D. Deshpande, "Conducting Polymers Functionalized with Phthalocyanine as Nitrogen Dioxide Sensors," *Sensors*, vol. 2, no. 5, Art. no. 5, May 2002, doi: 10.3390/s20500185.

[31] E. H. Kwon, H. An, M. B. Park, M. Kim, and Y. D. Park, "Conjugated polymer–zeolite hybrids for robust gas sensors: Effect of zeolite surface area on NO2 sensing ability," *Chemical Engineering Journal*, vol. 420, p. 129588, Sep. 2021, doi: 10.1016/j.cej.2021.129588.

[32] J. Sethi, M. Van Bulck, A. Suhail, M. Safarzadeh, A. Perez-Castillo, and G. Pan, "A label-free biosensor based on graphene and reduced graphene oxide dual-layer for electrochemical determination of beta-amyloid biomarkers," *Microchim Acta*, vol. 187, no. 5, p. 288, Apr. 2020, doi: 10.1007/s00604-020-04267-x.

[33] C. L. Chaffer and R. A. Weinberg, "A Perspective on Cancer Cell Metastasis," *Science*, vol. 331, no. 6024, pp. 1559–1564, Mar. 2011, doi: 10.1126/science.1203543.

[34] H. Sung, J. Ferlay, R. L. Siegel, M. Leversanne, I. Soerjomataram, A. Jemal, F. Bray., "Global Cancer Statistics 2020: GLOBOCAN Estimates of Incidence and Mortality Worldwide for 36 Cancers in 185 Countries," *CA: A Cancer Journal for Clinicians*, vol. 71, no. 3, pp. 209–249, 2021, doi: 10.3322/caac.21660.

[35] G. P. Currie, A.-M. Kennedy, and A. R. Denison, "Tools used in the diagnosis and staging of lung cancer: what's old and what's new?," *QJM: An International Journal of Medicine*, vol. 102, no. 7, pp. 443–448, Jul. 2009, doi: 10.1093/qjmed/hcp038.

[36] T. O. Tobore, "On the need for the development of a cancer early detection, diagnostic, prognosis, and treatment response system," *Future Sci OA*, vol. 6, no. 2, p. FSO439, doi: 10.2144/fsoa-2019-0028.

[37] Z. S. Lima, M. R. Ebadi, G. Amjad, and L. Younesi, "Application of Imaging Technologies in Breast Cancer Detection: A Review Article," *Open Access Maced J Med Sci*, vol. 7, no. 5, pp. 838–848, Mar. 2019, doi: 10.3889/oamjms.2019.171.

[38] L. Horn, C. M. Lovly, and D. H. Johnson, "Neoplasms of the Lung," in *Harrison's Principles of Internal Medicine*, 19th ed., D. Kasper, A. Fauci, S. Hauser, D. Longo, J. L. Jameson, and J. Loscalzo, Eds. New York, NY: McGraw-Hill Education, 2014. Accessed: Dec. 08, 2021. [Online]. Available: accessmedicine.mhmedical.com/content.aspx?aid=1137770458

[39] H. J. Park, S. H. Lee, and Y. S. Chang, "Recent advances in diagnostic technologies in lung cancer," *Korean J Intern Med*, vol. 35, no. 2, pp. 257–268, Mar. 2020, doi: 10.3904/kjim.2020.030.

[40] P. Novellis, S. R. Cominesi, F. Rossetti, M. Mondoni, V. Gregorc, and G. Veronesi, "Lung cancer screening: who pays? Who receives? The European perspectives," *Transl Lung Cancer Res*, vol. 10, no. 5, pp. 2395–2406, May 2021, doi: 10.21037/tlcr-20-677.

[41] K. Begg and M. Tavassoli, "Review: biomarkers towards personalised therapy in cancer," vol. 4, no. 2, pp. 26–30, Jun. 2017, Accessed: Dec. 08, 2021. [Online]. Available: https://www.drugtargetreview.com/article/23631/biomarkers-personalised-therapy-cancer/

[42] Y. Zhang, M. Li, X. Gao, Y. Chen, and T. Liu, "Nanotechnology in cancer diagnosis: progress, challenges and opportunities," *J Hematol Oncol*, vol. 12, no. 1, p. 137, Dec. 2019, doi: 10.1186/s13045-019-0833-3.

[43] L. Díaz de León-Martínez *et al.*, "Identification of profiles of volatile organic compounds in exhaled breath by means of an electronic nose as a proposal for a screening method for breast cancer: a case-control study," *J Breath Res*, vol. 14, no. 4, p. 046009, Sep. 2020, doi: 10.1088/1752-7163/aba83f.

[44] W. Filipiak *et al.*, "Dependence of exhaled breath composition on exogenous factors, smoking habits and exposure to air pollutants," *J Breath Res*, vol. 6, no. 3, p. 10.1088/1752-7155/6/3/036008, Sep. 2012, doi: 10.1088/1752-7155/6/3/036008.

[45] M. Hakim *et al.*, "Volatile organic compounds of lung cancer and possible biochemical pathways.," *Chemical reviews*, 2012, doi: 10.1021/cr300174a.

[46] C. A. Acevedo, E. Y. Sanchez, J. G. Reyes, and M. E. Young, "Volatile profiles of human skin cell cultures in different degrees of senescence," *J Chromatogr B Analyt Technol Biomed Life Sci*, vol. 878, no. 3–4, pp. 449–455, Feb. 2010, doi: 10.1016/j.jchromb.2009.12.033.

[47] X. Chen, F.Xu, Y. Wang,Y. Pan, D. Lu, P. Wang, K. Yang, E. Chen, W. Zhang., "A study of the volatile organic compounds exhaled by lung cancer cells in vitro for breath diagnosis," *Cancer*, vol. 110, no. 4, pp. 835–844, Aug. 2007, doi: 10.1002/cncr.22844.

[48] L. Burd, J. Blair, and K. Dropps, "Prenatal alcohol exposure, blood alcohol concentrations and alcohol elimination rates for the mother, fetus and newborn," *J Perinatol*, vol. 32, no. 9, pp. 652–659, Sep. 2012, doi: 10.1038/jp.2012.57.

[49] M. Koureas, P. Kirgou, G. Amoutzias, C. Hadjichristodoulou, K. Gourgoulianis, and A. Tsakalof, "Target Analysis of Volatile Organic Compounds in Exhaled Breath for Lung Cancer Discrimination from Other Pulmonary Diseases and Healthy Persons," *Metabolites*, vol. 10, no. 8, p. 317, Aug. 2020, doi: 10.3390/metabo10080317.

[50] A. Bajtarevic, C. Ager, M. Pienz, M. Klieber, K. Schwarz, W. Miekisch, J. Schubert, A. Amann., "Noninvasive detection of lung cancer by analysis of exhaled breath," *BMC Cancer*, vol. 9, no. 1, p. 348, Sep. 2009, doi: 10.1186/1471-2407-9-348.

[51] Z. Jia, H. Zhang, C. N. Ong, A. Patra, Y. Lu, C. T. Lim, T. Venkatesin., "Detection of Lung Cancer: Concomitant Volatile Organic Compounds and Metabolomic Profiling of Six Cancer Cell Lines of Different Histological Origins," *ACS Omega*, vol. 3, no. 5, pp. 5131–5140, May 2018, doi: 10.1021/acsomega.7b02035.

[52] M. Phillips, R. N. Cataneo, A. R. C. Cummin, A. J. Gagliardi, K. Gleenson, J. Greenberg, R.A. Maxfield, W. N. Rom., "Detection of lung cancer with volatile markers in the breath," *Chest*, vol. 123, no. 6, pp. 2115–2123, Jun. 2003, doi: 10.1378/chest.123.6.2115.

[53] D. Poli, P. Carbognani, M. Corradi, M. Galdoni, O. Acampa, B. Balbi, L. Bianchi, M. Rusca, A. Mutti., "Exhaled volatile organic compounds in patients with non-small cell lung cancer: cross sectional and nested short-term follow-up study," *Respiratory Research*, vol. 6, no. 1, p. 71, Jul. 2005, doi: 10.1186/1465-9921-6-71.

[54] R. F. Machado *et al.*, "Detection of lung cancer by sensor array analyses of exhaled breath," *Am J Respir Crit Care Med*, vol. 171, no. 11, pp. 1286–1291, Jun. 2005, doi: 10.1164/rccm.200409-1184OC.

[55] J. S. Stenehjem, T. E. Robsahm, M. Bråtveit, S. O. Samuelsen, J. Kirkeleit, and T. K. Grimsrud, "Aromatic hydrocarbons and risk of skin cancer by anatomical site in 25 000 male offshore petroleum workers," *Am J Ind Med*, vol. 60, no. 8, pp. 679–688, Aug. 2017, doi: 10.1002/ajim.22741.

[56] Z. Li, Y. Li, L. Zhan, L. Meng, X. Huang, T. Wang, Y. Li, Z. Nie., "Point-of-Care Test Paper for Exhaled Breath Aldehyde Analysis via Mass Spectrometry," *Anal. Chem.*, vol. 93, no. 26, pp. 9158–9165, Jul. 2021, doi: 10.1021/acs.analchem.1c01011.

[57] S. Janfaza, B. Khorsand, M. Nikkhah, and J. Zahiri, "Digging deeper into volatile organic compounds associated with cancer," *Biol Methods Protoc*, vol. 4, no. 1, p. bpz014, Nov. 2019, doi: 10.1093/biomethods/bpz014.

[58] X. Zhang, X. Ren, Y. Zhong, K. Chingin, and H. Chen, "Rapid and sensitive detection of acetone in exhaled breath through the ambient reaction with water radical cations," *Analyst*, vol. 146, no. 16, pp. 5037–5044, Aug. 2021, doi: 10.1039/D1AN00402F.

[59] P. R. Galassetti *et al.*, "Breath ethanol and acetone as indicators of serum glucose levels: an initial report," *Diabetes Technol Ther*, vol. 7, no. 1, pp. 115–123, Feb. 2005, doi: 10.1089/dia.2005.7.115.

[60] S. Das and M. Pal, "Review—Non-Invasive Monitoring of Human Health by Exhaled Breath Analysis: A Comprehensive Review," *J. Electrochem. Soc.*, vol. 167, no. 3, p. 037562, Feb. 2020, doi: 10.1149/1945-7111/ab67a6.

[61] H. P. Chan, C. Lewis, and P. S. Thomas, "Oxidative Stress and Exhaled Breath Analysis: A Promising Tool for Detection of Lung Cancer," *Cancers*, vol. 2, no. 1, Art. no. 1, Mar. 2010, doi: 10.3390/cancers2010032.

[62] J. E. Belizário, J. Faintuch, and M. G. Malpartida, "Breath Biopsy and Discovery of Exclusive Volatile Organic Compounds for Diagnosis of Infectious Diseases," *Frontiers in Cellular and Infection Microbiology*, vol. 10, p. 783, 2021, doi: 10.3389/fcimb.2020.564194.

[63] A. Di Gilio, C. Annamaria, L. Angela, P. Jolanda, F. Laura, M. Teresa, V. Niccolo, B. Roberto, G. Domenico, G. De Gianluigi, T. Sabina., "Breath Analysis for Early Detection of Malignant Pleural Mesothelioma: Volatile Organic Compounds (VOCs) Determination and Possible Biochemical Pathways," *Cancers*, vol. 12, no. 5, Art. no. 5, May 2020, doi: 10.3390/cancers12051262.

[64] A. Čipak Gašparović, M. Lidyia, D. Nadia, S. Stefanie, P. Iskra, V. Josip, S. Sanda, S. Christoph, B. Marija., "Chronic Oxidative Stress Promotes Molecular Changes Associated with Epithelial Mesenchymal Transition, NRF2, and Breast Cancer Stem Cell Phenotype," *Antioxidants (Basel)*, vol. 8, no. 12, p. E633, Dec. 2019, doi: 10.3390/antiox8120633.

[65] M. Phillips, R. N. Cataneo, C. Saunders, P. Hope, P. Schmitt, and J. Wai, "Volatile biomarkers in the breath of women with breast cancer," *J. Breath Res.*, vol. 4, no. 2, p. 026003, Mar. 2010, doi: 10.1088/1752-7155/4/2/026003.

[66] D. C. Deacon, E. A. Smith, and R. L. Judson-Torres, "Molecular Biomarkers for Melanoma Screening, Diagnosis and Prognosis: Current State and Future Prospects," *Frontiers in Medicine*, vol. 8, p. 440, 2021, doi: 10.3389/fmed.2021.642380.

[67] M. R. Van Scott, J. Chandler, S. Olmstead, J. M. Brown, and M. Mannie, "Airway Anatomy, Physiology, and Inflammation," in *The Toxicant Induction of Irritant Asthma, Rhinitis, and Related Conditions*, W. J. Meggs, Ed. Boston, MA: Springer US, 2013, pp. 19–61. doi: 10.1007/978-1-4614-9044-9_2.

[68] S. Das, S. Pal, and M. Mitra, "Significance of Exhaled Breath Test in Clinical Diagnosis: A Special Focus on the Detection of Diabetes Mellitus," *J Med Biol Eng*, vol. 36, no. 5, pp. 605–624, 2016, doi: 10.1007/s40846-016-0164-6.

[69] M. Karla Lombello Coelho, D. Nunes da Silva, and A. César Pereira, "Development of Electrochemical Sensor Based on Carbonaceal and Metal Phthalocyanines Materials for Determination of Ethinyl Estradiol," *Chemosensors*, vol. 7, no. 3, Art. no. 3, Sep. 2019, doi: 10.3390/chemosensors7030032.

[70] M. Rondanelli, P. Fedrica, I. Vittoria, F. Milena Anna, P. Gabriella, I. Giancarlo, N. Mara, A. A. Tariq, P.Simone, C. Clementina., "Volatile Organic Compounds as Biomarkers of Gastrointestinal Diseases and Nutritional Status," *J Anal Methods Chem*, vol. 2019, Sep. 2019, doi: 10.1155/2019/7247802.

[71] P. Finamore C. Pedone, D. Lelli, L. Costanzo, B. I. Rossi, A. De Vincentis, S. Grasso, P. F. Romana, G. Pennazza, M. Santonico, A. R Incalzi., "Analysis of volatile organic compounds: an innovative approach to heart failure characterization in older patients," *J Breath Res*, vol. 12, no. 2, p. 026007, 06 2018, doi: 10.1088/1752-7163/aa8cd4.

[72] K. Schmidt and I. Podmore, "Current Challenges in Volatile Organic Compounds Analysis as Potential Biomarkers of Cancer," *Journal of Biomarkers*, vol. 2015, p. e981458, Mar. 2015, doi: 10.1155/2015/981458.

[73] J. K. Wickliffe, T. H. Stock, J. L. Howard, E. Fraham, B. R. Simon-Friedt, K. Montgomery, M.J. Wilson, M. Y Lichveld, E. Harville., "Increased long-term health risks attributable to select volatile organic compounds in residential indoor air in southeast Louisiana," *Sci Rep*, vol. 10, no. 1, p. 21649, Dec. 2020, doi: 10.1038/s41598-020-78756-7.

[74] P. Pignatti, D. Visca, S. Ioukides, A. Martson, J. C Alffenaar, G. B Migliori,A.Spanevello., "A snapshot of exhaled nitric oxide and asthma characteristics: experience from high to low income countries," *Pulmonology*, Dec. 2020, doi: 10.1016/j.pulmoe.2020.10.016.

[75] B. S. Yadav, G. Bade, R. Guleria, and A. Talwar, "Exhaled Breath Temperature and Systemic Biomarkers for Assessment of Airway Inflammation in Asthmatics," *J Assoc Physicians India*, vol. 69, no. 7, pp. 11–12, Jul. 2021.

[76] P. Montuschi, "Pharmacotherapy of Patients with Mild Persistent Asthma: Strategies and Unresolved Issues," *Front Pharmacol*, vol. 2, p. 35, Jul. 2011, doi: 10.3389/fphar.2011.00035.

[77] M. Sharifi-Rad, N. V. Anil Kumar, P. Zucca, E. M. Varoni, L. Dini, E.Panzarini,J. Rajkovic, P. V Tsouh Farou, E. Azzini, I.Peluso., "Lifestyle, Oxidative Stress, and Antioxidants: Back and Forth in the Pathophysiology of Chronic Diseases," *Frontiers in Physiology*, vol. 11, p. 694, 2020, doi: 10.3389/fphys.2020.00694.

[78] N. Drabińska, C. Flynn, N.Ratcliffe, I. Bollumo, A. Myridakis, O. Gould, M.Fois., "A literature survey of all volatiles from healthy human breath and bodily fluids: the human volatilome," *J. Breath Res.*, vol. 15, no. 3, p. 034001, Apr. 2021, doi: 10.1088/1752-7163/abf1d0.

[79] D.-K. Lee, E. Na, S. Park, J. H. Park, J. Lim, and S. W. Kwon, "In Vitro Tracking of Intracellular Metabolism-Derived Cancer Volatiles via Isotope Labeling," *ACS Cent. Sci.*, vol. 4, no. 8, pp. 1037–1044, Aug. 2018, doi: 10.1021/acscentsci.8b00296.

[80] R. Sudi, T. R, V. Biligere, T. S. P, and T. M, "Usage of Volatile Organic Compounds for Detection of Diabetes Mellitus in Exhaled Breath," *International Journal of Engineering Research & Technology*, vol. 9, no. 12, Jul. 2021, Accessed: Dec. 08, 2021. [Online]. Available: https://www.ijert.org/research/usage-of-volatile-organic-compounds-for-detection-of-diabetes-mellitus-in-exhaled-breath-IJERTCONV9IS12067.pdf, https://www.ijert.org/usage-of-volatile-organic-compounds-for-detection-of-diabetes-mellitus-in-exhaled-breath

[81] V. Saasa, T. Malwela, M. Beukes, M. Mokgotho, C.-P. Liu, and B. Mwakikunga, "Sensing Technologies for Detection of Acetone in Human Breath for Diabetes Diagnosis and Monitoring," *Diagnostics (Basel)*, vol. 8, no. 1, Jan. 2018, doi: 10.3390/diagnostics8010012.

[82] C. S. Probert, I. Ahmed, T. Khalid, E. Johnson, S. Smith, and N. Ratcliffe, "Volatile Organic Compounds as Diagnostic Biomarkers in Gastrointestinal and Liver Diseases," p. 7.

[83] S. M. Gordon, J. P. Szidon, B. K. Krotoszynski, R. D. Gibbons, and H. J. O'Neill, "Volatile organic compounds in exhaled air from patients with lung cancer," *Clin Chem*, vol. 31, no. 8, pp. 1278–1282, Aug. 1985.

[84] E. Gashimova, A. Temerdasher, V. Porkhanov, I. Polyakov, D. Perunov, A. Azaryan, E. Dmitrieva., "Investigation of different approaches for exhaled breath and tumor tissue analyses to identify lung cancer biomarkers," *Heliyon*, vol. 6, no. 6, p. e04224, Jun. 2020, doi: 10.1016/j.heliyon.2020.e04224.

[85] A. E. Omer, G. Shaker, S. Safari-Naeini, H. Kokabi, G. Alquie, F.Dashours, R. M. Shubair., "Low-cost portable microwave sensor for non-invasive monitoring of blood glucose level: novel design utilizing a four-cell CSRR hexagonal configuration," *Sci Rep*, vol. 10, no. 1, p. 15200, Sep. 2020, doi: 10.1038/s41598-020-72114-3.

[86] Y. Puentes-Osorio, P. Amariles, M. Á. Calleja, V. Merino, J. C. Díaz-Coronado, and D. Taborda, "Potential clinical biomarkers in rheumatoid arthritis with an omic approach," *Autoimmunity Highlights*, vol. 12, no. 1, p. 9, May 2021, doi: 10.1186/s13317-021-00152-6.

[87] K. D. Davis, N. Aghaepour, A.H.Ahn, M.S.Angst, D. Borsook, T. D. Wager, A. D. Wasan,M.A. Pelleymounter., "Discovery and validation of biomarkers to aid the development of safe and effective pain therapeutics: challenges and opportunities," *Nat Rev Neurol*, vol. 16, no. 7, pp. 381–400, Jul. 2020, doi: 10.1038/s41582-020-0362-2.

[88] Z. Li, J. Shu, B. Yang, Z. Zhang, J. Huang, and Y. Chen, "Emerging non-invasive detection methodologies for lung cancer (Review)," *Oncology Letters*, vol. 19, no. 5, pp. 3389–3399, May 2020, doi: 10.3892/ol.2020.11460.

[89] S. Kisely, E. Crowe, and D. Lawrence, "Cancer-Related Mortality in People With Mental Illness," *JAMA Psychiatry*, vol. 70, no. 2, pp. 209–217, Feb. 2013, doi: 10.1001/jamapsychiatry.2013.278.

[90] I. Azzouz, M. S. Khan, A. C. Bishop, and K. Bachari, *Recent Advances in Targeting Clinical Volatile Organic Compounds (VOC)*. IntechOpen, 2021. doi: 10.5772/intechopen.96436.

[91] J. W. Lim, D. Ha, J. Lee, S. K. Lee, and T. Kim, "Review of Micro/Nanotechnologies for Microbial Biosensors," *Frontiers in Bioengineering and Biotechnology*, vol. 3, p. 61, 2015, doi: 10.3389/fbioe.2015.00061.

[92] A. Haleem, M. Javaid, R. P. Singh, R. Suman, and S. Rab, "Biosensors applications in medical field: A brief review," *Sensors International*, vol. 2, p. 100100, Jan. 2021, doi: 10.1016/j.sintl.2021.100100.

[93] N. Nasiri and C. Clarke, "Nanostructured Gas Sensors for Medical and Health Applications: Low to High Dimensional Materials," *Biosensors*, vol. 9, no. 1, p. 43, Mar. 2019, doi: 10.3390/bios9010043.

[94] H. Nazemi, A. Joseph, J. Park, and A. Emadi, "Advanced Micro- and Nano-Gas Sensor Technology: A Review," *Sensors (Basel)*, vol. 19, no. 6, Mar. 2019, doi: 10.3390/s19061285.

[95] Q.-W. Zhang, L.-G. Lin, and W.-C. Ye, "Techniques for extraction and isolation of natural products: a comprehensive review," *Chin Med*, vol. 13, p. 20, Apr. 2018, doi: 10.1186/s13020-018-0177-x.

[96] M. García-Nicolás, N. Arroyo-Manzanares, J de Dios Hernandez, I. Guillen, P. Vizcaino, M. Sanchez-Rubio, I. Lopez, P. Vinas., "Ion mobility spectrometry and mass spectrometry coupled to gas chromatography for analysis of microbial contaminated cosmetic creams," *Anal Chim Acta*, vol. 1128, pp. 52–61, Sep. 2020, doi: 10.1016/j.aca.2020.06.069.

[97] X. Chen, R. Hu, L. Hu, Y. Huang, W. Shi, Q. Wei, Z. Li., "Portable Analytical Techniques for Monitoring Volatile Organic Chemicals in Biomanufacturing Processes: Recent Advances and Limitations," *Frontiers in Chemistry*, vol. 8, p. 837, 2020, doi: 10.3389/fchem.2020.00837.

[98] A. Ghasemi, H.Amiri, H. Zare, M. Mansoor, A. Hasnzadeh, A. Beyzar,A. Z. Aref, M. Karimi,M. R.Hamblin., "Carbon nanotubes in microfluidic lab-on-a-chip technology: current trends and future perspectives," *Microfluid Nanofluidics*, vol. 21, no. 9, Sep. 2017, doi: 10.1007/s10404-017-1989-1.

[99] G. W. Hunter, S. Akbar, S. Bhansali, M. Daniele, P. J.Hesketh, P. Manickam, R. L. Vander wal., "Editors' Choice—Critical Review—A Critical Review of Solid State Gas Sensors," *J. Electrochem. Soc.*, vol. 167, no. 3, p. 037570, Jan. 2020, doi: 10.1149/1945-7111/ab729c.

[100] D. M. C. Rodrigues, R. N. Lopes, M. A. R. Franco, M. M. Werneck, and R. C. S. B. Allil, "Sensitivity Analysis of Different Shapes of a Plastic Optical Fiber-Based Immunosensor for Escherichia coli: Simulation and Experimental Results," *Sensors (Basel)*, vol. 17, no. 12, p. 2944, Dec. 2017, doi: 10.3390/s17122944.

[101] B. Troia, A. Paolicelli, F. De, and V. M. N. Passaro, "Photonic Crystals for Optical Sensing: A Review," in *Advances in Photonic Crystals*, V. Passaro, Ed. InTech, 2013. doi: 10.5772/53897.

[102] R. V. Nair and R. Vijaya, "Photonic crystal sensors: An overview," *Progress in Quantum Electronics*, vol. 34, no. 3, pp. 89–134, May 2010, doi: 10.1016/j.pquantelec.2010.01.001.

[103] I. Cretescu, D. Lutic, and L. R. Manea, *Electrochemical Sensors for Monitoring of Indoor and Outdoor Air Pollution*. IntechOpen, 2017. doi: 10.5772/intechopen.68512.

[104] N. R. Stradiotto, H. Yamanaka, and M. V. B. Zanoni, "Electrochemical sensors: a powerful tool in analytical chemistry," *J. Braz. Chem. Soc.*, vol. 14, pp. 159–173, Apr. 2003, doi: 10.1590/S0103-50532003000200003.

[105] J. M. Pingarrón *et al.*, "Terminology of electrochemical methods of analysis (IUPAC Recommendations 2019)," *Pure and Applied Chemistry*, vol. 92, no. 4, pp. 641–694, Apr. 2020, doi: 10.1515/pac-2018-0109.

[106] S. E. Root, S. Savagatrup, A. D. Printz, D. Rodriquez, and D. J. Lipomi, "Mechanical Properties of Organic Semiconductors for Stretchable, Highly Flexible, and Mechanically Robust Electronics," *Chem. Rev.*, vol. 117, no. 9, pp. 6467–6499, May 2017, doi: 10.1021/acs.chemrev.7b00003.

[107] S. Tajik H. Beitollahi, F. Gaukari Najad, S.I. Sheikh, K.Zhang, H. Won Jang, M.Shokouhimehr., "Recent developments in conducting polymers: applications for electrochemistry," *RSC Advances*, vol. 10, no. 62, pp. 37834–37856, 2020, doi: 10.1039/D0RA06160C.

[108] D. Khokhar, S. Jadoun, R. Arif, and S. Jabin, "Functionalization of conducting polymers and their applications in optoelectronics," *Polymer-Plastics Technology and Materials*, vol. 59, Sep. 2020, doi: 10.1080/25740881.2020.1819312.

[109] R. Khalil, S. Homaeigohar, D. Häußler, and M. Elbahri, "A shape tailored gold-conductive polymer nanocomposite as a transparent electrode with extraordinary insensitivity to volatile organic compounds (VOCs)," *Sci Rep*, vol. 6, no. 1, Art. no. 1, Sep. 2016, doi: 10.1038/srep33895.

[110] M. M. Ayad, N. Salahuddin, and I. M. Minisy, "Detection of some volatile organic compounds with chitosan-coated quartz crystal microbalance," *Designed Monomers and Polymers*, vol. 17, no. 8, pp. 795–802, Nov. 2014, doi: 10.1080/15685551.2014.918019.

[111] M. Hijazi, "Sensitive and selective ammonia gas sensor based on molecularly functionalized tin dioxide working at room temperature," p. 151.

[112] N. Uehara, "Polymer-functionalized gold nanoparticles as versatile sensing materials," *Anal Sci*, vol. 26, no. 12, pp. 1219–1228, 2010, doi: 10.2116/analsci.26.1219.

[113] V. O. Okechukwu, V. Mavumengwana, I. A. Hümmelgen, and M. A. Mamo, "Concomitant in Situ FTIR and Impedance Measurements To Address the 2-Methylcyclopentanone Vapor-Sensing Mechanism in MnO2–Polymer Nanocomposites," *ACS Omega*, vol. 4, no. 5, pp. 8324–8333, May 2019, doi: 10.1021/acsomega.8b03589.

[114] K. J. Dunst, K. Cysewska, P. Kalinowski, and P. Jasiński, "Polypyrrole based gas sensor for ammonia detection," *IOP Conference Series Materials Science and Engineering (Online)*, vol. 104, no. 1, p. 8, Jan. 2016.

[115] A. M. Smolin, N. P. Novoselov, T. A. Babkova, S. N. Eliseeva, and V. V. Kondrat'ev, "Use of composite films based on poly(3,4-ethylenedioxythiophene) with inclusions of palladium nanoparticles in voltammetric sensors for hydrogen peroxide," *J. Anal. Chem.*, vol. 70, no. 8, pp. 967–973, Aug. 2015, doi: 10.1134/S1061934815080171.

[116] A. Sonu, A. Baraket, S. Boudjaoui, J. Gallardo, N. Zine, M. Sigaud, M. Hangouet, A. Alcacer, A. Streklas, J. Bausells, A. Errachid., "Solid State Gas Sensor Based on Polyaniline Doped with [3,3′-Co(1,2-C2B9H11)2]−1 for Detection of Acetone:

Diagnostic to Heart Failure Disease," *Proceedings*, vol. 2, no. 13, Art. no. 13, 2018, doi: 10.3390/proceedings2131086.

[117] B. Yeole, T. Sen, D. Hansora, and S. Mishra, "Electrical and Gas Sensing Behaviour of Polypyrrole/silver Sulphide Nanocomposites," *American Journal of Sensor Technology*, vol. 4, no. 1, Art. no. 1, Mar. 2017, doi: 10.12691/ajst-4-1-2.

[118] P. Krcmar, I. Kuritka, J. Maslik, P. Urbanek, P. Bazant, M.Machovsky, P.Suly,P.Merka., "Fully Inkjet-Printed CuO Sensor on Flexible Polymer Substrate for Alcohol Vapours and Humidity Sensing at Room Temperature," *Sensors*, vol. 19, no. 14, Art. no. 14, Jan. 2019, doi: 10.3390/s19143068.

[119] M. A. L. dos Reis, F. Thomazi, J. D. Nero, and L. S. Roman, "Development of a Chemiresistor Sensor Based on Polymers-Dye Blend for Detection of Ethanol Vapor," *Sensors (Basel)*, vol. 10, no. 4, pp. 2812–2820, Mar. 2010, doi: 10.3390/s100402812.

[120] D. Maity, M. Manoharan, and R. T. Rajendra Kumar, "Development of the PANI/MWCNT Nanocomposite-Based Fluorescent Sensor for Selective Detection of Aqueous Ammonia," *ACS Omega*, vol. 5, no. 15, pp. 8414–8422, Apr. 2020, doi: 10.1021/acsomega.9b02885.

[121] S. Han, X. Zhuang, W. Shi, X. Yang, L. Li, and J. Yu, "Poly(3-hexylthiophene)/polystyrene (P3HT/PS) blends based organic field-effect transistor ammonia gas sensor," *Sensors and Actuators B: Chemical*, vol. 225, pp. 10–15, Mar. 2016, doi: 10.1016/j.snb.2015.11.005.

[122] Y. Yang, "HYBRID OF P3HT AND ZnO@GO NANOSTRCTURED PARTICLES FOR INCREASED NO2 SENSITIVITY," p. 31.

[123] M. Šetka, J. Drbohlavová, and J. Hubálek, "Nanostructured Polypyrrole-Based Ammonia and Volatile Organic Compound Sensors," *Sensors (Basel, Switzerland)*, vol. 17, no. 3, Mar. 2017, doi: 10.3390/s17030562.

[124] L.-C. Chang, H.-N. Wu, C.-Y. Lin, Y.-H. Lai, C.-W. Hu, and K.-C. Ho, "One-pot synthesis of poly (3,4-ethylenedioxythiophene)-Pt nanoparticle composite and its application to electrochemical H2O2 sensor," *Nanoscale Research Letters*, vol. 7, no. 1, p. 319, Jun. 2012, doi: 10.1186/1556-276X-7-319.

[125] C. Duc, M.-L. Boukhenane, J.-L. Wojkiewicz, and N. Redon, "Hydrogen Sulfide Detection by Sensors Based on Conductive Polymers: A Review," *Frontiers in Materials*, vol. 7, 2020, Accessed: Apr. 19, 2022. [Online]. Available: https://www.frontiersin.org/article/10.3389/fmats.2020.00215

[126] S. Pandey, "Highly sensitive and selective chemiresistor gas/vapor sensors based on polyaniline nanocomposite: A comprehensive review," *Journal of Science: Advanced Materials and Devices*, vol. 1, no. 4, pp. 431–453, Dec. 2016, doi: 10.1016/j.jsamd.2016.10.005.

[127] F. Croisier and C. Jérôme, "Chitosan-based biomaterials for tissue engineering," *European Polymer Journal*, vol. 49, no. 4, pp. 780–792, Apr. 2013, doi: 10.1016/j.eurpolymj.2012.12.009.

[128] A. Madaci, G. Raffin, C. Pages, C. Jose, M. Martin, H. Ferkous, A. Bouzid, J. Bausells, A. Alcacer, A. Errachid, N. Jaffrezic-Renault ., "A microconductometric ethanol sensor prepared through encapsulation of alcohol dehydrogenase in chitosan: application to the determination of alcoholic content in headspace above beverages," *J Mater Sci: Mater Electron*, vol. 32, no. 13, pp. 17752–17763, Jul. 2021, doi: 10.1007/s10854-021-06311-9.

[129] Z. Pang, E. Yildirim, M. A. Pasquinelli, and Q. Wei, "Ammonia Sensing Performance of Polyaniline-Coated Polyamide 6 Nanofibers," *ACS Omega*, vol. 6, no. 13, pp. 8950–8957, Apr. 2021, doi: 10.1021/acsomega.0c06272.

[130] M. Hao, R. Zhang, X. Jia, X, Gao, Z, Gao, L, Cheng, Y, Qui., "A polymer based self-powered ethanol gas sensor to eliminate the interference of ultraviolet light," *Sensors and Actuators A: Physical*, vol. 332, p. 113173, Dec. 2021, doi: 10.1016/j.sna.2021.113173.

[131] J.-C. Chiou, C.-C. Wu, and T.-M. Lin, "Sensitivity Enhancement of Acetone Gas Sensor using Polyethylene Glycol/Multi-Walled Carbon Nanotubes Composite Sensing Film with Thermal Treatment," *Polymers*, vol. 11, no. 3, Art. no. 3, Mar. 2019, doi: 10.3390/polym11030423.

[132] S. G. Surya, S. Khartoon, A. Lahcen, A. T. H. Nguyen, B. B. Dzantiev, N. Tarannum, K. N. Salama., "A chitosan gold nanoparticles molecularly imprinted polymer based ciprofloxacin sensor," *RSC Adv.*, vol. 10, no. 22, pp. 12823–12832, Mar. 2020, doi: 10.1039/D0RA01838D.

[133] A. A. Escárcega-Galaz, D. I. Sánchez-Machado, J. López-Cervantes, A. Sanches-Silva, T. J. Madera-Santana, and P. Paseiro-Losada, "Characterization data of chitosan-based films: Antimicrobial activity, thermal analysis, elementary composition, tensile strength and degree crystallinity," *Data in Brief*, vol. 21, pp. 473–479, Dec. 2018, doi: 10.1016/j.dib.2018.09.121.

[134] F. Zouaoui, S. Bourouina-Bacha, M. Bourouina, N. Jaffrezic-Renault, N. Zine, and A. Errachid, "Electrochemical sensors based on molecularly imprinted chitosan: A review," *TrAC Trends in Analytical Chemistry*, vol. 130, p. 115982, Sep. 2020, doi: 10.1016/j.trac.2020.115982.

[135] Z. Wang, L. He, J. Lv, and M. Kimura, "Electrodeposition of thin chitosan membrane in freestanding SU-8 microfluidic channel for molecular addressing by capillary effect," *Mater. Res. Express*, vol. 6, no. 4, p. 045403, Jan. 2019, doi: 10.1088/2053-1591/aafce2

[136] F. Kus, C. Tasaltin, M. Albakour, A. G. Gürek, and İ. Gürol, "Macromolecular hexa-asymmetric zinc(II) phthalocyanines bearing triazole-modified triphenylene core: Synthesis, spectroscopy and analysis towards volatile organic compounds on Surface Acoustic Wave devices," *J. Porphyrins Phthalocyanines*, vol. 23, no. 04n05, pp. 477–488, Apr. 2019, doi: 10.1142/S1088424619500342.

[137] V. V. Singh, G. Gupta, R. Sharma, M. Boopathi, P. Pandey, K. Ganesan, B. Singh, D. C. Tiwari, R. Jain, R. Vijayaraghavan., "Detection of chemical warfare agent Nitrogen Mustard-1 based on conducting polymer phthalocyanine nanorod modified electrode," *Synthetic Metals*, vol. 159, no. 19, pp. 1960–1967, Oct. 2009, doi: 10.1016/j.synthmet.2009.07.001.

[138] G. I. Dzhardimalieva and I. E. Uflyand, "Design and synthesis of coordination polymers with chelated units and their application in nanomaterials science," *RSC Adv.*, vol. 7, no. 67, pp. 42242–42288, Aug. 2017, doi: 10.1039/C7RA05302A.

[139] L. Cao and C. Wang, "Metal–Organic Layers for Electrocatalysis and Photocatalysis," *ACS Cent. Sci.*, vol. 6, no. 12, pp. 2149–2158, Dec. 2020, doi: 10.1021/acscentsci.0c01150.

[140] X. Zhou *et al.*, "Nanomaterial-based gas sensors used for breath diagnosis," *Journal of Materials Chemistry B*, vol. 8, no. 16, pp. 3231–3248, 2020, doi: 10.1039/C9TB02518A.

[141] A. F. Abdulameer, M. H. Suhail, O. Gh. Abdullah, and I. M. Al-Essa, "Fabrication and characterization of NiPcTs organic semiconductors based surface type capacitive–resistive humidity sensors," *J Mater Sci: Mater Electron*, vol. 28, no. 18, pp. 13472–13477, Sep. 2017, doi: 10.1007/s10854-017-7186-x.

[142] R. Paolesse, S. Nardis, D. Monti, M. Stefanelli, and C. Di Natale, "Porphyrinoids for Chemical Sensor Applications," *Chem. Rev.*, vol. 117, no. 4, pp. 2517–2583, Feb. 2017, doi: 10.1021/acs.chemrev.6b00361.

[143] J. Brunet, A. Pauly, C. Varenne, and B. Lauron, "On-board phthalocyanine gas sensor microsystem dedicated to the monitoring of oxidising gases level in passenger

compartments," *Sensors and Actuators B: Chemical*, vol. 130, no. 2, pp. 908–916, Mar. 2008, doi: 10.1016/j.snb.2007.10.074.

[144] M. W. Urbanczyk and E. Maciak, "Palladium and Metal-Free Phthalocyanine Bilayer Structures for Hydrogen Detection in the SAW Sensor System Based on Interaction Speed," *Sensors Journal, IEEE*, vol. 6, pp. 1178–1185, Nov. 2006, doi: 10.1109/JSEN.2006.881343.

[145] J. Dong, "Experimental and modeling studies of colloidal dispersion stability of CuPc pigment nanoparticles in aqueous solution," *Theses and Dissertations Available from ProQuest*, pp. 1–290, Jan. 2012, [Online]. Available: https://docs.lib.purdue.edu/dissertations/AAI10156350

[146] M. Singh, N. Kaur, and E. Comini, "The role of self-assembled monolayers in electronic devices," *J. Mater. Chem. C*, vol. 8, no. 12, pp. 3938–3955, Mar. 2020, doi: 10.1039/D0TC00388C.

[147] T. Liu, C. Burger, and B. Chu, "Nanofabrication in polymer matrices," *Progress in Polymer Science*, vol. 28, no. 1, pp. 5–26, Jan. 2003, doi: 10.1016/S0079-6700(02)00077-1.

[148] R. Zhou, F. Josse, W. Göpel, Z. Z. Öztürk, and Ö. Bekaroğlu, "Phthalocyanines as Sensitive Materials for Chemical Sensors," *Applied Organometallic Chemistry*, vol. 10, no. 8, pp. 557–577, 1996, doi: 10.1002/(SICI)1099-0739(199610)10:8<557::AID-AOC521>3.0.CO;2-3.

[149] P. Gaudillat, F. Jurin, B. Lakard, C. Buron, J.-M. Suisse, and M. Bouvet, "From the Solution Processing of Hydrophilic Molecules to Polymer-Phthalocyanine Hybrid Materials for Ammonia Sensing in High Humidity Atmospheres," *Sensors*, vol. 14, no. 8, Art. no. 8, Aug. 2014, doi: 10.3390/s140813476.

[150] Z. Şen, D. K. Tarakci, I. Gürol, V. Ahsen, and M. Harbeck, "Governing the sorption and sensing properties of titanium phthalocyanines by means of axial ligands," *Sensors and Actuators B: Chemical*, vol. 229, pp. 581–586, Jun. 2016, doi: 10.1016/j.snb.2016.01.145.

[151] M. Harbeck, Z. Şen, D. Erbahar, G. Gümüş, and E. Musluoğlu, "Gas sensing with hexafluoroisopropanol substituted phthalocyanines and vic-dioximes: a comparative study," *Turk J Chem*, p. 12.

[152] M. Wu *et al.*, "Sensitive and Selective Electrochemical Sensor Based on Molecularly Imprinted Polypyrrole Hybrid Nanocomposites for Tetrabromobisphenol A Detection," *Analytical Letters*, vol. 52, no. 16, pp. 2506–2523, Nov. 2019, doi: 10.1080/00032719.2019.1617298.

[153] S. Kurosawa, N. Kamo, D. Matsui, and Y. Kobatake, "Gas sorption to plasma-polymerized copper phthalocyanine film formed on a piezoelectric crystal," May 01, 2002. https://pubs.acs.org/doi/pdf/10.1021/ac00203a009 (accessed Mar. 23, 2021).

[154] M. Harbeck, C. Taşaltın, I. Gürol, E. Musluoğlu, V. Ahsen, and Z. Z. Öztürk, "Preferential sorption of polar compounds by fluoroalkyloxy substituted phthalocyanines for the use in sorption based gas sensors," *Sensors and Actuators B: Chemical*, vol. 150, no. 2, pp. 616–624, Oct. 2010, doi: 10.1016/j.snb.2010.08.031.

[155] C. Tasaltin, I. Gurol, M. Harbeck, E. Musluoglu, V. Ahsen, and Z. Z. Ozturk, "Synthesis and DMMP sensing properties of fluoroalkyloxy and fluoroaryloxy substituted phthalocyanines in acoustic sensors," *Sensors and Actuators B: Chemical*, vol. 150, no. 2, pp. 781–787, Oct. 2010, doi: 10.1016/j.snb.2010.07.056.

[156] L. Zhihua, Z. Xucheng, S. Jiyong, Z. Xianbo, H. Xiaowei, T. E. Tahir, M. Holmes ., "Fast response ammonia sensor based on porous thin film of polyaniline/sulfonated nickel phthalocyanine composites," *Sensors and Actuators B: Chemical*, vol. 226, pp. 553–562, Apr. 2016, doi: 10.1016/j.snb.2015.10.062.

[157] M. Sülü, A. Altındal, and Ö. Bekaroğlu, “Synthesis, characterization and electrical and CO2 sensing properties of triazine containing three dendritic phthalocyanine,” *Synthetic Metals*, vol. 155, no. 1, pp. 211–221, Oct. 2005, doi: 10.1016/j.synthmet.2005.08.005.

[158] A. Rydosz, E. Maciak, K. Wincza, and S. Gruszczyński, “Microwave-based sensors with phthalocyanine films for acetone, ethanol and methanol detection,” *Sensors and Actuators B: Chemical*, vol. 237, Jul. 2016, doi: 10.1016/j.snb.2016.06.168.

Chapter III

Analysis of the technologies used for the design of a VOCs sensor

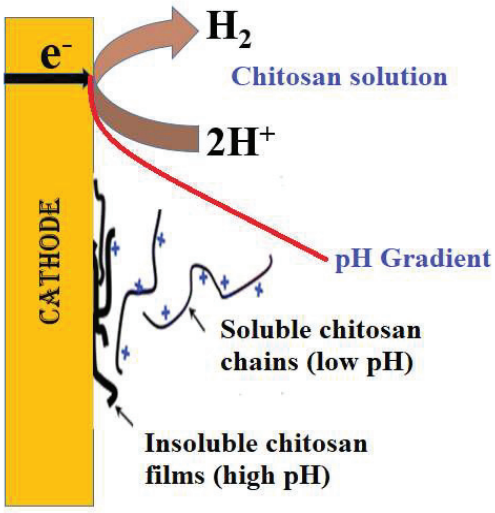

Electrodepositeed chitosan film on Au electrode wafer

III.1. Introduction

Within the scope of this research, a VOC sensor will be developed through the experimental procedure explained in this chapter. The usage of microelectrodes, surface characterization, manufacture of sensitive layers, and sensor response analysis were all implemented. This chapter will first focus on presenting an overview of the laboratory equipment and devices utilized in this work before describing the methods of producing the sensor and highlighting the detection techniques used. It will also be discussed how to measure and characterize the surfaces used. These techniques have not been developed in the state-of-the-art; thus, we will briefly review the operational principle. In the second half, we'll go over the gas analysis platform we built as part of this work. The instrumentation used will be explained first, and then we will concentrate our development efforts on gas sensor manufacturing. We will wrap up this chapter by discussing the transducer's modeling and characterization findings. It is the final phase in the sensor production process, allowing us to test its functioning before functionalizing it to detect certain VOCs such as acetone, ethanol, and methanol.

III.2 Analytical and electrochemical measurements in a controlled environment

III.2.1 Laboratory Instruments

As illustrated in Figure 10, all electrochemical approaches for the functionalization of the gas sensor require an electrochemical faraday cell with three electrodes: a reference electrode (RE) Ag/AgCl, a platinum counter electrode (CE), and a gold working electrode (Working Electrode WE).

Micro conductometric chips developed by CNM-CSIC in Barcelona have been used in the study. The silicon chip dimension was 7.3 x 4.1 mm. The devices occupied a designed finger of 60-µm width; the finger partitioning is like the finger width. The interdigitated electrode areas were described with a dimension diameter of 1.2 mm for the 4 rounded devices and 1.74 x 0.9 mm for the middle rectangular electrode. Our research team elsewhere demonstrated the flowchart of the fabrication process [1].

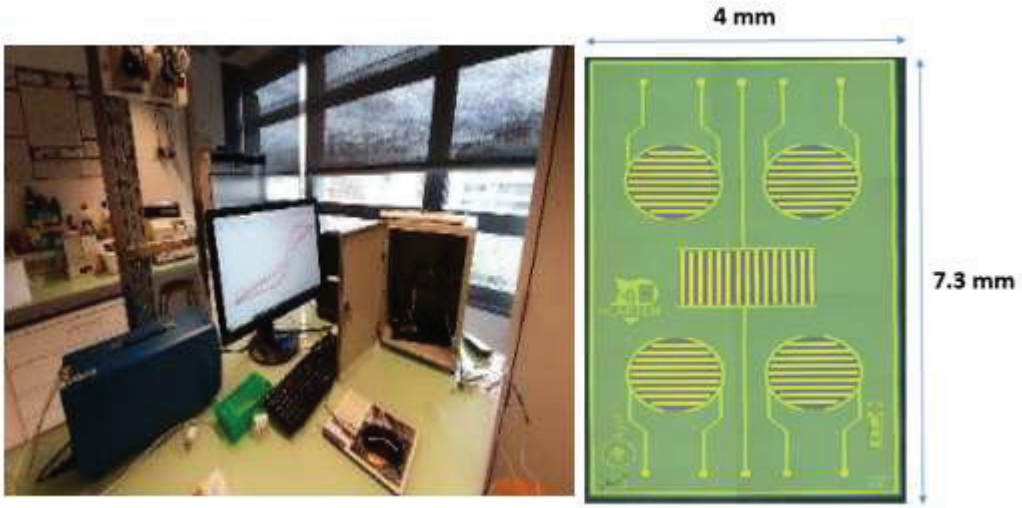

Figure 10. Photo of Potentiostat and the faraday electrochemical cell containing the reference, counter, and working interdigitated electrode

For electrochemical measurements, this faraday electrochemical cell is coupled to a potentiostat. The Figure 11 below depicts the 3-electrode configuration's similar electrical setup [2].

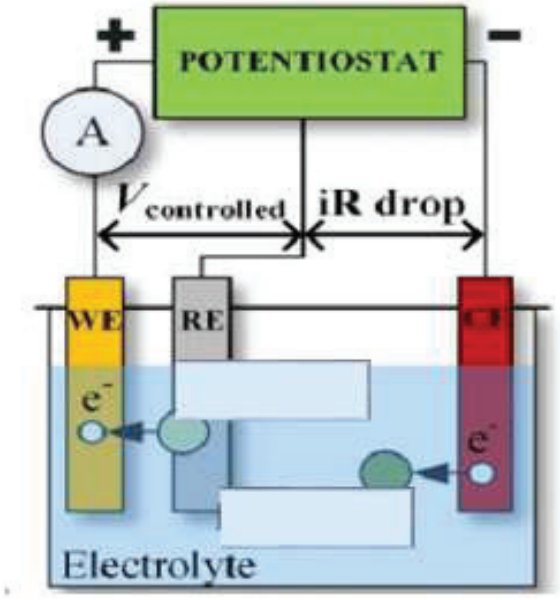

Figure 11. In an electrolyte, the equivalent circuit of the 3-electrode circuit

III.3. Techniques for electrochemical measurements

The potentiostat is essential for the chemical characterization of electrodes before and after functionalization. It enables the creation of measurement methods such as chronoamperometry (CA), cyclic voltammetry (CV), and even electrochemical impedance spectroscopy [3].

The CA involves monitoring the current's temporal evolution after a constant potential is applied to the working electrode as a function of time (t) [4]. Our study utilizes it during the electrode's functionalization, and it will be detailed later in the manuscript.

The CV is formulated by measuring the current generated by a potential linear sweep over a predetermined interval at a constant sweep speed [5]. We can run several CV cycles with the instrument in succession, each depicted by a plot of the recorded current against the applied potential. The resulting graph is known as a voltammogram. It is an electrochemical method for determining how the electrons travel between the working electrode and the electrolyte. It is beneficial for visualizing the redox characteristics of electroactive species in solution or chemical compounds on the electrode's surface.

The research employed this approach to control the electrode's surface state and functionalize and characterize the deposited membrane [6]. The voltammogram of a gold microelectrode immersed in a solution of $[Fe(CN)_6]^{3-}$ / $[Fe(CN)_6]^{4-}$ buffered with phosphate-buffered saline (pH = 7.6) is shown in the Figure 12.

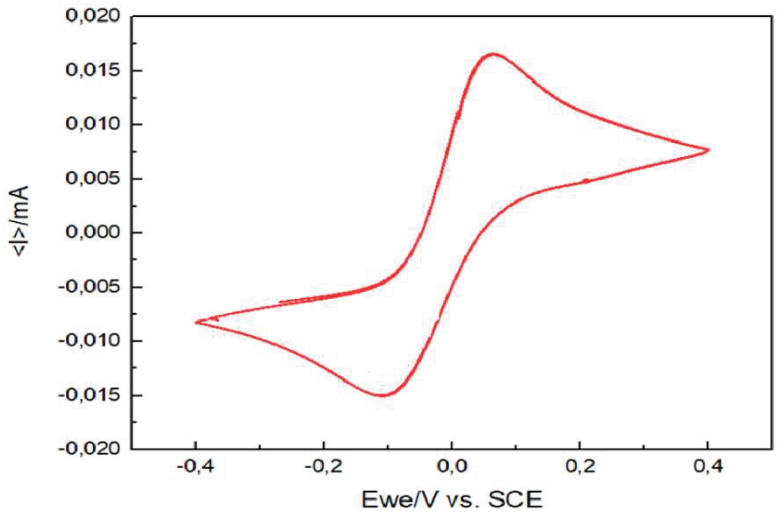

Figure 12. Voltammogram of a bare gold microelectrode with a solution of $[Fe (CN) 6]^{3-}$ /$[Fe (CN) 6]^{4-}$ buffered with PBS (pH = 7.4), sweep speed 50 mV / s

The oxidizing/reducing coupling parameters were used in our work because the potentials at which the current peaks (-0.1V / 0.1V) for a gold surface are widely mentioned in the literature [7]. The application of these potentials does not damage the electrode surface. The double wave visible on the graph corresponds to the oxidation and reduction of the two species at the electrode surface [8]. The measured current value is proportional to the area accessible to species in the solution. As a result, we can utilize this method to determine if a gold surface is blocked after the electrodeposition of a chitosan-sensitive membrane.

III.4. Conductometric measurements by IDE's sensors

The operating principle of an interdigitated electrode sensor (IDE) is the same as that of a capacitor. Indeed, an IDE is immersed in an ionic solution called electrolyte which is electrically conductive. The presence of ions, electrically charged, ensures the character solution driver. The conductive properties of this solution are measured by a conductometric analysis. Its principle can be explained by analogy with the operation of an electric capacitor with parallel plates. The latter is composed of two plane reinforcements, parallel, of the same shape, of surface A and spaced by a distance d. When applying a potential on these plates, they are charged on both sides, which generates an internal electric field. The nature of this field depends on the position of the plates. We define the properties of the dielectric medium placed between the 2 flat electrodes by the capacitance (C) and the conductance (G), shown in Figure 13.

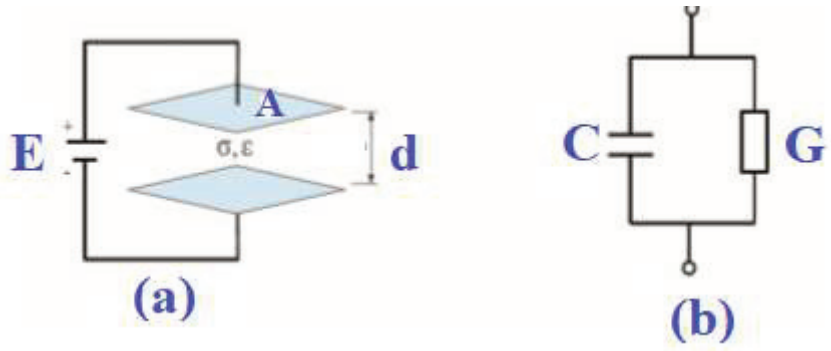

Figure 13. Conductimetry Operating Principle

(a) measurement of a dielectric space, (b) electrical circuit equivalent

The following formulae can be used to determine these variables:

- A: the area of the flat electrode (μm^2)
- d: distance between the electrodes (µm)
- σ: electrical conductivity of the medium (S/m)
- ε_0: vacuum permittivity, $\varepsilon_0 = 8{,}8542.10^{-6}$ (pF/µm)

- εr: relative permittivity of the medium
- C_0: capacitance per unit area (pF / μm^2)

The conductivity σ is a quantitative characteristic of the medium to be analyzed. An aqueous medium depends on ions concentration, ionic conductivity, and temperature. The defined factor (A / d) depends only on the sensor's geometry, generally assimilated to a constant K, the cell constant of the sensor [9]. The electric field formed by the application of potential on the sensor is shown in Figure 14, as reported by Dey et al. [10].

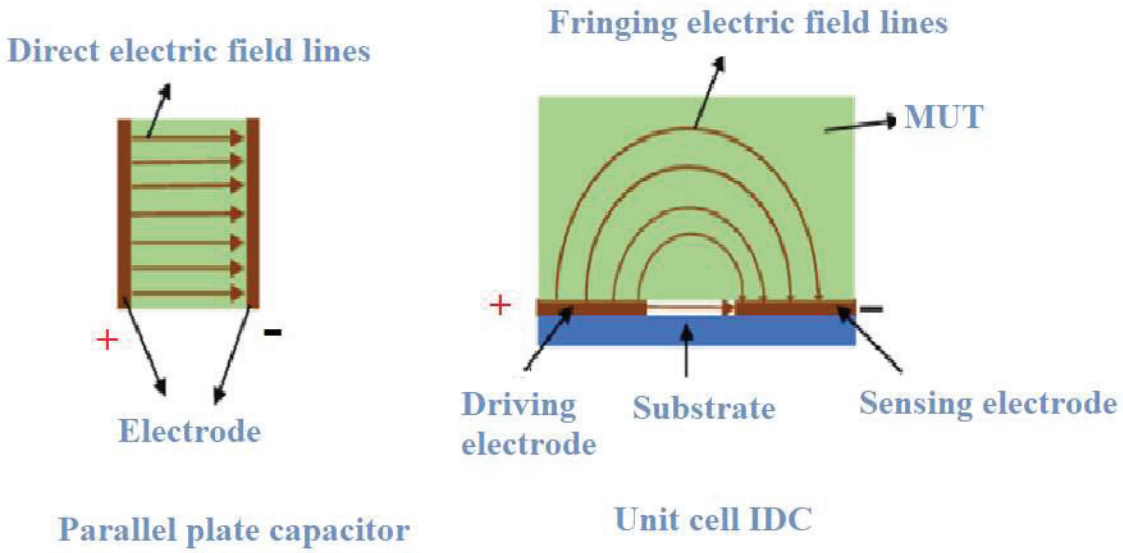

Figure 14. Electric field produced by applying a voltage to the sensor

As a result, the capacitor's geometry influences the electric field created. When an analyte is added to the medium being studied, it changes the field lines created by the electric field. The sensor's equipment allows for the measurement of variations in the electric field (current flowing in the electrode) and the conversion of the medium's conductivity [11]. The device relates to the detection of the analyte at hand.

An IDE sensor works in the same way as a planar capacitor in terms of operation. As shown in Figure 15: an IDE consists of a series of positively and negatively polarized electrodes arranged in the form of interlaced combs.

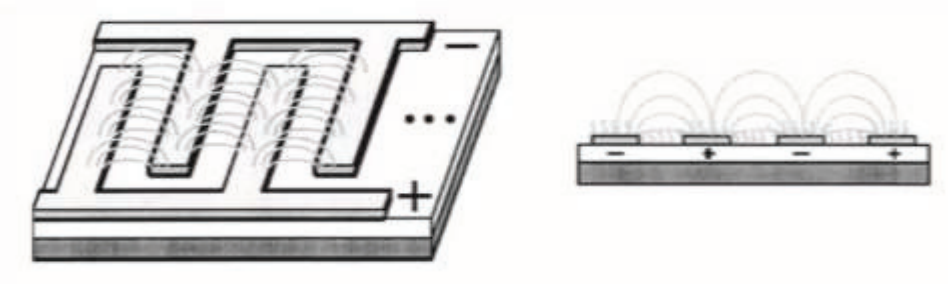

Figure 15. Structure of an interdigitated electrode

III.5. Instruments for laboratory characterization

III.5.1. The Atomic Force Microscopy

The Atomic Force Microscopy (AFM) is a technique for mapping nanometric solid, conductive, or insulating surfaces using near-field microscopy. It is based on the contact between the surface of the sample and a micro lever with a radius of curvature (10 nm) tip.

The optical deflected tips system is based on the detection of a laser beam reflected off the back of the micro-lever by a photodiode 4 dials, as shown in Figure 16.

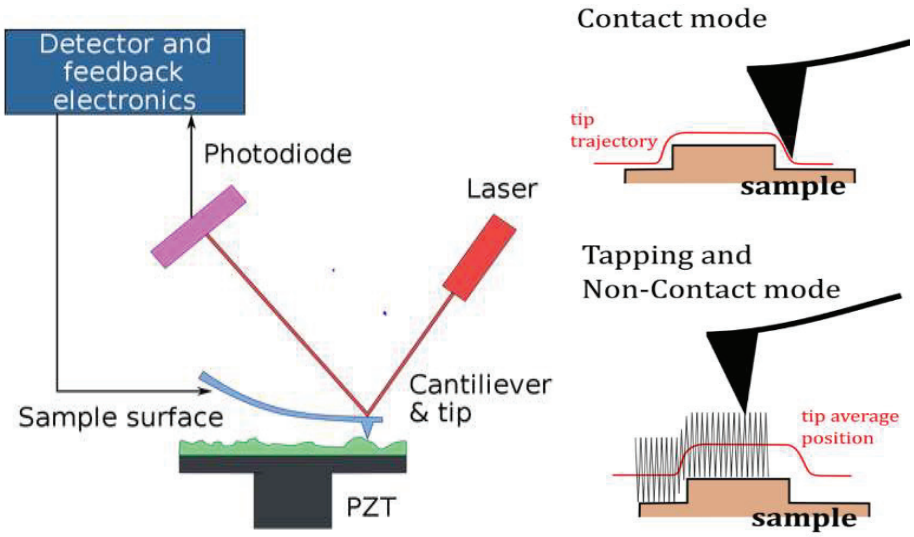

Figure 16. The AFM principle of operation

(a) Atomic Force Microscope (b) AFM Imaging Modes

There are two ways to use it. Static mode, also known as contact mode, involves moving the sample across the surface to scan the surface. The sample surface is in touch with the tip. The results of the repulsive interaction can be traced back to the surface's topology. This technique

can be used on both resistant and rough samples. The dynamic or "tapping" mode oscillates the micro-lever so that the tip taps the surface intermittently in the down position. It is feasible to return to the topology of rough and deformable surfaces by studying the phase and amplitude of oscillations.

III.5.2. Fourier Transform Infrared spectroscopy

IR spectroscopy is an analytical technique for characterizing molecular groups and establishing the bonding compounds' nature in a sample [12]. Polychromatic radiation is used to illuminate the model during the analysis. The piece has absorbed part of the radiation because the transmitted beam's intensity is lower than the incident beams. The electric charges of the molecule interact with the electromagnetic field of radiation, causing the dipole moment to change. When the field frequency coincides with the molecule's vibrational frequency, the resulting interaction excites the vibration of bonds, resulting in energy absorption from the excitation wave. The frequency at which the radiation is absorbed corresponds to a permissible transition between two vibrational states of the molecule, and the type of the bonds, the mass of the atoms involved, and the surrounding environment determine it, allowing for the determination of the presence of chemical functions in the sample, among other things.

Transmission and reflection are two different radiation/matter interactions used by infrared absorption spectroscopy. The most common method for determining a material's absorbance is to compare the intensity of transmitted radiation to the intensity of incident radiation [13]. This concept necessitates the use of thin samples. For gases and liquids, this method of analysis is ubiquitous. The in-line analyzes cannot be used because the materials in this study are electrodes. As a result, we worked in the Attenuated Total Reflectance mode (ATR).

The use of a crystal in contact with the sample to be studied is required for this procedure. This technique generates an evanescent wave at the crystal/sample contact, with an electric field attenuating along the normal to the surface. This field can be coupled with the material's vibration modes, resulting in absorption [14]. The refractive index, among other factors, determines the depth of penetration of the evanescent wave into the material.

We selected to deal with a germanium crystal since it has a high refractive index (n = 4), making it unique. As a result, we restrict the depth of analysis to focus on the surface of our sample.

A broadband light source generates the beam, which contains the whole spectrum of wavelengths to be measured. The light goes via a Michelson interferometer, which works on the following principle shown in Figure 17.

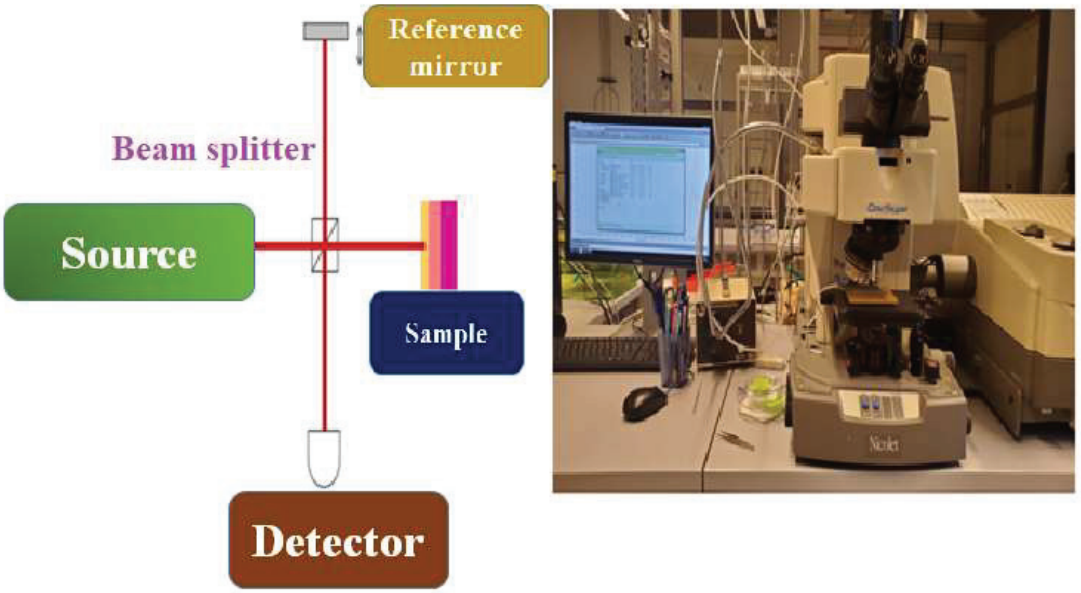

Figure 17. Michelson interferometer schematic and a view of the micro and nano biotechnology

ISA LYON platform

The IR beam passes via a splitter, which divides the beam into two equal-intensity beams [15]. One beam is focused on a stationary mirror, while the other is focused on a moving mirror [16]. At the separator's level, the two beams are reflected and recombined; depending on the distance traveled by the two beams, they interfere in different ways. If the distance traveled by the two beams is identical (or separated by a wavelength), interference is in phase (or constructive). The optical path of this emerging beam is increased by 2d if the moveable mirror is shifted from "d," and the two beams are out of phase. As a result, the resulting signal is a displacement "d" function called an interferogram. We convert the interferogram data to spectra reflecting the light absorbed as a function of wavenumber using the Fourier transformation [17].

The Analysis is made with a "NEXUS (THERMO - OMNIC software)" spectrometer that includes a "Globar" source, a "KBr" splitter, and a "DTGS" detector. The spectra were captured in ATR on a germanium crystal in monoreflexion at 45 degrees (Spectra Tech Thunderdome attachment). And to obtain a scope with a resolution of 4 cm^{-1}, 256 accumulations are performed.

III.5.3. The scanning electron microscope

Scanning electron microscopy (SEM) is a technique for obtaining high-resolution pictures of a sample's surface, based on the electron-matter interaction principle [18]. The block diagram is depicted in Figure 18.

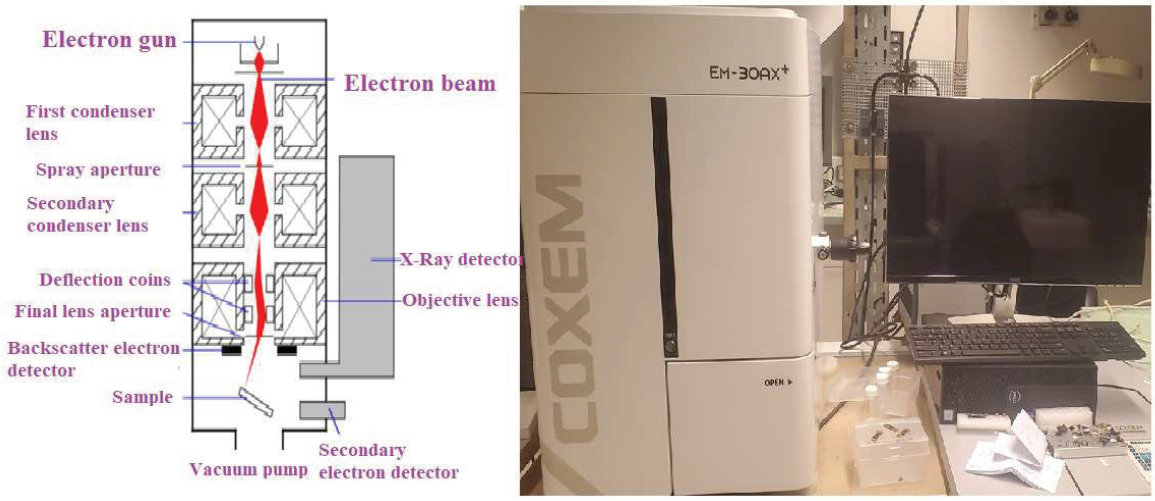

Figure 18. A schematic diagram of a scanning electron microscope (SEM) and a perspective of the MNBT Lab (ISA LYON) platform

The interaction between the probe electrons and the sample generates low-energy secondary electrons propelled towards the detector when the electron beam is projected onto the material to be examined [19]. Each impact on the sample's surface produces an electrical signal, the strength of which is determined by the nature of the selection and its topography at the place in question. It is possible to obtain a map of the scanned area by scanning the beam over the sample. The surface morphologies of the sensing materials membranes were studied using scanning electron microscopy (SEM) (COXEM EM-30AX+). The instrument is installed in our team MNBT (ISA LYON). This SEM is fitted with Energy Dispersive Spectroscopy EDS analysis equipment. We can use this technique to perform elemental analysis on the material. Notwithstanding, following that, the de-excitation generates atom-specific X-rays, which we may examine to learn more about the atom's chemical makeup. The detection of X photons in energy dispersion is usually done with a detector made of a silicon crystal diode doped with lithium or a germanium.

III.5.4. Thermogravimetric Analysis

Thermogravimetric analysis (TGA) is a thermal analysis method in which the mass of a sample is estimated based on temperature or time, and the surrounding environment. In this method,

changes in the mass range can be recognized with a high degree of accuracy [20]. The principle of TGA as depicted in Figure 19.

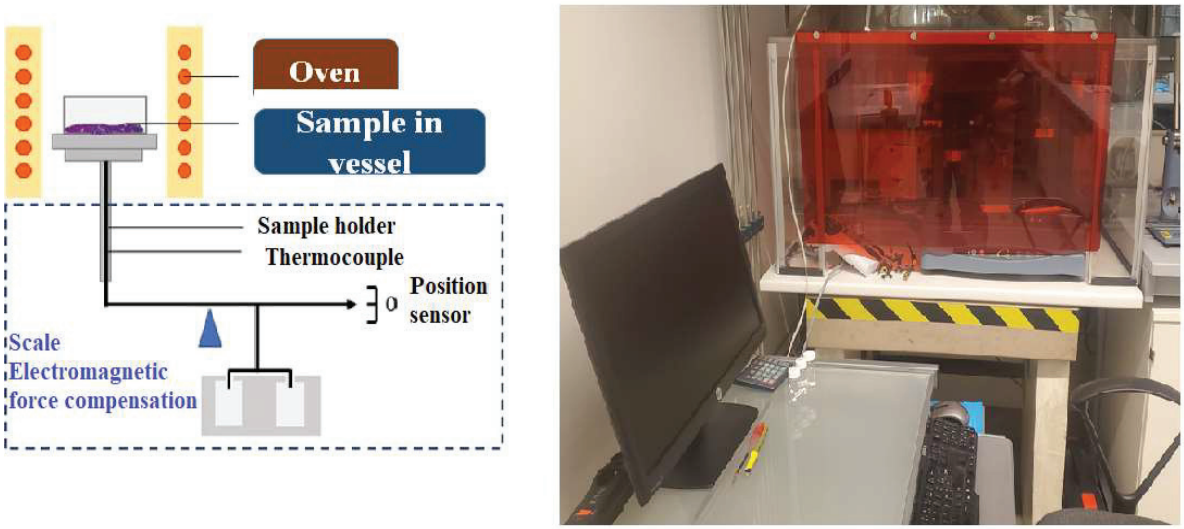

Figure 19. A schematic diagram of a thermogravimetric instrument
and a view of the MNBT Lab (ISA Lyon) platform (TA Instruments series Q50)

The sample is heated at a controlled rate in a specific environment (air, N_2, CO_2, He, Ar, etc.) in the TGA. The change in the substance's weight as a function of temperature or time is recorded. For a known beginning weight of the material, the temperature is increased at a fixed rate, and the weight changes are registered as a function of temperature at various time intervals [21]. The thermogravimetric curve, often known as a TGA thermogram, is a graph of weight change as a function of temperature.

III.6. The platform for detecting and analyzing VOCs

Conductometric detections of volatile organic compounds were made possible by applying a significant amplitude of sinusoidal potential difference (10 mV peak to peak at 0 V) to each pair of interdigitated electrodes (microelectrodes) with an optimized frequency of 10 kHz produced by a limited frequency waveform generator. These factors were solely included to reduce faradaic activity, double-layer charging, and concentration polarization at the microelectrode surface. The Standard Research System Lock-in Amplifier SR510 was utilized to generate the differential output signal between the working electrode and the reference electrode (Figure 20).

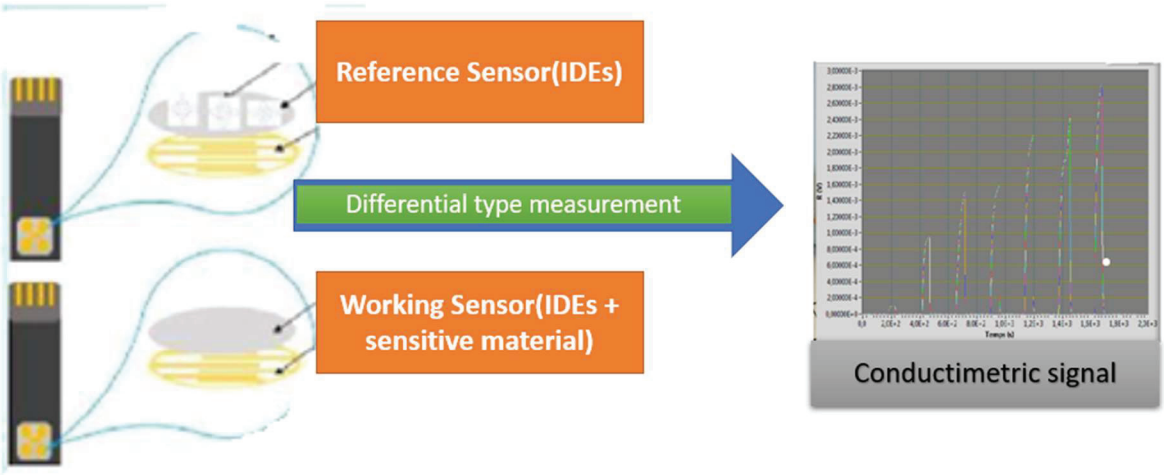

Figure 20. The components of the VOC detection platform

III.6.1. The "Lock-in amplifier"

The "Lock-in amplifier" shown in Figure 21, is a highly efficient method for detecting and measuring low-amplitude AC signals. Despite the presence of large noise sources, accurate measurements can be made. This system employs phase-sensitive signal detection to precisely isolate signal components in sensor output at a predetermined frequency and phase. Noise at frequencies other than the reference frequency is rejected, therefore the measurements are unaffected. As a result of the "Lock-in Amplifier" we may use conductometric measurements to examine the gas sensor's response. It has an output that can generate a sinusoidal signal stimulation with adjustable frequency and amplitude. We restore the sensor's reaction to input A of the "Lock-In" once it has been excited. It is also feasible to carry out differential conductometric measurements. A second input B is coupled to a VOC-insensitive reference sensor. This mode of operation will be discussed in the next sections where differential measurements were practically adopted.

Figure 21. Front view of Lock-In Amplifier

Phase-sensitive detection

To extract a signal from a noisy environment, Lock-in amplifiers leverage the knowledge of the signal's time dependence. A lock-in amplifier multiplies its input with a reference signal, also known as down-mixing or heterodyne/homodyne detection. It then filters the result using an adjustable low-pass filter. Demodulation, also known as phase-sensitive detection, isolates the signal at the desired frequency from all other frequency components. The reference signal generated by the lock-in amplifier or supplied by an external source to the lock-in amplifier and the experiment. The reference signal is typically a sine wave, although it can also take other shapes. Using demodulation with a pure sine wave, selective measurement at the fundamental frequency or any of its harmonics is possible. Some instruments utilize a square wave [22], which records all of the signal's odd harmonics, potentially generating systematic measuring inaccuracies. We will look at both the time and frequency domains to understand lock-in detection, first for mixing and filtering.

Dual-phase demodulation

This method necessitates the creation of a reference signal. The "Lock-In" generates a fixed frequency AC pulse that excites the gas sensor. The sensor's response is then measured at the same frequency by the latter. The reference signal created by Lock-In in Figure 22 is the result of a square signal of frequency. The output signal is proportional to.

$$V_{sig} * \cos\theta$$
$$\theta = \theta_{sig} - \theta_{ref}$$

The phase difference between the signal and the Lock-In reference oscillator corresponds to this value. It is possible to get this phase difference equal to zero by modifying ref. In this situation, the signal Vsig is being measured. The output will be zero if the phase difference is 90 degrees. Simple phase locking is defined as a lock-in that consists of a single PSD [23]. By introducing a second PSD module, phase dependence can be eliminated, the signal at the output of the sensor is multiplied by the signal from the reference oscillator shifted by 90 °: $V_L * \sin(\omega_L + \theta_{ref} + 90°)$.

The second low-pass filter's output signal is then:

$$V_{psd2} = \frac{1}{2} * V_{sig} * V_L * \sin(\theta_{sig} - \theta_{ref})$$
$$V_{psd2} \sim V_{sig} * \sin\theta$$

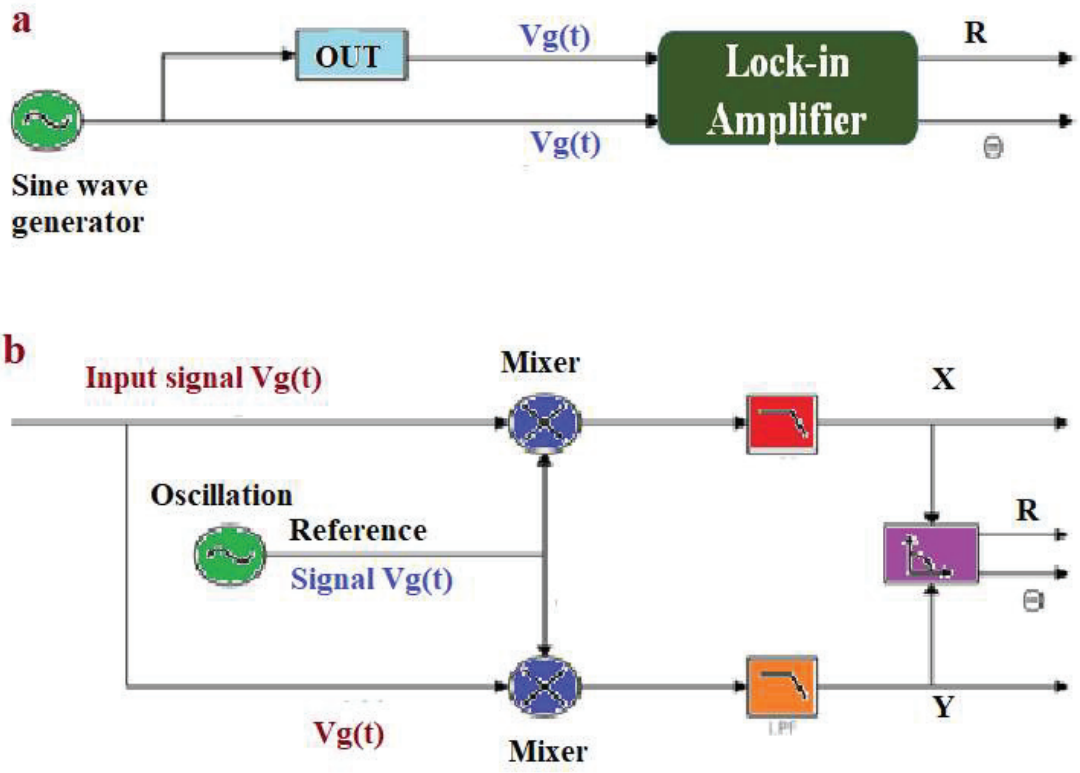

Figure 22. (a) An example of a lock-in measurement. (b) Lock-in amplification schematic working mode

The Lock-in Amplifier therefore measures two types of variables, one proportional to cosθ and the other proportional to sinθ according to the following equations:

$$X = V_{sig} * \cos\theta$$
$$Y = V_{sig} * \sin\theta$$

These two variables describe the signal as a vector in relation to the Lock-In's reference oscillator. The in-phase component is X, while the quadrature component is Y. We subtract the phase dependency. To calculate the norm of the vector R, which gives us the formula:

$$R = \sqrt{(X^2 + Y^2)} = V_{sig}$$

R thus allows us to obtain the amplitude of the signal at the output of the sensor and does not depend on any phase shift. Furthermore, the phase difference θ can be measured according to the following equation:

$$\theta = \tan^{-1}(\frac{Y}{X})$$

Figure 22 (b) shows that the lock-in amplifier must split up the input signal to demodulate it with two different phases. Contrary to analog instruments, digital technology overcomes any losses in SNR and mismatch between the channels when splitting the signal.

Differential measurements

Lock-in enables differential measurements, which is a separate measurement mode. It's not uncommon for measurement findings in gas detection applications to be heavily influenced by ambient factors (temperature, humidity, etc.). We can use differential configuration to break free from the medium in measuring.

Its concept is based on the employment of two IDEs, one of which is passive and the other of which is active. In trying to detect the presence of analyte gas in the media, a membrane sensitive to the desired VOC is put on the operational IDE. The other IDE (reference IDE) has been passivated to be insensitive to this VOC. Figure 23 depicts the setup in use.

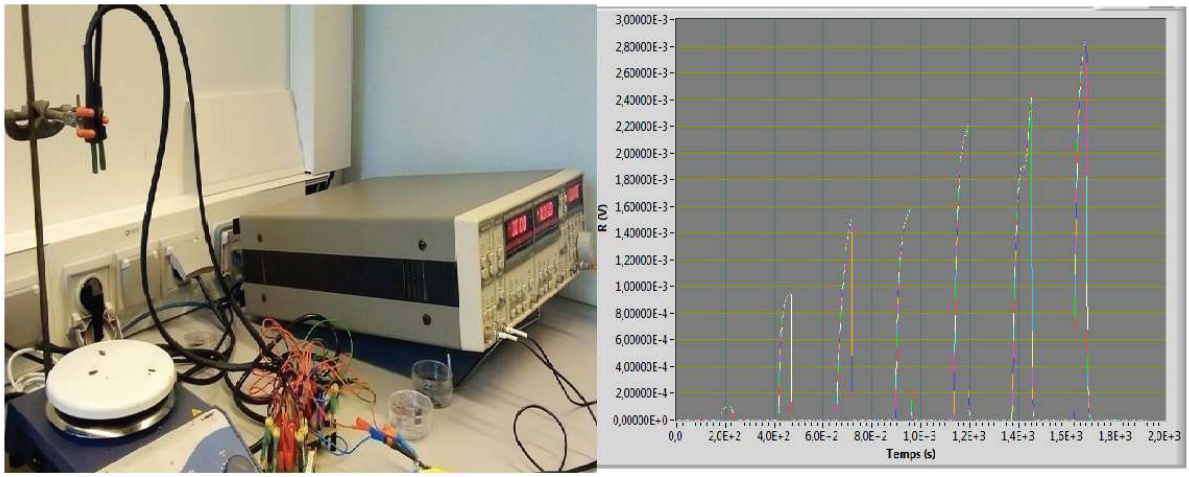

Figure 23. Lock-In configuration from LabVIEW applying differential measurement

One of the active microelectrode's combs is connected to one of the passive electrode's combs, and the assembly is then connected to the Lock-In Amplifier's output (sinusoidal signal). The currents circulating in the two microelectrodes are monitored using parallel resistors R linked to the Lock-In Amplifier's inputs A and B (Figure 24).

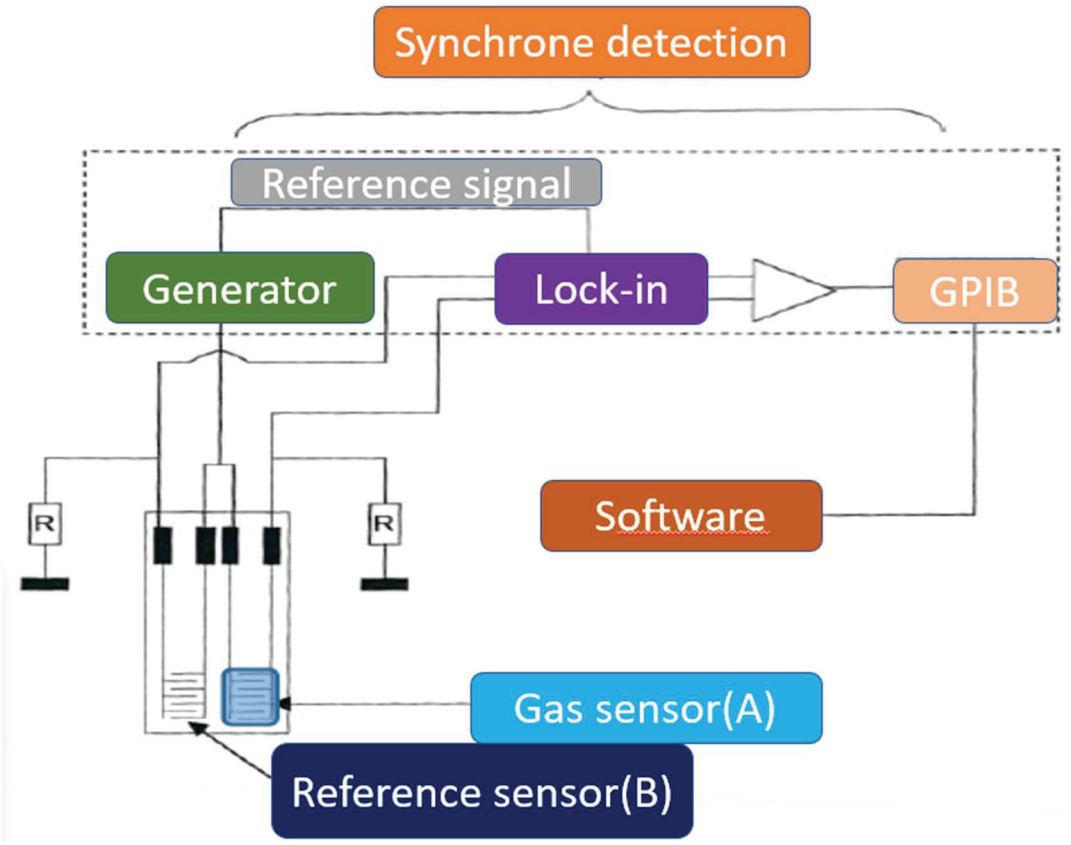

Figure 24. Configuration of lock-in differential measurements

After then, the Lock-In calculates the differential current between the two microelectrodes. When the analyte is detected, the current flowing through the active microelectrode changes, causing it to change, allowing us to measure a difference in the medium's conductivity. This technique allows for more exact measurement findings that are standardized and independent of the electrode's environment. Non-specific signals, such as species absorption on sensors, can also be eliminated using this strategy.

Interface for measuring conductivity

The software LabVIEW was used to create a human-machine interface (HMI) for controlling the Lock-In. A GPIB (General Purpose Interface Bus) link supplied with measuring equipment connects the Lock-In to the PC. Figure 24 depicts the intended HMI. It allows to customize measurement parameters such as acquisition time, amplitude and frequency of the excitation AC signal, and I-V measurement type (single or differential). On the graph depicted, the sensor's response (variable R previously mentioned equivalent to the voltage at the sensor's output) is exhibited in real-time. Finally, the acquisition findings are stored in a text file on the

computer and processed using the Origin software. Now that we've gone over the entire module instrumentation, we'll move on to the final module created as the design phase.

III.6.2. Basic principles of headspace analysis

A headspace sample is typically made in a vial that contains the analyte, dilution solvent, matrix modifier, and headspace [24]. In a sample vial's headspace or gas section, volatile components from complex sample mixes can be separated from non-volatile sample components and segregated. The gas sensor connected to the lock-in amplifier through signals detects a sample of the gaseous compounds above the aqueous phase in the headspace (Figure 25).

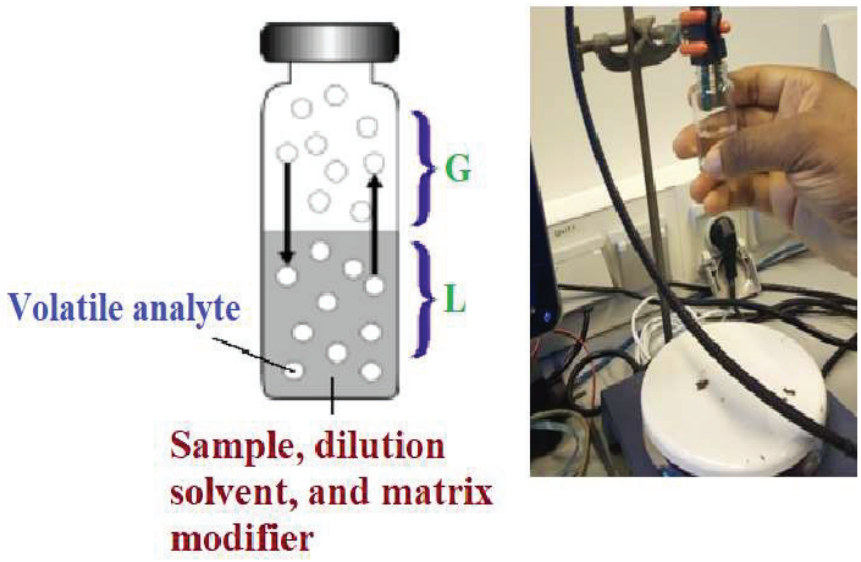

Figure 25. Phases of the Headspace Vial

G = the gas phase (headspace)

The gas phase is commonly referred to as the headspace and lies above the condensed sample phase.

S = the sample phase

The sample phase contains the compound(s) of interest. It is usually a liquid or solid combined with a dilution solvent or a matrix modifier.

Once the sample phase has been loaded to the vial and sealed, volatile components diffuse into the gas phase until the headspace reaches equilibrium, as shown by the arrows. After that, the sample is obtained from the headspace.

III.6.3 Potassium Chloride Conductometric Analysis

To determine how effective our IDEs sensors are, we examine their response to changes in the conductivity of the aqueous medium, particularly about the frequency f of the fixed signal and the resistance R utilized. Titration of a potassium chloride KCl solution was performed in this experiment. μ-IDEs were immersed in 25 mL of distilled water, and then, we gradually added volumes of KCl at varying concentrations to adjust the medium's concentration. The following is an explanation of how the titration is done:

Stock solutions were prepared from Alfa Ultrapure KCI, and the samples were weighed in a temperature-controlled room using a Mettler BSC1000 balance. The water was prepared using a Culligan deionizing system and had a specific resistance more significant than 18 x 10^6 Ωcm^{-1} at delivery and about 5 x 10^6 Ωcm^{-1} in the cells. All preparation of solutions is carried out in a fume hood under a nitrogen atmosphere to prevent contamination. 1M mother solution of KCl solution was prepared by weighing 7.459 g of KCl pellets and poured into 100 mL flask then topped to the lower meniscus of the 100 mL flask. Other concentrations were obtained by dilution of a factor 10. Other concentrations for each measurement was obtained through double dilution formulation.

The KCl measurements were done using the Lock-in Amplifier at a different frequency (2 kHz, 10 kHz, 50 kHz, and 100 kHz) to find out at which frequency the chip is responding to the conductivity of the KCl solution even at low concentrations. It took 1 minute for every KCl solution measurement. A measurement is represented in Figure 26.

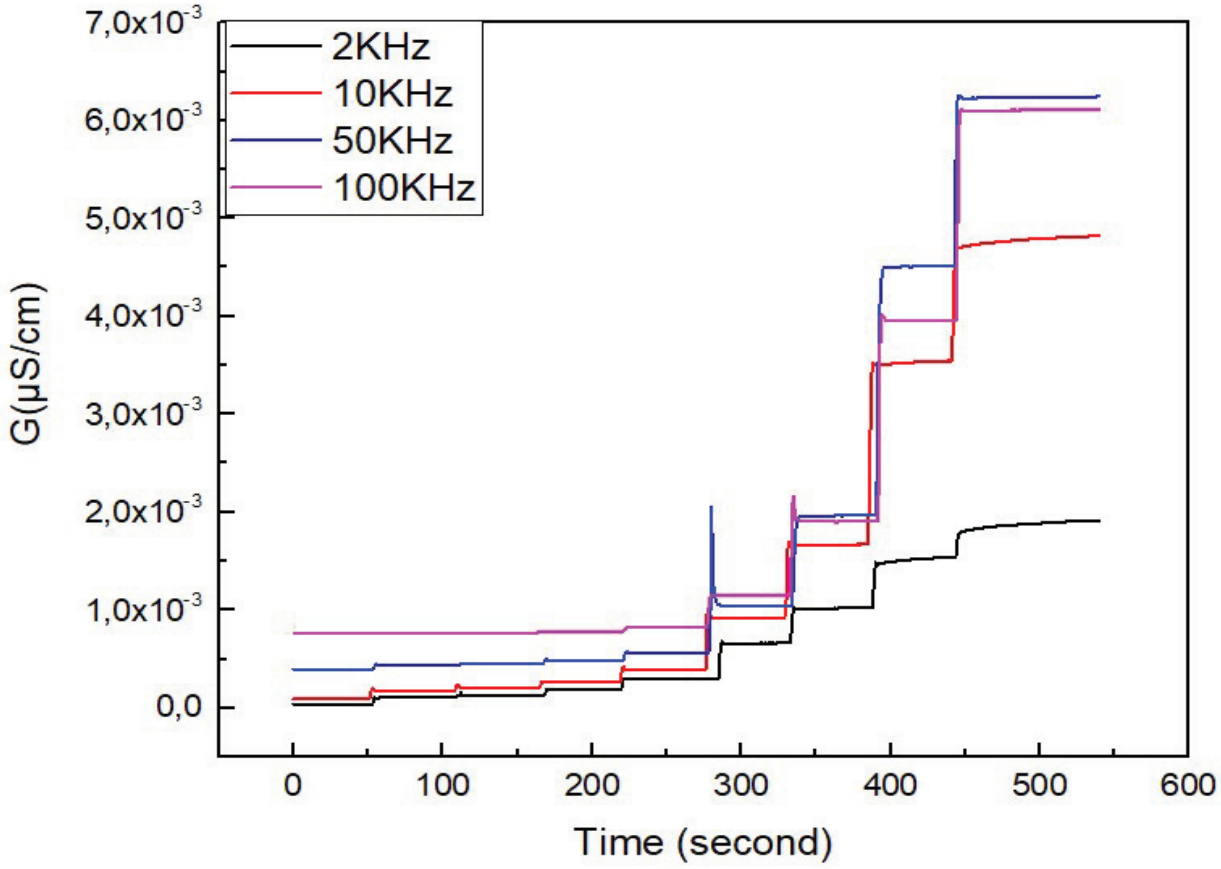

Figure 26. Kinetics of KCl detection at different frequencies

From the above result of KCl measurements with our chip at different frequencies, the frequencies at 2, 50 and 100 kHz show that conductometric signals at lower concentrations are not much visible, except for 10 kHz, which offers a significant response to KCl solutions even at low concentrations (Figure 27). Secondly, the chitosan membrane for conductive measurement is mostly affected by humidity due to its hygroscopic nature [25]. To overcome the situation, preliminary a differential measurement was carried out between the two sensors, that is the microelectrode without sensitive membrane (Reference sensor) and microelectrode with sensitive material deposited (working electrode). The response become more at 10 kHz than other frequencies. Henceforth, these two reasons allow us to make our gas detection measure at 10 kHz. The plot of conductance against KCl concentrations (M) was plotted from the above Kinetics. Even though the conductance of 50 and 100 kHz has the most prominent signal at a very high concentration, that is not good enough to be considered because they do not respond at a low concentration of KCl solutions.

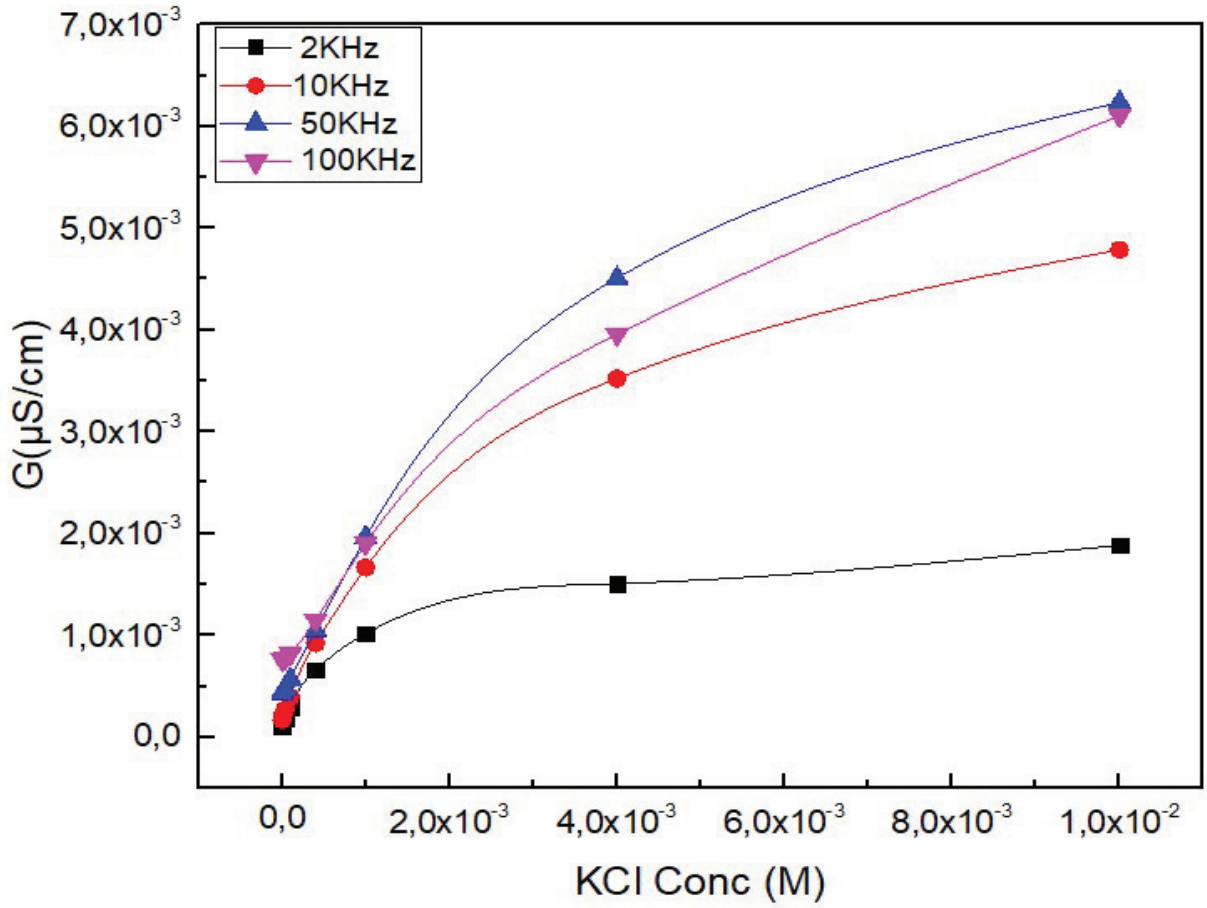

Figure 27. Calibration plot of conductance against KCl concentrations at different frequencies

III.7. Membrane preparation

III.7.1. Electrodeposition of chitosan

The electrochemical parameters for the deposit were tuned based on prior bibliographic studies conducted in our laboratory [1]. Therefore, the approach is based on gradually increasing the pH of the solution by adding 1M sodium hydroxide solution, allowing the precipitation of chitosan during the application of the potential. After a protracted homogenization, this approach creates a homogeneous chitosan solution.

- Chitosan solution (50 mL):

• 0.286 mL of acetic acid

• 49.714 mL of ultrapure water

• 0.5 g of chitosan

• Homogenization with magnetic stirring until complete dissolution

• Adjustment of the pH to 5 by adding 1M soda

The voltage provided by AC was varied as the second stage in optimizing the electrodeposition protocol. A preliminary CV of the produced chitosan solution was performed with a potential ranging from -0.8 V to 0.8 V and a scanning speed of 100 mV / s. The curve obtained is shown in Figure 28.

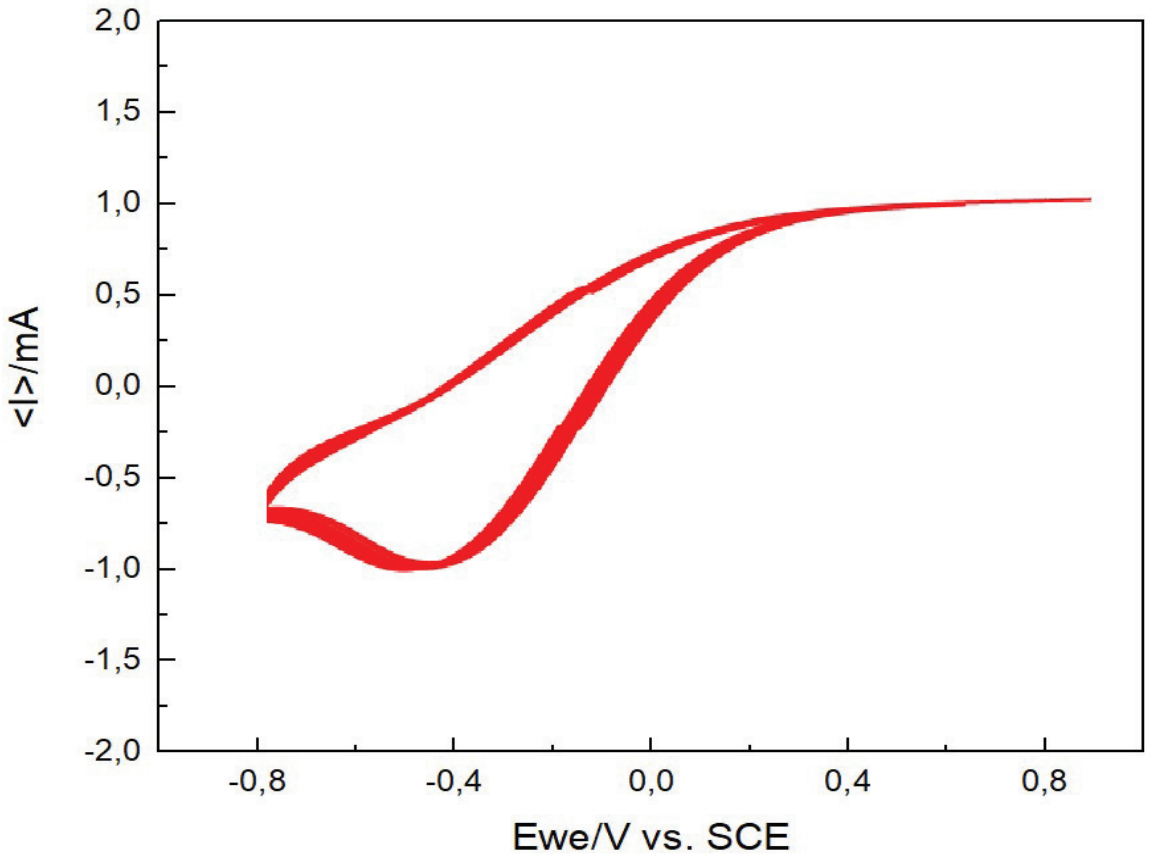

Figure 28. Cyclic voltammetry of a 1% chitosan solution

A cathode peak characterizes the electrodeposition of the polymer. The peak's intensity steadily declines, indicating polymer precipitation on the gold surface. As a result of this test, we may conclude that a constant voltage between -0.4 and 0.4 V is best for the AC, which we subsequently used. CA deposition is carried out by applying a voltage of -1.4 V based on these results. The deposition duration will be varied to investigate the effect of membrane thickness on the detecting system. The chronoamperometric curve acquired during a deposit for 5 minutes is shown in Figure 29. We can see that the intensity remains constant after 3 minutes, implying that the amount deposited does not change significantly over time.

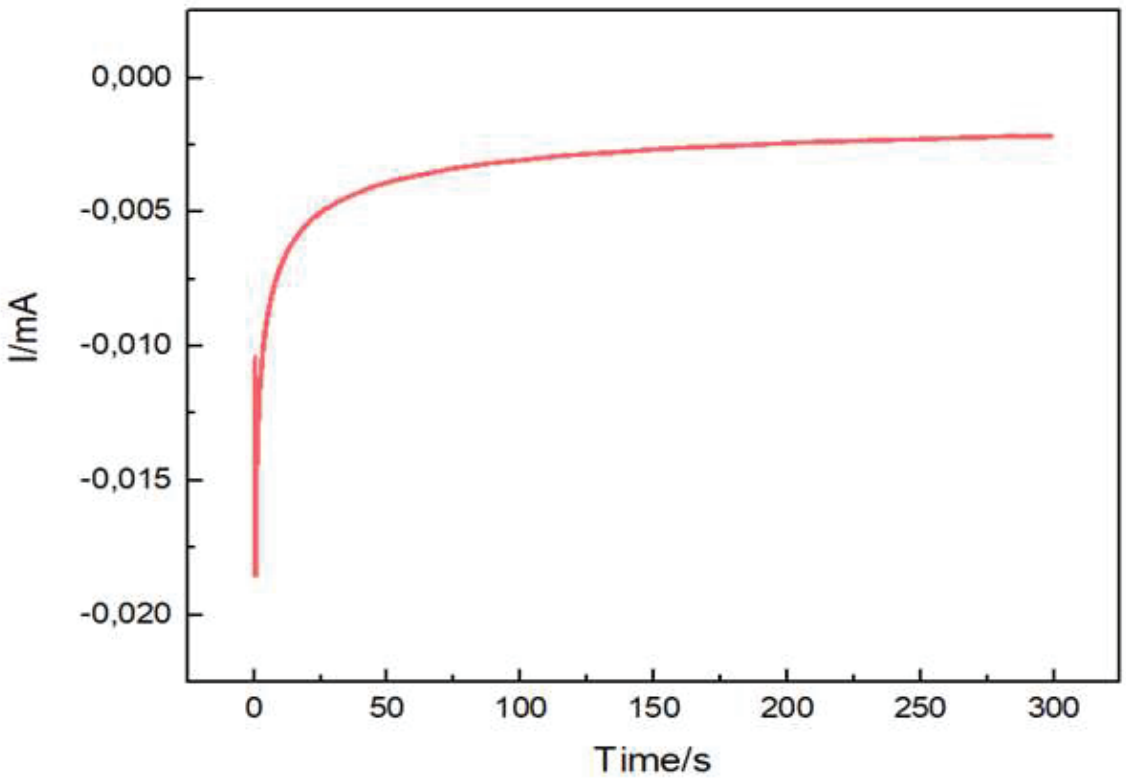

Figure 29. Chronoamperogram in a 1% chitosan solution at -1.4 V

The electrodeposited membrane was subjected to an electrochemical (CV) evaluation in a 5mM Fe(II)/Fe(III) solution buffered with PBS to investigate its blocking nature of bare gold. The following is how to make the solution that allows for this characterization:

- 5 mM ferrocyanide/ferricyanide solution

• 200 mL of ultrapure water + 1 tablet of PBS

• 0.4224 g of $Fe(CN)_6^{4-}$

• 0.3292 g of $Fe(CN)_6^{3-}$

The voltammogram obtained is presented in Figure 30.

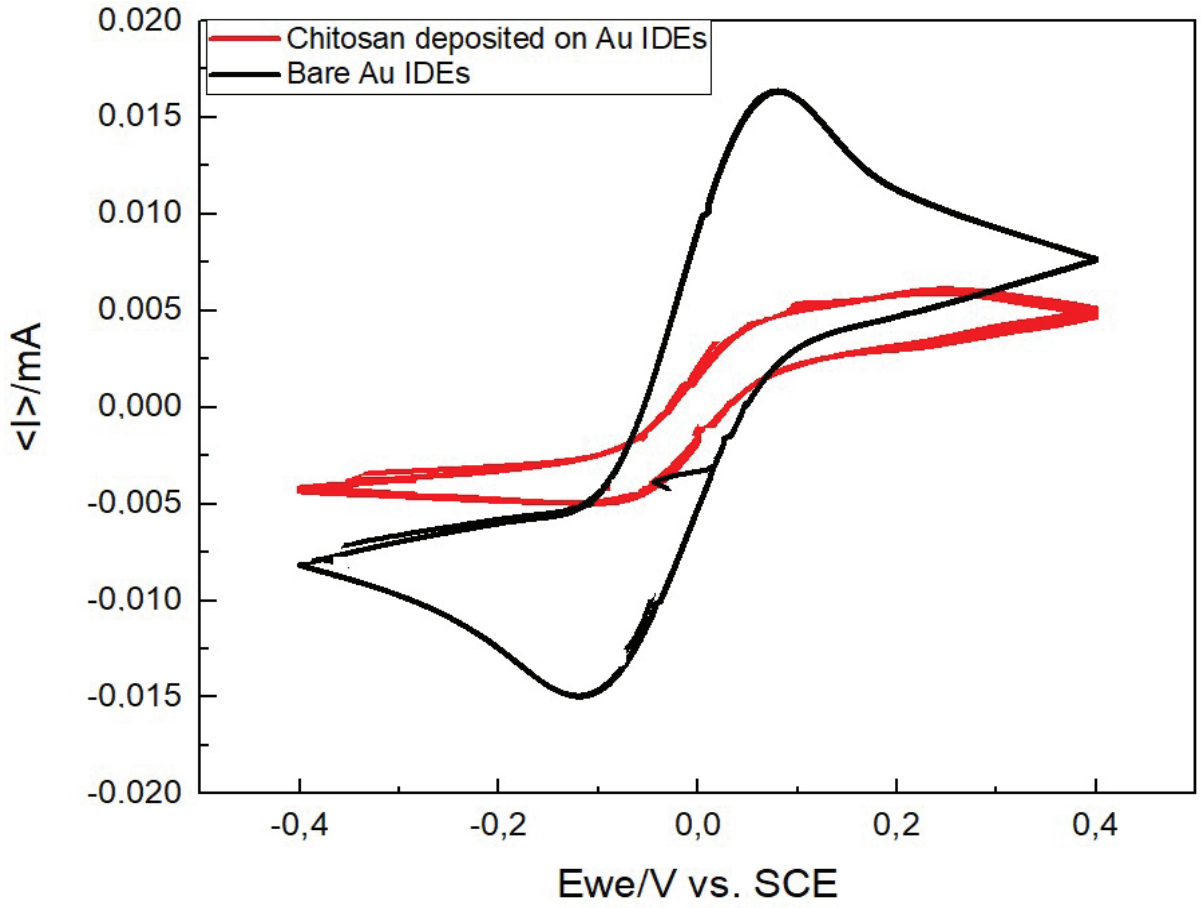

Figure 30. Voltammogram of an electrode before and after electrodeposition of chitosan

The redox peaks associated with a gold surface may be seen on both curves. We also notice a decrease in peak current, indicating that the deposit is present on the electrode's surface. Chitosan is not an electrical insulator; instead, the polymer allows electrons to be exchanged with the metallic electrodes.

We'll focus on the sensor's response in the presence of analytes now that we've perfected the method of electrodeposition of the membrane on the sensor's surface. The appendices will outline the final methodology that was optimized during this section (Figures S6 to S10).

III.7.2. Electrospinning process

PVC/NiPc mixture was prepared by dissolving 4.12 g of PVC powder in 15 mL of DMF/THF mixture (volume ratio of 1/1), at a temperature of 50°C and under a stirring speed of 500 rpm, a clear solution of the polymer was obtained after 3 h mixing. To eliminate air bubbles and stabilize the solution, it was kept at room temperature for 1 h. In parallel, a suspension of NiPc was prepared by dissolving blueish NiPc 1mg/mL in THF for overnight stirring. The solution

of PVC polymer and the NiPc suspension were mixed in a volume ratio of 4:1 respectively for further electrospinning processes.

Vertical regime of electrospinning setup was used (fig. 31). After preparation, PVC polymer/NiPc solution was loaded into a 5 mL disposable plastic syringe fitted with a Spray Base pump system and pumped with different flow rates 0.1-1mL/hr. Distance between orifice of the needle and stainless-steel flat plate collector was kept constant 15cm. Size of the blunt stainless needle was 22 gauge. Applied Voltage was in range of 7.0-18kV. Deposition time of the PVC/NiPc nanofibers for all samples was around 1min. Electrospinning process was done under normal condition (T=298 K, Pressure= 1 atm and relative humidity 40% to 50%).

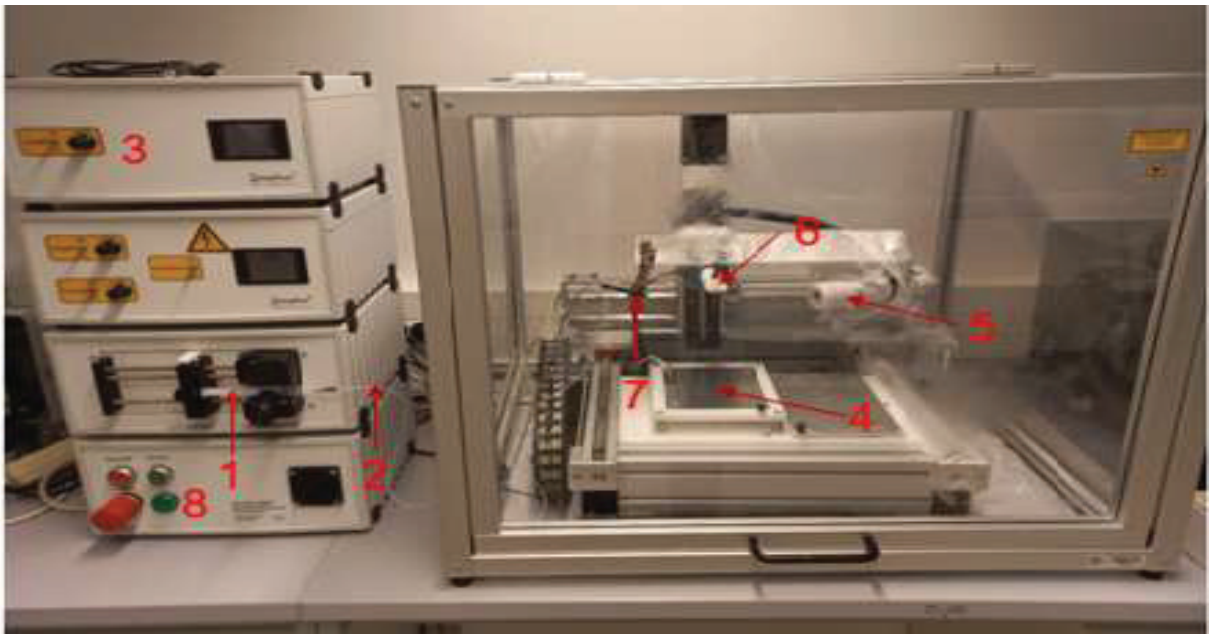

Figure 31. Electrospinning setup (1) Syringe mounted in syringe pump. (2) Tube. (3) High voltage power supply. (4) Flat plate collector. (5) CCD Camera. (6) Blunt needle with capillary tube (emitter). (7) Illumination (laser). (8) XYZ belt driven stage controller

The analysis system is based on measuring the conductance of our working electrode about a reference electrode, as mentioned in the introduction. The sort of membrane put on our sensor's surface, its thickness, and the gaseous species present, as well as their concentration, all influence its conductivity. For each type of membrane, each of these properties must be investigated.

III.8. Analytical cell for VOC detection using microsensor

A comprehensive analysis system is required to regulate all aspects mentioned above. Our first system used a cylindrical cell (Figure 32).

Figure 32. Cylindrical cell for VOC measurement

This cell has a large enough volume in comparison to the size of our sensor to allow us to create a homogeneous environment around it. The cap contains an aperture that allows the conductivity meter wiring to be routed while keeping the system tight. Finally, gas can be channeled to the sensor through two gaps on the side of the chamber.

We employ a commercial gas generator, the Liquid Calibration Unit (LCU), marketed by the business "Ionicon," to produce the gas that allows us to test our sensor, as shown in Figure 33.

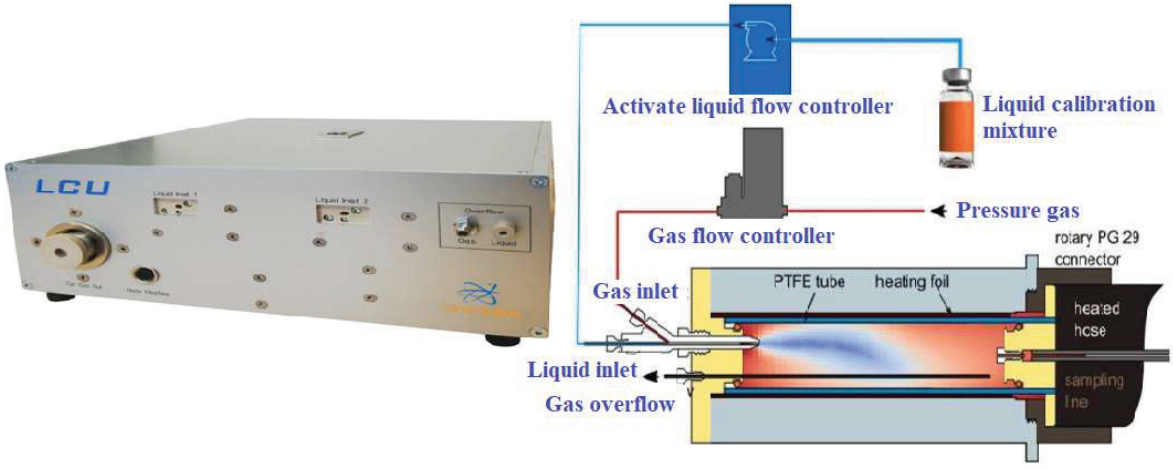

Figure 33. Views of LCU

(a) LCU front view (b) LCU operation schematic

This device not only allows to nebulize low-concentration aqueous solutions into a known-concentration gas, but it also maintains a consistent relative humidity regardless of the concentration of analytes. It accomplishes this by utilizing two pumps capable of supplying liquid flow rates varying from 0 to 50 L/min in a neutral gas nebulizer. According to industry norms, the gas flow can be regulated from 0 to 1000 cm^3 per minute ("Standard Cubic Centimeter per Minute" - sccm). We can sweep a whole field of analyte concentrations by changing these parameters. Figure 34 depicts a diagram of the entire analytical system.

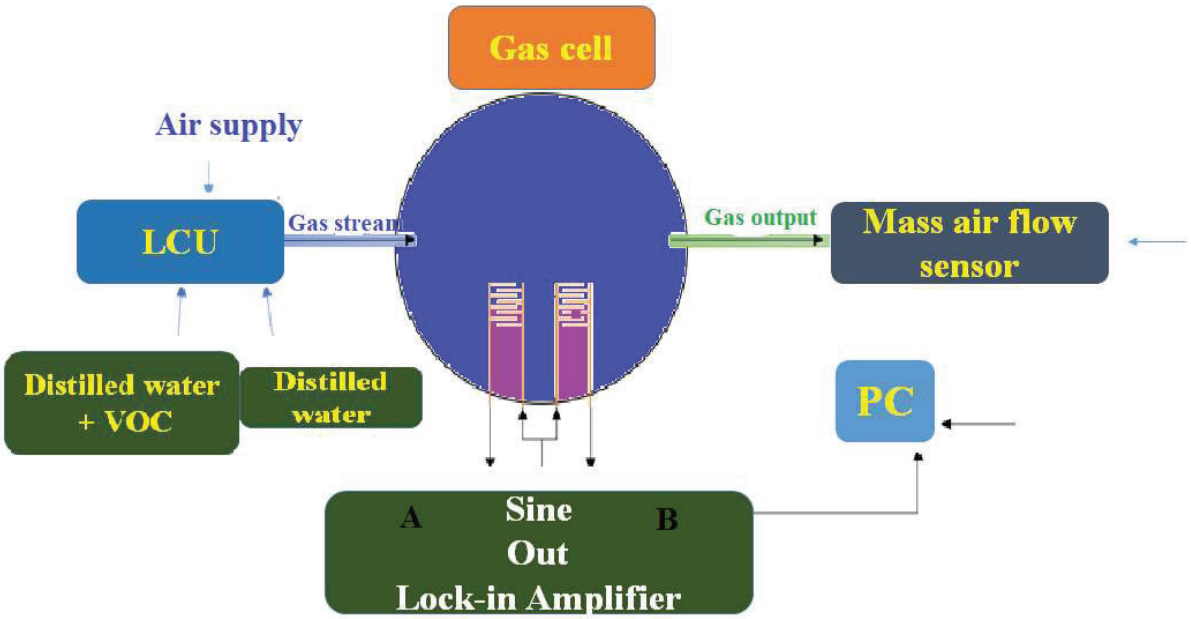

Figure 34. The components of the detection platform

III.9. Sensor response

The sensor initially reacted to a gas made up of a mixture of water and acetone. Still, the signal stayed steady even when the acetone concentrations fluctuated by a few ppm. We subjected the sensor to gases with considerable fluctuations in acetone concentrations to better understand how it reacts to acetone. The sensor was immersed in the gaseous headspace of a liquid solution to make these measurements. The headspace is created by evaporating a liquid solution, managed by a liquid-gas equilibrium system. As a result, the concentration of species in the gas phase is determined by their aqueous phase concentrations. As a result, the sensor was subjected

to pure acetone, a 50 percent acetone-water combination, and a gas containing water vapor solely. Figure 35 depicts the outcome of this investigation.

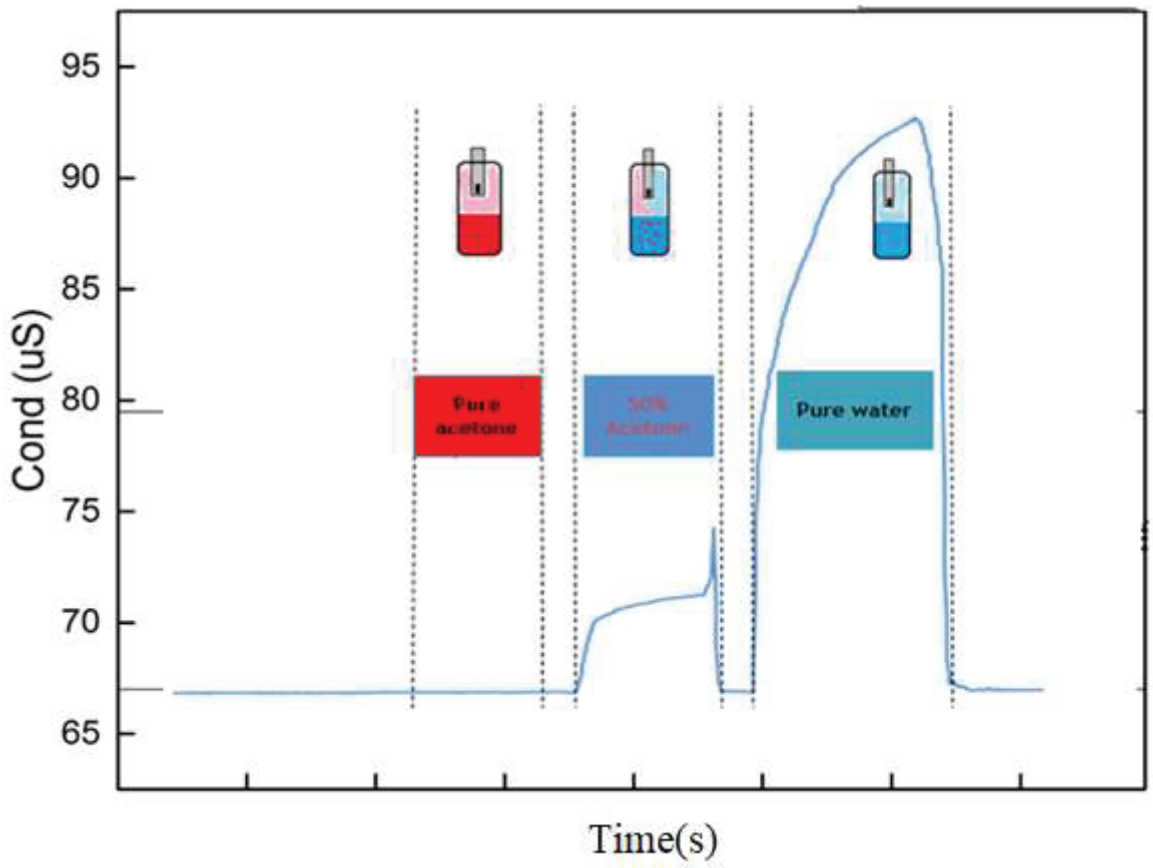

Figure 35. Conductometric headspace acetone detection

The principle of reaction of chitosan with acetone or other VOCs has not yet been well defined in the literature. The response of a sensitive layer of chitosan is dependent on the presence of water molecules and oxygen species near the chitosan particles [26]. This theory is illustrated in the mechanism of absorption of oxygen species from the surface of chitosan (Figure 36).

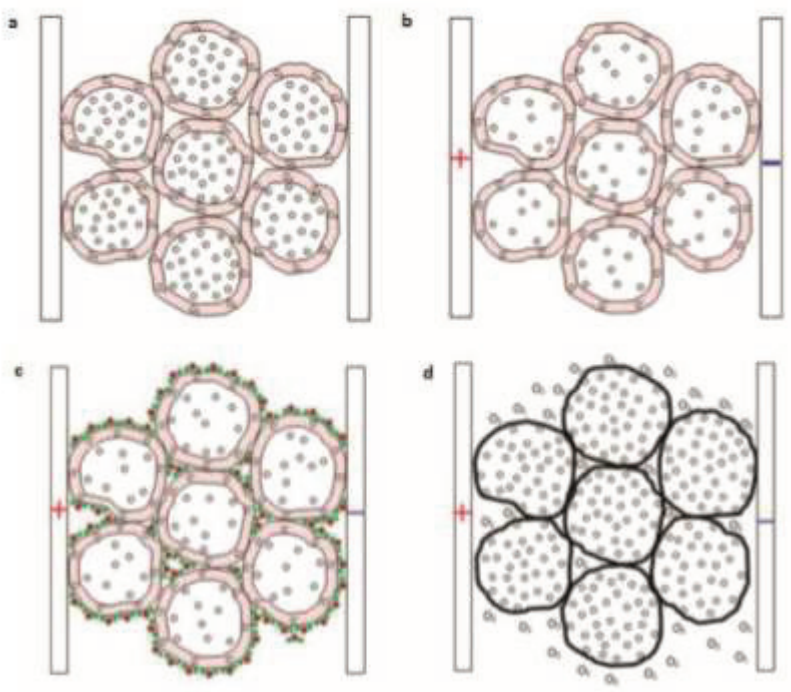

Figure 36. A chitosan sensor's response mechanism

(a) oxygen molecule absorption, (b) oxygen species production,

(c) water molecule exposure, electron release (reproduced from Ref 27)

The oxygen atoms contained in the medium are chemically absorbed on the surface of the chitosan film when it is exposed to ambient air as reported from Nasution et al [27]. (a). The number of free electrons circulating randomly in the conduction band reduces when exposed to a potential layer. Absorbed oxygen species trap electrons, passing from one chitosan particle to another. The sensor's resistance increases as a result, and the sensor's responsiveness decreases typically. The saturation of oxygen species determines this phenomenon under a predetermined equilibrium (b).

However, when the sensor is exposed to a particular flow of VOC enriched carrier gas, the gas flow contains a certain number of water molecules, which reflects the relative humidity level of the gas. These water molecules will impact the film and alter the chemical equilibrium that has been created. The molecules adhering to the chitosan particles' surfaces will react with the O- species, causing O_2 to degas and stored electrons to be released (c and d). Figure 36 depicts the mechanism that governs this reaction:

$$Chit - NH_2 + 2O^- + H_2O \leftrightarrow Chit - NH_2 + O_2 + H_2O + 2e^-$$

Surface tension is also created on the chitosan film by water molecules. This voltage encourages electron mobility by allowing oxygen species to escape. It is again accessible in the conduction band, increasing the membrane's electrical conduction. On the other hand, free electrons may find it challenging to move between available particles due to gaps between nearby particles. Figure 7 shows how the carbon chain of chitosan promotes electron circulation by forming hydrogen bonds between the hydrogen of amine groups and the oxygen of water molecules. These hydrogen bridges serve as an electrical link between particles, allowing electrons to flow freely. As a result of this notion, the sensitive layer's conductivity is strongly reliant on water molecules in the gas. In this way, we can expect its behavior to be influenced by the gas's relative humidity. Due to the presence of many water molecules, the response of our sensor will be enhanced at a high relative humidity rate.

On the other hand, VOCs are not included in the information supplied thus far. Water molecules, no VOCs, are the most susceptible to chitosan. By altering the circulation of electrons in the conduction band, the presence of VOCs in the carrier gas modifies fluctuations in membrane conductivity. Since acetone molecules have a molecular vibration that affects the water molecules on the film's surface, the previously created surface tension is then broken, resulting in the vaporization of the water molecules. As a result, the interaction between water molecules and oxygen species is diminished, which significantly affects the film's increased conductivity owing to the existence of water molecules.

Sensitivity

Because these sensors are designed to detect gas concentrations in the ppb range, it was vital to investigate the impact of sensitivity. Using many working electrodes simultaneously was one of the options explored. It is crucial to ensure that the reference electrode does not generate any signal in the presence of humid air to do this. Otherwise, we would have to utilize twice as many reference electrodes as active electrodes, but each sensor only has four of them. As a result, we conducted measurements with the various electrodes under the same conditions, namely 91 percent relative humidity (RH) at room temperature. The data in Figure 37 show that the reference has minimal effect on the magnitude of our signal. In the case of humid air, we can therefore avoid the usage of an internal connection.

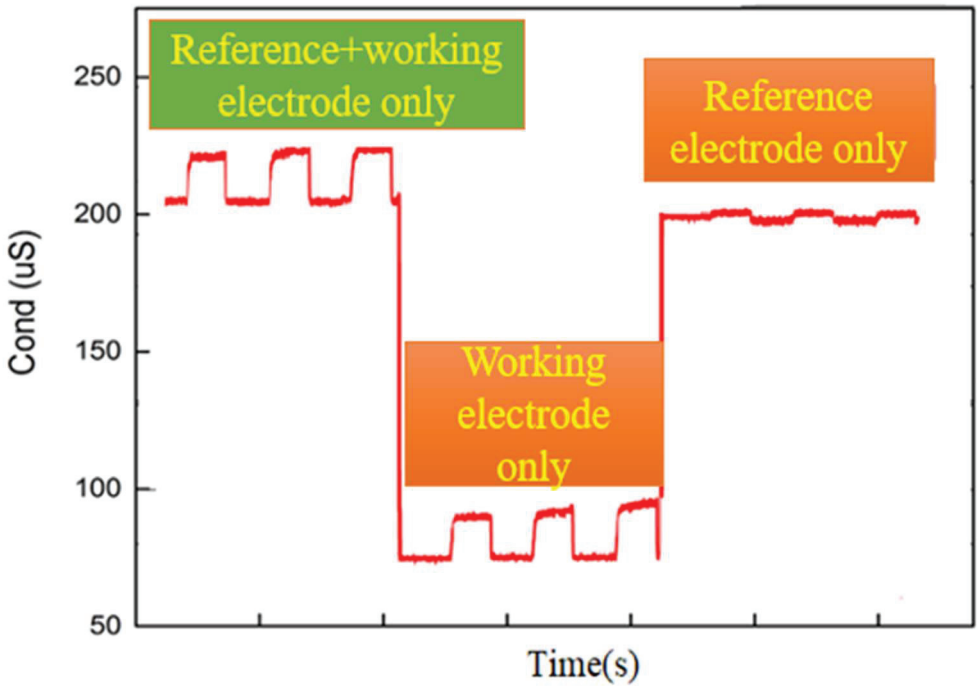

Figure 37. Signal resulting from the internal reference (IDE=reference and Chitosan on IDE=working)

The following experiments were chosen to employ three chitosan-functionalized electrodes connected. In the first plot one IDE with chitosan deposited on it connected to conductimeter and measure the signal, again 3 IDEs deposited with chitosan were connected in series to detect acetone. It was observed that the signal when 3 working electrodes were connected in series produced a higher signal. Figure 38 shows the results of an analysis performed under the previously described parameters. The increase in signal intensity is proportional to the number of electrodes employed, as can be seen. This enables us to produce higher signal-to-noise (S/N) signals at lower humidity levels than previously possible.

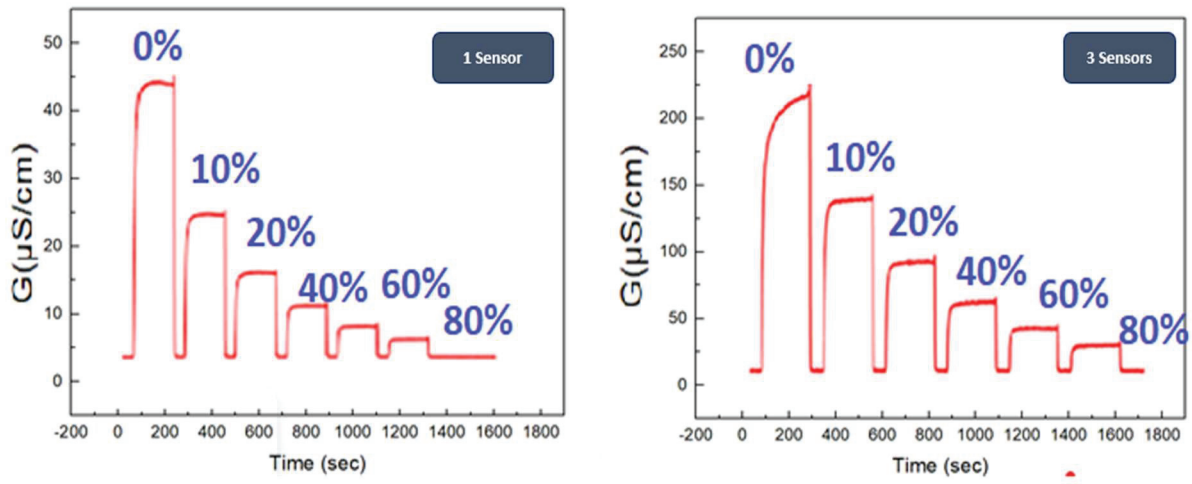

Figure 38. Acetone detection connecting multiple electrodes

III.10. Adaptation to GC-MS

System geometry

Another objective concerning these gas sensors is to adapt them to existing analysis systems. In our case, it is a matter of coupling them to a gas phase chromatography apparatus. The gas flow rates used in chromatography being much lower than those used in the cell, 1000 mL/min against 1.5 mL/min in GC, we have studied the impact this will have on the signal. For this we designed a cell with an adapted geometry (Figure 39).

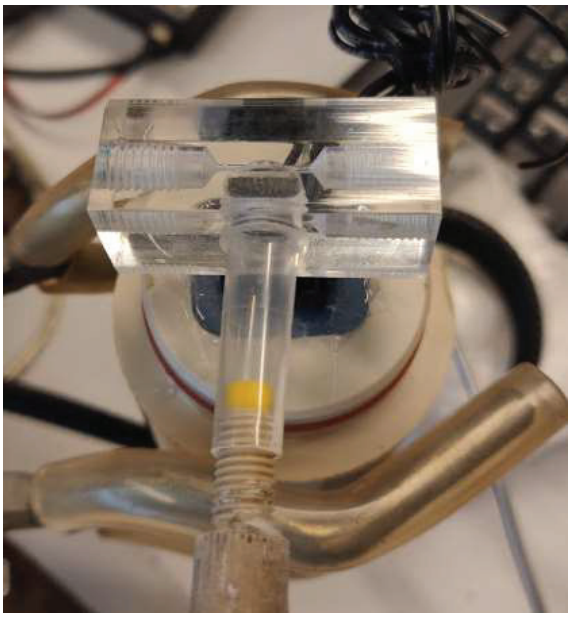

Figure 39. Gas cell for low flow rates

The carrier gas flow, at the outlet of the chromatographic column, was conveyed by a transfer line and arrived in front of the sensor in order to maximize the adsorption of water molecules and thus obtain a more intense and more reproducible signal.

Injection system

Another major difference that appears when adapting the system to the chromatograph, is that the injection of the gas to be analyzed, which was continuous, becomes instantaneous and discontinuous. Indeed, in the previous configurations, we fixed a gas flow using the LCU, then we waited for the stabilization of the sensor to determine the amplitude of the signal, on the other hand in a GC the injection is made in a punctual way with a specific volume. For this we have simulated an "instantaneous" injection system using a 6-way valve and a 250 µL sampling loop. This system, schematized in Figure 40, allowed us obtained, by the conductimeter, the results presented in Figure 41.

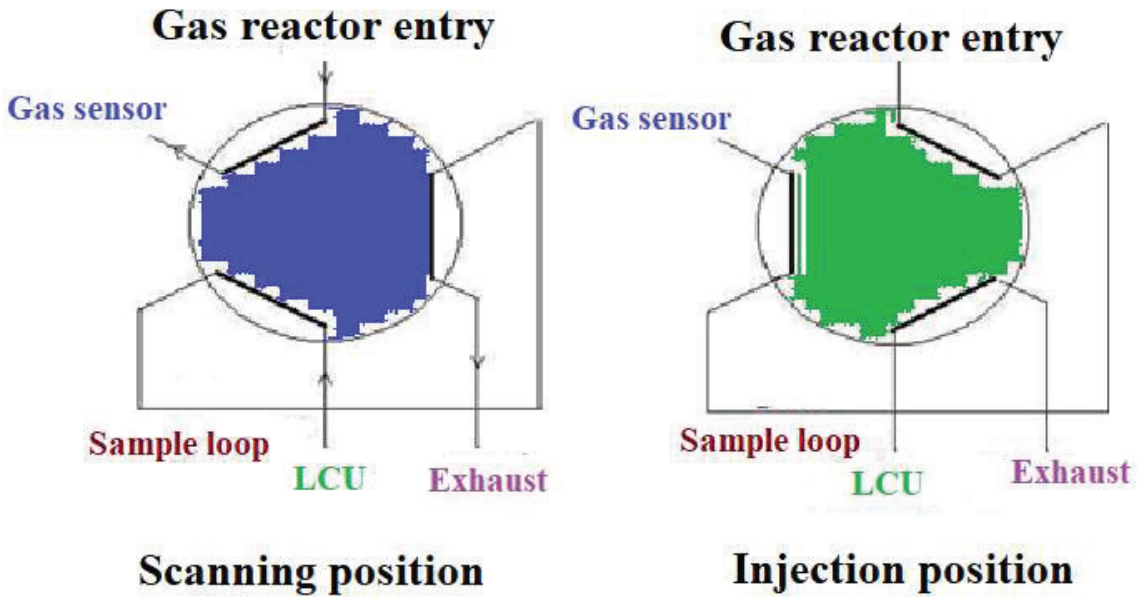

Figure 40. Diagram of the instant injection system

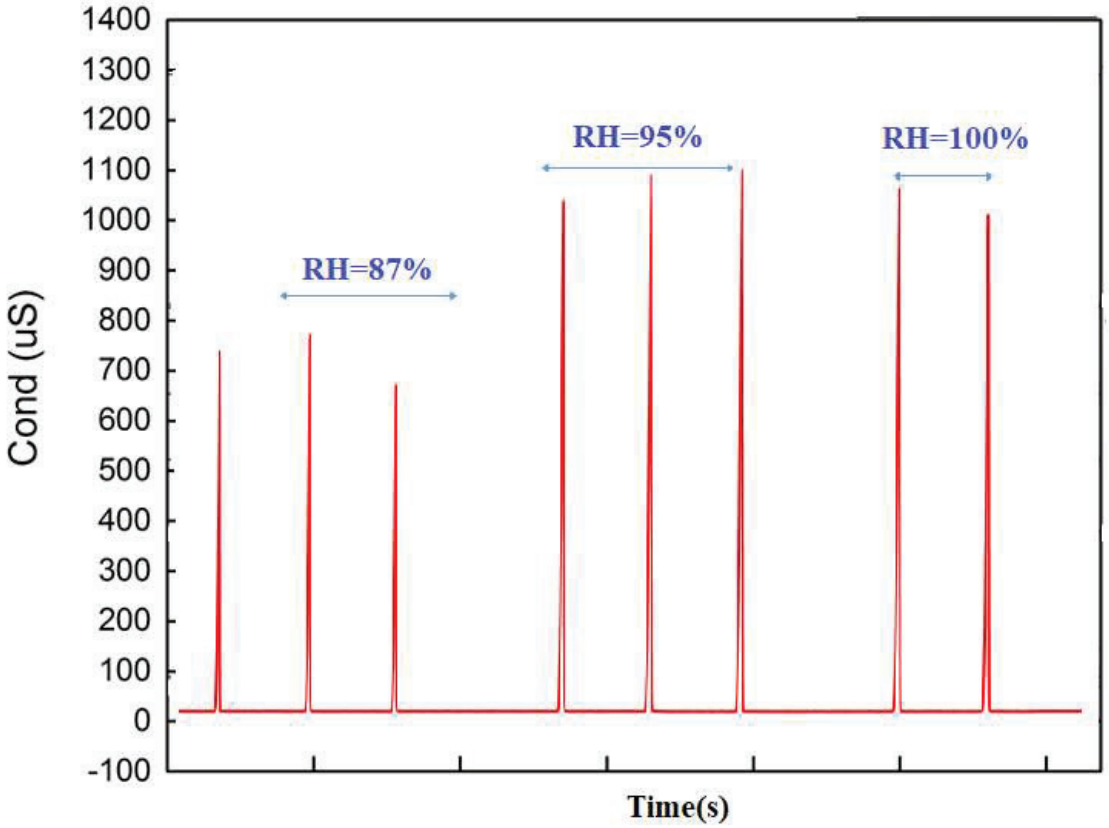

Figure 41. Conductometric measurements on an instantaneous injection system

Firstly, we can see that the surface of the peaks acquired varies with the humidity of the gas, implying that there may be a correlation between these two variables.
Secondly, at a temperature of 25°C, we were able to observe more sensitive results with a gas flow greater than 2 mL/min.

We can connect the GC to the cell now that it permits low-flow analysis, and the sensor can operate with instantaneous injection. The first step will be to analyze the gas using GC-MS to identify the chemical of interest to us, in this case, water, and determine its retention time within the column. We may then direct the gas flow to the sensor using a valve.
The GC column separates the gases, and we can identify each compound by associating a retention time with it using the mass spectrometer. This temporal element, termed retention time, will allow us to compare our sensor's response to each gas we have looked at. Because this research is focused solely on a chitosan membrane with previously established selectivity, moisture will be the primary gas of interest.
Two peaks can be seen in the total ionic current (TIC). The diluent gas, nitrogen, has the most extensive surface area and 4.5 min. The elution of water created by the LCU with a 100% RH is represented by the mass spectrum corresponding to the peak of 8.2 minutes (Figure 42, 43).

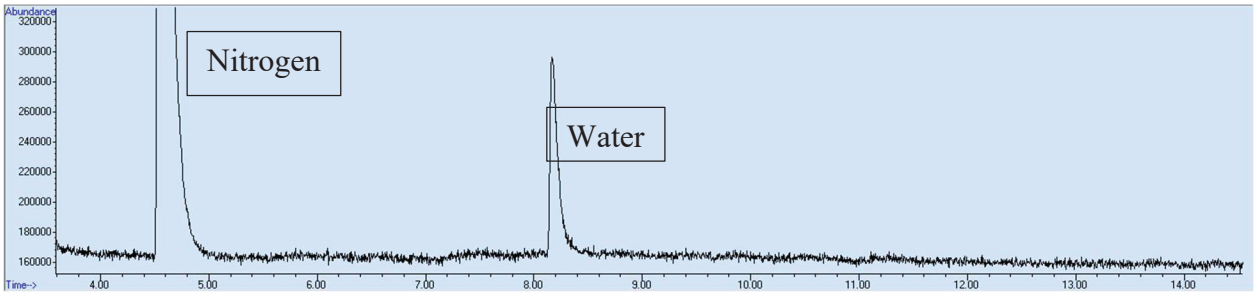

Figure 42. Chromatogram of the wet gas (RH 100%) generated by the LCU

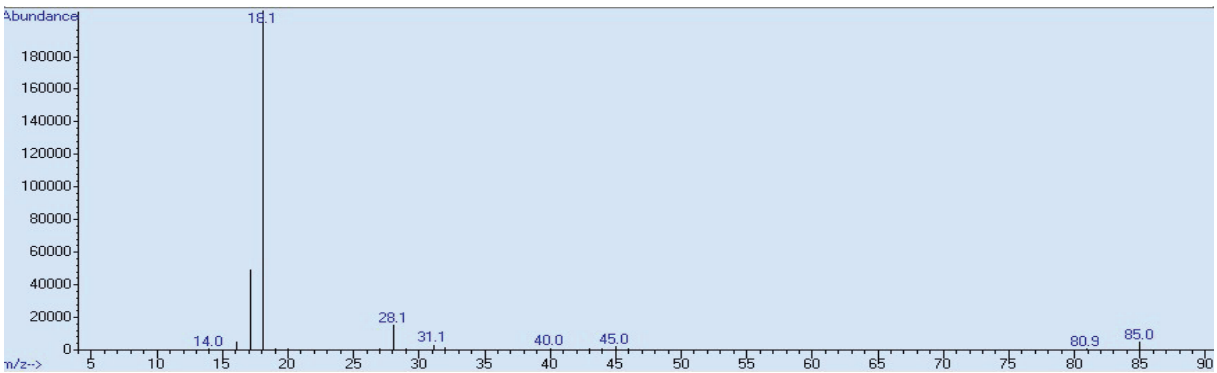

Figure 43. Mass spectrum of water

Figure 44 shows the results obtained during the coupling of our micro-sensor for analysis with a carrier gas at 3.7 mL/min.

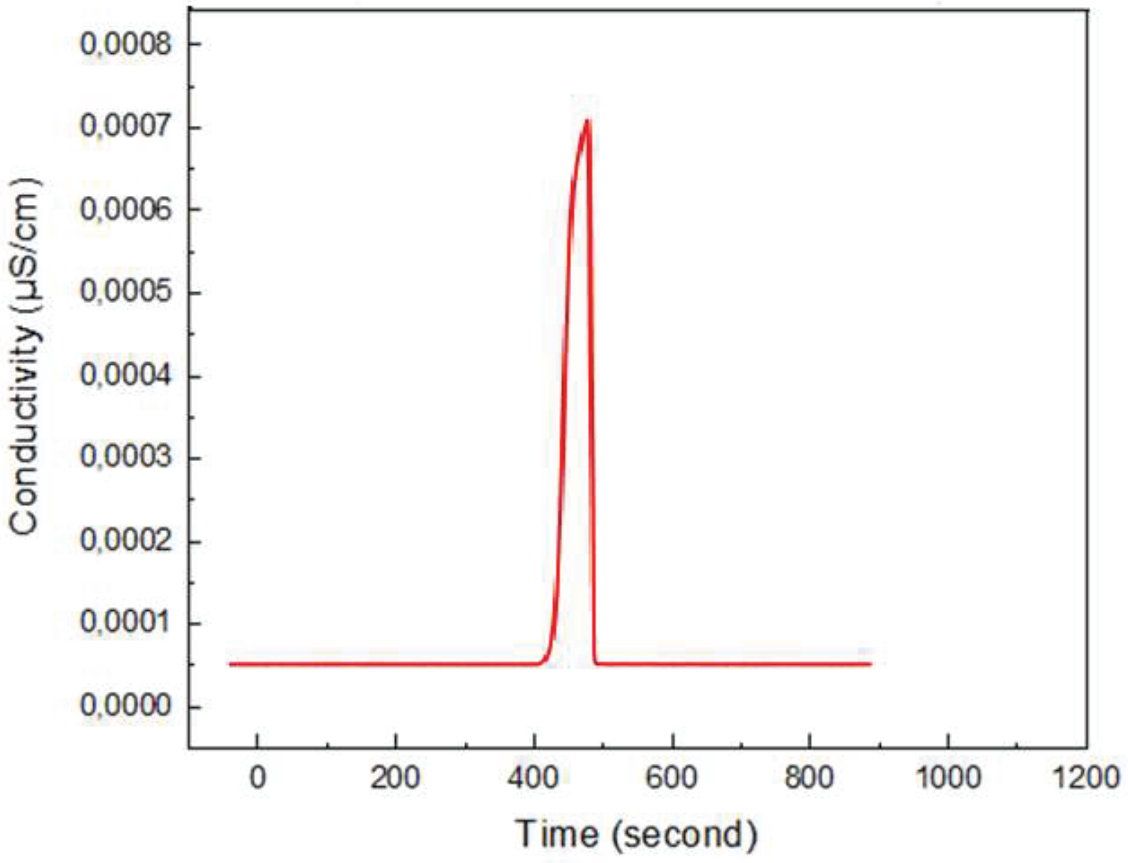

Figure 44. Sensor signal produced by water from coupled GC

Consequently, we notice that there is a signal at the column output. As a result, the sensor can detect minute quantities at low flow rates, as demonstrated by prior devices. Furthermore, the repeatability of our results is good, allowing us to contemplate employing this method for quantification. Finally, a gas dilutor has been validated to address this quantitative element and the potential of testing our sensors on various gases.

Gas dilutor

We built a gas dilutor to evaluate the affinity of our sensor for numerous gases and be able to do quantitative analyses. The latter is based on Messer-supplied and certified gas cylinders with

known concentrations and a flow controller to establish the dilution factor to be applied. The following equation determines the ultimate gas concentration:

$$C_f = C_i * \frac{F_G}{F_G + F_D}$$

Cf: Final gas concentration

Ci: concentration of gas in the bottle

F_G: Bottle gas flow

F_D: Diluent gas flow rate

The principle of the diluter is therefore based on the use of 3 commercial bottles with gas concentrations of 300,000 ppm, 150,000 ppm and 1,000 ppm. The flow rates achievable by the flow controllers made it possible to scan a range of concentrations extending from 100 to 300,000 ppm. The measurements were carried out using a GC-MS, on three common gases present in the standard cylinders: methane (CH_4), ethane (C_2H_6) and carbon dioxide (CO_2). Figure 45 represents the surfaces obtained as a function of the concentrations of methane. It can therefore be seen that the system responds linearly. The uncertainties represented here by the prediction envelope were calculated for a confidence rate of 95%.

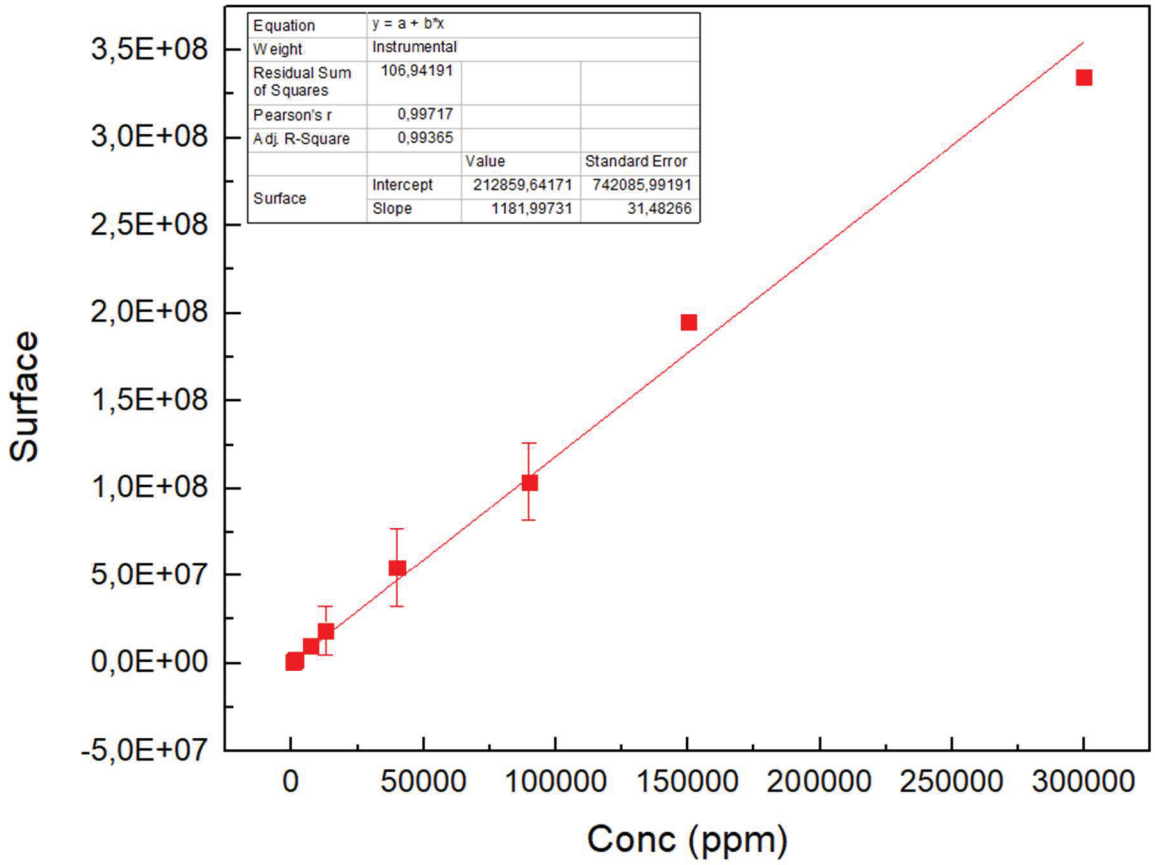

Figure 45. Gas dilutor validation for methane

III.11. Conclusions

We worked on a polymeric chitosan membrane during our research for the functionalization of the sensor by an acetone-sensitive layer. We chose a method for preparing an acid chitosan solution, the various processes were tuned to produce a homogeneous and repeatable deposit on the IDE's surface. A functionalization procedure based on cyclic voltammetry (CV) electro-addressing of the chitosan membrane on the surface of the microelectrode has been optimized. The functionalized sensors were evaluated (bottles containing a mixture of distilled water and solvents). The sensor is sensitive to the water molecule and provides fast response and recovery times and a stable and reproducible signal.

The sensors were then put in a gas flow. The sensor's response to gas flow at various relative humidity levels has been proven. Because the reaction of our sensor increases with the level of humidity, the qualities of our membrane have been validated. Because the study aims to

quantify the minor changes in humidity caused by adding species in solution, this feature is quite promising.

Finally, the sensor's reaction was tested with gas chromatography analysis settings. We can evaluate the selectivity of our sensor against these gases without needing to work with pure samples using this technique for separating gases in a mixture. Also, the use of a gas diluter, which was validated, allows for working with wide range of concentrations and avoids some of the issues that occur using numerous samples.

III.12. References

[1] A. Madaci, G. Raffin, C. Pages, C. Jose, M. Martin, H. Ferkous, A. Bouzid, J. Bausells, A. Alcacer, A. Errachid, N. Jaffrezic-Renault., "A microconductometric ethanol sensor prepared through encapsulation of alcohol dehydrogenase in chitosan: application to the determination of alcoholic content in headspace above beverages," *J Mater Sci: Mater Electron*, vol. 32, no. 13, pp. 17752–17763, Jul. 2021, doi: 10.1007/s10854-021-06311-9.

[2] M. Ender, J. Illig, and E. Ivers-Tiffée, "Three-Electrode Setups for Lithium-Ion Batteries," *J. Electrochem. Soc.*, vol. 164, no. 2, p. A71, Dec. 2016, doi: 10.1149/2.0231702jes.

[3] N. Elgrishi, K. J. Rountree, B. D. McCarthy, E. S. Rountree, T. T. Eisenhart, and J. L. Dempsey, "A Practical Beginner's Guide to Cyclic Voltammetry," *J. Chem. Educ.*, vol. 95, no. 2, pp. 197–206, Feb. 2018, doi: 10.1021/acs.jchemed.7b00361.

[4] J.-F. Lemineur, J.-M. Noël, C. Combellas, and F. Kanoufi, "Optical monitoring of the electrochemical nucleation and growth of silver nanoparticles on electrode: from single to ensemble nanoparticles inspection," *Journal of Electroanalytical Chemistry*, vol. 872, p. 114043, Sep. 2020, doi: 10.1016/j.jelechem.2020.114043.

[5] C. Montella, V. Tezyk, E. Effori, J. Laurencin, and E. Siebert, "Linear sweep and cyclic voltammetry of porous mixed conducting oxygen electrode: Formal study of insertion, diffusion and chemical reaction model," *Solid State Ionics*, vol. 359, p. 115485, Jan. 2021, doi: 10.1016/j.ssi.2020.115485.

[6] J. M. Pingarrónm, J. Labuda, J. Barek, C. M. A. Brett, M. F. Camoes, M. Fojita, D. B. Hibbert., "Terminology of electrochemical methods of analysis (IUPAC Recommendations 2019)," *Pure and Applied Chemistry*, vol. 92, no. 4, pp. 641–694, Apr. 2020, doi: 10.1515/pac-2018-0109.

[7] F. Ruffino and M. G. Grimaldi, "Nanoporous Gold-Based Sensing," *Coatings*, vol. 10, no. 9, Art. no. 9, Sep. 2020, doi: 10.3390/coatings10090899.

[8] C. Sandford, A. M. Edwards, J. K. Klunder, P. D. Hickey, M. Li, K. Barman, S. M. Sigman, S. H. White, D. S. Minteer., "A synthetic chemist's guide to electroanalytical tools for studying reaction mechanisms," *Chemical Science*, vol. 10, no. 26, pp. 6404–6422, 2019, doi: 10.1039/C9SC01545K.

[9] S.-J. Lee, Y.-J. Park, and H.-L. Choi, "Efficient sensor network planning based on approximate potential games," *International Journal of Distributed Sensor Networks*, vol. 14, no. 6, p. 1550147718781454, Jun. 2018, doi: 10.1177/1550147718781454.

[10] N. Dey, A. S. Ashour, W. S. Mohamed, and N. G. Nguyen, *Acoustic Sensors for Biomedical Applications*. Springer, 2018.

[11] D. Grieshaber, R. MacKenzie, J. Vörös, and E. Reimhult, "Electrochemical Biosensors - Sensor Principles and Architectures," *Sensors (Basel)*, vol. 8, no. 3, pp. 1400–1458, Mar. 2008, Accessed: Dec. 17, 2021. [Online]. Available: https://www.ncbi.nlm.nih.gov/pmc/articles/PMC3663003/

[12] A. Tinti, V. Tugnoli, S. Bonora, and O. Francioso, "Recent applications of vibrational mid-Infrared (IR) spectroscopy for studying soil components: a review," *j. cent. eur. agric.*, vol. 16, no. 1, pp. 1–22, 2015, doi: 10.5513/JCEA01/16.1.1535.

[13] A. M. Hofmeister, E. Keppel, and A. K. Speck, "Absorption and reflection infrared spectra of MgO and other diatomic compounds," *Monthly Notices of the Royal Astronomical Society*, vol. 345, no. 1, pp. 16–38, Oct. 2003, doi: 10.1046/j.1365-8711.2003.06899.x.

[14] A. Agrawal, A. Singh, S. Yazdi, A. Singh, G. K. Ong, K. Bustillo, R. W. Johns, E. Ringe, D. J. Milliron ., "Resonant Coupling between Molecular Vibrations and Localized Surface Plasmon Resonance of Faceted Metal Oxide Nanocrystals," *Nano Lett.*, vol. 17, no. 4, pp. 2611–2620, Apr. 2017, doi: 10.1021/acs.nanolett.7b00404.

[15] J. C. Tarafdar and R. Raliya, *Nanotechnology*. Scientific Publishers, 2012.

[16] C. Guo and S. C. Singh, *Handbook of Laser Technology and Applications: Lasers Applications: Materials Processing and Spectroscopy (Volume Three)*. CRC Press, 2021.
[17] A. Lacan, F. M. Breon, A. Rosak, F. Brachet, L. Roucayrol, P. Etcheto, C. Casteras, Y. Salaun., "A static Fourier transform spectrometer for atmospheric sounding: concept and experimental implementation," *Optics Express*, vol. 18, no. 8, p. 8311, 2010, doi: 10.1364/OE.18.008311.
[18] F. Krumeich, "Properties of Electrons, their Interactions with Matter and Applications in Electron Microscopy," Laboratory of Inorganic Chemistry, ETH Zurich, Vladimir-Prelog Weg 1, 8093 Zurich, Switzerland p. 24.
[19] A. Suri, A. Pratt, S. Tear, C. Walker, and M. El-Gomati, "Next generation secondary electron detector with energy analysis capability for SEM," *J Microsc*, vol. 279, no. 3, pp. 207–211, Sep. 2020, doi: 10.1111/jmi.12867.
[20] A. M. Zambrano Arévalo *et al.*, "Conceptual approach to thermal analysis and its main applications," *Prospectiva*, vol. 15, no. 2, pp. 117–125, Dec. 2017, doi: 10.15665/rp.v15i2.1166.
[21] A. A. Escárcega-Galaz, D. I. Sánchez-Machado, J. López-Cervantes, A. Sanches-Silva, T. J. Madera-Santana, and P. Paseiro-Losada, "Characterization data of chitosan-based films: Antimicrobial activity, thermal analysis, elementary composition, tensile strength and degree crystallinity," *Data in Brief*, vol. 21, pp. 473–479, Dec. 2018, doi: 10.1016/j.dib.2018.09.121.
[22] D. G. B. Armen, "Phase sensitive detection: the lock-in amplifier," Department of Physics and Astronomy 401 Nielsen Physics Building The University of Tennessee Knoxville, Tennessee 37996-1200 p. 40.
[23] K. Huang, Y. Geng, X. Zheng, D. Chen, Z. Cai? M. Wang, Z. Zhu, Z. Wang., "A Wide-Band Digital Lock-In Amplifier and Its Application in Microfluidic Impedance Measurement," *Sensors (Basel)*, vol. 19, no. 16, p. E3519, Aug. 2019, doi: 10.3390/s19163519.
[24] P.-C. Wang, Y. Dan, and L.-H. Liu, "Effect of thermal treatment on conductometric response of hydrogen gas sensors integrated with HCl-doped polyaniline nanofibers," *Mater. Chem. Phys.*, vol. 144, no. 1–2, pp. 155–161, Mar. 2014, doi: 10.1016/j.matchemphys.2013.12.035.
[25] F. Zouaoui, S. Bourouina-Bacha, M. Bourouina, N. Jaffrezic-Renault, N. Zine, and A. Errachid, "Electrochemical sensors based on molecularly imprinted chitosan: A review," *TrAC Trends in Analytical Chemistry*, vol. 130, p. 115982, Sep. 2020, doi: 10.1016/j.trac.2020.115982.
[26] S. H. Othman, N. R. A. Kechik, R. A. Shapi'i, R. A. Talib, and I. S. M. A. Tawakkal, "Water Sorption and Mechanical Properties of Starch/Chitosan Nanoparticle Films," *Journal of Nanomaterials*, vol. 2019, p. e3843949, Mar. 2019, doi: 10.1155/2019/3843949.
[27] T. I. Nasution, I. Nainggolan, S. D. Hutagalung, K. R. Ahmad, and Z. A. Ahmad, "The sensing mechanism and detection of low concentration acetone using chitosan-based sensors," *Sensors & Actuators: B. Chemical*, vol. Complete, no. 177, pp. 522–528, 2013, doi: 10.1016/j.snb.2012.11.063.

Chapter IV

Development of a chitosan/nickel phthalocyanines composite based conductometric micro-sensor for methanol detection

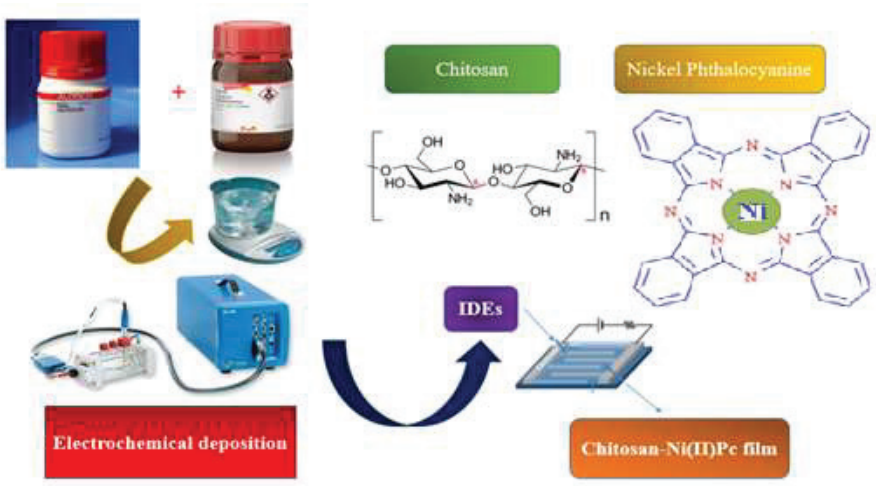

IV.1. Introduction

Methanol concentration in human blood can be measured non-invasively in exhaled breath [1], similar to ethanol, which is commonly used by legal enforcement agencies [2]. The main objective is thus to detect methanol selectively in the presence of a significantly greater ethanol environment, which is common after sipping contaminated alcoholic beverages and during therapy where ethanol is employed as an antidote [3]. Fraudsters in some countries use methanol instead of ethanol in homemade wine because it is less expensive and more frequently available. As a result, increasing public aware- ness about the lethal implications of consuming counterfeit alcohol supplied on the black market is critical [4]. Simple ways for screening alcoholic beverages to prevent methanol poisoning may be even more intriguing [5]. When methanol poisoning is not detected early enough, it can cause blindness, organ failure, and even death [6]. There is currently no methanol detector available for early breath analysis diagnosis or screening of contaminated beverages.

Furthermore, advanced development in analytical technologies for detecting and measuring methanol in clinical matrices raised significant concern for their application in evaluating volatile organic diagnostic potential for different types of diseases [7]. VOCs were initially analyzed by analytical techniques such as coupled gas chromatography with mass spectroscopy or chemiluminescence [8]. Each of these techniques has its own merits and demerits [9]. Indeed, the GC-MS operates to separate the VOCs in a chromatography column, then their identification by mass spectroscopy [10]. This technique has a low detection limit of about one hundred ppb and good selectivity. However, it involves complex measurement procedures and imposes expensive laboratory measurements. As for chemiluminescence, it consists of studying the light produced by returning to the ground state of a molecule previously excited by a chemical reaction [11]. It has the advantage of being a portable technique, however, it causes analytical difficulties for multiple detections of distinct species [12]. As such, these traditional ways of analyzing VOCs become time-consuming, convoluted, very expensive, and unsuitable for widespread screening. In this respect, discovering a rapid, reliable, economical, and portable method is of uppermost need before breath analysis attains a clinical reality [13]. Researchers paid much attention worldwide in numerous gas species detection, quite many transduction principles focused with a high percentage pointed at the miniaturized ones. The main form of operation studied in sensing approaches and promoting sensing results is here outlined: sensing transducers based on nanomaterials [14], acoustic wave [15], cantilever resonance [16, 17], resistance or capacitive changes [18]. The last among the sensor is the conductometric sensor.

Conductometric gas sensors are most widely among the known and utilized researched devices for controlling dangerous and flammable gases in medical diagnosis, industrial processes, and environmental studies. Conductometric sensors feature a straightforward design that consists of only two components: a sensitive conducting layer and contact electrodes. A DC voltage, usually applied, in the range of 1-10 V, to the device to produce the measurement, and the current flowing through the electrodes is monitored as the response.

Chemical species interact with the sensitive layer, changing its electrical conductivity as a result. The change in resistance/conductivity of a sensitive layer because of processes (adsorption, chemical reactions, diffusion, catalysis, charge transfer) occurring on the surface of the sensing area is the base of conductometric sensor functioning [19]. Change in electrical conductivity as a response is due to the interactions between chemical species (Analyte) and the sensitive film.

This study will focus on implementing chitosan sensitive membrane doped with gas sensitive ionophores developed based on the previous research where only chitosan was employed for the detection of gaseous compounds [20].

Metallophthalocyanines are a group of coordination compounds, which tend to have the capability to act as a chemically reactive and sensitive film as a factor of enormous physical properties impelled upon them through interaction with a large number of VOCs [21].

Early researchers described phthalocyanine sensors [22-24]. These researchers reported that NO_2 has large effects (6–8 orders of magnitude) on the conductivity of some sublimated phthalocyanine films. It is hoped that suitable substitutions of metals in the cavity and organic substituents at the periphery of the phthalocyanine structure can be used to develop gas specificity. Chemical and electrochemical oxidation methods were used to investigate the direct integration of phthalocyanine into conducting polyaniline, polypyrrole, and polythiophene. The chemical sensitivity analyses of conducting polymers functionalized with copper and nickel phthalocyanine, particularly polyaniline (PANI CuPc) polypyrrole (PPy NiPc), and polythiophene, are the focus of this work (PT CuPc). The chemical vapors of nitrogen dioxide, ammonia, and alcohol were investigated on these polymers. They are mostly used as thin-film semiconducting gas sensors solely for the detection of various VOCs. However, the main properties of phthalocyanines in detection abilities for environmentally relevant volatile organic compounds are particularly, their ionization potential's ability, which can as well be varied by metal-ion insertion and besides by the attachment of other atoms or groups that trigger or diminish the ionization potential in preference of their position in the electro-negativity scale [25]. An important approach to get control of some of the physical limitations of most

phthalocyanines, including the bad processability and higher crystallinity for chemosensing, comprises combining these materials with polymers [26], such as polyvinyl alcohol (PVA), polystyrene (PS), polymethyl methacrylate (PMMA) [27], etc. Phthalocyanines are functionalized in the polymer through dissolution, in a common solvent and deposited by a common solution processing. These techniques are solvent casting, spin coating, electrostatic layer-by-layer technique, or in some cases, to see the possibility of electrochemical deposition [9]. Ali and coworkers [28] reported that phthalocyanine blended polymeric materials were demonstrated to be less crystal-line, have higher conductivity, and more efficient gas sensing than pure phthalocyanines. This paves the way for the careful fabrication and design of an optimized thin film having different degrees of sensitivity, selectivity, and stability (3S). However, these films are considered to undergo high chemical and thermal stability concerning many environmental conditions. The films are easily made through the following coating techniques as, sublimation, spraying, spin, and smearing coating, or through electrochemical deposition. Previous studies have classified the interactions between the Pc and VOCs into the irreversible chemical affinity, reversible (normal charge-transfer) chemical reaction, or in some time, bulk sorption [28].

In other to achieve a more efficient gas sensor in terms of sensitivity, selectivity, and stability towards gas detection, we here electrodeposited a chitosan biopolymer film on the gold substrate and later doped it with nickel phthalocyanine as a sensitive composite film on the gold electrode. Both processes were conducted separately, due to the incompatibility of solvent solubility. A conductometric methanol sensor, working at ambient temperature was then obtained.

IV.2. Materials and Methods

IV.2.1. Chemicals and Reagents

All reagents and solvents in this work were of analytical reagent grade and were used as received without further purification. Chitosan lower molecular weight (deacetylated chitin, degree of acetylation 85-95 % Mw = 230 kDa), glacial acetic acid (99.9 %), nickel phthalocyanine (NiPc) (dye content 85 %), THF (98 %), 0.1 M sodium hydroxide solution, potassium chloride (99.0 %), ethanol (99.5 %), methanol 99.9 %) and acetone (99.0 %) were all procured from Sigma Aldrich.Ultra-pure water (UPW) (resistivity > 180 Ohm.cm) was used throughout this research work, which was obtained from a Millipore System.

IV.2.2. Fabrication and Cleaning of Encapsulated Interdigitated Microelectrodes

Interdigitated gold microelectrode chip was fabricated using silicon technology including physical vapor deposition technique and photolithography, as described in Figure 46. The fabrication procedures were carried out in CNM-CSIC, Barcelona, Spain. The size of the silicon chip was 7300 × 4000 µm. Finger width was 60 µm.

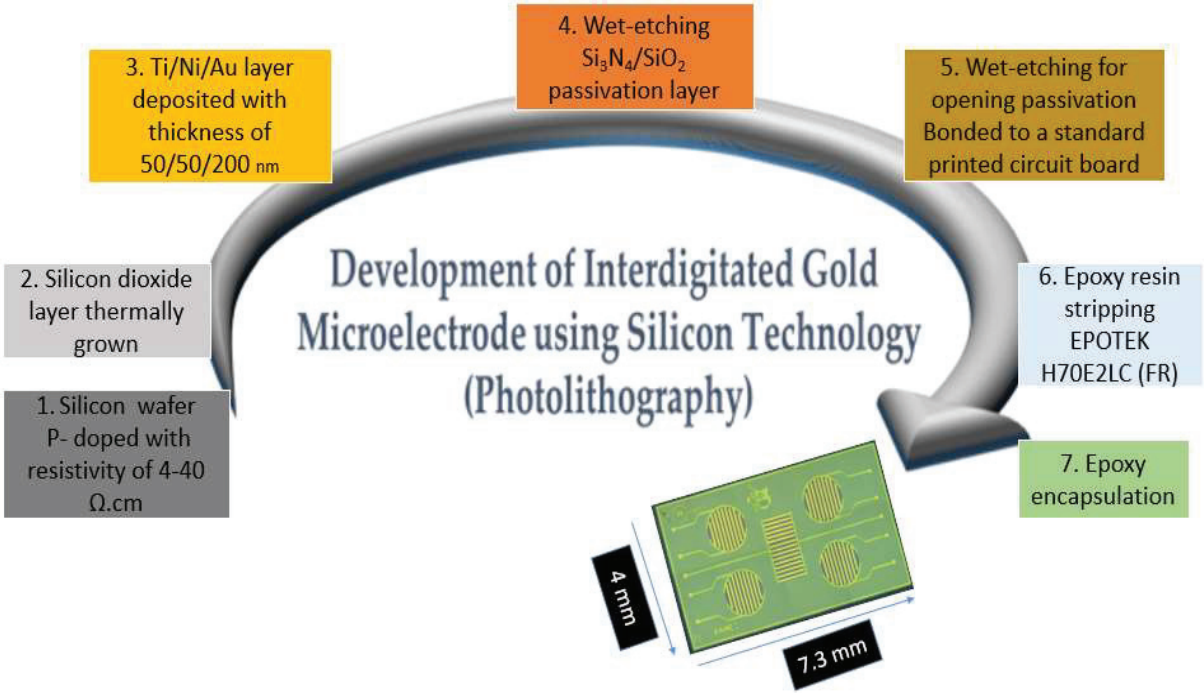

Figure 46. Different steps for the fabrication of interdigitated gold microelectrodes

The finger distance was similar to the finger width. The interdigitated electrodes areas present the following dimensions: diameter of 1200 µm for the 4 circular devices, and 1740 µm× 900 µm for the central rectangular device. Immediately after the microelectrode was manufactured, we fixed it on the printed circuit board, connected it through wire bonding, and passivated it with epoxy resin.

IV.2.3. Instrumentation

The electrodeposition of chitosan was carried out using an EC-Lab 9.9 potentiostat, in a conventional three-electrode system. The experiments were proceeded at room temperature in a dark and grounded metal Faraday box, using the gold interdigitated electrode as the working electrode, Ag/AgCl (saturated KCl) electrode as the reference electrode, and a platinum counter electrode.

The surface morphologies and energy-dispersive X-ray (EDX) analysis of the bare encapsulated microelectrode, of chitosan on a gold electrode, and of NiPc doped in chitosan film deposited on gold electrode were studied using scanning electron microscopy (SEM) (COXEMEM-30AX+).

Thermogravimetric analysis (TGA) was carried out using a thermal gravimetric analyzer TA Instruments Q50. The atmosphere is air at a flow rate of 90 mL/min. Fourier Transform Infrared (FTIR) spectroscopy was carried by applying a vacuum microscope continuous (Nicolet-Thermo Fisher, UK), coupled to an infrared spectroscopy Nexus specular reflectance mode, with an MCT detector. Spectra were registered, through a resolution of 4 cm^{-1}, in the wavenumber range of 4000 and 400 cm^{-1} at room temperature.

Conductometric detections of VOCs was achieved by applying to each of the paired interdigitated electrodes (sensor) a small amplitude sinusoidal voltage (10 mV peak to peak) with 10 kHz frequency generated by a very low-frequency waveform generator (Standard Research System). These parameters were employed to limit faradaic processes, multiple layer charging, and polarisation at the microelectrode surface. These conditions were optimized in KCl solutions [29]. The differential output signal was recorded between the working and the reference pair of the interdigitated electrodes, utilizing a Standard Research System lock-in amplifier SR510 and the response time of the gas sensor was registered.

These measurements were done by placing the NiPc/ chitosan modified interdigitated electrodes (working electrode) and the chitosan modified interdigitated electrodes (reference electrode) in the headspace over a liquid phase in a cylindrical vessel like container. The differential measurement of conductance (ΔG) was detected against time. The recovery was obtained when the sensor was removed from the headspace after peak maximum was reached and passed to the air.

IV.2.4. Preparation of Chitosan and Nickel Phthalocyanine Solutions

The fabricated interdigitated microelectrodes chip was cleaned through sonication in acetone, ethanol, and deionized water, each step during ten min under ultra- sonication. Later, the chip was rinsed with distilled water, and dried under nitrogen flow in a fume hood, then the electrode was placed in UV/Ozone procleaner (BioForce) for at least 30 min before electrodeposition of chitosan on the electrode surface as described below.

The chemical composition of the chitosan solution was 0.55 g of chitosan powder (lower molecular weight) completely dissolved in 2 % (v/v) of glacial acetic acid by overnight stirring. The pH was adjusted to 6.5 by drop addition of 0.1 M NaOH solution into the chitosan solution

while agitating with a magnetic stirrer, The chitosan (Figure 47A) was used as film matrix. Whereas suspension of NiPc was prepared by dissolving blueish NiPc (Figure 47B) at 1 mg/mL in THF for overnight stirring, due to low solubility of phthalocyanine.

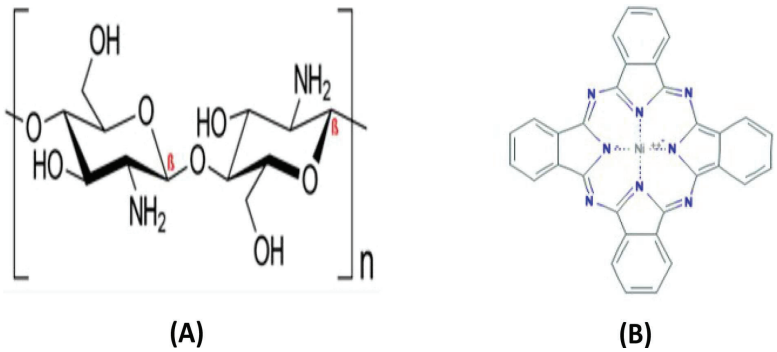

Figure 47. Chemical structures of Chitosan (A) and Nickel phthalo-cyanine (B)

Chronoamperometric deposition technique was carried out by putting chitosan solution in a 5 mL beaker, where the working electrode (Au interdigitated electrode), reference electrode Ag/AgCl, counter electrode (Pt-electrode) was all immersed, connected to EC LAB Potentiostat. A constant potential of 1.4 V was applied for 5 min. The cathodic current at the electrode, measured as a function of time, fluctuated according to the diffusion of H^+ from the bulk solution towards the sensor surface. The current (mA) continued to increase until it became stable within 5 min when the chitosan film was electro-deposited on the gold surface. The reference chips were washed with deionized water dried under nitrogen flow and then baked in an oven for about two hours. The obtained sensor was then ready for gaseous detection. The working chips with chitosan deposited electrode were washed with distilled water, then, dried with nitrogen, dipped into a solution of 1 mg/mL of nickel phthalocyanine in THF for 20 min, dried under nitrogen flow after washing with distilled water. The fabricated working sensor was also annealed in a furnace at 50°C for 2 h.

IV.3. Results and Discussion

IV.3.1. Electrochemical Growing Chitosan Film on Interdigitated Electrodes (IDEs)

Physical and chemical parameters of chitosan solution such as viscosity, electrical conductivity, pH, and chitosan concentration can affect the suitability of the chitosan deposited on the gold electrode surfaces [30]. CA electro-deposition of chitosan solution using 1 % w/v favored a highly sensitive gas sensor [29]. An increase in acid concentration may lead to an increase in

gas adsorption due to a higher degree of protonation [31]. Chitosan film was grown onto the gold substrate to form a thin film and the highly controlled deposition improved the mechanical and electrical contact between the polymeric membrane and the gold surface [32].

It's worth noting that each glucosamine in chitosan makes it a polycationic polymer with one NH_2 group and two OH groups per unit. These three groups are extremely reactive and have a significant impact on the polymer's characteristics. Chitosan's high functionality allows it to be chemically modified in a variety of ways [33]. Figure 48 shows chronoamperometric deposition of chitosan on the gold microelectrode.

Surface modification was achieved by the introduction of sensitive nanomaterials such as nickel phthalocyanine. A current of 20 µA was observed, because of the proton reduction, and the current decreases since chitosan film were formed on the IDEs. The working chip was then dipped in a 1 mg/mL of NiPc in THF solution for 20 min before baking in the furnace in the same conditions as the reference sensor.

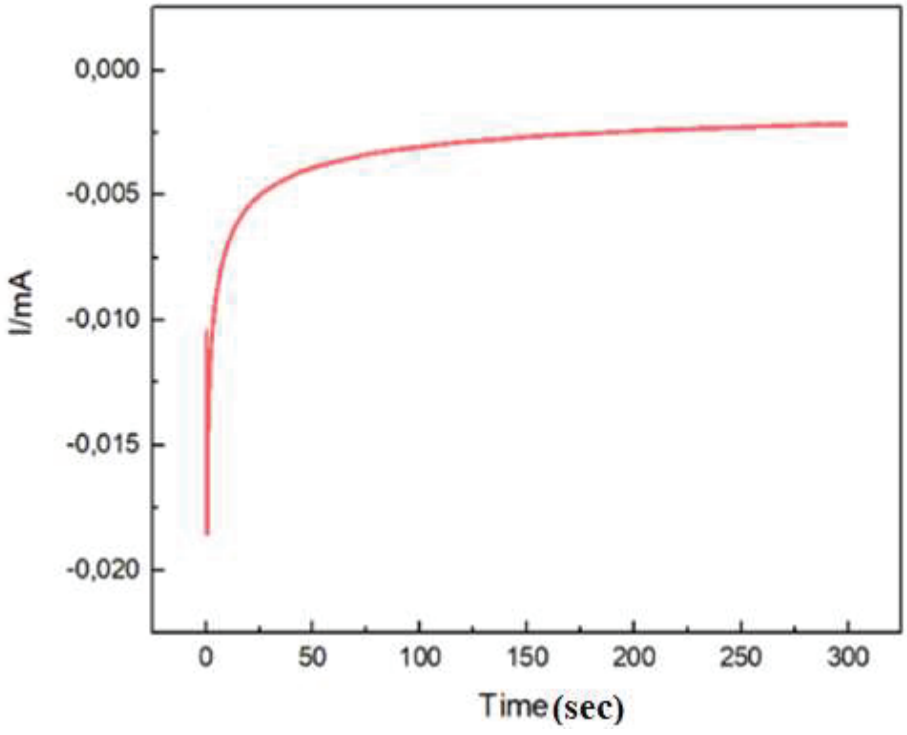

Figure 48. Chronoamperometric measurement monitoring of electro- deposition of chitosan

SEM images of the bare chip, chitosan deposited on chip and chitosan doped NiPc deposited on chip are presented in appendix, Figures S12 (a,b,c) respectively. EDS analyses were carried out on bare Au, Au- chitosan, and Au-chitosan doped NiPc to study the change in the surface

composition (Figures S13, S14, S15 in Appendix and Table 9). On bare Au, gold and Si are abundant.

Table 9. EDS analysis

	Element	Atomic percentage
Bare IDEs	C	16.94
	O	32.65
	Ni	1.21
	Si	39.70
	Au	9.29
Chitosan film on IDEs	C	57.03
	O	34.12
	Na	7.32
	Si	0.72
	Au	0.82
NiPc/Chitosan on IDEs	C	81.24
	O	16.30
	Ni	1.42
	Si	1.25

(a) bare electrode on-chip, (b) electrodeposited chitosan on-chip and (c) electrodeposited chitosan doped with NiPc on-chip

An increase in carbon was noticed after deposition of chitosan, Si and Au largely decreased and Na is visible due to NaOH for pH adjustment of chitosan solution. Significant detection of nitrogen is difficult, due to low composition in chitosan molecule, oxygen from chitosan compound was detected by EDS analysis. Nickel and carbon increment were observed when analyzing Au-chitosan doped NiPc.

The surface of the bare interdigitated gold electrode on a silicon wafer was subjected to FTIR analysis. Bands at 2859 and 1036 cm^{-1} which is said to be associated with Au [34] and the bands at 1169 and 1036 cm^{-1} are considered to be Si-O stretching [35]. FTIR spectra for the electrodeposited chitosan film showed important absorption bands identifying the characteristics of functional groups, which were recorded in the middle infrared (4000 cm^{-1} to 500 cm^{-1}). The infrared spectra for chitosan biopolymers as shown in Figure 49.

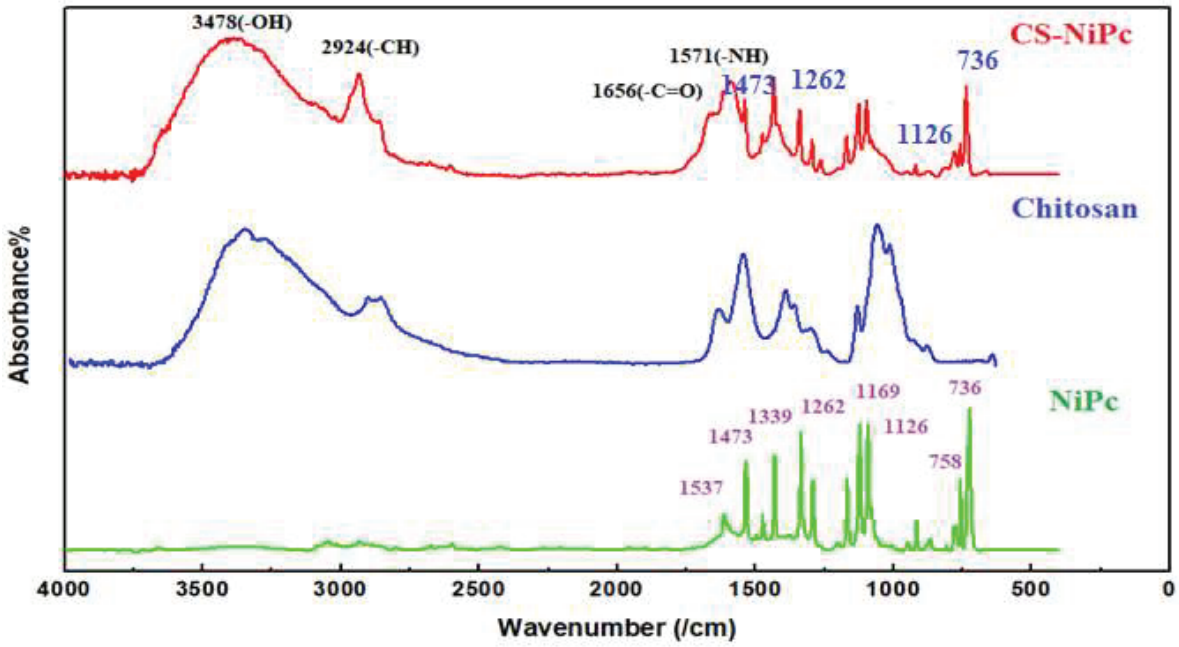

Figure 49. FTIR overlap spectra from pure chitosan film (blue curve) and chitosan film doped with NiPc (red curve) and pure NiPc (green curve)

The stretching vibrations of the -OH bond of the prepared chitosan was found at 3366.3 cm^{-1} and that for C-H was observed at 2932.5 cm^{-1}. The absorption peaks at 1656.88 cm^{-1}, 1585.3 cm^{-1}, 1432.2 cm^{-1}, 1339 cm^{-1} were associated with the presence of the C=O stretching of the amide I band, bending vibrations of the N-H (N-acetylated residues, amide II band), C-H bending, O-H bending respectively. The peak at 1169.0 cm^{-1} assigned for anti-symmetric stretching of (C-O-C) bridge, 1078 cm^{-1}, and 1025.18 cm^{-1} anticipated to the skeletal vibration involving C-O stretching [32, 36, 37]. However, the FTIR spectra of electrodeposited chitosan doped with NiPc (well-observed onto pure NiPc spectrum) has bands of chitosan at 3366, 1585, 1415, 1078, and 1036 cm^{-1}, and bands of NiPc at 1537, 1473, 1432, 1339, 1262, 1169, 1126, 1096, 758 and 736 cm^{-1} [38, 39, 28].

As suggested previously, the FTIR vibration peaks of phthalocyanines originate from pyrrole, benzene ring, and metal-ligand [42]. The peak at 918 cm^{-1} can be assigned to Ni ligand vibration [39-41]. The peaks at 1293 cm^{-1} and 1432 cm^{-1} are due to the C-N and the C-C bonds stretching in pyrroles [40]. The peaks at 736 cm^{-1} and 758 cm^{-1} are corresponding to the C-H out-of-plane mode, and 1126 cm^{-1} corresponds to an in-plane bending in the benzene ring. These indicate that the NiPc individual molecule does not change either in powder or nanowires. However, we can find the difference in the FTIR spectra of powder and nanowires caused by the change of crystal structure. Commonly, the peaks at 724 cm^{-1} and 1293 cm^{-1} in NiPc nanowires are used

to identify the orientation in phthalocyanines, while these two characteristic peaks are located at 736 cm^{-1} and 1339 cm^{-1} for NiPc powder [41]. The peaks at 780 cm^{-1} and 1174 cm^{-1} are the signature for the β-MPc, which appeared apparently in NiPc powder, while was missing in NiPc nanowires [42], not observed here.

TGA analysis was conducted on lower molecular weight chitosan samples and results are presented in Appendix Figure S18. The weight loss process of chitosan under air is divided into three phases of the thermal degradation pattern. The first stage started to degrade at around 180°C and degradation terminated at around 650°C. During the first thermal process from ambient temperature to 180°C, the sample lost 9.70 % of its weight. This loss of mass corresponds to a loss of moisture. The second and the third thermal degradation of chitosan are from 180 to 385°C and from 385 to 650°C. At these temperatures, we observed the chitosan decomposition and scission of the polymer chain through two mechanisms. At 650°C in which chitosan attained nearly complete decomposition, we observe a weight loss of 99.3 %. The chitosan-blend showed similar decomposition ranges but with higher remaining weights at each temperature [43], this is because the decomposition of chitosan leads to rapid weight loss [44]. Chitosan weight loss of 9.7 %, (Appendix Figure S18) as such enables us to calculate the exact mass of chitosan for the solution preparation. Additionally, the ability of chitosan to start degrading at 180°C allows us to bake our fabricated sensor made from chitosan at 50°C without any risk of decomposition. The same way, TGA analysis of chitosan doped with NiPc was studied accordingly, the different degradation stages were observed as in pure chitosan (Figure S19 in Appendix). The TGA profile, under air, in Figure 50, demonstrates the stages of mass loss of chitosan doped with NiPc.

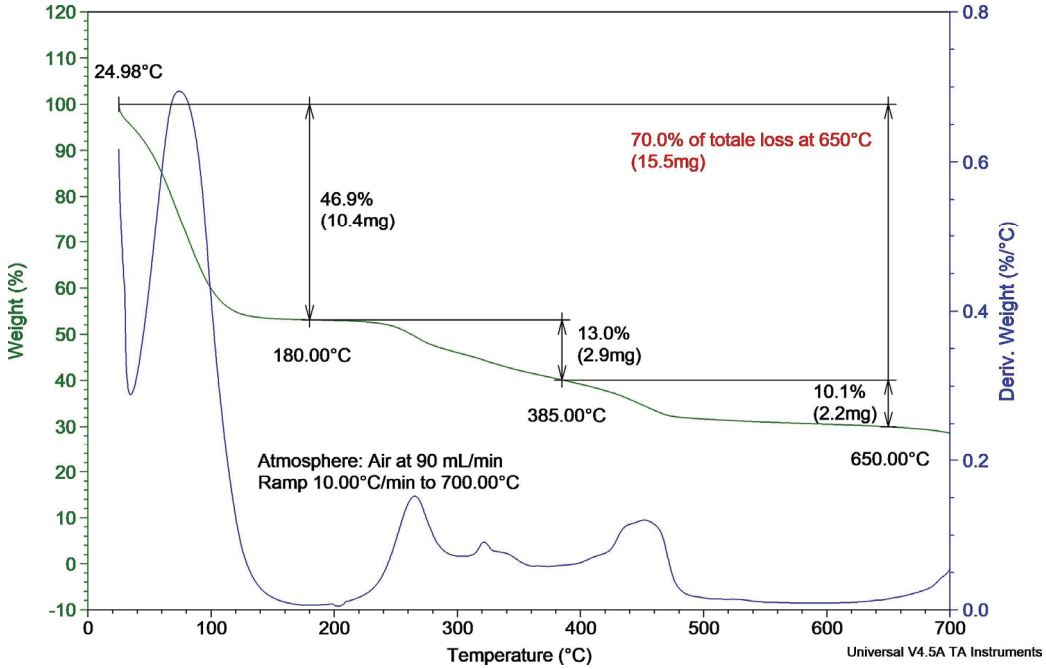

Figure 50. TGA analysis to determine the thermal degradation properties of low molecular weight chitosan doped with NiPc

We can observe a first stage of loss of 46.9 % from the ambient temperature to 180°C, possibly corresponding to water and/or solvent. Above 180°C, we can see the degradation into two mechanisms: from 180 to 385°C (13.0 %) and the third stage of 10.1 % from 385 to 650 °C. The total loss is 70 % at 650°C. The chitosan and NiPc remained stable afterward. This also corresponds to the results obtained by Modibanne et al. [42] and by Rajic and Stojakovic [45].

IV.3.2. Preparation of Gas Samples

Gaseous samples of acetone, ethanol and methanol were sampled from the headspace above aqueous solutions of known concentrations between 0-100 %.

The concentrations of the aforementioned solvents in the gas phase above the aqueous solution depend on Henry's law constants, of the given analytes in water and were converted from Henry's law from the third version equation reported at (25°C) by Sander in 1999 [46].

$$kHo = ca/pg \quad (1)$$

Here, ca is the concentration of a species in the aqueous phase and pg is the partial pressure of that species in the gas phase. Where H^o refers to Henry's law constants for the standard condition, its unit is M/atm (2) For the listed solvents above at (25°C) i.e, methanol, ethanol, and acetone, Henry's law constants value of 2.2×10^2 M/atm, 1.9×10^2 M/atm, and 0.2×10^2 M/atm were considered respectively [47]. Tables 10, 11, and 12 describe the calculated

equilibrium gas-phase concentrations of acetone, ethanol, and methanol above the aqueous phase.

Table 10. Equilibrium gaseous phase concentrations above an aqueous methanol solution at 25°C following Henry's law constants as reported by Sender et al [46]

S/N	% volumetric concentration	Concentration of methanol in the aqueous phase (M)	Concentration of methanol in the gaseous phase (%v/v)
1	0%	0	0
2	10%	2.48	1.13
3	20%	4.95	2.25
4	40%	9.9	4.5
5	60%	14.85	6.75
6	80%	19.8	9
7	100%	24.75	11.25

Table 11. Equilibrium gaseous phase concentrations above an aqueous ethanol solution at 25°C per Henry's law constants as reported by Sender et al [46]

S/N	% Volumetric concentration	Concentration of ethanol in the aqueous phase (M)	Concentration of ethanol in the gaseous phase (v/v%)
1	0%	0	0
2	10%	1.71	0.90
3	20%	3.41	1.79
4	40%	6.82	3.58
5	60%	10.23	5.37
6	80%	13.23	7.16
7	100%	17.05	8.95

Table 12. Equilibrium gaseous phase concentrations above an aqueous acetone solution at 25°C per Henry's law constants as reported by Sender et al [46]

S/N	% Volumetric concentration	Concentration of acetone in the aqueous phase (M)	Concentration of acetone in the gaseous phase (v/v%)
1	0%	0	0
2	10%	1.35	5.63
3	20%	2.7	11.26
4	40%	5.4	22.52
5	60%	8.1	33.78
6	80%	10.8	45.04
7	100%	13.5	56.03

Conductometric detection of several VOCs (methanol, acetone, chloroform, and water) were performed in the gaseous phase above pure liquid compounds, at room temperature 25°C, as shown in Figure 51a. The conductivity of the film, read by the lock-in amplifier, increased dramatically when exposed to the headspace of pure solvents. The sensor shows good sensitivity towards methanol, 4.5 times higher than towards ethanol, 10 times higher than towards acetone, and 7.5 times higher than towards water, with no single response when exposed to chloroform.

Variation of the absorption curves in the presence of dry air and methanol or ethanol vapors is important in the Q-band region (600-640 nm) rather than in the Soret band for a CuPcOH film. A six times higher effect is observed with methanol compared to ethanol [48]. The sensing mechanism is related to the rearrangement of the electrical dipole in the bulk thin film due to the interaction of phthalocyanine and analytes, in other words, the interaction generates modulation in the disposable electronic levels for π-π* transitions of the phthalo-cyanine ring. The same phenomenon was observed with ZnTTBPc (zinc tetra-tertiary-butyl phthalocyanine) film in the presence of methanol and was modeled as weak bonding between test alcohol molecule and the central Zn atom, which perturbs the π-π* transitions [49].

For measuring the selectivity of the sensor toward acetone, ethanol, and methanol, we exposed some concentrations ranging from 5.67-56.06, 0.9-8.95, and 1.13-11.25 (%v/v) of acetone, ethanol, and methanol respectively. Measurements in the headspace of different methanol/water solutions are given in Figure 51b. Measurements in the headspace of different acetone/water solutions and ethanol/water solutions are given respectively in Figure S21A and S21B, in Appendix. It can be seen clearly that the conductance of the sensor increases with an increase

in the concentration of methanol in the liquid phase. To check the repeatability of the sensor, three measurements were carried out.

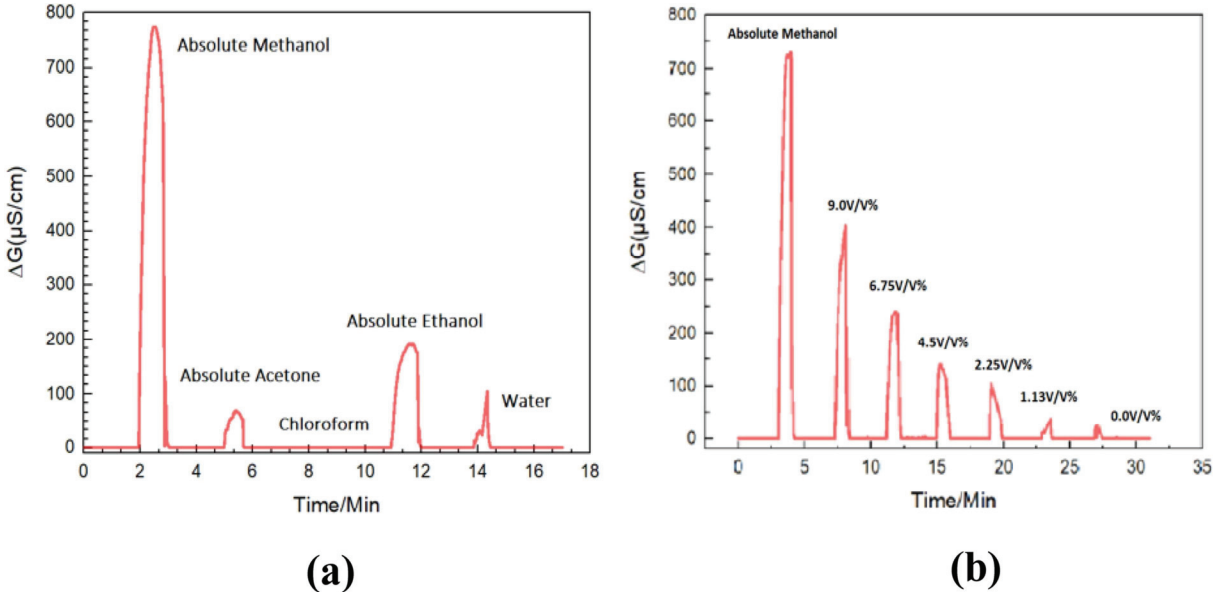

Figure 51. Conductometric detection of several VOCs (methanol, acetone, chloroform, and water)

(a) Detection of gas-phase concentration for pure liquid phase of methanol, acetone, chloroform, ethanol, water (b) Detection of gas-phase concentration for different methanol/water solutions NiPc/chitosan sensor, using a lock-in amplifier

The response time of the sensor is short, around one to thirty-one seconds, whereas the time to be recovered back to the baseline immediately after removal of the headspace measurement, is around thirty-eight seconds. The calibration curve for methanol, ethanol, and acetone are presented in Figure 52.

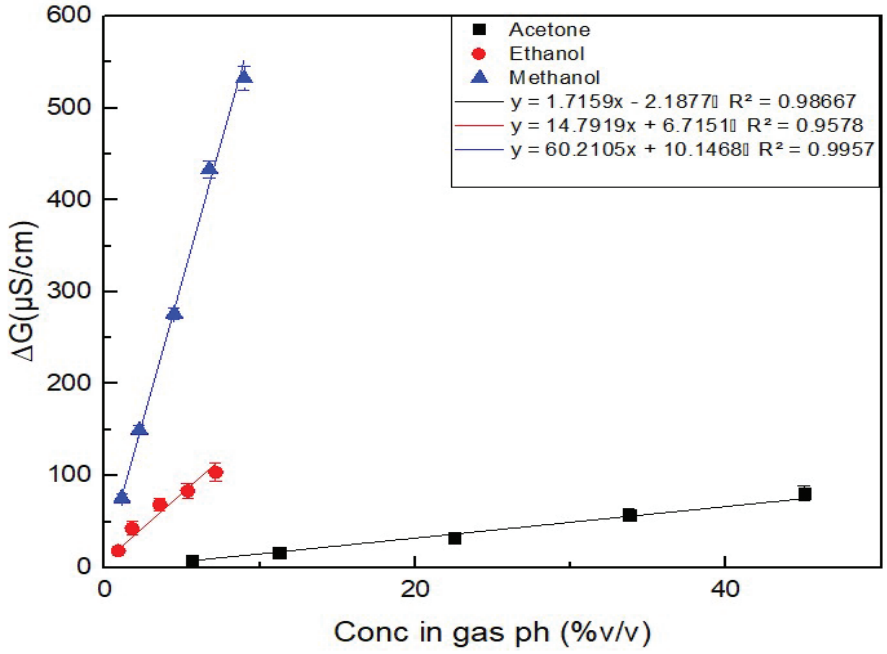

Figure 52. Calibration curve of the gas-phase concentrations of acetone, ethanol, and methanol

The sensor-based on chitosan doped NiPc provides us with a detection limit for methanol to be 0.07 v/v% (700 ppm) in the gaseous phase during the headspace measurement, this concentration corresponds to 0.15 M in the aqueous phase (4.8 g/L of methanol diluted in water).

The relative standard deviation for the described sensor ranged from 3% for higher concentrations to around 10% for lower concentrations. Chitosan/NiPc conductometric sensor maintains its stability for almost three months when stored in a plastic container at room temperature. Methanol was detected after every 4 days. Over this period the sensor still retained almost 92% of its original response A lot of methanol sensors have been fabricated (Table 13) but this is the first time that chitosan doped with NiPc is used for the conductometric detection of methanol. Compared to the other methanol sensors, this one presents a short response time, a large dynamic range but a rather high detection limit. The addition of nano-materials could improve the detection limit.

The calibration plots, from Figure 52, highlight the linearities of change in conductivity for acetone, ethanol, and methanol versus concentration in the gas-phase. Methanol sensor with the best linearity slot of R2 = 0.99688, was also observed to have the best sensitivity of 60.21 $\mu S.cm^{-1}$ (v/v), 35 times higher than acetone (1.71 $\mu S.cm^{-1}$ (v/v)) and 4 times higher than ethanol (14.79 $\mu S.cm^{-1}$(v/v)) respectively.

We noticed from Figure 51a that the detection signal of the gaseous phase pure methanol was at 575 $\mu S.cm^{-1}$ and that of pure water to be 98 $\mu S.cm^{-1}$.

Table 13. Comparison of the analytical performances of methanol sensors based on different sensitive materials

Methanol sensors	Response time	Dynamic range (ppm)	LOD (ppm)	Ref.
graphene oxide/polyindole/ conductivity	7 s	1.14–11.36	0.015	[50]
Pd doped SnO_2 nanoparticles/ conductivity (350 °C)	10 s–25 s	1–1000	1	[6]
TiO_2 doped CdS/ amperometry	10 s	0–6	0.18	[51]
ADH/Amperometry	5 s	0.1–40	10	[52]
PtAuAg nanotubes/ Amperometry	12 s	1–400	1	[53]
Chitosan-NiPc/ Conductometry	25 s–32 s	500–3500	700	This work

Even though chitosan is hygroscopic, the hydrophilic ability of the NiPc coupled with the differential measurement decreases the signal of the water and limits its interfering effect. From Figure 53, it comes that the methanol signal is increased by a factor of 11 % in the presence of 1/10 of ethanol and by a factor of 3 % in the presence of 1/10 of acetone. The effect of acetone is in the range of the measurement error whereas the effect of ethanol is 4 times higher than this error.

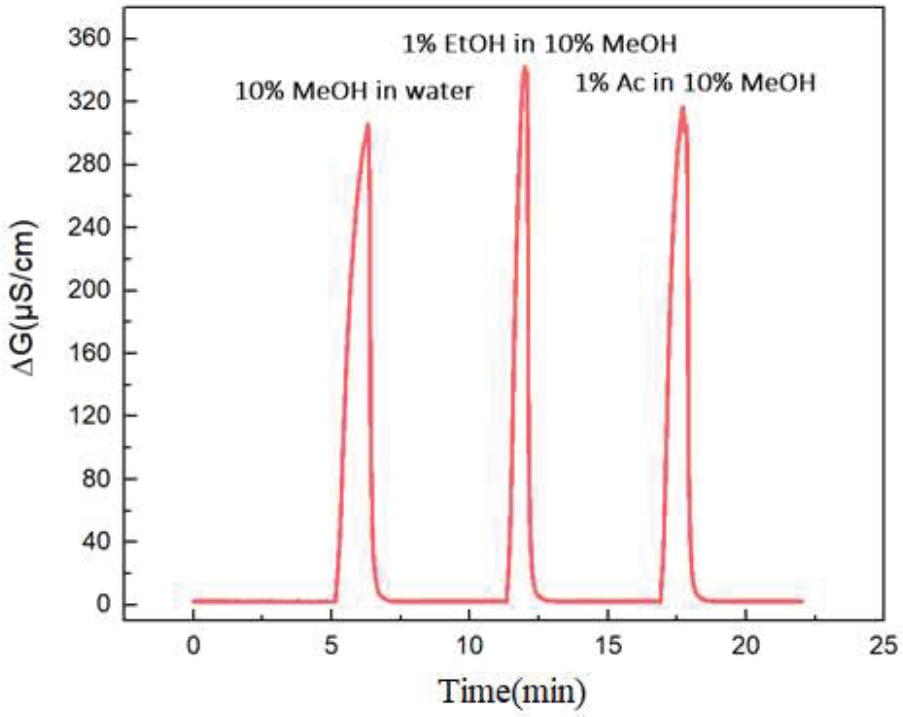

Figure 53. Effect of the presence of 1/10 of ethanol and of acetone compared to methanol on the sensor signal

Rubbing alcohol is a product made from 95 % methanol, is used as a liquid on barbecues or fireplaces or as an antifreeze solvent. In addition, if used at home, it is a powerful cleaner for stubborn dirt, polishing numerous surfaces, removing stains.

Following the detection of absolute methanol and a 90 % methanol/water combination in the gaseous phase, the detection of a commercial rubbing alcohol in the gaseous phase was conducted as presented in Figure 54.

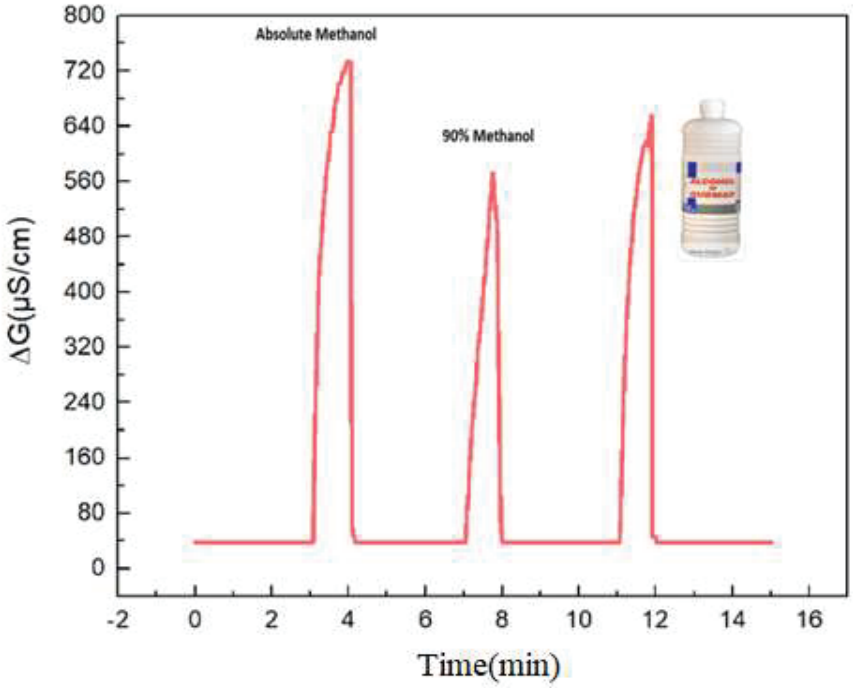

Figure 54. Detection of gas-phase concentrations for different meth- anol/water solutions and commercial rubbing alcohol, with the chitosan/NiPc sensor

For the commercial sample, the conductivity was 6.45 × 10^2 μS/cm. This data represents a gaseous phase volume of 10.54±0.24v/v%. In the aqueous phase, the alcohol has a molar concentration of 23.3±1.25 M. This corresponds to 94.0±1.5v/v%, which is in good agreement with the supplier's figure of 95 %.

Previously described chemiresistor gas/vapor sensors based on polyaniline nanocomposite for detecting methanol in perfumes and dyes have a detection range of 0.31 mM–3.5 mM [54]. The developed microconductometric methanol sensor has a relatively large detection limit (22 mM). Pre-functionalization of the microconductometric chip with nanomaterials such as zeolite [55], could improve this detection limit. Measurements of methanol in exhaled breath could be another application for this methanol sensor [56]. Exhaled methanol (MeOH) can provide a non-invasive assessment of intestinal flora.

IV.4. Conclusion

In this study, a highly sensitive gas sensor based on chitosan composites doped with NiPc, was successfully developed. Analytical techniques such as FTIR, EDX, and TGA were employed to characterize the sensing composite layer. Excellent thermal stability of the sensing layer has been observed. Acetone, ethanol, and methanol gas-sensing properties of the films prepared at

optimum conditions were studied at atmospheric temperature using differential measurements at a frequency of 10 kHz. The sensor is selective, sensitive, stable and presents a short response time towards methanol detection. Presently, there exists no methanol detector working at ambient temperature for early diagnosis by breath analysis or for screening of adulterated beverages.

IV.5. References

[1] O. Laakso, M. Haapala, T. Pennanen, T. Kuitunen, and J.-J. Himberg, "Fourier-Transformed Infrared Breath Testing After Ingestion of Technical Alcohol," *Journal of Forensic Sciences*, vol. 52, no. 4, pp. 982–987, Accessed: Nov. 08, 2021.

[2] R. F. Borkenstein and H. W. Smith, "The Breathalyzer and its Applications," *Med Sci Law*, vol. 2, no. 1, pp. 13–22, Oct. 1961, doi: 10.1177/002580246200200103.

[3] J. A. Kraut, "Approach to the Treatment of Methanol Intoxication," *Am J Kidney Dis*, vol. 68, no. 1, pp. 161–167, Jul. 2016, doi: 10.1053/j.ajkd.2016.02.058.

[4] Z. Nekoukar*, Z. Zakarieai, F. Taghizaden, F. Musavi, E. S.Banimostafavi, A.Sharifpour, N. Ebrahim Ghuchi, M.Fakhar, R. Tabaripour, S. Safariavaei*, "Methanol poisoning as a new world challenge: A review," *Ann Med Surg (Lond)*, vol. 66, p. 102445, Jun. 2021, doi: 10.1016/j.amsu.2021.102445.

[5] A. T. Güntner, S. Abegg, K. Königstein, P. A. Gerber, A. Schmidt-Trucksäss, and S. E. Pratsinis, "Breath Sensors for Health Monitoring," *ACS Sens.*, vol. 4, no. 2, pp. 268–280, Feb. 2019, doi: 10.1021/acssensors.8b00937.

[6] J. van den Broek, S. Abegg, S. E. Pratsinis, and A. T. Güntner, "Highly selective detection of methanol over ethanol by a handheld gas sensor," *Nat Commun*, vol. 10, no. 1, p. 4220, Sep. 2019, doi: 10.1038/s41467-019-12223-4.

[7] K. Schmidt and I. Podmore, "Current Challenges in Volatile Organic Compounds Analysis as Potential Biomarkers of Cancer," *Journal of Biomarkers*, vol. 2015, p. e981458, Mar. 2015, doi: 10.1155/2015/981458.

[8] O. Lawal, W. M. Ahmed, T. M. E. Nijsen, R. Goodacre, and S. J. Fowler, "Exhaled breath analysis: a review of 'breath-taking' methods for off-line analysis," *Metabolomics*, vol. 13, no. 10, p. 110, 2017, doi: 10.1007/s11306-017-1241-8.

[9] Y. Adiguzel and H. Kulah, "Breath sensors for lung cancer diagnosis," *Biosens. Bioelectron.*, vol. 65, pp. 121–138, Mar. 2015, doi: 10.1016/j.bios.2014.10.023.

[10] E. A. Reber, "Gas Chromatography-Mass Spectrometry (GC-MS): Applications in Archaeology," in *Encyclopedia of Global Archaeology*, C. Smith, Ed. Cham: Springer International Publishing, 2018, pp. 1–17. doi: 10.1007/978-3-319-51726-1_340-2.

[11] T. L. Mathew, P. Pownraj, S. Abdulla, and B. Pullithadathil, "Technologies for Clinical Diagnosis Using Expired Human Breath Analysis," *Diagnostics (Basel)*, vol. 5, no. 1, pp. 27–60, Feb. 2015, doi: 10.3390/diagnostics5010027.

[12] L. Al-Mashat, R. Kaner, H. Tran, K. Kalantar-zadeh, and W. Wlodarski, "Layered Surface Acoustic Wave Hydrogen Sensor Based on Polyethylaniline Nanofibers," *Procedia Chemistry*, vol. 1, pp. 220–223, Sep. 2009, doi: 10.1016/j.proche.2009.07.055.

[13] S. Nag, "Development of Conductive Nanocomposite Sensors for Anticipated Diagnostic of Diseases," phdthesis, Université de Bretagne Sud, 2014. Accessed: Aug. 20, 2020. [Online]. Available: https://tel.archives-ouvertes.fr/tel-01193327

[14] H. Nazemi, A. Joseph, J. Park, and A. Emadi, "Advanced Micro- and Nano-Gas Sensor Technology: A Review," *Sensors*, vol. 19, no. 6, Art. no. 6, Jan. 2019, doi: 10.3390/s19061285.

[15] A. Mujahid and F. L. Dickert, "Surface Acoustic Wave (SAW) for Chemical Sensing Applications of Recognition Layers," *Sensors (Basel)*, vol. 17, no. 12, p. E2716, Nov. 2017, doi: 10.3390/s17122716.

[16] J. Xu, M. Bertke, H. S. Wasisto, and E. Peiner, "Piezoresistive microcantilevers for humidity sensing," *J. Micromech. Microeng.*, vol. 29, no. 5, p. 053003, Apr. 2019, doi: 10.1088/1361-6439/ab0cf5.

[17] H.-W. Lee, J.Park, H. Lee, C. Kim, J. Lee, W. Kim, R. Ryu, J. Ahn, E.Lee, S. Kim, J.Jeon,Y. Yang, E. Choi, H. Lee., "Development of novel on-line capillary gas chromatography-based analysis method for volatile organic compounds produced by aerobic fermentation," *J Biosci Bioeng*, vol. 127, no. 1, pp. 121–127, Jan. 2019, doi: 10.1016/j.jbiosc.2018.07.007.

[18] D. Barauskas, D. Pelenis, G. Vanagas, D. Viržonis, and J. Baltrušaitis, "Methylated Poly(ethylene)imine Modified Capacitive Micromachined Ultrasonic Transducer for Measurements of CO_2 and SO_2 in Their Mixtures," *Sensors*, vol. 19, no. 14, Art. no. 14, Jan. 2019, doi: 10.3390/s19143236.

[19] G. Korotcenkov, V. Brinzari, and B. K. Cho, "Conductometric gas sensors based on metal oxides modified with gold nanoparticles: a review," *Microchim Acta*, vol. 183, no. 3, pp. 1033–1054, Mar. 2016, doi: 10.1007/s00604-015-1741-z.

[20] D. Shantini, I. Nainggolan, T. I. Nasution, M. N. Derman, R. Mustaffa, and N. Z. Abd Wahab, "Hexanal Gas Detection Using Chitosan Biopolymer as Sensing Material at Room Temperature," *Journal of Sensors*, vol. 2016, p. e8539169, Mar. 2016, doi: 10.1155/2016/8539169.

[21] L. Zhihua, Z. Xucheng, S. Jiyong, Z. Xianobo, H. Xiaowei, H. Tahir, M. Holmes., "Fast response ammonia sensor based on porous thin film of polyaniline/sulfonated nickel

phthalocyanine composites," *Sensors and Actuators B: Chemical*, vol. 226, pp. 553–562, Apr. 2016, doi: 10.1016/j.snb.2015.10.062.

[22] F. I. Bohrer, C. Colesniuc, J. Park, M. Ruidiaz, I.Schuller, A. Kummel, W. Trogler., "Comparative Gas Sensing in Cobalt, Nickel, Copper, Zinc, and Metal-Free Phthalocyanine Chemiresistors," *J. Am. Chem. Soc.*, vol. 131, no. 2, pp. 478–485, Jan. 2009, doi: 10.1021/ja803531r.

[23] J. Brunet, A. Pauly, C. Varenne, and B. Lauron, "On-board phthalocyanine gas sensor microsystem dedicated to the monitoring of oxidising gases level in passenger compartments," *Sensors and Actuators B: Chemical*, vol. 130, no. 2, pp. 908–916, Mar. 2008, doi: 10.1016/j.snb.2007.10.074.

[24] A. Kumar, R. Meunier-Prest, and M. Bouvet, "Organic Heterojunction Devices Based on Phthalocyanines: A New Approach to Gas Chemosensing," *Sensors*, vol. 20, no. 17, p. 4700, Aug. 2020, doi: 10.3390/s20174700.

[25] X. Duan, Y. Zhang, H. Wang, F. Dai, G. Yang, and Y. Chen, "A phthalocyanine sensor array based on sensitivity and current changes for highly sensitive identification of three toxic gases at ppb levels," *New J. Chem.*, vol. 44, no. 31, pp. 13240–13248, Aug. 2020, doi: 10.1039/D0NJ02025G.

[26] S. Radhakrishnan and S. D. Deshpande, "Conducting Polymers Functionalized with Phthalocyanine as Nitrogen Dioxide Sensors," *Sensors*, vol. 2, no. 5, Art. no. 5, May 2002, doi: 10.3390/s20500185.

[27] D. S. Chandrasakaran, I. Nainggolan, T. Ikhsan, and M. N. B. Derman, "Ammonia Gas Sensor Based on Chitosan Biopolymer," *Materials Science Forum*, pp. 429–434, 2015, doi: 10.4028/www.scientific.net/MSF.819.429.

[28] F. Ali, S. B. Khan, T. Kamal, Y. Anwar, K. A. Alamry, and A. M. Asiri, "Anti-bacterial chitosan/zinc phthalocyanine fibers supported metallic and bimetallic nanoparticles for the removal of organic pollutants," *Carbohydrate Polymers*, vol. 173, pp. 676–689, Oct. 2017, doi: 10.1016/j.carbpol.2017.05.074.

[29] A. Madaci, G. Raffin, C. Pages, C. Jose, M. Martin, H. Ferkous, A. Bouzid, J. Bausells, A. Alcacer, A. Errachid, N. Jaffrezic-Renault *l.*, "A microconductometric ethanol sensor prepared through encapsulation of alcohol dehydrogenase in chitosan: application to the determination of alcoholic content in headspace above beverages," *J Mater Sci: Mater Electron*, vol. 32, no. 13, pp. 17752–17763, Jul. 2021, doi: 10.1007/s10854-021-06311-9.

[30] S. G. Surya, S. Khatoon, A. Lahcen, A. Nguyen, B. Dzantiev, N. Tarannum, K.Salama., "A chitosan gold nanoparticles molecularly imprinted polymer based ciprofloxacin

sensor," *RSC Adv.*, vol. 10, no. 22, pp. 12823–12832, Mar. 2020, doi: 10.1039/D0RA01838D.

[31] N. L. Lukman Hekiem, A.A. Md Ralib, M. A. Mohd Hatta, F.B. Ahmad, A. N. Nordin,R. Ab. Rahim, N. F. Za¨bah., "Effect of chitosan dissolved in different acetic acid concentration towards VOC sensing performance of quartz crystal microbalance overlay with chitosan," *Materials Letters*, vol. 291, p. 129524, May 2021, doi: 10.1016/j.matlet.2021.129524.

[32] R. Jayalakshmi and J. Jeyanthi, "Spectroscopic investigation of carbon nanotube as nano-filler entrapped in chitosan hydrogel beads," *Journal of Molecular Structure*, vol. 1237, p. 130386, Aug. 2021, doi: 10.1016/j.molstruc.2021.130386.

[33] F. Zouaoui, S. Bourouina-Bacha, M. Bourouina, N. Jaffrezic-Renault, N. Zine, and A. Errachid, "Electrochemical sensors based on molecularly imprinted chitosan: A review," *TrAC Trends in Analytical Chemistry*, vol. 130, p. 115982, Sep. 2020, doi: 10.1016/j.trac.2020.115982.

[34] H. Forootanfar, "Biological synthesis of Au, Ag and Au-Ag bimetallic nanoparticles by A-Amylase," *Digest Journal of Nanomaterials and Biostructures*, vol. 6, pp. 1419–1426, 2011, Accessed: Jul. 05, 2021. [Online]. Available: http://research.kmu.ac.ir/webdocument/load.action?webdocument_code=2000&masterCode=95001279

[35] S. Saravanan and R. S. Dubey, "Synthesis of SiO2Nanoparticles by Sol-Gel Method and Their Optical and Structural Properties," p. 8.

[36] S. Yasmeen, M. Kabiraz, B. Saha, M. Qadir, M. Gafur, and S. Masum, "Chromium (VI) Ions Removal from Tannery Effluent using Chitosan-Microcrystalline Cellulose Composite as Adsorbent," *International Research Journal of Pure and Applied Chemistry*, vol. 10, pp. 1–14, Jan. 2016, doi: 10.9734/IRJPAC/2016/23315.

[37] H. Y. C.-Eulalio, J. F. B.-Rodrigues, K. O.-Santos, C. Peniche, and M. V.-LiaFook, "Characterization and thermal properties of chitosan films prepared with different acid solvents," *Revista Cubana de Química*, vol. 31, no. 3, pp. 309–323, Accessed: Jul. 05, 2021. [Online]. Available: https://www.redalyc.org/journal/4435/443561090001/html/

[38] G. de la Torre, P. Vázquez, F. Agulló-López, and T. Torres, "Role of Structural Factors in the Nonlinear Optical Properties of Phthalocyanines and Related Compounds," *Chem. Rev.*, vol. 104, no. 9, pp. 3723–3750, Sep. 2004, doi: 10.1021/cr030206t.

[39] K.-C. Ho and Y.-H. Tsou, "Chemiresistor-type NO gas sensor based on nickel phthalocyanine thin films," *Sensors and Actuators B: Chemical*, vol. 77, no. 1–2, pp. 253–259, Jun. 2001, doi: 10.1016/S0925-4005(01)00742-0.

[40] X. Wang, W. Wu, H. Ju, T. Zou, Z. Qiao, H. Gong, H. Wang., "Experimental and theoretical studies of the structure and optical properties of nickel phthalocyanine nanowires," *Materials Research Express*, vol. 3, p. 125002, Dec. 2016, doi: 10.1088/2053-1591/3/12/125002.

[41] S. Khene, K. Lobb, and T. Nyokong, "Characterization of nickel tetrahydroxy phthalocyanine complexes and the electrocatalytic oxidation of 4-chlorophenol: Correlation of theory with experiments," *Inorganica Chimica Acta*, vol. 362, no. 14, pp. 5055–5063, Nov. 2009, doi: 10.1016/j.ica.2009.08.019.

[42] K. D. Modibane, T. Pesha, T. C. Maponya, K. E. Ramohlola, G. R. Monama, M.E. Makhatha, E. Makhado, M. J. Hato., "Electrochemical studies on the corrosion protection of aluminum metal in acid media by unsubstituted and 4-tetranitro substituted nickel(II) phthalocyanine inhibitors for hydrogen fuel cells," *International Journal of Corrosion and Scale Inhibition*, vol. 10, no. 1, Art. no. 1, 2021, Accessed: Jul. 05, 2021. [Online]. Available: http://ijcsi.pro/papers/electrochemical-studies-on-the-corrosion-protection-of-aluminum-metal-in-acid-media-by-unsubstituted-and-4-tetranitro-substituted-nickelii-phthalocyanine-inhibitors-for-hydrogen-fuel-cells/

[43] N. Nady and S. Kandil, "Novel Blend for Producing Porous Chitosan-Based Films Suitable for Biomedical Applications," *Membranes*, vol. 8, no. 1, p. 2, Jan. 2018, doi: 10.3390/membranes8010002.

[44] L. Cui, S. Gao, X. Song, L. Huang, H. Dong, J. Liu, F. Chen, S. Yu., "Preparation and characterization of chitosan membranes," *RSC Advances*, vol. 8, no. 50, pp. 28433–28439, 2018, doi: 10.1039/C8RA05526B.

[45] N. Z. Rajić and D. R. Stojaković, "Synthesis and Characterization of Some Nitro-Substituted Phthalocyanines of Nickel(II), Cobalt(II) and Copper(II)," *Journal of Coordination Chemistry*, vol. 19, no. 4, pp. 295–301, Mar. 1989, doi: 10.1080/00958978909408832.

[46] R. Sander, "Compilation of Henry's Law Constants for Inorganic and Organic Species of Potential Importance in Environmental Chemistry," p. 107.

[47] J. R. Snider and G. A. Dawson, "Tropospheric light alcohols, carbonyls, and acetonitrile: Concentrations in the southwestern United States and Henry's Law data," *Journal of*

Geophysical Research: Atmospheres, vol. 90, no. D2, pp. 3797–3805, 1985, doi: 10.1029/JD090iD02p03797.

[48] J. Spadavecchia, G. Ciccarella, L. Valli, and R. Rella, "A novel multisensing optical approach based on a single phthalocyanine thin films to monitoring volatile organic compounds," *Sensors and Actuators B: Chemical*, vol. 113, no. 1, pp. 516–525, Jan. 2006, doi: 10.1016/j.snb.2005.03.110.

[49] S. Uttiya, T. Kerdcharoen, and S. V. and S. Pratontep, "Effect of Structural Transformation on the Gas-Sensing Properties of Phthalocyanine Thin Films," *Journal of the Korean Physical Society*, vol. 52, no. 5, pp. 1575–1579, May 2008, doi: 10.3938/jkps.52.1575.

[50] K. Phasuksom, W. Prissanaroon-Ouajai, and A. Sirivat, "A highly responsive methanol sensor based on graphene oxide/polyindole composites," *RSC Adv.*, vol. 10, no. 26, pp. 15206–15220, Apr. 2020, doi: 10.1039/D0RA00158A.

[51] C.-F. Fong, C.-L. Dai, and C.-C. Wu, "Fabrication and Characterization of a Micro Methanol Sensor Using the CMOS-MEMS Technique," *Sensors*, vol. 15, no. 10, Art. no. 10, Oct. 2015, doi: 10.3390/s151027047.

[52] Q. Liu and J. R. Kirchhoff, "Amperometric detection of methanol with a methanol dehydrogenase modified electrode sensor," *Journal of Electroanalytical Chemistry*, vol. 601, no. 1–2, pp. 125–131, Mar. 2007, doi: 10.1016/j.jelechem.2006.10.039.

[53] Q. Qiu, N. Jiang, L. Ge, X. Li, and X. Chen, "The electrochemical sensor for methanol detection based on trimetallic PtAuAg nanotubes," *J Mater Sci*, vol. 55, no. 33, pp. 15681–15694, Nov. 2020, doi: 10.1007/s10853-020-05146-9.

[54] S. Pandey, "Highly Sensitive and Selective Chemiresistor Gas/Vapor Sensors based on Polyaniline Nanocomposite: A comprehensive review," *Journal of Science: Advanced Materials and Devices*, vol. 1, Oct. 2016, doi: 10.1016/j.jsamd.2016.10.005.

[55] J. Park and H. Tabata, "Gas Sensor Array Using a Hybrid Structure Based on Zeolite and Oxide Semiconductors for Multiple Bio-Gas Detection," *ACS Omega*, vol. 6, no. 33, pp. 21284–21293, Aug. 2021, doi: 10.1021/acsomega.1c01435.

[56] K. Toma, K. Iwasaki, G. Zhang, K. Litani, T. Arakawa, Y. Iwasaki, K. Mitsubayashi., "Biochemical Methanol Gas Sensor (MeOH Bio-Sniffer) for Non-Invasive Assessment of Intestinal Flora from Breath Methanol," *Sensors (Basel)*, vol. 21, no. 14, p. 4897, Jul. 2021, doi: 10.3390/s21144897.

Chapter V

Electrospun PVC polymer/nickel phthalocyanines composite fiber arrays for the conductometric detection and identification of volatile organic compounds

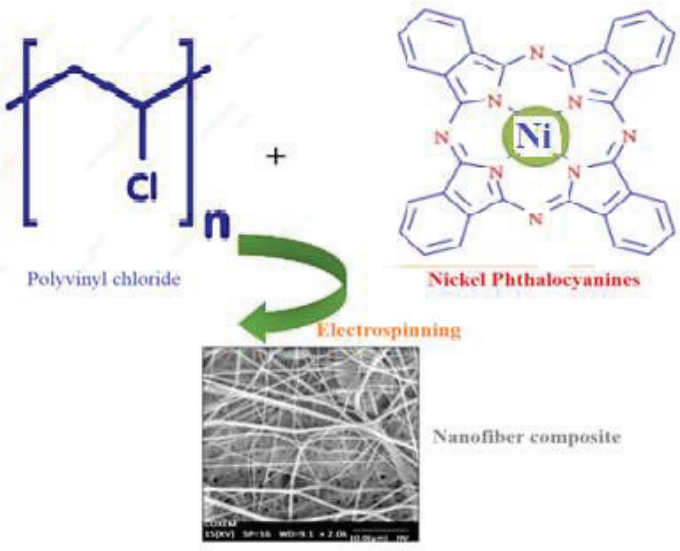

V.1. Introduction

Methanol (MeOH) is commonly utilized in laboratories and industries as solvents or cleaning agents [1]. Methanol is a frequent feedstock for a variety of critical compounds and a possible energy carrier alternative to hydrogen [2]. Inhaling significant amounts of methanol vapor can result in headaches, tiredness, nausea, impaired vision, convulsion, and even blindness, tumors, and cancer [1]. The wide range of applications for MeOH, as well as its toxic effects and the desire to fine-tune its synthesis under extreme conditions, all of these factors point to the necessity for methanol sensors that are both reliable and selective. The American Conference of Governmental Industrial Hygienists (AGGIH) recommends a released threshold for methanol vapor concentration of 200 ppm for repeated exposure without severe health effects during the working day (8 h). Originally, non-invasive analytical pieces of equipment such as PTR-ToF-MS, GC-MS, and chemiluminescence gas analyzers were known for methanol detection and measurements for early diagnostic techniques [3]. With these techniques, conventional VOC analysis becomes time-consuming, expensive, and unsuited for extensive screening [4]. Sensors are good candidates for the low-cost detection of VOCs. Chemical species interact with the sensitive layer of the sensor, changing its electrical conductivity as a result. The change in resistance/conductivity of a sensitive layer because of processes (adsorption, chemical reactions, diffusion, catalysis, charge transfer) occurring on the surface of the sensing area is the base of conductometric sensor functioning [5].

Electrospinning is a low-cost, effective technique for creating ultra-thin polymer and composite fibers having diameters ranging from a few nanometers to a few micrometers (Figure 44) [6]. It requires utilizing a high voltage to polymer solutions or melts ejected from micro syringe pumps through electrostatic stretching [7]. Over the last two decades, this technique has gained significant attention. It was used to actively spin more than a hundred polymers into ultra-fine fibers [8].

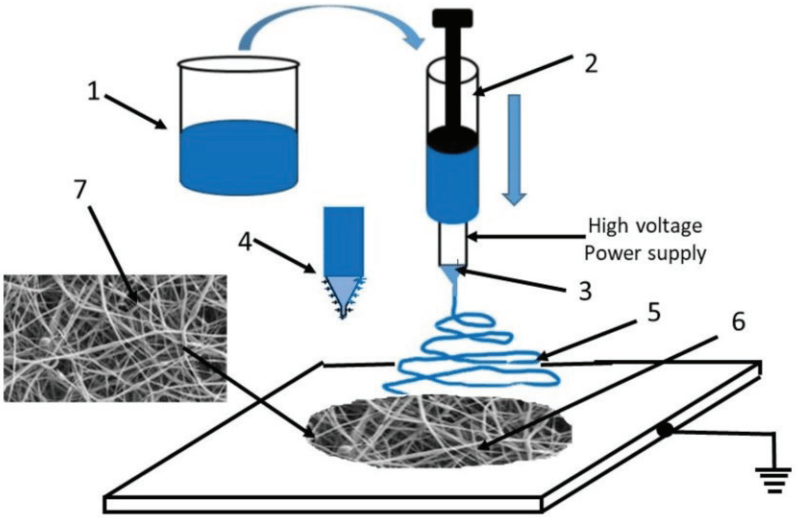

Figure 55. Electrospinning setup

(1) polymer solution, (2) syringe, (3) needle, (4) Blunt needle with capillary tube (emitter), (5) polymer stretching, (6) Flat plate collector, (7) nanofiber (laser).

Electrospun fibers with several properties, fine structure, tunable membrane, thickness, and an attractive large specific surface area are indicators of the best prospects for a sensing application's configuration [9]. So far, sensor scientists have carried out numerous studies to develop amazingly gas sensors capable of detecting NH_3, H_2S, CO, and others [10]. Nickel-phthalocyanines are a class of coordination compounds that can act as a chemically reactive and sensitive film due to the enormous physical properties of interactions with a wide range of volatile organic compounds [11-27]. Compared to pure phthalocyanines, polymers-phthalocyanines mixed materials are less crystalline, and have high electrical conductivity, and are more effective in gas sensing properties [17]. This opens the door to the meticulous manufacture and design of a thin film with high sensitivity, selectivity, and stability (3S) [18]. We investigated the activities for COVs sensing of the electrospun polyvinyl chloride doped with the NiPc deposited on interdigitated electrodes, in this study. The ideal conditions for nanofiber manufacturing were explored using characterization techniques like scanning electron microscopy, FTIR, and TGA.

V.2. Results and Discussion

V.2.1. Optimization of the electrospinning process

Electrospinning of a 15% and 11% w/v PVC solution in a 1:1 v/v DMF/THF solution proved relatively easy and is suggested that electrospinning of PVC in the THF/DMF solution is more favorable [19]. Four parameters were explored to investigate the electrospinning process and generate smooth nanofibers. Polymer concentration, NiPc concentration, applied voltage, and flow rate are critical parameters that have a direct impact on nanofiber shape [20]. Thus, we produced 15% and 11% PVC solutions and then varied flow rates and voltages. Furthermore, the distance between the needle and the collector in the electrospinning setup had restrictions. Nanofibers were placed on the substrate's surface to determine the best electrospinning settings. The collection period was 3 min, which resulted in dense polymer deposition and allowed the experiment to be completed in a fair amount of time. Experiments that determine Taylor cone, stability of jet, and fabrication of nanofibers are summarized in appendix Table S23.
The parameters of the electrospinning technique for the formation of PVC nanofibers on the interdigitated gold electrode substrate were successfully optimized. We observed that 15% wt. polymer content, flow rate of 1.5 mL/h, and 12 cm between the needle and the collector are the most impressive parameters for fabricating consistent bead free nanofibers.

V.2.2. Characterization of electrospun PVC-NiPc nanofibers

V.2.2.1. Scanning electron microscopy

Scanning electron microscopy (SEM) scans of electrospun 15% PVC nanofibers and that of PVC-NiPc nanofibers are shown in Figure 56.

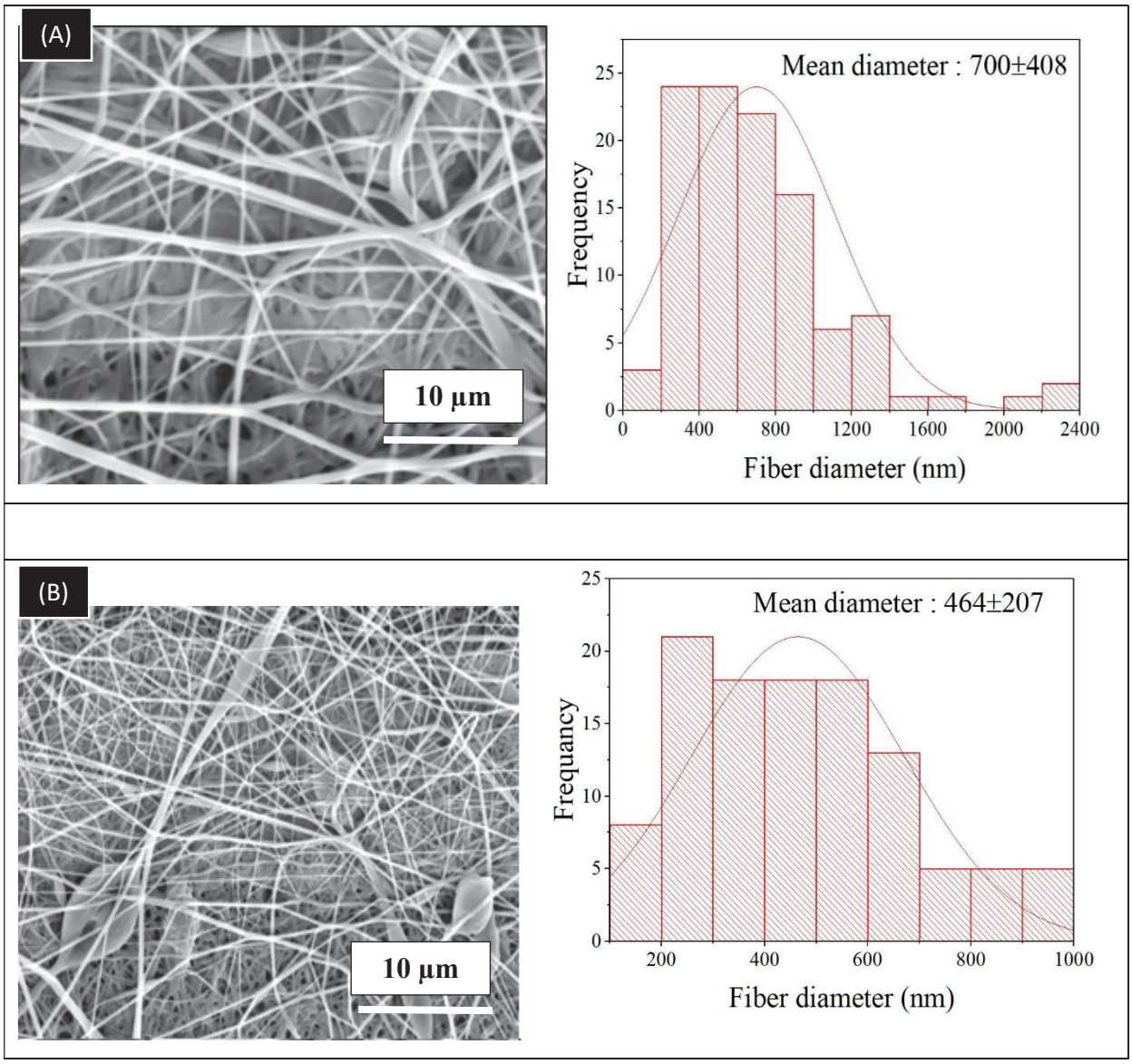

Figure 56. SEM scans and diameter distribution histograms of fibrous mats

(A) PVC nanofibers (B) PVC-NiPc nanofibers electrospun at 1.5 mL/h, 17.4 kV

The morphological surface of the produced nanofibers is presented in Figure 45A depicts fibrous mats obtained from the electrospinning of PVC on interdigitated electrodes. In agreement with the histogram of PVC nanofiber size distribution, PVC nanofibers (NFs) present an average diameter within the range of 700 ± 408 nm. PVC-NiPc nanofibers were found to be dark at the first glance, because of the bluish color of NiPc. The size distribution of PVC NFs average diameter had reduced within the range of 464 ± 207 nm (Figure 45B). This size reduction might be due to the reduced viscosity and increased conductivity of the PVC-NiPc solution.

After electrospinning PVC nanofibers on the substrate, optical images were obtained on bare chip, chip covered with electrospun PVC nanofibers and chip covered with electrospun PVC/NiPc nanofibers (Figure S24 in Appendix). EDS analysis were then performed on the electrospun PVC nanofiber chip. In Figures S26, S27, S28, S29 and in Table S30 in Appendix, we discovered carbon in abundance (77.88%) and some quantity of chlorine (9.45%) due to PVC nanofibers. After doping PVC nanofiber with NiPc, the atomic percentage composition was investigated. NiPc was distributed on the surface PVC nanofiber, as evidenced by the nearly equal percentage number of carbon atoms of about (75.64%) and the presence of (1.14%) Ni at the surface of the fibrous mats.

TGA and FTIR characterization of the electrospun fibers is presented in the Appendix.

V.2.3. VOC differential measurements

The VOC differential detection performance of PVC/NiPc fibrous mats on the interdigitated electrode as working sensor and using only PVC nanofiber as the reference sensor is shown in Figure 46. Sensor operated at optimum conditions (T = 293K, Pressure = 1 atm). The analytical measurement of methanol begins by accounting for the essential sensor parameters, which are response and recovery time of the device, as shown in appendix Figure S35. The response time is 13 s and the recovery time is 25 s.

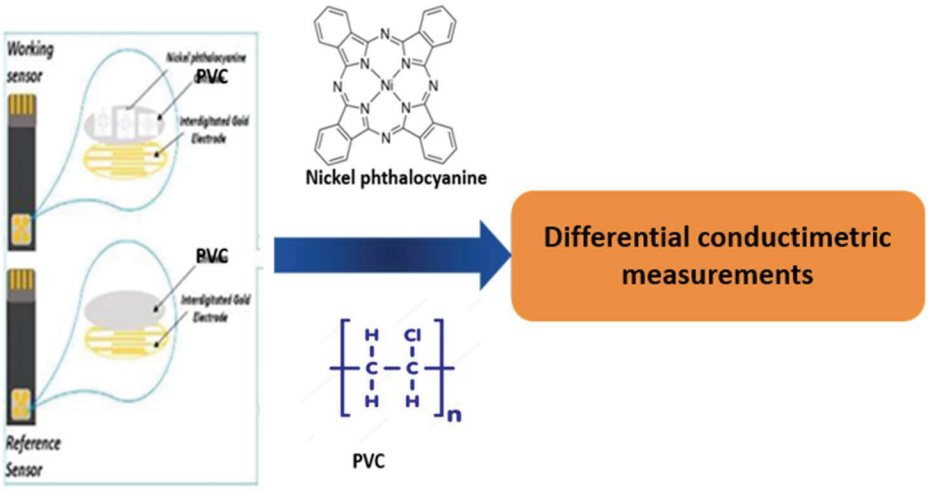

Figure 57. Differential measurements for VOC detection

The sensor response of five different VOCs was tested initially, as shown in Figure 47A.

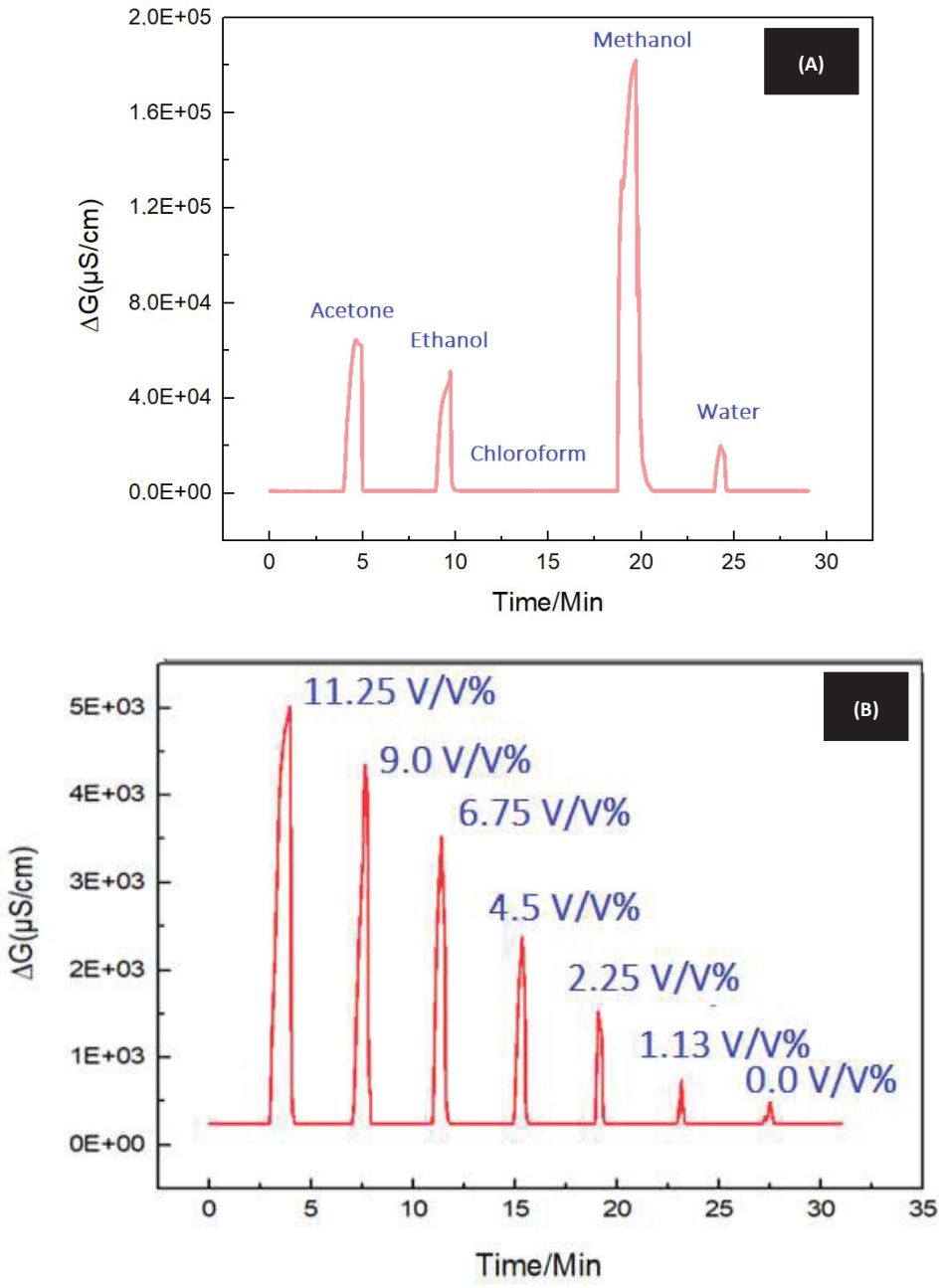

Figure 58. Conductometric sensor responses of five different VOCs

(a) VOCs' detection kinetics (b) gaseous phase of methanol detection kinetics by electrospun PVC nanofiber doped with NiPc using a lock-in amplifier (T = 293 K, Pressure = 1 atm)

The sensor response towards methanol is much higher than for ethanol, acetone, and water, with no response when exposed to chloroform. The sensing mechanism should be related to the rearrangement of the electrical dipole in the bulk thin film due to the interaction of phthalocyanine and analytes (alcohols and acetone), in other words, the interaction generates

modulation in the electronic levels for π -π* transitions of the phthalocyanine ring [21]. After testing the sensor's selectivity of the VOCs as depicted in Figure 47A, the sensor was exposed to successive decreasing concentrations of methanol (Figure 47B) and of acetone (Figure S33) and of ethanol (Figure S34). When the concentration of methanol was 0%, the sensor was exposed to pure water and the measured conductivity, corresponding to 100% of humidity, is then $4.4x10^2$ µS/cm. This low value is due to the hydrophobicity of the PVC matrix and to the differential measurement system. When the concentration of methanol was 11.25%, the measured signal was $5x10^3$ µS/cm, the contribution of 89% of humidity is less than 10% of this signal, which is in the range of the experimental error in this range of concentration. The sensors were exposed to different concentrations of acetone, ethanol, and methanol to ascertain the sensitivity of each of the three VOCs accordingly. The linearity of the methanol calibration curve was verified in the range of 0v/v% to 11.25v/v%. The sensor has a sensitivity of 505 µS/cm $(v/v)^{-1}$ and a limit of detection of 15 ppm, as demonstrated in the calibration curve in Figure 48.

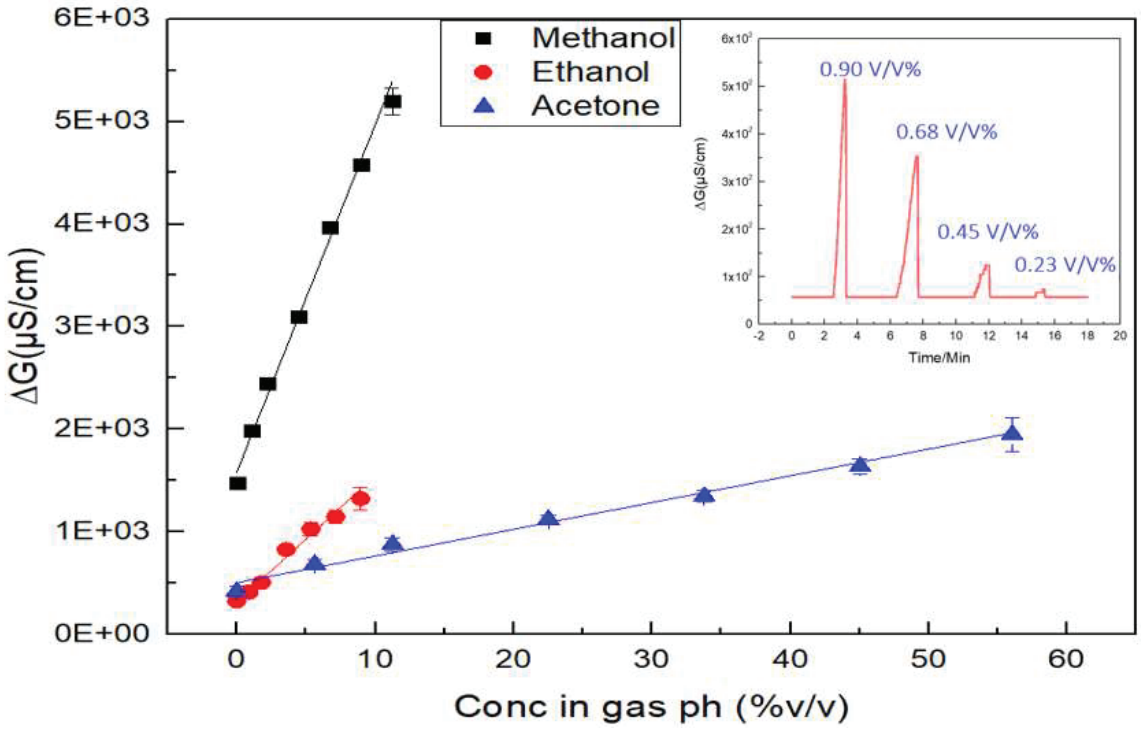

Figure 59. Calibration curves of the gaseous phase of VOCs sensitivities by electrospun PVC nanofiber incorporated NiPc using a lock-in amplifier (T = 293K, Pressure = 1 atm)

The sensor was 4 times more sensitive to methanol than to ethanol and 19 times more sensitive to methanol than to acetone.

In our previous work, using a film of chitosan doped with NiPc [22], a conductivity value of 400 µS/cm was obtained for 9.0 v/v% of methanol whereas with PVC-NiPc fibrous mats, the obtained conductivity value was 4400 µS/cm for the same concentration, showing the interest of the fibrous mats for increasing the sensitivity of detection.

For the same sensor, the relative standard deviation ranges from 8% for lower concentrations to 2% for higher concentrations. The sensor retains its detection performance for seven weeks, when every four days, methanol was tested. The sensor kept nearly 88% of its initial response after this time.

The effect of the presence of 1/10 of acetone on the methanol peak is in the range of the measurement error whereas the effect of 1/10 of ethanol on the methanol peak is 4 times higher than this error.

V.2.4. Application of methanol sensor

Commercial rubbing alcohol is a product made from methanol and is used as a liquid onto barbecues or fireplaces or as solvent or antifreeze. In addition, if used at home, it is a powerful cleaner for stubborn dirt.

The sensor initially detected absolute methanol, followed by a 90% methanol/water mixture and then the commercial rubbing alcohol, as seen in the diagram above (Appendix S37). The conductivity value for rubbing alcohol is consistent with a concentration of 9.9±0.46 v/v% in the gas phase. The expected concentration of rubbing alcohol is 22.2±0.6 M, equivalent to 91.5 ± 3.7% in compliance with the concentration specified by the provider, 95%.

Table S36 in Appendix summarizes different types of electrospun polymer nanofibers describing the nature of the polymer, the gas tested, the response time, the dynamic range and the detection limits for some VOCs.

V.3. Conclusions

The current research proposes a one-step elaboration of electrospun nanofibrous mats and optimization of the electrospinning parameters to generate PVC electrospun nanofibers doped with NiPc. According to our research, the most optimal parameters for fabricating continuous non-beaded nanofibers were 15 weight percent PVC polymer, 1.5 mL/h flow rate, and 12 cm distance between needle and collector.

The findings revealed that nanofiber morphology is greatly influenced by the applied voltage, flow rate, and polymer concentration in solution and the adhesion and stability of nanofiber

deposition on the substrate surface. PVC/NiPc-NFs, synthesized electrospun nanofibers, were employed to make the VOC conductometric sensor. Sensor demonstrated good sensing performance for methanol. In the future, to fabricate an efficient gas sensor for biomedical, industrial, and environmental applications, we wish to couple our sensor with a LCU and GC-MS to enable detection at a much lower concentration.

V.4. References

[1] C. I. L. Justino, T. A. Rocha-Santos, A. C. Duarte, and T. A. Rocha-Santos, "Review of analytical figures of merit of sensors and biosensors in clinical applications," *TrAC Trends Anal. Chem.*, 29(10) (2010) 1172–1183, doi: 10.1016/j.trac.2010.07.008.

[2] F. Schorn, J. L. Breuer, R. C. Samsun, T. Schnorbus, B. Heuser, R. Peters, D. Stolten., "Methanol as a renewable energy carrier: An assessment of production and transportation costs for selected global locations," *Adv. Appl. Energy*, 3 (2021) 100050, doi: 10.1016/j.adapen.2021.100050.

[3] D. S. Chandrasakaran, I. Nainggolan, T. Ikhsan, and M. N. B. Derman, "Ammonia Gas Sensor Based on Chitosan Biopolymer," *Mater. Sci. Forum*, (2015) 429–434, doi: 10.4028/www.scientific.net/MSF.819.429.

[4] Z. Jia, A. Patra, V. K. Kutty, and T. Venkatesan, "Critical Review of Volatile Organic Compound Analysis in Breath and In Vitro Cell Culture for Detection of Lung Cancer," *Metabolites*, 9 (2019) 52, doi: 10.3390/metabo9030052.

[5] G. Korotcenkov, V. Brinzari, and B. K. Cho, "Conductometric gas sensors based on metal oxides modified with gold nanparticles: a review." *Microchim. Acta*, 183 (2016) 1033–1054. doi: 10.1007/s00604-015-1741-z

[6] E. Correa, M. E. Moncada, O. D. Gutiérrez, C. A. Vargas, and V. H. Zapata, "Characterization of polycaprolactone/rGO nanocomposite scaffolds obtained by electrospinning," *Mater. Sci. Eng. C*, 103 (2019) 109773, doi: 10.1016/j.msec.2019.109773.

[7] J. Avossa, R. Paolesse, C. Di Natale, E. Zampetti, G. Bertoni, F. De Cesare, G. Scarrascia-mugrozza, A. Macagnano., "Electrospinning of Polystyrene/Polyhydroxybutyrate Nanofibers Doped with Porphyrin and Graphene for Chemiresistor Gas Sensors," *Nanomaterials*, 9, (2) (2019) 2, doi: 10.3390/nano9020280.

[8] J. K. Y. Lee, N. Chen, S. Peng, P. Li, L. Tian, N. Thakor, S. Ramakrishna., "Polymer-based composites by electrospinning: Preparation & functionalization with nanocarbons," *Prog. Polym. Sci.*, 86 (2018) 40–84, doi: 10.1016/j.progpolymsci.2018.07.002.

[9] J. Xue, T. Wu, Y. Dai, and Y. Xia, "Electrospinning and Electrospun Nanofibers: Methods, Materials, and Applications," *Chem. Rev.*, 119(8) (2019) 5298–5415, doi: 10.1021/acs.chemrev.8b00593.

[10] Z.-M. Huang, Y.-Z. Zhang, M. Kotaki, and S. Ramakrishna, "A review on polymer nanofibers by electrospinning and their applications in nanocomposites," *Compos. Sci. Technol.*, 15(63) (2003) 2223–2253, doi: 10.1016/S0266-3538(03)00178-7.

[11] C. Tasaltin, I. Gurol, M. Harbeck, E. Musluoglu, V. Ahsen, and Z. Z. Ozturk, "Synthesis and DMMP sensing properties of fluoroalkyloxy and fluoroaryloxy substituted phthalocyanines in acoustic sensors," *Sens. Actuators B Chem.*, 150(2) (2010) 781–787, doi: 10.1016/j.snb.2010.07.056.

[12] A. Kumar, R. Meunier-Prest, and M. Bouvet, "Organic Heterojunction Devices Based on Phthalocyanines: A New Approach to Gas Chemosensing," *Sensors*, 20(17) (2020) 4700, doi: 10.3390/s20174700.

[13] A. Kumar, N. Alami mejjati, R. Meunier-prest, A. Krystianiak, O. Heintz, E. Lesniewka, C. H. Devillers, M. Bouvet., "Tuning of interfacial charge transport in polyporphine/phthalocyanine heterojunctions by molecular geometry control for an efficient gas sensor," *Chem. Eng. J.*, 429 (2022) 132453, doi: 10.1016/j.cej.2021.132453.

[14] F. I. Bohrer, C. Colesniuc, J. Park, M. Ruidiaz, I. Schuller, A. Kummel, W. Trogler., "Comparative Gas Sensing in Cobalt, Nickel, Copper, Zinc, and Metal-Free Phthalocyanine Chemiresistors," *J. Am. Chem. Soc.*, 131(2) (2009) 478–485, doi: 10.1021/ja803531r.

[15] A. Kumar, J. Brunet, C. Varenne, A. Ndiaye, and A. Pauly, "Phthalocyanines based QCM sensors for aromatic hydrocarbons monitoring: Role of metal atoms and substituents on response to toluene," *Sens. Actuators B Chem.*, 230 (2016) 320–329, doi: 10.1016/j.snb.2016.02.032.

[16] Z. Şahin, R. Meunier-Prest, F. Dumoulin, A. Kumar, Ü. Isci, and M. Bouvet, "Tuning of organic heterojunction conductivity by the substituents' electronic effects in phthalocyanines for ambipolar gas sensors," *Sens. Actuators B Chem.*, 332, (2021) 129505, doi: 10.1016/j.snb.2021.129505.

[17] R. Zhou, F. Josse, W. Göpel, Z. Z. Öztürk, and Ö. Bekaroğlu, "Phthalocyanines as Sensitive Materials for Chemical Sensors," *Appl. Organomet. Chem.*, 10(8) (1996) 557–577, doi: 10.1002/(SICI)1099-0739(199610)10:8<557::AID-AOC521>3.0.CO;2-3.

[18] A. F. Abdulameer, M. H. Suhail, O. Gh. Abdullah, and I. M. Al-Essa, "Fabrication and characterization of NiPcTs organic semiconductors based surface type capacitive–resistive humidity sensors," *J. Mater. Sci. Mater. Electron.*, 28(18) (2017) 13472–13477, doi: 10.1007/s10854-017-7186-x.

[19] C. Carrizales, S. Palfrey, R. Rincon, T. M. Eubanks, A. Kuang,M. J.McClure,G. L. Bowlin, J. Macossay., "Thermal and mechanical properties of electrospun PMMA, PVC, Nylon 6, and Nylon 6,6," *Polym. Adv. Technol.*, 19(2) (2008) 124–130, doi: 10.1002/pat.981.

[20] S. Sundarrajan and S. Ramakrishna, "Fabrication of nanocomposite membranes from nanofibers and nanoparticles for protection against chemical warfare stimulants," *J. Mater. Sci.*, 42(20) (2007) 8400–8407, doi: 10.1007/s10853-007-1786-4.

[21] J. Spadavecchia, G. Ciccarella, L. Valli, and R. Rella, "A novel multisensing optical approach based on a single phthalocyanine thin films to monitoring volatile organic compounds," *Sens. Actuators B Chem.*, 113(1) (2006) 516–525, doi: 10.1016/j.snb.2005.03.110.

[22] I. Musa, G. Raffin, M. Hangouet, M. Martin, A. Alcacer, Nadia Zine, F. Bellagambi, N. Jaffrezic-Renault, A. Errachid, Development of a chitosan/nickel phthalocyanine composite based conductometric micro-sensor for methanol detection, *Electroanalysis*, on line, doi: 10.1002/elan.202100707

Chapter VI
General Conclusions

We have developed a new class of novel transducers based on the utilization of interdigitated gold microelectrodes (µIDEs). These µIDEs were made on a silicon substrate (microchips measuring 7.3 x 4 mm) in a cleanroom using traditional microelectronics production processes. This microelectrode arrangement makes it possible to detect and measure the presence of a target molecule in a gaseous medium using conductometric measurement techniques. Different designs of µIDEs were considered and manufactured for these purposes. In this investigation, only the classic design of µIDEs was studied among these microelectrode types. The application of our study findings to these cutting-edge microelectrodes will undoubtedly boost the sensitivity of our sensors.

The effort of creating and optimizing the sensor in this context was centered on determining the impact of the µIDE's geometric parameters on the sensor's response. For detecting gaseous analytes, characteristics such as digit size, spacing, and thickness were debated, carefully investigated, and adjusted. Following the validation of the transducer, the designed encapsulated sensors were first cleaned and tested in aqueous environments using the method of adding various concentrations of KCl. The conductometric data were compared to a mathematical model that depicted the events that occur at the interface of polarized µIDEs in a liquid media. The conductometric measurements allowed us to validate the transducer's fabrication and use in a liquid medium. After then, the entire model was converted to a gaseous medium. Consequently, we developed an effective transducer capable of measuring the presence and concentrations of VOCs in a gaseous medium using conductometric measurements.

The research goal is to develop a sensor that can measure the concentration of VOC molecules selectively. Most VOCs concentrations in saintly patients have been reported to be in the hundreds of parts per billion (ppb), with a general trend to ppm. We need to use a sensitive and VOC-selective polymer membrane to functionalize our sensor in this scenario.

We have opted to work with chitosan for our research, a fascinating biopolymer with intriguing physical and chemical properties. On the one hand, we have thus created a process for creating an acid chitosan solution, the different phases of which have been optimized to achieve a homogeneous and repeatable deposit on the µIDE's surface. A functionalization process based on the electro-addressing of the chitosan membrane to the microelectrode surface was devised in the other section. CV also characterized the membranes as well designed. The functionalized sensors were put to the test using conductometric analyses. But later, the chronoamperometry technique was shown more suitable for chitosan deposition on gold microelectrode surface.

It was based on the usage of LabVIEW software; we control the "Lock-In Amplifier" measuring device that provides our sensor (sinusoidal signal) and evaluates the sensor response when exposed to VOCs. To achieve this strategy, numerous instrumentation parameters, amplitude, and frequency of the excitation signal were evaluated and tuned for our sensor. As a result, the complete platform produced during this project allows us to adjust the numerous parameters involved with conductometric analyses and evaluate the response of our sensor in different configurations. With this in mind, we suggested first investigating the behavior of our chitosan membrane to verify the polymer's physical and chemical properties. The functionalized sensors were tested in stationary gaseous environments (cylinders holding a mixture of distilled water and solvents). Our sensor is sensitive to the VOC molecules, with fast reaction and recovery times (40 seconds) and a consistent and repeatable signal.

Furthermore, experiments have revealed that our membrane is more selective for methanol than for other interfering chemicals like ethanol and acetone. The sensor's reaction to a gas flow at various relative humidity levels was studied and optimized. Sensor response influenced by humidity level, to a maximum RH rate of 70%, the qualities of our membrane have been proven. Because the study's goal is to monitor the breath expelled by the patient, which can be compared to a gas flow saturated with moisture, this feature is somewhat encouraging. After that, the sensor's response was tested against various VOC concentrations. The final sensor created has a detection limit of 1000 ppm against methanol, which is insufficient for the project's goals, as we need to approach a lower concentrations range. In this regard, we proposed doping the chitosan membrane with VOC-sensitive molecules to boost the sensitivity of our sensor. are a group of organometallic compounds, which tend to have the capability to act as a chemically reactive and sensitive film as a factor of enormous physical properties impelled upon them through interaction with many volatile organic compounds.

On the one hand, we've devised a method for chemically modifying the chitosan membrane by doping in a solution of 1 mg/ml THF solution such that nickel phthalocyanine can be incorporated into their structure. This form of cation allows the molecule to be polarized, which aids in trapping VOC molecules in the membrane. SEM and FTIR studies evaluated the functionalized nickel phthalocyanines allowing us to validate the chemical modification method. Functionalizing sensor using the CA technique has been tweaked to co-electrodeposit chitosan-NiPc doped surface IDE at a doping rate of 10%. FTIR and AFM technologies were used to characterize membranes. The conductometric analysis of functionalized sensors, the insertion of NiPc and making differential measurements changed the behavior of our sensor

completely. According to tests, humidity no longer affects the conductivity signal of the VOC detection.

A sensitive gas sensor was developed based on chitosan composites doped with NiPc. Analytical techniques such as FTIR, SEM, EDS, AFM, XPS, and TGA were employed to characterize the composite-sensing layer. Excellent thermal stability of the sensing layer has been observed. Acetone, ethanol, and methanol gas-sensing properties of the films prepared at optimum conditions were studied at atmospheric temperature using lock-in amplifier differential measurements at 10 kHz. The sensor is selective, sensitive, and stable towards methanol. Presently, there exists no methanol detector for early diagnosis by breath analysis or for screening of alcoholic beverages.

To explore more in fabricating a highly sensitive, selective, and stable gas sensor, we use the electrospinning of polymer composites. Electrospinning is a low-cost, high-efficiency method for producing ultra-thin polymer and composite fibers with diameters ranging from a few nanometers to a few micrometers. Electrostatic stretching of polymer solutions or melts ejected by microsyringe pumps necessitates a high voltage. This method has got a lot of attention in the previous two decades. More than a hundred polymers were actively spun into ultra-fine fibers using electrospinning. Electrospun fibers with various materials, a fine structure, a tunable membrane, thickness, and an appealing broad specific surface indicate the best structure prospects for a sensing application.

This research employs a vertical electrospinning device with polyvinyl chloride as a sensitive polymer membrane.

The present study provides a one-step elaboration of electrospun membrane nanofibrous mats and optimizes electrospinning parameters to make PVC-NFs with no beading mixed with NiPc. According to our research, the best parameters for generating continuous non-beaded nanofibers were 15% PVC polymer, 1.5 mL/h flow rate, and 12 cm distance between needle and collector.

The researchers discovered that the applied voltage, flow rate, and polymer concentration in solution and the adhesion and stability of nanofiber deposition on the substrate surface significantly impact nanofiber morphology. It has a sizeable homogeneous zone of nanofiber collection.

The VOC sensor was made with PVC-NFs, which were electrospun nanofibers manufactured. The sensor displayed good detecting capability during electrochemical testing of the constructed conductometric gas sensor for VOC detection. We hope to connect our sensor with

a LCU and a GC-MS in the future to create an efficient gas sensor for biomedical, industrial, and environmental applications. This will allow detection at low concentrations.

The sensors produced will provide clinicians in charge of patients with real-time data on the concentration of conditions biomarkers. Furthermore, they will make the patient's care easier because the created sensors will be quick, simple to use, and reusable. As a result, these sensors will enable the early detection of disease syndrome or, if appropriate, the clinical monitoring of patients' vital data and screening laced beverages. As a result, a more comprehensive examination of the sensory response to various VOC combinations is on the horizon for future research in this field. Furthermore, the findings of this thesis point to the following phase, which is the confrontation of e-noses with real-world objects. VOC biomarkers in a patient's breath can be used to make an early diagnosis of cancer and other related VOC biomarkers of various diseases.

Appendix

Chips used in this study [1]

The silicon wafer (<100 > orientation p-type wafer) is first wet oxidized, resulting in an 800 nm thick silicon oxide layer. "Physical Vapor Deposition" is then used to deposit metal layers (PVD). The deposit's thickness was 200 nm for the gold layer and 150 nm for the platinum layer. The thicknesses are sufficient to assure the metal layer's adherence. Thin titanium and nickel auxiliary layers were also deposited over silicon oxide before improving the compliance of the higher layers (50 nm for gold and 15 nm for platinum). Finally, a 400 nm thick silicon oxide/silicon nitride passivation layer is deposited via plasm-enhanced chemical vapor deposition (PECVD).

Following the validation of the microelectrode design, a layout is created using modeling software and executed on a substrate in a clean environment. The CNM, Barcelona in Spain, oversaw manufacturing the microelectrodes.

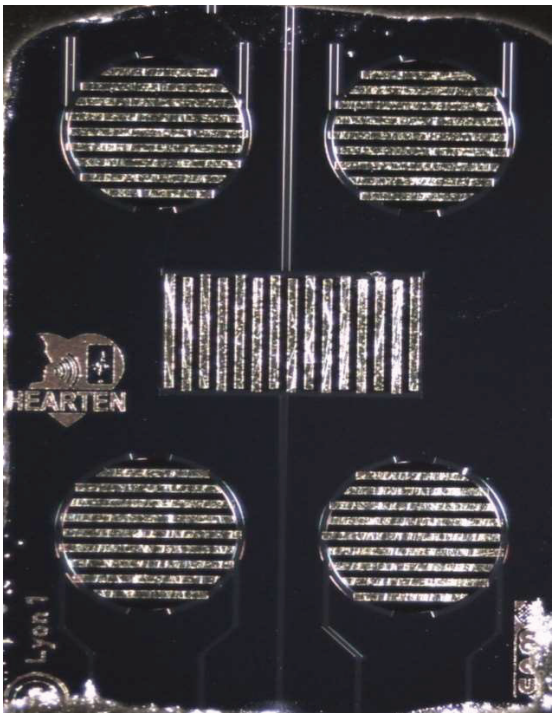

S 1. Encapsulated micro conductometric chips

The obtained chips were cleaned using the schematic protocols as shown in the figure below.

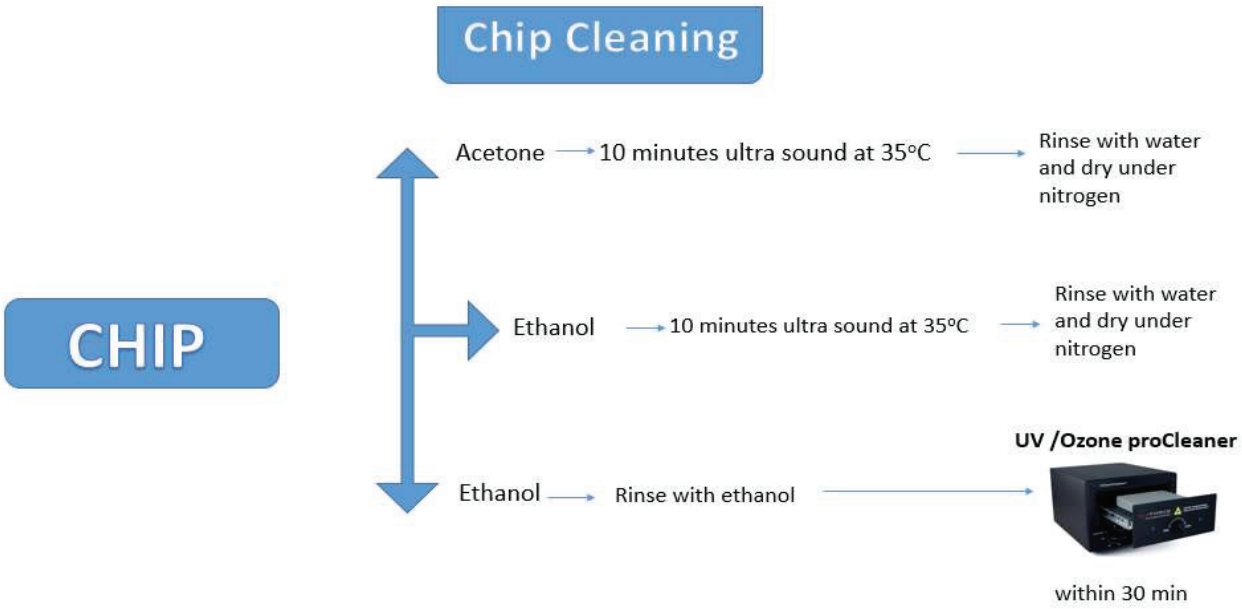

S 2. Chips cleaning

To be sure that, the chip is well cleaned, we use an optical microscope device to view the cleanliness of the chips, as demonstrated in the figure below.

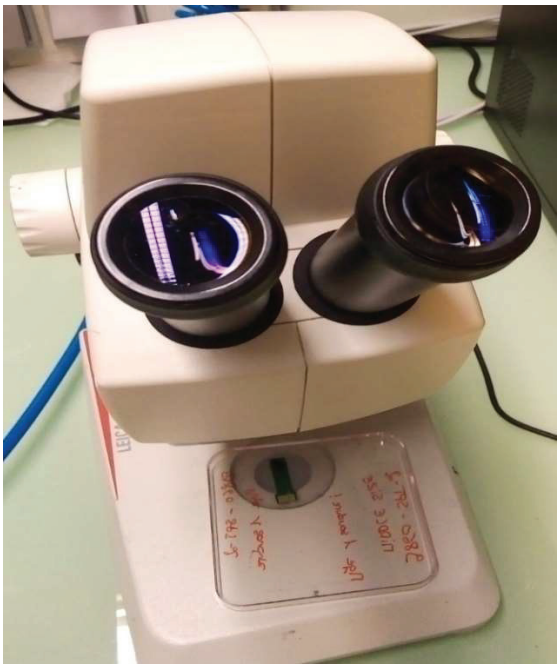

S 3. Optical microscope for viewing chips

KCl Analysis

Upon getting satisfied that the chips are cleaned, we went ahead to sort out the conductivity working efficiency of the interdigitated electrodes using KCl titration experiment with lock-in amplifier as depicted in the coming figure.

S 4. Conductivity measurements of KCl solution using interdigitated electrodes

Chitosan used in this study

Chitosan is a polysaccharide made from chitin, the world's second most prevalent polysaccharide after cellulose. Several outstanding features of chitosan provided unique prospects for the development of biomedical applications. The presence of amino groups in the chitosan structure may be protonated, giving solubility in dilute acidic aqueous solutions. In this study, we used many varieties of chitosan before settling on lower molecular weight, as shown in the figure below, because it gives us the most remarkable results.

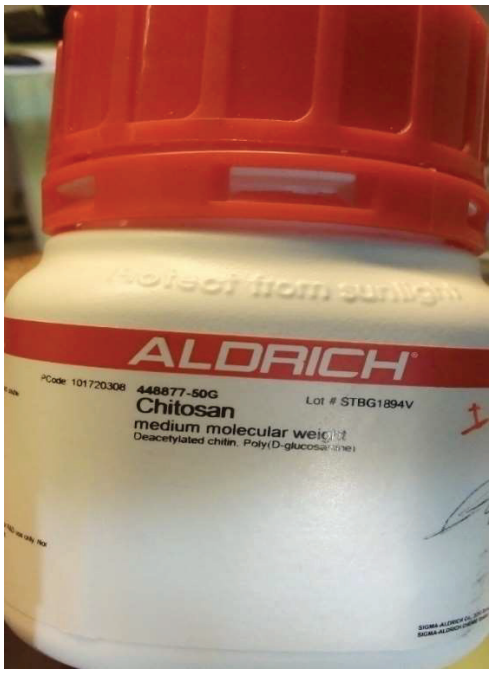

S 5. Medium molecular weight chitosan is the sensitive membrane for gas sensors

All the chitosan used in this study were purchased from Sigma Aldrich without further modification.

Preparation of Chitosan solution

The chemical composition of the chitosan solution was: 1% (v/v) of acetic acid, 1% (w/v) of chitosan; (medium molecular weight). The pH was adjusted at 6.5 by carefully adding a drop of 1M NaOH after 24 hours of agitation at a 550-rpm magnetic stirrer (Figure S6). The chitosan solution was used for electrodeposition of the membrane.

S 6. Preparation of 1 %(w/v) chitosan solution

Preparation of Nickel Phthalocyanines solution

We measure 1 mg/mL of NiPc in THF solvent and allow agitation of 300 rpm for 24 hours. The dissolved solution of NiPc is depicted in Figure S7.

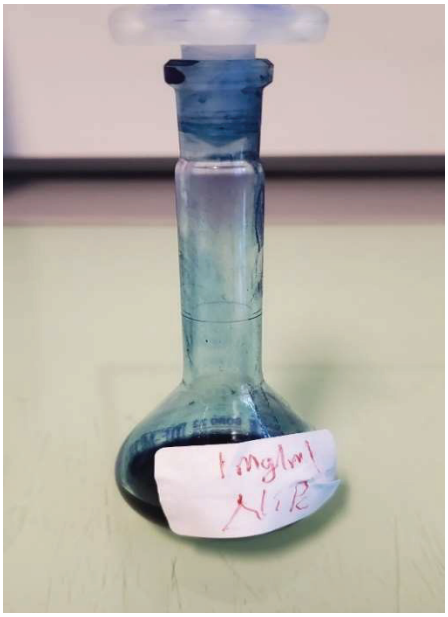

S 7. NiPc solution sensitive material

CA Electrodeposition procedure

Chronoamperometry deposition technique was carried out by putting some amount of chitosan solution in a 5 mL beaker, where the working electrode (Au-chitosan membrane), Reference electrode Ag/AgCl, Counter electrode (Pt-electrode) are all immersed in the chitosan solution, connected to EC LAB Potentiostat and set the constant potential of -1.4 V for 5 minutes (see conditions in Figure S8). The current of the electrode was measured as a function of time (Figure S9).

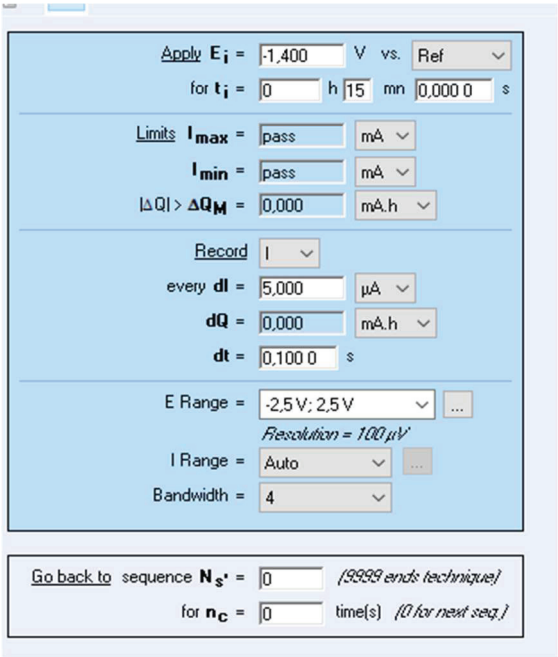

S 8. Chronoamperometry parameters for chitosan deposition

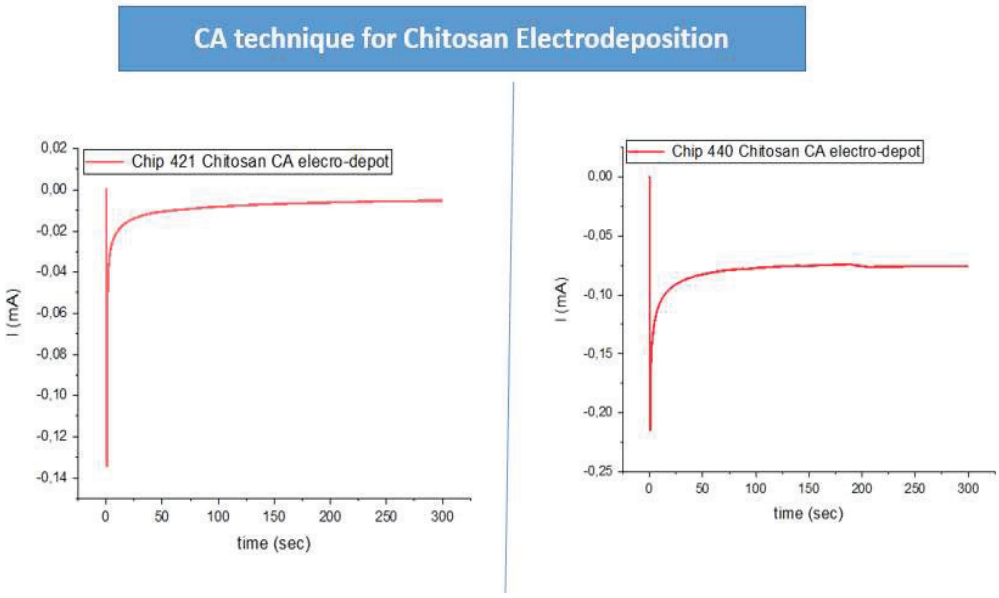

S 9. Voltammogram for chitosan deposition

After the deposition, the chip is carefully rinsed, dried under nitrogen flow in the fume hood, then baked in a furnace (see Figure S10) at 50ºC for 2 hours. The working electrode chip is immersed in the solution of NiPc for 5 minutes before baking in a furnace.

S 10. Furnace for baking electrodeposited chitosan chip

The optical microscope was used to view the chip to ascertain the change of structure of the chip to be sure the chitosan is well deposited on the gold electrode surface, as can be seen in Figure S11: cleaned chip, chip covered with chitosan, and a chip covered with chitosan doped with NiPc

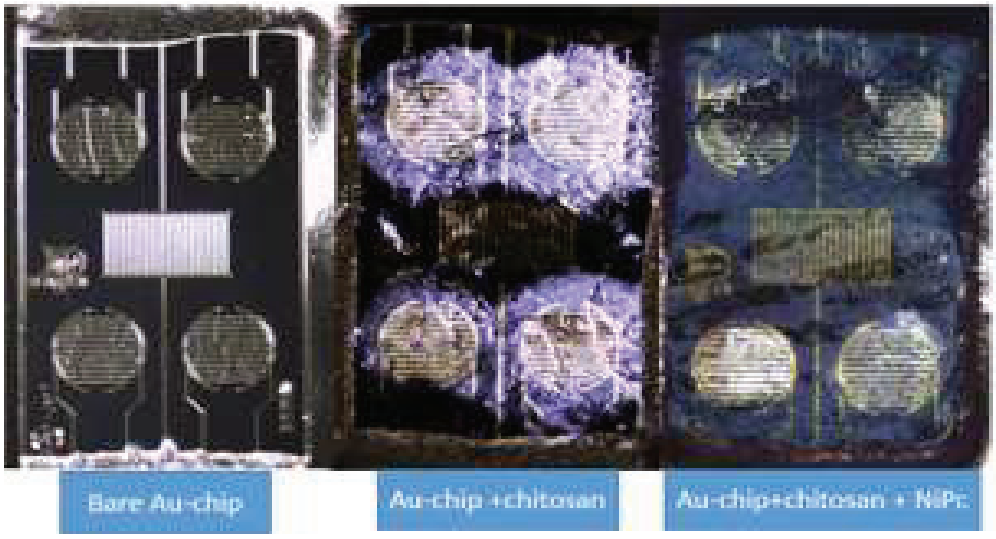

S 11. Optical microscopic view of the clean chip, the chip covered with chitosan and chip covered with chitosan doped NiPc

SEM Analysis

An image of the surface of the chip (gold electrode) with chitosan and NiPc deposited as a sensitive membrane were snapped using SEM. The picture depicts an excellent deposition. The surface morphologies of the chitosan on gold electrode together with chitosan on gold covered with NiPc membranes were studied using scanning electron microscopy (SEM) (COXEM EM-30AX^{+}).

S 12. SEM Image of (a) bare chip, (b) chitosan deposited on chip and (c) Chitosan doped NiPc deposited on chip

The atomic composition of the materials was also confirmed using EDS elemental analysis, as demonstrated in Figures S13, S14, S15.

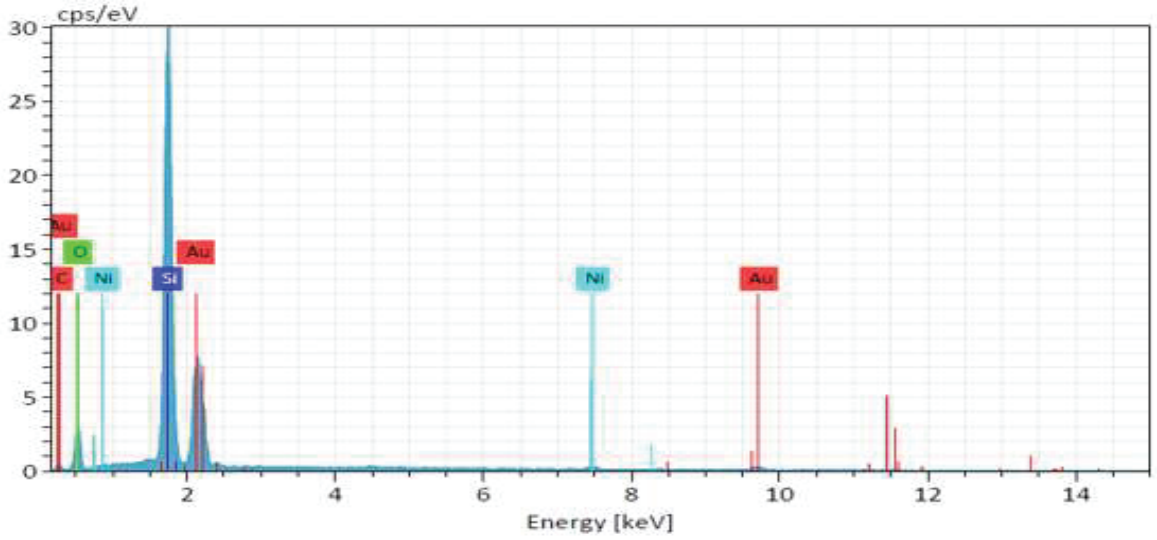

reference 1

Element	At. No.	Netto	Mass [%]	Mass Norm. [%]	Atom [%]	abs. error [%] (1 sigma)	rel. error [%] (1 sigma)
Si	14	21931	46.81	38.75	45.29	2.02	4.31
Au	79	8308	44.98	37.23	6.20	1.83	4.07
O	8	1579	21.17	17.52	35.95	4.27	20.19
C	6	203	4.96	4.10	11.22	1.91	38.57
Ni	28	220	2.90	2.40	1.34	0.26	8.94
		Sum	**120.82**	**100.00**	**100.00**		

S 13. EDS of the bare chip

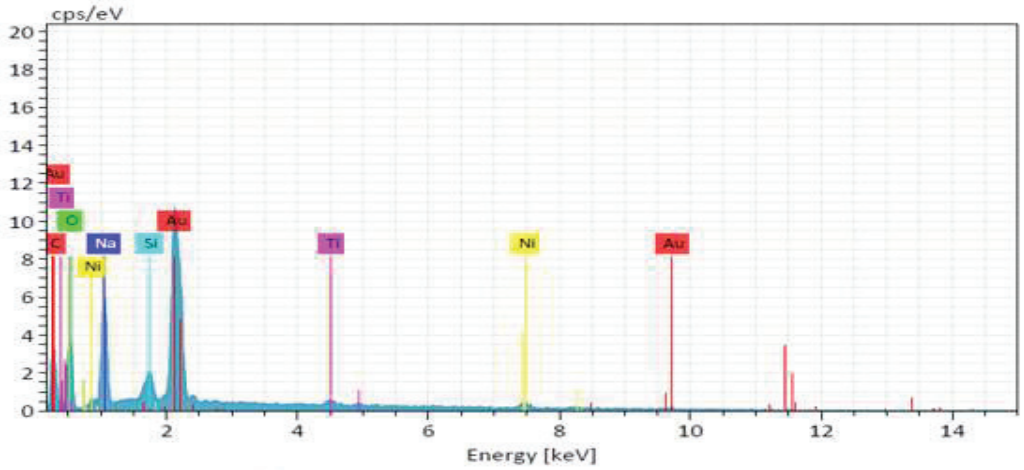

reference-WE2 1

Element	At. No.	Netto	Mass [%]	Mass Norm. [%]	Atom [%]	abs. error [%] (1 sigma)	rel. error [%] (1 sigma)
Au	79	13703	35.65	41.59	5.58	1.42	3.98
C	6	2322	17.16	20.02	44.06	3.16	18.45
O	8	2465	16.69	19.47	32.17	3.04	18.21
Na	11	4011	10.56	12.33	14.18	0.74	6.96
Ni	28	341	2.87	3.35	1.51	0.22	7.69
Si	14	1127	1.55	1.81	1.70	0.11	7.35
Ti	22	349	1.23	1.44	0.80	0.11	8.61
		Sum	**85.71**	**100.00**	**100.00**		

S 14. EDS of chip covered with chitosan

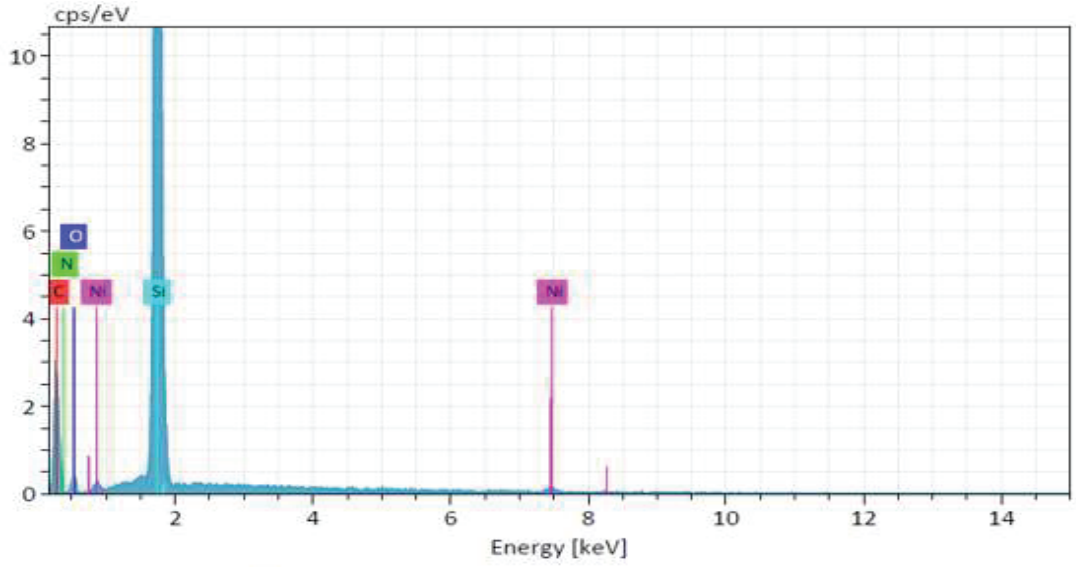

421_NiPc 0

Element	At. No.	Netto	Mass [%]	Mass Norm. [%]	Atom [%]	abs. error [%] (1 sigma)	rel. error [%] (1 sigma)
C	6	2748	63.28	51.83	67.01	11.18	17.67
Si	14	33638	40.71	33.34	18.43	1.74	4.28
N	7	97	9.36	7.67	8.50	4.76	50.83
O	8	380	7.20	5.90	5.73	2.22	30.86
Ni	28	208	1.54	1.26	0.33	0.15	9.89
		Sum	**122.10**	**100.00**	**100.00**		

S 15. EDS of chip covered with chitosan-NiPc

FTIR Analysis

Fourier Transform Infrared (FTIR) spectra were obtained out using a (Nicolet-Thermo Fisher, UK) coupled to an Attenuated Total Reflectance (ATR) mode with a thunder dome (Spectra-tech) sample holder with a germanium crystal coupled with a mono reflection at 45°. FTIR was used to obtain information and confirmation of the doping of phthlocyanine in the chitosan membrane for assessing the chemical bonds and compositions of chitosan composite; the quantification of the FTIR peak areas was carried out with Software (Nicolet-Thermo Fisher, UK) after a proper normalization procedure. The step-by-step results were obtained from bare chip, chip covered with chitosan, and chip covered with chitosan-NiPc.

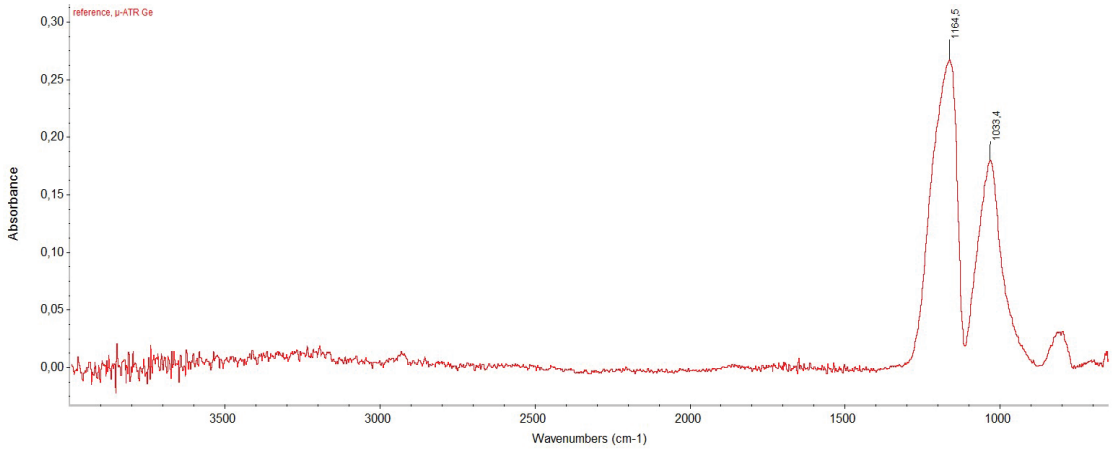

Spectrum from reference bare chip

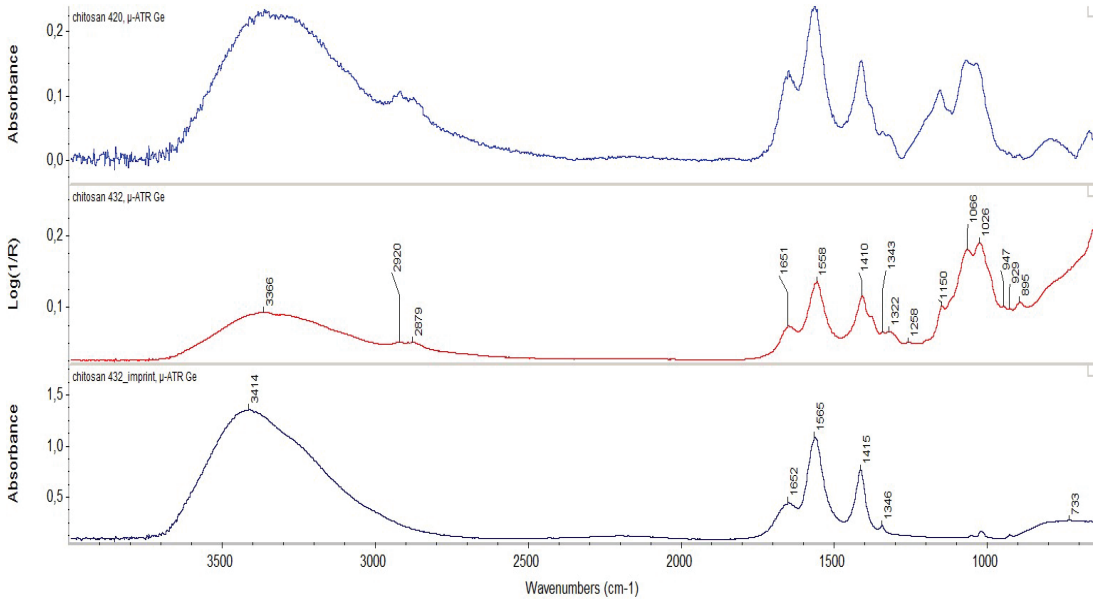

S 16. Spectra from chitosan 420, chitosan 432, and his imprint left on crystal

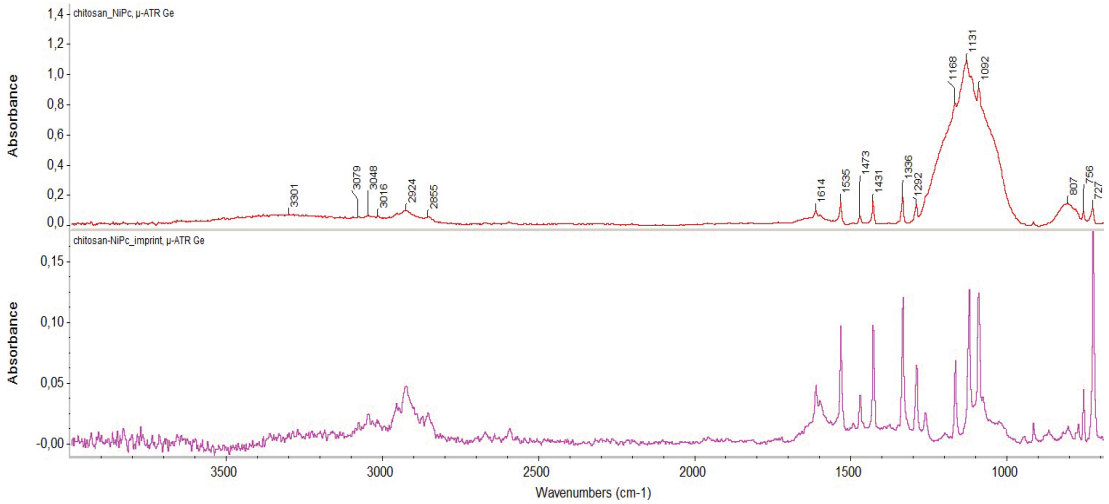

S 17. Spectra from Chitosan+NiPc and the imprint left on the crystal after analysis

TGA Analysis

Chitosan powder was subjected to TGA analysis. The TGA results demonstrate chitosan has a loss weight of 9.7%, enabling us to calculate the exact mass of chitosan for the solution prepared for the deposition. The decomposition temperature of chitosan is around 180ºC. With this, our sample baked at 50ºC is in the course without fear of being decomposed. The TGA provides us with three degradation stages: at 180°C, the second stage at 385°C, and the third stage being at 650°C. Therefore, the thermal stability of the products is from ambient temperature to around 180°C. The analysis showed that both physical forms presented three degradation steps, with the chitosan losing a little more mass during each step. The TGA results are depicted inFigures S18 for chitosan, S19 for nickel-phthalocyanine and S20 for chitosan doped with nickel-phthalocyanine.

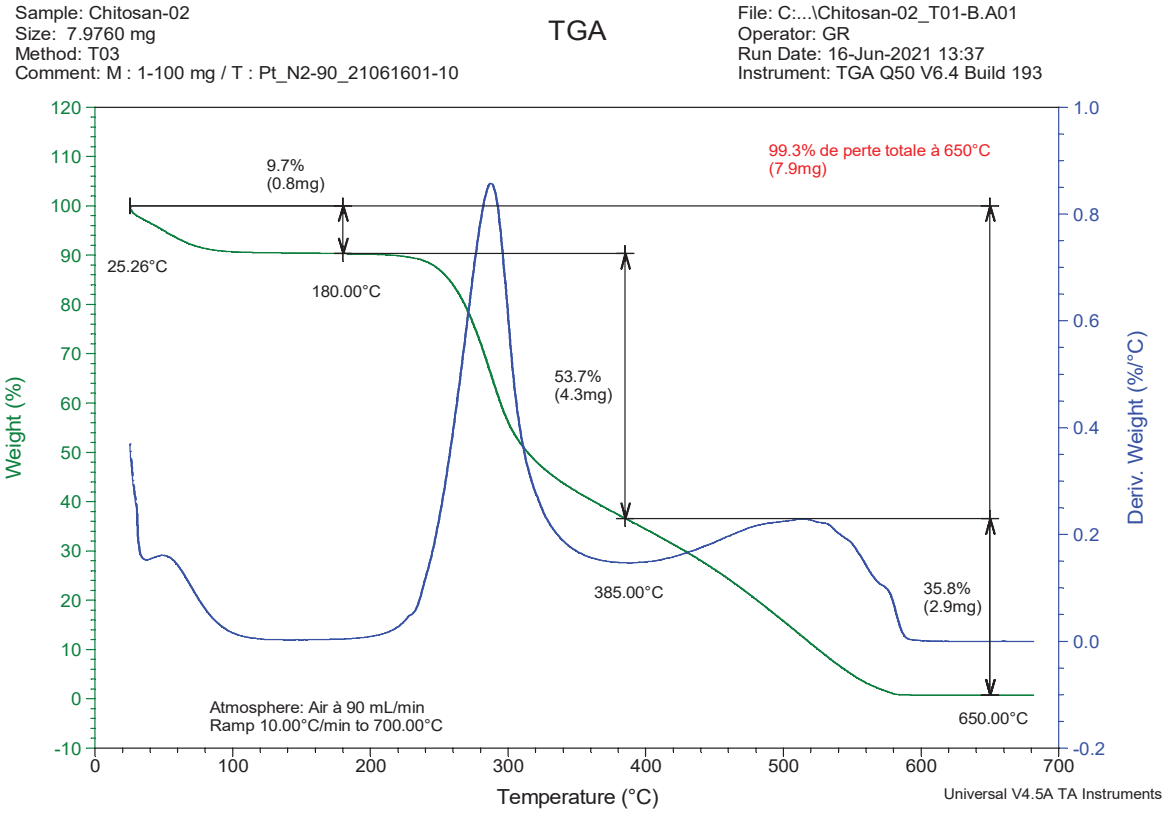

S 18. TGA of chitosan

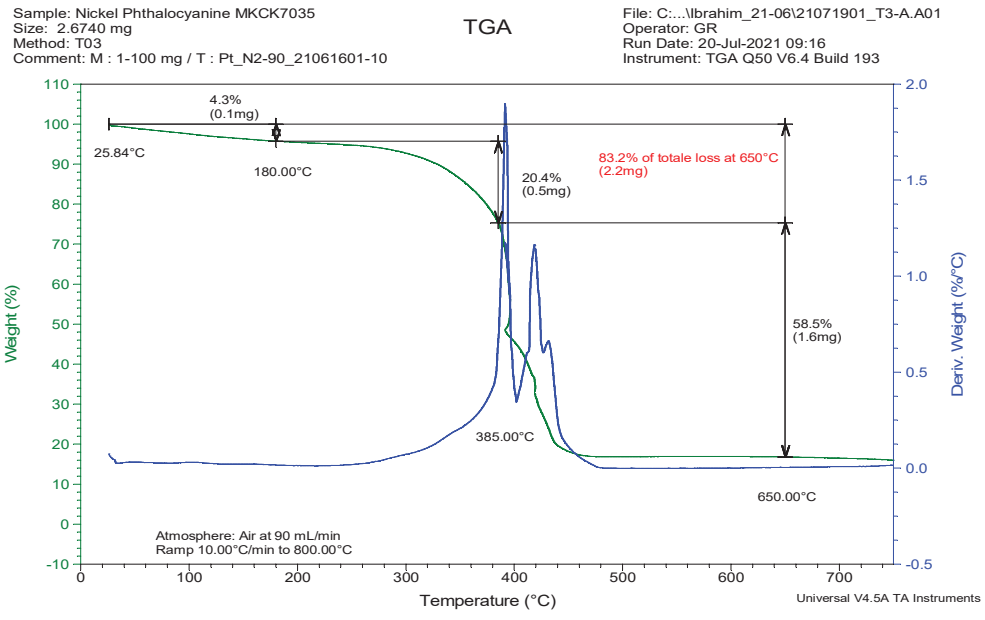

S 19. TGA of NiPc

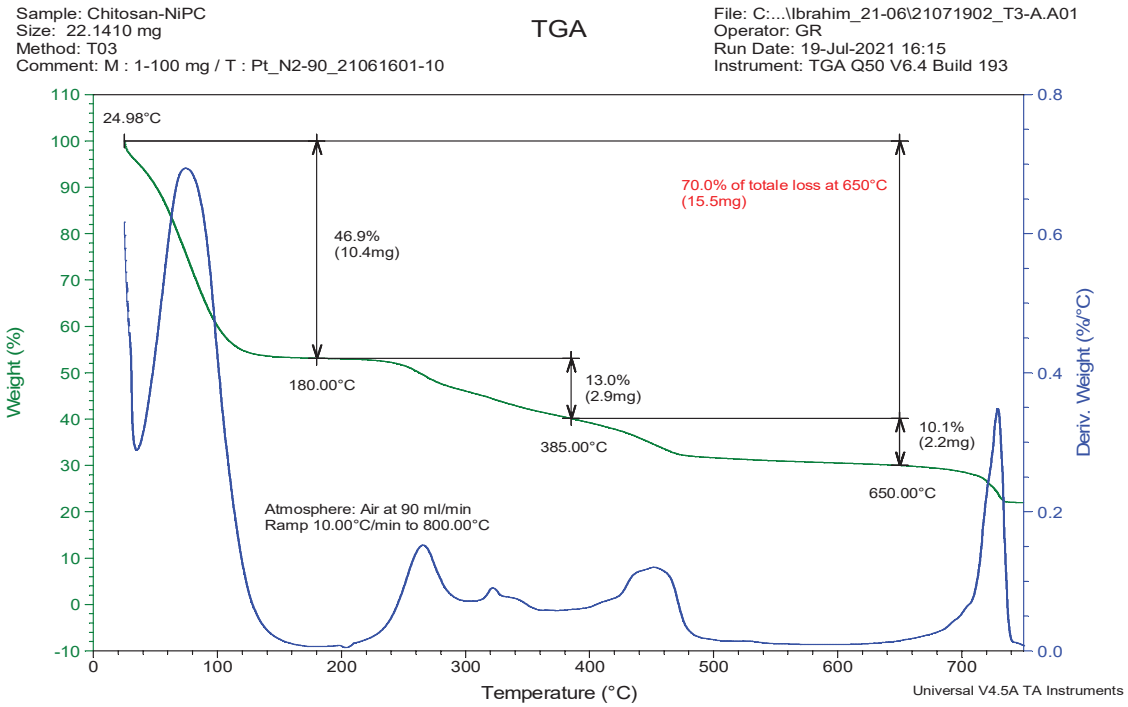

S 20. TGA of chitosan-NiPc

VOC Detection

Gaseous methanol, ethanol, and alcohol sample were collected from the headspace above aqueous solutions of known concentrations and detected using a Lock-in amplifier in a differential mode. The VOCs detection of different aqueous concentrations range (10-100%) is given in Figure S21(A) for acetone and S21(B) for ethanol.

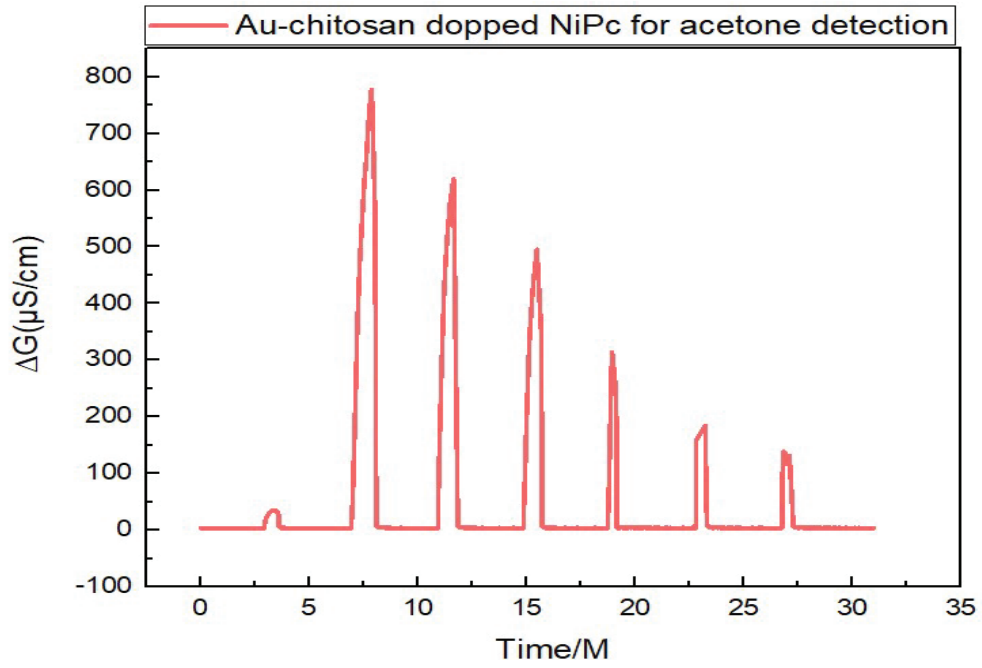

S 21 (A). Detection of gas-phase acetone solutions with chitosan-NiPc

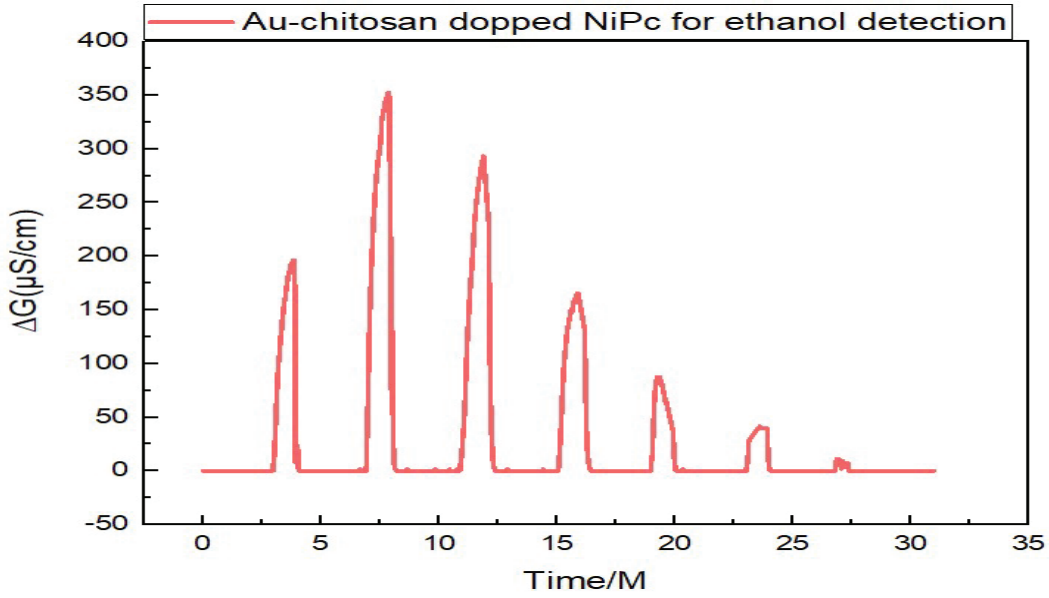

S21 (B). Detection of gas-phase ethanol solutions with chitosan-NiPc

PVC used in this study

One of the candidates that can be used for the sensor is polyvinyl chloride (PVC) third most used polymer. Besides having a wide variety of applications in different spheres due to inexpensiveness in synthesis, chemical resistivity, good insulating properties, and availability on a large scale, such materials have found proper utilization in sensor technologies. Poly (Vinyl chloride) PVC was purchased from Sigma-Aldrich, used without further purification.

Preparation of electrospinning membrane

PVC solution was prepared by dissolving the PVC powder in the DMF/THF systems (ratio volume of 50/50) at a temperature of 50°C and a stirring speed of 300 rpm with an 11%, 15%, and 17% PVC weight concentration. Mixing was carried out for 3 h until the PVC dissolved completely. The prepared solution was kept at room temperature for 1 h to remove air bubbles and stabilize, as shown in Figure S22.

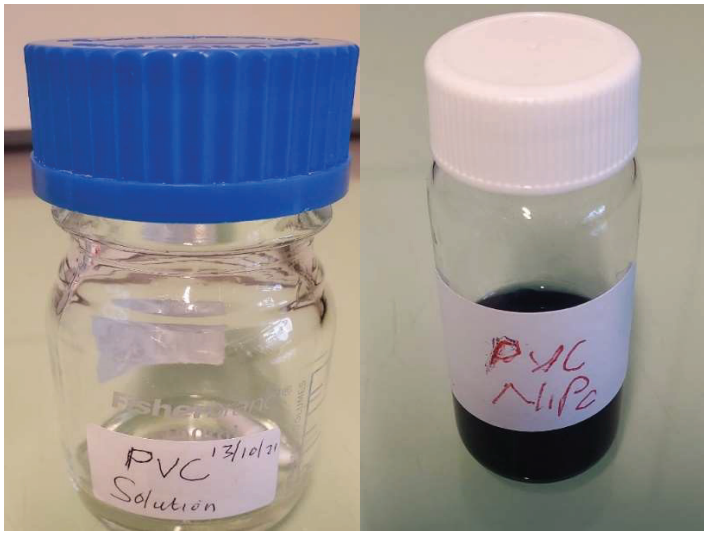

S 22. Solution of PVC and PVC doped with NiPc

An electrospinning machine was used to carry out the process of nanofiber fabrication, the electrospun fiber was sprayed on interdigitated electrodes. The tested parameters for electrospinning process are presented in Table S23.

Experiment No.	Concentration	Applied Voltage	Flow rate
1	11%	8.63 kV	0.2 mL/h
2	11%	8.6 kV	1.5 mL/h
3	11%	9.68 kV	2.0 mL/h
4	11%	10.28 kV	3.0 mL/h
5	15%	8.35 kV	0.2 mL/h
6	15%	9.11 kV	0.3 mL/h
7	15%	10.5 kV	0.4 mL/h
8	15%	15.11 kV	0.5 mL/h
9	15%	10.65 kV	0.5 mL/h
10	15%	17.74 kV	0.5 mL/h

S 23. Tested parameters for the electrospinning process, for 11 and 15% PVC solution

Figure S24 depicts the optical microscope images of bare chip, chip covered with electrospun with PVC nanofiber and chip covered with electrospun with PVC nanofiber incorporated with NiPc.

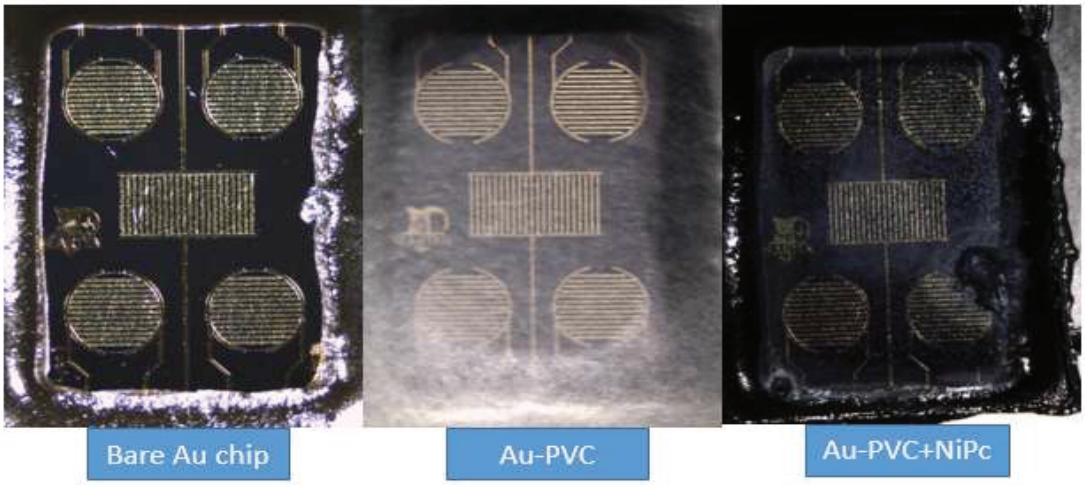

S 24. Optical microscope image from bare chip, chip covered with electrospun with PVC nanofiber, and chip covered with electrospun with PVC nanofiber incorporated with NiPc

SEM and EDS Analysis

The SEM samples were sputter-coated with gold to prevent charging during SEM imaging. Image processing software Image (NIH) and microscopic observations of the SEM image were used to measure the diameter of the electrospun nanofibers from the SEM micrographs. Nanofibers morphologies were determined, as demonstrated in Figure S25.

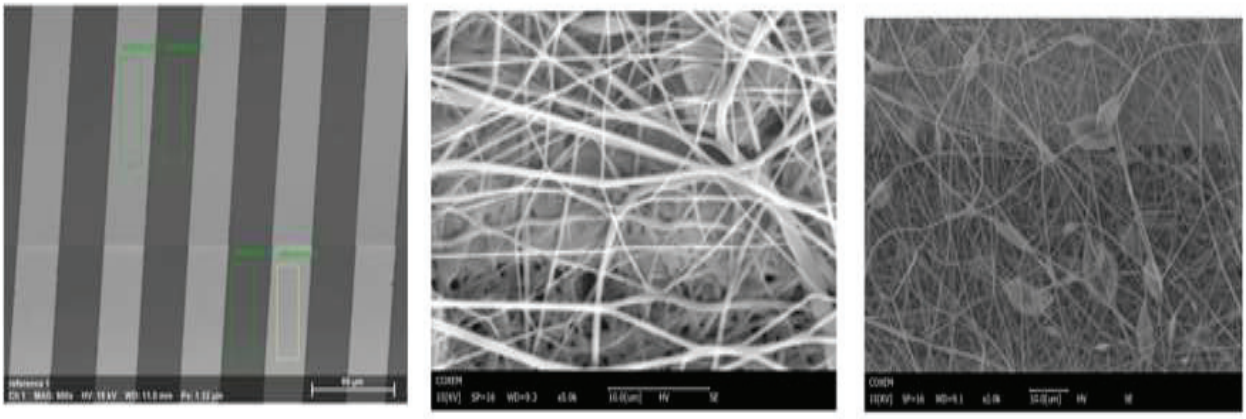

S 25. SEM image of bare chip, chip covered with electrospun with PVC nanofiber, and chip covered with electrospun with PVC nanofiber incorporated with NiPc

The atomic composition of the nanofiber was also confirmed using EDS elemental analysis, as demonstrated in the Figure S26, S27, S28 and Table S29.

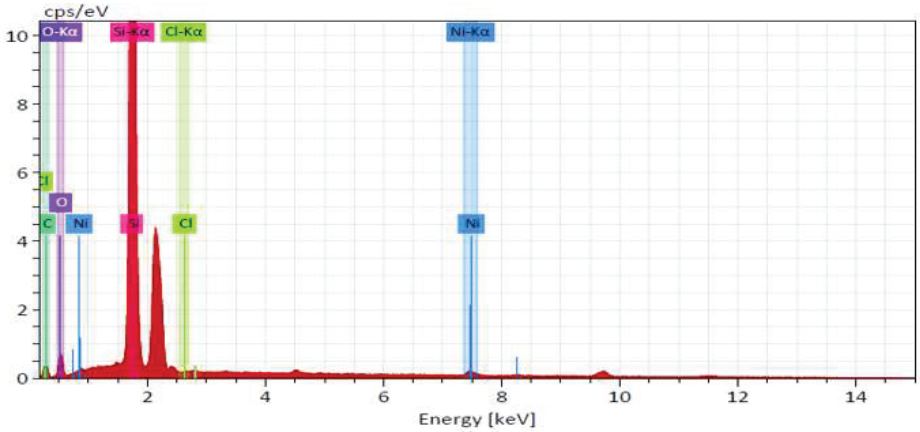

Element	At. No.	Netto	Mass [%]	Mass Norm. [%]	Atom [%]	abs. error [%] (1 sigma)	rel. error [%] (1 sigma)
Si	14	225088	28.59	60.37	43.67	1.21	4.24
C	6	3157	10.05	21.23	35.91	1.75	17.37
O	8	5581	7.20	15.21	19.31	1.13	15.70
Ni	28	2519	1.51	3.20	1.11	0.08	5.51
Cl	17	0	0.00	0.00	0.00	0.00	1.32
		Sum	47.36	100.00	100.00		

S 26. EDS analysis of bare chip

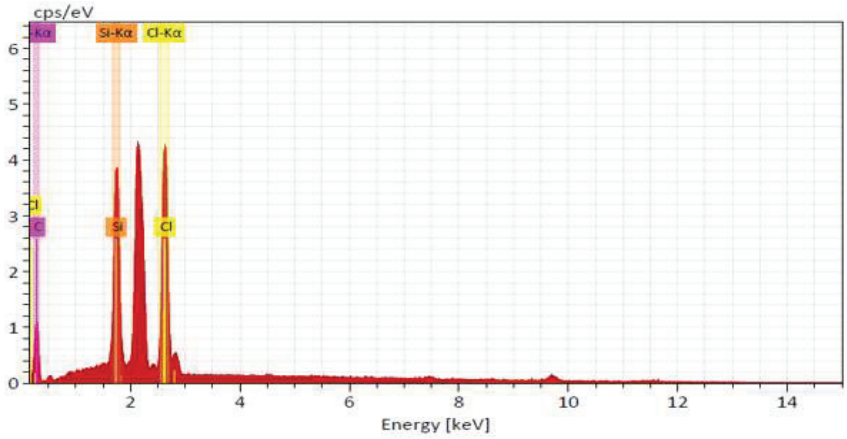

Map

Element	At. No.	Netto	Mass [%]	Mass Norm. [%]	Atom [%]	abs. error [%] (1 sigma)	rel. error [%] (1 sigma)
C	6	8772	24.29	59.89	77.88	3.49	14.37
Cl	17	55842	8.70	21.45	9.45	0.32	3.65
Si	14	42393	5.35	13.20	7.34	0.25	4.67
O	8	1004	2.21	5.46	5.33	0.53	23.75
		Sum	40.55	100.00	100.00		

S 27. EDS analysis of chip electrospun with PVC nanofiber

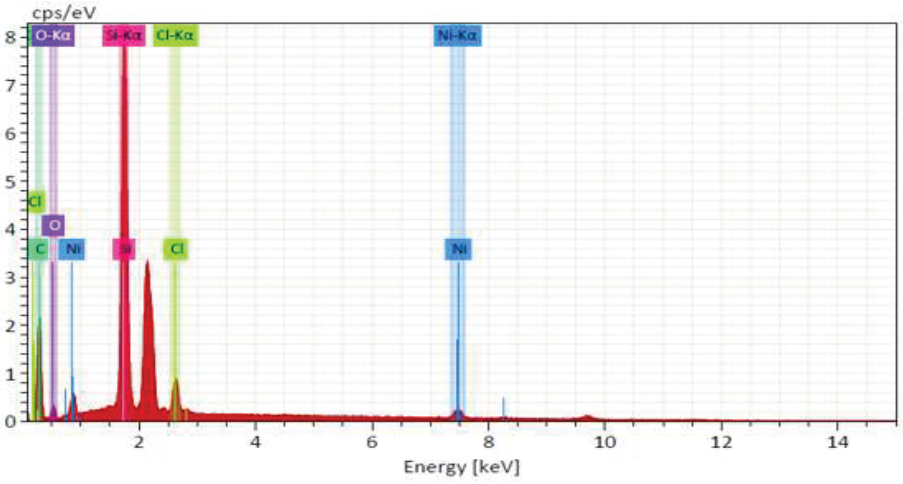

Element	At. No.	Netto	Mass [%]	Mass Norm. [%]	Atom [%]	abs. error [%] (1 sigma)	rel. error [%] (1 sigma)
C	6	17158	30.55	59.03	75.64	4.01	13.14
Si	14	91392	12.88	24.89	13.64	0.56	4.37
O	8	2454	4.39	8.49	8.17	0.82	18.64
Ni	28	3664	2.24	4.34	1.14	0.11	4.75
Cl	17	9702	1.68	3.25	1.41	0.08	5.05
		Sum	51.75	100.00	100.00		

S 28. EDS analysis of chip electrospun with PVC nanofiber doped NiPc

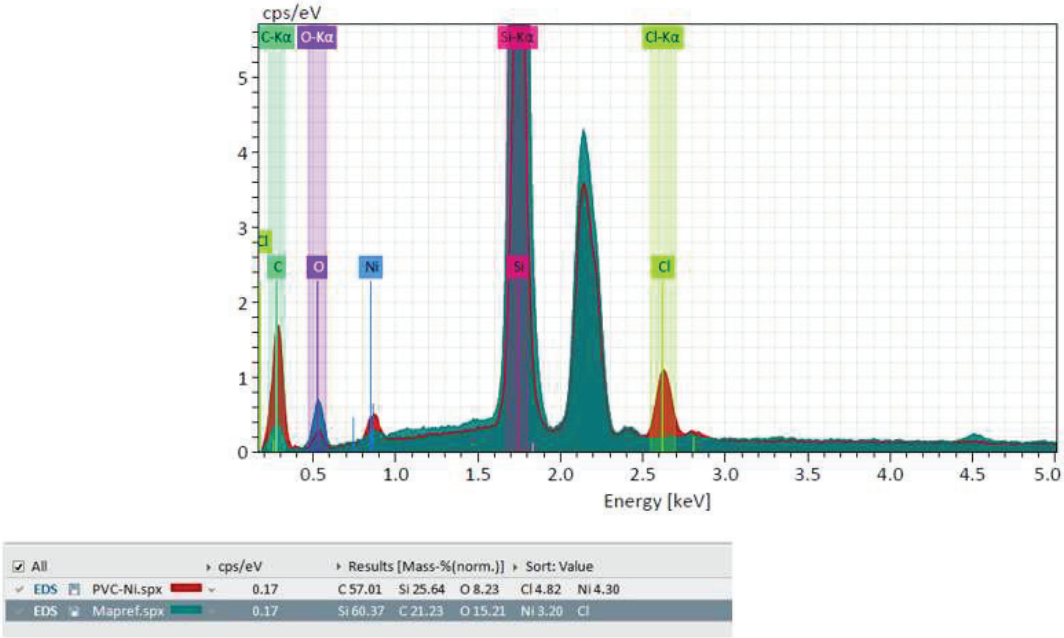

S 29. Superimposition of bare chip and the PVC nanofiber incorporated NiPc on IDEs

Material	Element	Atomic percentage (%)
PVC Nanofiber on IDEs	C	77.88
	O	5.33
	Cl	9.45
	Si	7.34
PVC-NiPc Nanofiber on IDEs	C	75.64
	O	8.17
	Ni	1.47
	Si	13.64
	Cl	1.41

S 30. EDS analysis of bare electrode on-chip, of electrospun PVC nanofiber on-chip and of electrospun PVC doped with NiPc on-chip nanofibers

FTIR Analysis

PVC membrane for assessing the chemical bonds and compositions of nanofiber, the quantification of the FTIR peak areas was carried out with Software (Nicolet-Thermo Fisher, UK) after a proper normalization procedure.

Before detecting the analytes, we can use this FT-IR approach to acquire the membrane's distinctive peaks. The CH_2 asymmetric stretching vibration mode displays peaks at 2970.5 cm^{-1} and 2925.9 cm^{-1} in the FTIR spectra of PVC nanofibers, while the C-H aliphatic bending bond has a height of 1434 cm^{-1}. C-H near Cl has a peak of 1257 cm^{-1}, with C-C bonds at 1000-1100 cm^{-1} and C-Cl bonds at 900-980 cm^{-1}. The spectrum of electrospun PVC nanofiber was shown in the diagram below, which corresponds to the characterization done by Pandey. Nickel phthalocyanine bands were found according to the FT-IR results of electrospun PVC nanofiber mixed with NiPc depicted in (Figure S31) and also proves the finding made by Modibane and his team when characterizing NiPc using FT-IR analysis. Peaks at 1541.0, 1476.1, 1343.9, 1296.2, 1172.3, and 1129.6 cm^{-1}, as well as PVC-related bands that were highlighted above, were all visible after carrying out FTIR analysis of PVC-NiPc [3].

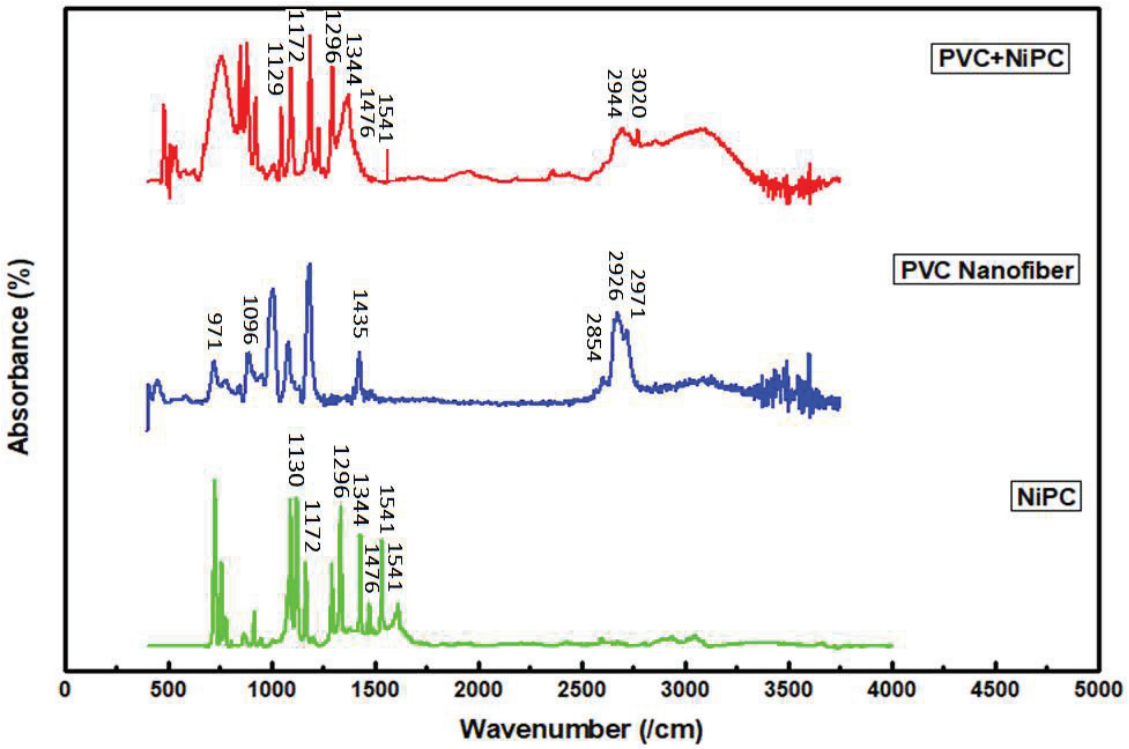

S 31. FT-IR overlap spectra from pure NiPc (green curve), pure PVC fiber (blue curve) and PVC-NiPc fiber (red curve)

TGA Analysis

The thermal properties of the samples were analyzed by thermogravimetric analysis (TGA). The studies were performed using TA instruments (Q50 Series). Scans were made from 20°C to 800°C with a heating rate of 10°C/min to 1000°C, under an N_2 flux at 90 mL/min, to prevent thermo-oxidative processes. The first derivative of the weight loss profile (DTGA) was drawn to identify the prominent degradation peaks of the systems. TGA data were also used to evaluate the actual weight composition of the blend samples, based on thermal decomposition and final residue (at 700 °C) of pure PVC powder and electrospun nanofibers of the PVC.

The thermogravimetric analysis (TGA) curves of PVC fiber and NiPc are shown in Figure S32 (A and B). The thermogravimetric study conducted on ambient air conditions, discovered that the TGA curves for the PVC nanofiber mats and NiPc dye are comparable, with three distinct stages of thermal loss. The first mass loss between ambient temperature to 180°C corresponds to a loss of water and/or solvent. The second step of PVC thermal decomposition begins at about 180-200°C, followed by the third stage at 385°C and finally at 650°C. PVC nanofibers degrade similarly as PVC powder when exposed to heat. As a result, the products' thermal stability is roughly 180-200°C. The fibrous mats fabricated from PVC dissolved in THF is more

rigid than fibrous mats made with DMF or made by mixing solvents. The rapid evaporation of THF resulted in high crystalline fibrous mats with a solid exothermal peak around 380ºC. On the other hand, DMF evaporated, lowering the fibrous mats melting temperature. THF and DMF mixed solvents improved fibrous mats characteristics [2]. Figure S32C shows how the weight of the PVC-NiPc fibrous mats decreases as the system's temperature rises. The DTG curve depicts the sample's multistep mass decrease. The percentage weight loss is about 9.2% in the 23–180 °C region (the first step), which is most likely due to water desorption from the system's surface. In the temperature ranges of 180 to 385 and 560–982°C, respectively, a second and third steps form as the temperature rises. As the temperature rises, PVC may be lost, allowing the parent phthalocyanine core to combine with nearby molecules due to the zigzag curve obtained while is likely to be oxidation reaction of nickel. The weight loss proceeded until 560°C, when the significant deterioration point was reached. Furthermore, TGA and DTG studies demonstrate that PVC-NiPc presents a good thermal stability, with the predominant point of disintegration occurring between 385 and 560 °C. This behavior suggests that it could be used in applications requiring greater thermal stability.

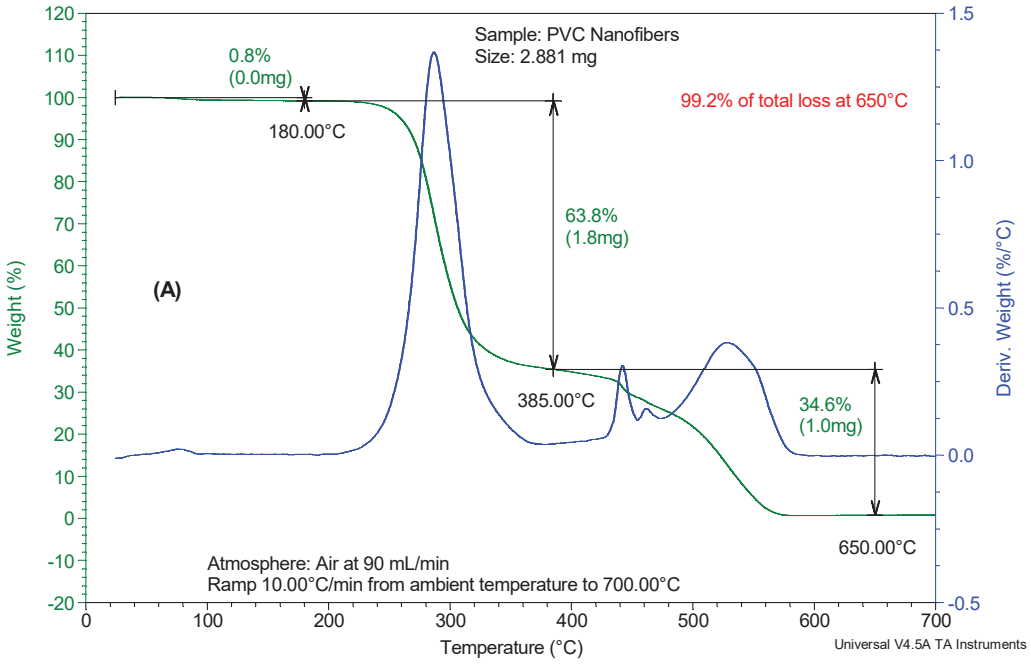

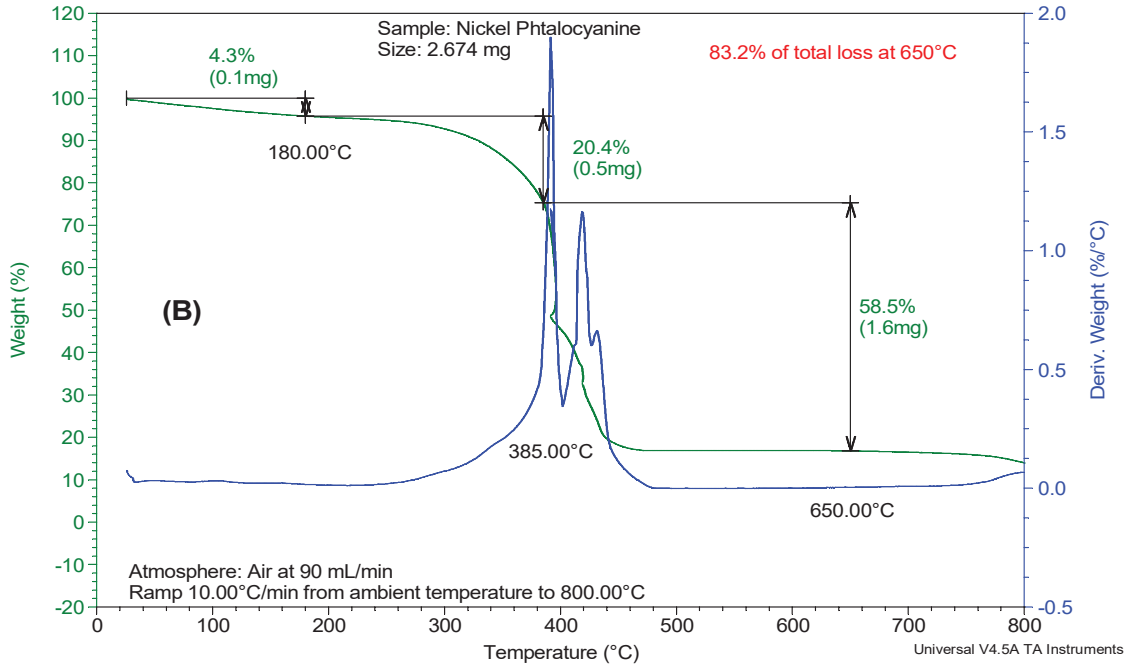

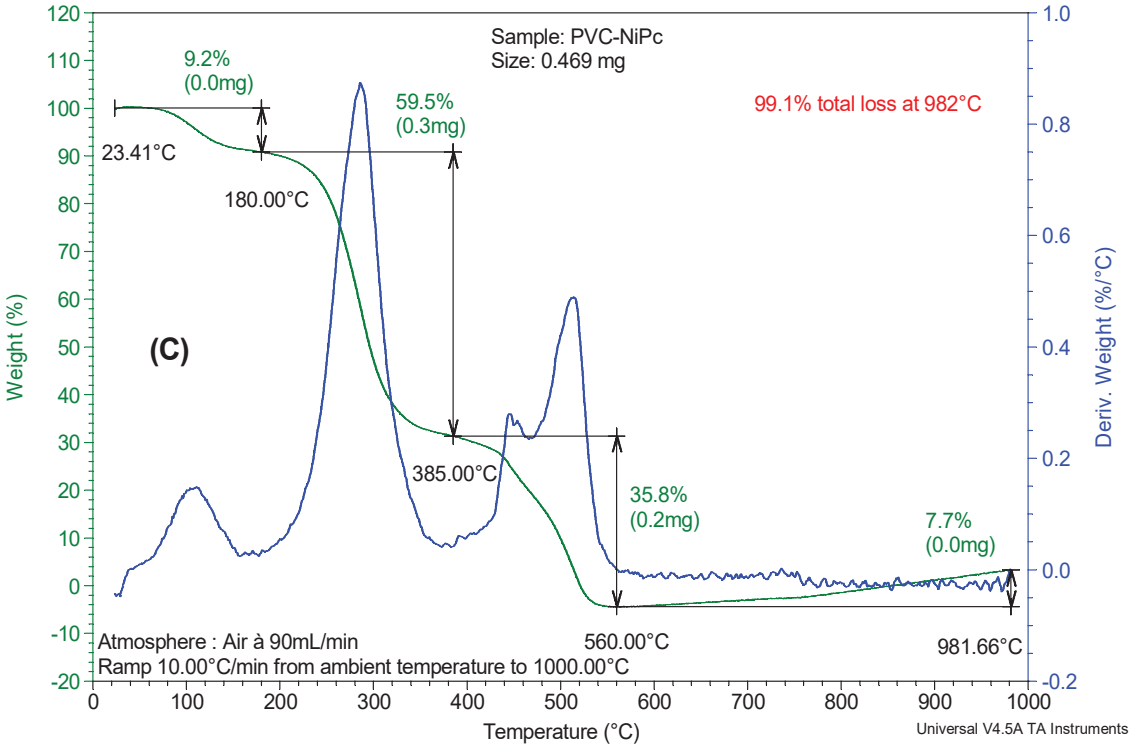

S 32. TGA of (A) pure PVC nanofiber, (B) pure NiPc and, (C) PVC-NiPc fiber

VOC Detections

Gaseous methanol, ethanol, and alcohol sample were collected from the headspace above the aqueous solutions of known concentrations and detected using a Lock-in amplifier in a differential mode. The VOCs detection of different concentrations is given in Figure S33 and S34 for acetone and for ethanol respectively.

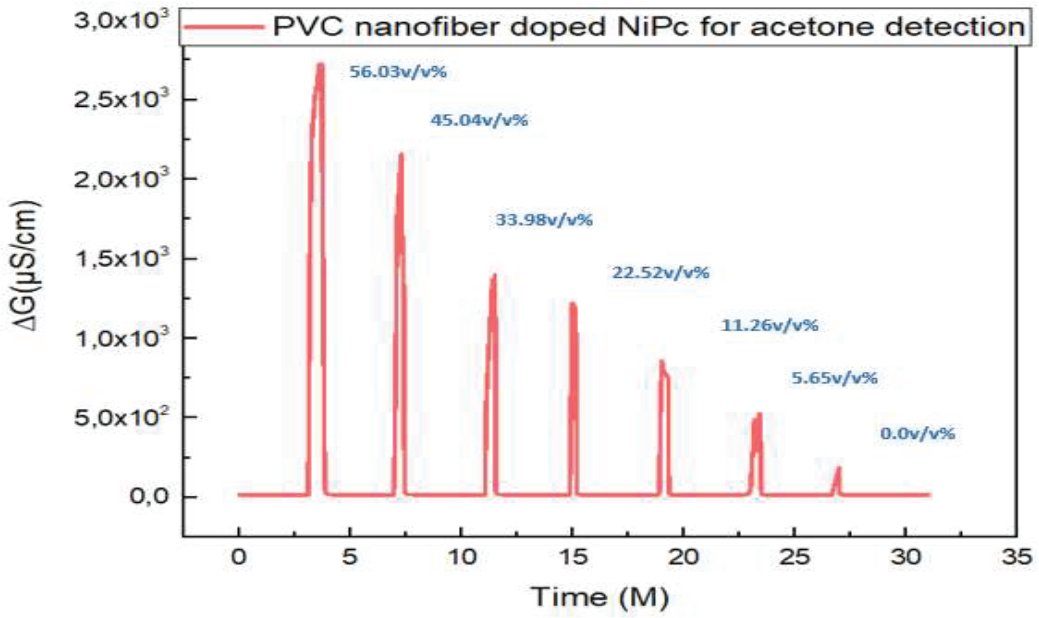

S 33. Detection of gas-phase acetone solutions with PVC nanofiber-NiPc

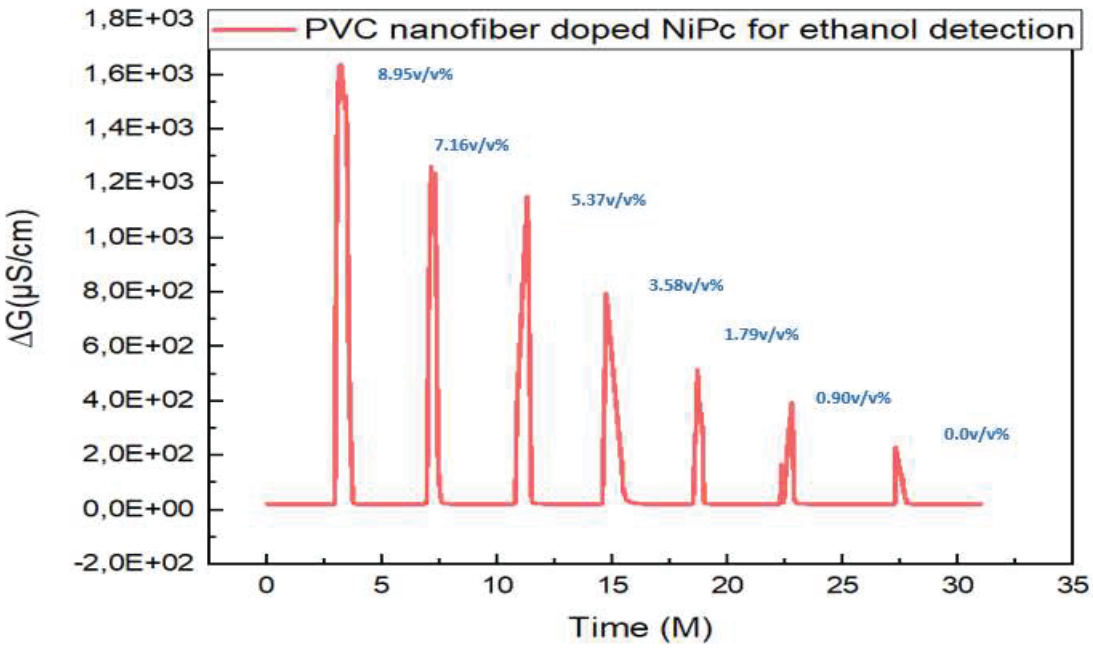

S 34. Detection of gas-phase ethanol solutions with PVC nanofiber-NiPc

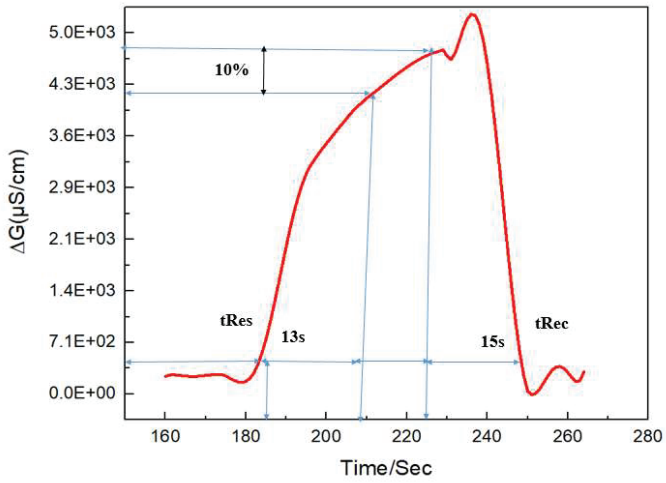

S 35. Determination of the response time (tRes) and of the recovery time tRec on the real-time analysis of the conductometric signal of sensor for methanol gas phase concentration of 11.25 v/v% (T = 293 K, Pressure = 1 atm)

Type of sensor	Polymer materials	Array of fibers	Tested gas	Response time (s)	Dynamic range (ppm)	Detection limit (ppm)	Ref
Acoustic	PAA-PVA	Nonwoven	NH_3	35	50-200	50	[6]
	PAA-PVA	Nonwoven	NH_3	300	0.13-5	0.13	[7]
Resistive	HCSA-PANI	Single	Alcohols	20	No data	No data	[8]
	PANI	Nonwoven	Amines	250	No data	100	[9]
	PMMA-PANI	Nonwoven	$(C_2H_5)_3N$	50	20-500	20	[10]
	CB-PECH	Oriented	VOCs	60	50-500	50	[11]
	PEO, PIB, PVP		$C_5H_{10}Cl_2$	45	5-300	5	[12]
Conductometric	PVC-NiPc	Nonwoven	CH_3OH	13	15-3500	15	This work

S 36. Different types of electrospun polymer nanofiber-based gas sensors

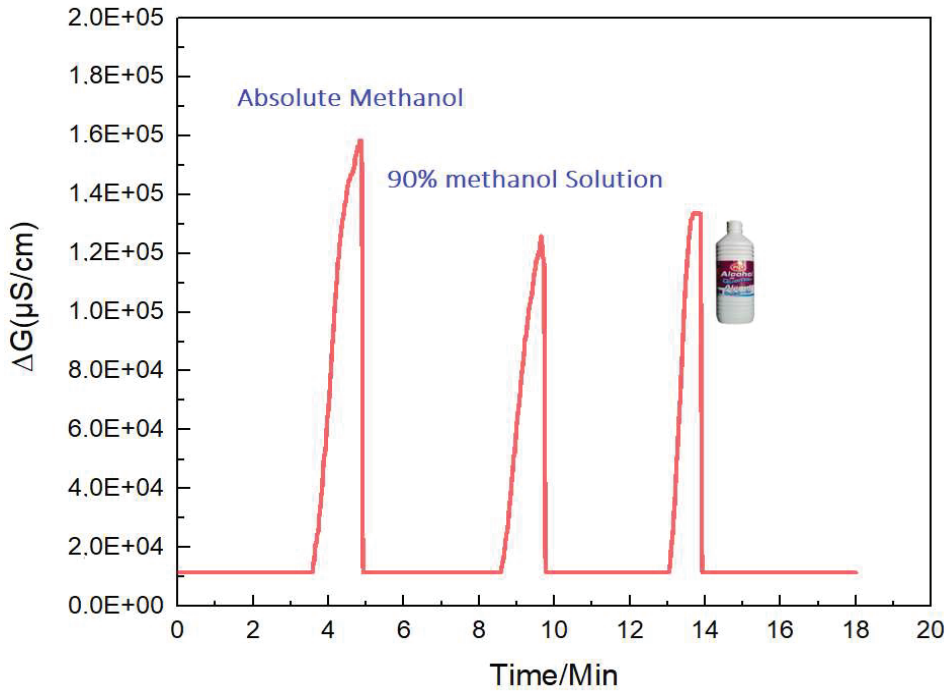

S 37. Detection of gas-phase concentration for different methanol/water solutions and for rubbing alcohol, with the electrospun PVC nanofiber doped with NiPc (T = 293K, Pressure = 1 atm)

References

1. A. Madaci, G. Raffin, M. Hangouet, C. Pages, C. Jose, M. Martin, H. Ferkous, A. Bouzid, J. Bausells, A. Alcacer, A. Errachid, and N. Jaffrezic-Renault, "A microconductometric ethanol sensor prepared through encapsulation of alcohol dehydrogenase in chitosan: application to the determination of alcoholic content in headspace above beverages," *J. Mater. Sci. Mater. Electron.*, 32(13) (2021) 17752–17763, https//doi.org/10.1007/s10854-021-06311-9.
2. E. Maccaferri, L. Mazzocchetti, T. Benelli, T. M. Brugo, A. Zucchelli, and L. Giorgini, "Rubbery nanofibers by co-electrospinning of almost immiscible NBR and PCL blends," *Mater. Des.*, 186 (2020) 108210, https//doi.org/10.1016/j.matdes.2019.108210.
3. K. D. Modibane , T. Peska, T.C. Maponya, K.E. Ramohlala, G.R. Monama, M.E. Makhatha, E. Makhado, M.J. Hato. "Electrochemical studies on the corrosion protection of aluminum metal in acid media by unsubstituted and 4-tetranitro substituted nickel(II) phthalocyanine inhibitors for hydrogen fuel cells," *Int. J. Corros. Scale Inhib.*, 10(1) (2021) 314-330, https//doi.org/10.17675/2305-6894-2021-10-1-18
4. B. Ding, J. Kim, Y. Miyazaki, and S. Shiratori, "Electrospun nanofibrous membranes coated quartz crystal microbalance as gas sensor for NH3 detection," *Sens. Actuators B Chem.*, 101(3) (2004) 373–380, https//doi.org/10.1016/j.snb.2004.04.008.
5. B. Ding, M. Yamazaki, and S. Shiratori, "Electrospun fibrous polyacrylic acid membrane-based gas sensors," *Sens. Actuators B Chem.*, 106(1) (2005) 477–483, https//doi.org/ 10.1016/j.snb.2004.09.010.
6. N. J. Pinto, I. Ramos, R. Rojas, P.-C. Wang, and A. T. Johnson, "Electric response of isolated electrospun polyaniline nanofibers to vapors of aliphatic alcohols," *Sens. Actuators B Chem.*, 129(2) (2008) 621–627, https//doi.org/10.1016/j.snb.2007.09.040.
7. Y. Gao, X. Li, J. Gong, B. Fan, Z. Su, and L. Qu, "Polyaniline Nanotubes Prepared Using Fiber Mats Membrane as the Template and their Gas-response Behavior," *J. Phys. Chem. C*, 112(22) (2008) 8215–8222, https//doi.org/10.1021/jp711601f.
8. S. Ji, Y. Li, and M. Yang, "Gas sensing properties of a composite composed of electrospun poly(methyl methacrylate) nanofibers and in situ polymerized polyaniline," *Sens. Actuators B Chem.*, 133(2) (2008) 644–649, https//doi.org/10.1016/j.snb.2008.03.040.
9. R. Kessick and G. Tepper, "Electrospun polymer composite fiber arrays for the detection and identification of volatile organic compounds," *Sens. Actuators B Chem.*, 117(1) (2006) 205–210, https//doi.org/10.1016/j.snb.2005.11.045.
10. B. Ding, M. Wang, J. Yu, and G. Sun, "Gas Sensors Based on Electrospun Nanofibers," *Sensors*, 9(3) (2009) 1609–1624, https//doi.org/10.3390/s90301609.